Advances in Natural and Technological Hazards Research

Sandeep
Parveen Kumar
Himanshu Mittal
Roshan Kumar *Editors*

Geohazards

Analysis, Modelling and Forecasting

Springer

Advances in Natural and Technological Hazards Research

Volume 53

The book series entitled *Advances in Natural and Technological Hazards* is dedicated to serving the growing community of scholars, practitioners and policy makers concerned with the different scientific, socio-economic and political aspects of natural and technological hazards.

The series aims to provide rapid, refereed publications of topical contributions about recent advances in natural and technological hazards research. Each volume is a thorough treatment of a specific topic of importance for proper management and mitigation practices and will shed light on the fundamental and applied aspects of natural and technological hazards.

Comments or suggestions for future volumes are welcomed.

Sandeep · Parveen Kumar · Himanshu Mittal ·
Roshan Kumar
Editors

Geohazards

Analysis, Modelling and Forecasting

Springer

Editors
Sandeep
Department of Geophysics
Banaras Hindu University
Varanasi, Uttar Pradesh, India

Himanshu Mittal
National Center for Seismology
New Delhi, India

Parveen Kumar
Wadia Institute of Himalayan Geology
Dehradun, Uttarakhand, India

Roshan Kumar
Department of Electronics and Information Technology
Miami College of Henan University
Kaifeng, China

ISSN 1878-9897 ISSN 2213-6959 (electronic)
Advances in Natural and Technological Hazards Research
ISBN 978-981-99-3954-1 ISBN 978-981-99-3955-8 (eBook)
https://doi.org/10.1007/978-981-99-3955-8

This Springer imprint is published by the registered company Springer Nature Singapore Pte Ltd.
The registered company address is: 152 Beach Road, #21-01/04 Gateway East, Singapore 189721, Singapore

Foreword

Turkey Earthquake of M7.8 on February 6, 2023 is the most recent example of natural geohazards, it has claimed over 50000 of human lives and has inflicted vast infrastructural damages. The extent of damages, economic losses and time frame required to recapitulate pre-earthquake scenario are still illusive. Since the advent of the theory of Plate Tectonics, concentration of strong earthquakes in the well-defined seismic belts, their recurrence interval as well as monitoring of stress generation/ accumulation, improved imaging of crustal structures have greatly enhanced our understanding of the process leading to catastrophic earthquakes. Although multiple seismological, geophysical, geochemical, hydrological and animal behavior, etc are collated and a few successes stories are reported as long, intermediate, and short-term precursors but prediction of an earthquake with precise location, magnitude, and time window still remains an unaccomplished challenge of earth sciences. Further, there is famous saying that earthquakes do no kill people, it is the collapse of buildings due to violent shaking caused by the traveling seismic waves account for the loss of lives and damage to standing structures. Given these recognition, major science and technical programs geared to co-up with growing geohazards of earthquake are aimed at developing the earthquake resistance society with a motto "Earthquake safe structures, the basis of the safe life".

The present edited book entitled "Geohazards: Analysis, Modelling and Forecasting" is an comprehensive attempt to share advances in several areas of geohazard quantification and their implementation by policymakers, city planners and above all by society. The most fascinating aspects are all the four co-editors; Dr. Sandeep, Dr. Parveen Kumar, Dr. Himanshu Mittal, and Dr. Roshan Kumar, are young emerging researchers with complimentary expertise and specializations, I congratulate them for choosing such a challenging theme of Seismic Geohazard for their maiden compilation. The book comprising of 12 chapters, authored by actively engaged researchers in wide spectrum of geohazards, cover three major components of the geohazard studies. For example, the Observation and Analysis of earthquakes occurrences, linkages with regional tectonics, stress-drop pattern, etc. Second set of presentation deal with modelling of geophysical, geochemical (radon) data to identify precursors or signal useful for early hazards warning. Importance of such

studies stems from the fact most rapidly advancing tools including artificial intelligence and machine learning are used to estimate potential seismic hazard. Finally, the background information on the site-specific amplification, source mechanism and stress-decay patterns are critical inputs to simulate end scenario hazards map, which under varied tectonic can be used to landslide vulnerability assessment, liquefaction in fault zone, tsunami risk assessment, and the use of early warning systems to avert disastrous effects. The end scenario hazards parameters also provide critical inputs to design for earthquake resistance infra-structure, an ultimate goal of geohazard studies. I am sure the simplimistic mode of presentation, highlighting the key issues of geohazard assessment, will be fruitful to both the subject specialists, policymakers as well as bring awareness among the common public and students. I wish good luck to co-editors and publishers for the success of the efforts and dedication.

Prof. Baldev Raj Arora, FNASc, FIASc.,
Former Director
Wadia Institute of Himalayan Geology
Dehradun, India

Preface

The growing vulnerability and exposure to failures in risk reduction and policy-making have increased the severity of geohazard impact many folds. This strongly demands an extensive understanding of various geohazards and their impetus. Furthermore, detailed geohazard analysis, modeling, and forecasting are needed to reduce the impacts of extreme events. This unique book volume includes chapters from renowned experts from different nations in response to the increased interest in understanding the geohazards. The geoscientists and all other researchers interested in methods for reducing geohazards are extremely interested in the subject. This book involves the geohazards aspects of the different domains on a single podium, making it significant and unique.

This book comprises a total of 12 chapters, which cover contemporary developments of modeling, and analysis techniques especially in the field of hazard and risk associated with earthquakes, vulnerability assessment for landslides, the assessment of tsunami risk in coastal regions, the implementation of early warning systems to prevent catastrophic consequences. While the book provides a fundamental knowledge of geohazards, the case studies illustrate recent developments in hazard reduction and disaster mitigation techniques. The purpose of compiling this book volume was to draw attention to the distinctive characteristics of the geohazards. For comprehending the many forms of geohazards modeling and forecasting, the book is an essential necessity for all researchers, scientists, students, and the industry. This book focuses on the recent trends and information on different geohazard types, ranging from earthquakes to landslides to Tsunamis. This book will significantly contribute to the acquisition of policy-relevant knowledge for risk reduction, which will provide direct benefits to the general public.

We are grateful to all the authors who produced such top-notch chapters for this book. We owe gratitude to all technical reviewers for giving up their time and expertise. Sincere appreciation is extended to the publishing team for their hard

work and effectiveness, which are evident in the book's final form. We think that by describing and comprehending geohazard's ideas from many angles, this book will advance knowledge and understanding in the field.

Varanasi, India — Sandeep
Dehradun, India — Parveen Kumar
New Delhi, India — Himanshu Mittal
Kaifeng, China — Roshan Kumar

About This Book

This book presents a comprehensive analysis of diverse aspects of geohazards. The growing vulnerability and exposure to failures in risk reduction and policy-making increase the severity of geohazard impacts by many folds. Therefore, detailed geohazard analysis, modeling and forecasting are needed to reduce the impacts of extreme events.

An interdisciplinary approach to hazard mitigation provides an advanced tool for risk reduction. The book thus summarizes recent modeling and analysis techniques for hazard assessment and risk mitigation. Topics discussed in the book are hazard and risk associated with earthquakes, vulnerability assessment for landslides and avalanches, the assessment of tsunami risk in coastal regions, the implementation of early warning systems to prevent catastrophic consequences, climate change risk modeling and risk communication.

The convergent approach with the aspects of natural, engineering, and social sciences attracts a vast audience working to advance disaster science. This book also significantly facilitates the acquisition of policy-relevant knowledge for risk reduction, which is beneficial to the general public.

Contents

About the Editors

Sandeep is working as an assistant professor in the Department of Geophysics, Banaras Hindu University (BHU) since 2016. He completed his Master's degree in Geophysics from Kurukshetra University and Ph.D. degree in Seismology from IIT Roorkee. His research interests include simulating strong ground motions and the statistical analysis and comparison of observed and simulated data. He is a lead or co-author of 32 journal articles in international peer-reviewed journals. Sandeep has also contributed to the scientific community as a reviewer of many research articles and projects. He has completed a project funded by the Department of Science and Technology (DST)–Science and Engineering Research Board (SERB) and is currently running a project sponsored by the Institute of Eminence (IoE) Cell, BHU. Recently, he has been selected for the prestigious Indian Society of Earthquake Science's Young Scientists award-2021 and Indian Geophysical Union's Dr. J.G. Negi Young Scientist award-2022 for his significant contributions in the field of seismology. In 2022, Sandeep also received a SERB International Research Experience (SIRE) fellowship to work on the upgradation of the earthquake early warning system at the University of Michigan, USA.

Parveen Kumar currently works as a scientist in the Wadia Institute of Himalayan Geology, Dehradun, India. Earlier, he was awarded a position as a post-doctoral fellow (funded by the University Grants Commission) to carry out his research work. He collaborated internationally in research with the Leibniz Institute for Applied Geophysics, Hanover, Germany. During his career, he has worked, and is still working, on several sponsored and consultancy projects. His research interests include strong motion seismology, earthquake hazard evaluation, geohazard assessment such as landslide and avalanche hazards, and earthquake source studies. He has carried out extensive fieldwork in the Himalayan belt to establish the seismicity detection network and investigate subsurface structure by the multichannel analysis of surface waves. He has published more than 30 research papers in SCI-indexed journals and has supervised several Ph.D. and Master's degree students. He holds a Ph.D. from the Indian Institute of Technology, Roorkee, India, and a Master's from Kurukshetra University, Kurukshetra, India.

Himanshu Mittal currently works as a scientist-E at the National Centre for Seismology, under the Ministry of Earth Sciences, New Delhi, India. Earlier, he worked as a research associate and scientist-C at the Indian Institute of Technology, Roorkee, India. He also worked as a research scientist (post-doc) for more than 5 years at National Taiwan University (NTU) and National Cheng Kung University (NCKU), Taiwan. He was responsible for various studies related to earthquake early warning (EEW) as well as strong-motion studies. Additionally, he served at Amity University, Jaipur, India, for 6 months as an associate professor. His major expertise is in strong-motion simulation, earthquake hazard assessment, site characterization, and EEW, among other areas. Recently, he has developed EEW systems for different regions worldwide. He was an active researcher in reporting the functioning of EEW in Taiwan during the Meinong earthquake of February 2016 and the Hualien earthquake of February 2018. He tested the functionality of an EEW system in India using the recorded earthquake data from Taiwan and completed extensive fieldwork in the Himalayan belt to establish a seismicity detection network in the Himalayas. He has published more than 40 research papers in SCI-indexed international journals and is actively engaged in collaboration with various national and international institutes.

Roshan Kumar currently works as an assistant professor at the Department of Electronic and Information Technology, Miami College of Henan University, China. Earlier, he completed his post-doc position at Zhejiang University, China. His research interests include earthquake early warning systems, seismic signal processing, and landslide warning systems. He holds a Ph.D. from the Indian Institute of Technology, Roorkee, India, and a Master's from Thapar University, India. To date, he has published more than 30 papers and also filed two Indian patents in his short academic career.

Chapter 1
Signature of Active Tectonics and Its Implications Towards Seismic Hazard in Western Part of Stable Peninsular India

Kapil Mohan, Naveen Kumar, Rakesh Dumka, and Sumer Chopra

Abstract The Dadra-Nagar Haveli and the surrounding region, in western India, have been facing moderate seismicity since 1856. Two historic events (Magnitude Ms 5 in 1935 and Magnitude Ms 5.7 in 1856) were reported in the past in this region. Additionally, more than 200 earthquakes ($1.0 \leq M \leq 5.7$) were also reported between M 1 and 5.7 in this area. The epicentre of these earthquakes follows the trend of the faults mapped in the study area. Current study is aimed to map the tectonic features in the region and their associated tectonic-geomorphic features to infer the tectonic behaviour and their impact on seismic hazard in the western part of India. The RIAT of the watersheds of main rivers has been estimated through the analysis of geomorphic indices like stream length (SL) gradient, hypsometric integral (HI), basin shape (BS) and valley floor (VF) and three classes (class II high ($1.3 \leq$ RIAT $<$ 1.5), class III—moderate ($1.5 \leq$ RIAT < 1.8), and class IV—low ($1.8 \leq$ RIAT)) have been found in the study area indicating it a seismically active region. The study area falls within the Panvel seismic zone and the recent seismicity has also been witnessed in the vicinity of N-S trending linear geological features. The presence of seismicity, faults with slickenside planes, shear zones with brittle nature, deformed dykes and extensional features suggests that the region has faced neotectonic activities and is even now active seismically. Through geological fieldwork, the evidence of past major seismic events (>5.5) is also found well preserved in the form of SSDS/seismites in quaternary sediments. The identified SSDS/seismites are mostly formed within the sandy silt, sandy gravel and clay beds; and include sills, dykes, suspended clast blocks, slump structures, and convolute bedding. The extent and dimension of these seismites indicate that the mechanism to trigger these and forces driven for

K. Mohan
National Center for Seismology, Ministry of Earth Sciences, New Delhi, India

N. Kumar (✉) · R. Dumka · S. Chopra
Institute of Seismological Research, Knowledge Corridor, Gandhinagar, Gujarat, India
e-mail: naveen5attri@gmail.com

N. Kumar
EDRC Hydel & Tunnels Larsen and Toubro Limited, Faridabad, India

Sandeep et al. (eds.), *Geohazards*, Advances in Natural and Technological Hazards Research 53, https://doi.org/10.1007/978-981-99-3955-8_1

the source of these features are shock waves of earthquake. The maximum moment magnitude of Mw 6.2 has been estimated based on the maximum displacement recorded along the normal active fault mapped in the study area, which trends N170°–N350°, with a sharp dip of 72° in the SW direction. The seismic hazard assessment of the area considering scenario earthquake of Mw 6.2 along this fault located east of Silvasa city has been estimated using the Stochastic Finite Fault Modelling simulation technique. A maximum peak ground acceleration (PGA) of the order of ~0.44 g has been assessed in the area with a maximum site amplification of 2.15.

Keywords Panvel seismic zone · Relative index of active tectonics · Soft sediment deformation · Seismic hazard assessment

1.1 Introduction

Neotectonics and active tectonics are the key geological agents, which are responsible for the modelling of present-day geomorphology on the earth. The tectonic processes are responsible for the many geological hazards to society. Among all the geological hazards, earthquakes have the most disturbing effect on society. In the field of earth science, the tectonic geomorphology is a rising domain due to its addition of distinctive tools like geodetics, geomorphology, geochronology. Additionally, these tools help in assessment of the deformation rate, incision upliftment, erosion and fault slip rates (Kumar et al. 2020b).

For a long time, the peninsular shield of India has been considered stable seismically and the region has the potential of generating only low-level seismicity at few places (De Montessus de Ballore 1911; Tandon and Chatterjee 1968; Krishnan 1968). However, this belief has been shattered after the occurrence of the 1967, Koyna Earthquake of M 6.2. The M 6.2 magnitude Koyna earthquake forced researchers to reconsider and reassess the seismic status of Peninsular India. The detailed studies conducted by (Chandra 1977; Auden 1949; Watts and Cox 1989; Bansal and Gupta 1998; Dole et al. 2000; Rajendran 1997; Sheth, 1998; Raj et al. 2003; Mohan et al. 2007; Kaplay et al. 2013, 2016; Naik and Awasthi 2003; Kale et al. 2016; Jade et al. 2017, Kumar et al. 2022, 2020a, b) show that, PFS zone, the Konkan coastal belt, Koyna are affected by tectonically generated deformation activities in the Deccan Volcanic region.

The profound accessibility of Geographic Information System and their role in the uninterpretation of digital elevation models has helped to the purposes of RIAT evaluation by means of geomorphic indices. The research on this subject are growing and have seen significant growth in last decades (Kumar et al. 2022). The GIS-based software enables to extract and analyse of landscapes with detailed information. The Assessment of RIAT from indices of geomorphic shows the rates of upliftment and deformation in the landscapes for the long time (Bull 1977; Kumar et al. 2022).

The current area under study is situated in western portion of DVP in the Western India (Fig. 1.1). Since late Triassic/early Jurassic to late Cretaceous periods, West

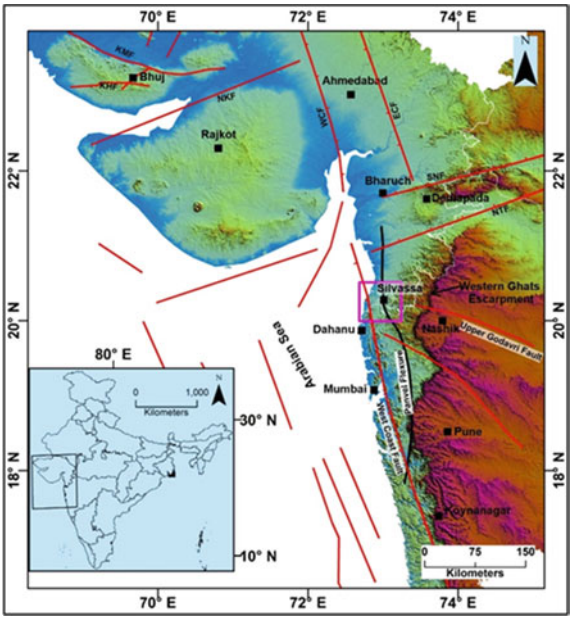

Fig. 1.1 The Tectonic map of Western India (after Biswas 1982; Sheth 1998), KMF-Kachchh Mainland Fault, KHF-Katrol Hill Fault, ECF-East Cambay Fault, WCF-West Cambay Fault, NKF-North Kathiawar Fault, SNF-Son-Narmada Fault, NTF-North Tapti Fault

Coast of India has evident persistent rifting events. The current study area is situated in the Panvel flexure seismic zone (Fig. 1.1), which is undergoing through earthquake events later 1618 (Rao 2005; Rao and Rao 1984; Kumar et al. 2020a) (https://isr.gujarat.gov.in/). Key purpose of this research is to evaluate the seismic hazard in area as there are no considerable studies associated to active tectonic and seismic hazard due active fault (s) in the area under study.

1.2 Geological Setting and Study Area

The area under study is situated in western parts of India (Fig. 1.1). In the west, it's confined by WCF (west coast fault), whereas in east is bounded by Western Ghats escarpment and the central portion is occupied by the Panvel flexure (Fig. 1.1). The Deccan basalt, trachyte and rhyolite complex dominates the study area with basic rock dykes. The central parts of the study area are occupied by alluvium these sediments are distributed in intermittent spots of major rivers (Kumar et al. 2022 and 2020a, b). During Pliocene, the Western Coast of is formed due to the faulting (Krishnan 1953). The WCF is the main tectonic structure in this part of India. Due to its NNW-SSE trend, the straight orientation in the west coast and up to the Gulf of Cambay in the north and continue to the south of Mumbai is considered to be due to this fault (Bombay) (Krishnan 1982).

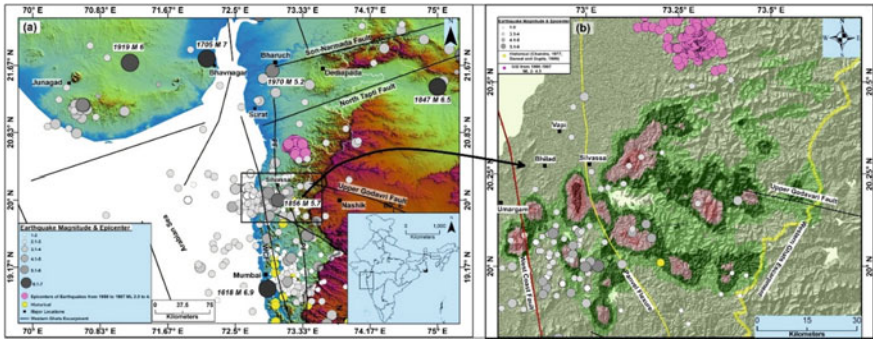

Fig. 1.2 **a** The Seismotectonic map of western India **b** The Seismotectonic map of the study area (After Kumar et al. 2020b)

1.3 Seismotectonics of the Study Area

The area is experiencing earthquakes since 1856. Two historical events (M_S5 in 1935 and $M_S5.7$ in 1856) were recorded in the study area especially concentrated in the southern part (Kumar et al. 2020b; Bansal and Gupta 1998; Chandra 1977). At present, the seismicity in the region endorses the active nature of the present tectonic features; epicentres of the earthquakes are focussed beside these tectonic units (Kumar et al. 2020a). A substantial number of earthquakes between M1 to 5.7 (Chandra 1977; Bansal and Gupta 1998 and Kumar et al. 2020b) are documented in the area under study. The disruption due to the tectonism is even now marked by several earthquakes in western India (Fig. 1.2).

1.4 Methodology

The targeted research work is distributed into three parts (i) evaluation of RIAT, (ii) soft-sediment deformation study and (iii) estimation of seismic hazard due to an active segment of the fault.

1.4.1 Evaluation of RIAT

For evaluation of the RIAT, the remote sensing (RS) and geographic information system (GIS) techniques are used. The network of streams and the demarcation of watershed boundaries are done utilizing Survey of India toposheet at 1:50,000 and SRT Digital Elevation Models (30 m) in the GIS system. The recognition of linear feature like faults, lineaments and dykes, processing of image, production of the FCC, and preparation of shaded relief maps are prepared. The indices, i.e., Bs, HI,

SL, Vf, are assessed and after calculation of all, sub-watersheds are classified in three category on the basis of the value of index. Finally, these values are added and each every sub-watershed has been grouped according to the value of the RIAT (Relative Index of Active Tectonics).

1.4.2 Soft Sediments Deformation (SSD) Structures

The study related to seismite (SSDS) is completed in the steps as follows:—seismites are identified, mapped in alluvial sediments pile up along Damanganga river banks in the study area. These seismites were measured and their association with the surrounding layers of sediments was done. Then the literature related to the seismites has been reviewed and the reasons (whether primary or secondary) behind the formation of these seismites are studied. In addition, the mechanism of trigger, the earthquake distribution and the manifestation of active faults in the region have been investigated.

1.4.3 Seismic Hazard Assessment Due to Active Fault Segment

To determine the seismic hazard of any area, the future earthquake potential valuation is mandatory. Precisely, it is essential to estimate the size of the earthquakes that might be produced by any specific fault. The magnitude of earthquake may be related to rupture parameters like length and displacement (Iida 1959; Tocher 1958; Chinnery 1969). To estimate these parameters, prior paleo-seismic and geologic studies of active faults are required. The parameters/data from the geological and geomorphic studies can be used to evaluate the time of historical earthquakes, the extent of displacement of each event, and the segmentation of the fault zone (Schwartz and Coppersmith 1986; Schwartz 1988; Coppersmith 1991) in the study area. To interpret these source features into estimates of earthquake size, the empirical relationship between rupture parameters and the measure of earthquake size, typically magnitude, is required (Wells and Coppersmith 1994).

Numerous published realistic relationships are available to relate magnitude to various fault rupture parameters, like fault rupture displacement versus rupture length and magnitude versus rupture area (subsurface and surface both), magnitude contrasted with total fault length (Tocher 1958; Iida 1959; Albee and Smith 1966; Chinnery 1969; Ohnaka 1978; Slemmons 1977, 1982; Acharya 1979; Bonilla and Buchanon 1970). There are research works also available that relate the seismic moment and magnitude to the rupture length, width, and an area of the rupture (as assessed from the amount of deformations at surface, the aftershock zone extent, or functions of earthquake source time) (Utsu 1970; Kanamori and Anderson 1975;

Wyss 1979; Singh et al. 1980; Purcaru and Berckhemer 1982; Darragh and Bolt 1987). The empirical relationships proposed by Wells and Coppersmith (1994) were well-tested and used in a number of significant studies in the seismic Hazard Assessment (Mohan et al. 2017, 2018, 2021). Therefore, the same relationship has been used in the present study to estimate the earthquake magnitude from the observed displacement, estimation of rupture area, rupture length and rupture width. The details are as follows.

1.4.3.1 Maximum Earthquake Magnitude

The length of surface rupture and the maximum displacement on continental fault traces are the most commonly used parameters to conclude magnitudes for paleo-earthquakes (Wells and Coppersmith 1994). Here, we have used the maximum displacement method (Wells and Coppersmith 1994) to calculate the maximum magnitude of an earthquake along the identified faults present in the study area.

Maximum Displacement Method

The maximum displacement method involves determining the maximum displacement (MD) estimated from the paleoseismological investigations associated with a paleoearthquake, and comparing that value to the maximum displacement measured or computed for an instrumentally recorded earthquake (Wells and Coppersmith 1994).

The empirical relationship between Moment magnitude (M) and MD will have the form of:

$$M = a + b * \log (MD)$$

Regressions coefficient derived by Wells and Coppersmith (1994) for Moment magnitudes (M) and maximum displacement (MD) are:

$$a = 6.69 \text{ and } b = 0.74$$

Along the normal active faults mapped in the study area, the maximum surface displacement of ~0.25 m is measured. Thus in the above equation with MD = 0.25, the possible Moment magnitude of Mw 6.2 is estimated.

1.4.3.2 Estimation of Seismic Hazard

The seismic hazard can be estimated using two different methodologies (i) Deterministic Seismic Hazard Assessment and (ii) Probabilistic Seismic Hazard Assessment.

In the case of seismic designing and retrofitting of structures, the DSHA has an advantage (McGuire 2001). The DSHA is also useful to check the worst-case scenarios (the largest magnitude at the closest distance) and in the training and plans for emergency response and post-earthquake recovery (McGuire 2001).

In the present study, the deterministic seismic hazard assessment has been conducted to estimate the seismic hazard due to the active segment of the Kilvani Fault (Fig. 1.3), where a displacement of 0.25 m was observed. The Strong motion simulation involves the rigorous mathematical exercise covering the earthquake source/rupture (geometry, nucleation, and propagation) and seismic wave propagation (between the source to the site) through different rock boundaries in the earth's crust. While passing through different subsurface layers, the seismic waves change (amplifies/deamplifies) and reach the site. Cancani (1904) initiated the simulation of strong motion (SM) by generating the SM parameters from the seismic intensity. Later on, Housner (1947) proposed the concept of black-box simulation for simulating SM by using white Gaussian noise. Presently, mainly five types of SM simulation techniques are available. These are (1) composite source modelling (Saikia and Herrmann 1985; Saikia 1993; Zeng et al. 1994; Yu 1994; Yu et al. 1995), (2) stochastic simulation (Boore 1983; Lai 1982; Boore and Atkinson 1987), (3) empirical Green function technique (EGF) (Hartzell 1978, 1982; Hadley and Helmberger 1980; Kanamori 1979; Mikumo et al. 1981; Irikura and Muramatu 1982; Irikura 1983, 1986; Muguia and Brune 1984; Hutchings 1985; Kamae and Irikura 1998; Irikura and Miyake 2011), (4) semi-empirical approach (Midorikawa 1993; Joshi and Midorikawa 2004; Joshi et al. 2001; Mohan 2014), and (5) Stochastic Finite Fault Source Modeling Technique (SFFMT) (Motazedian and Atkinson 2005). Every simulation technique follows certain conditions for the assumptions of source, path, and site effects and rarely estimates all three in one step. Due to advancements in the research methodologies, the SM simulation can be effectively done by dividing it into three major parts (i) source characterization and rupture propagation, (ii) wave propagation from source to base rock/Engineering bedrock (EBR), and (iii) wave propagation from EBR to surface considering near-surface effects gathered in the form of site amplification from geotechnical or/and geophysical parameters like Vs. Generally, one can choose any technique based on available input parameters (source, path and site conditions). The SFFMT is a well-tested SM technique of simulation and well tested in Gujarat by Chopra et al. (2010, 2013), Mohan et al. (2017, 2018, 2021) for seismic hazard assessment. In view of this, the technique has been selected to estimate the strong motion at a grid interval of 10 km $\times$ 10 km. A significant portion of the study area is covered with sediments. The United State Geological Survey (USGS) provided the worldwide Vs30 values based on the topographic slope (Allen and Wald 2009). The Vs30 values in the study region vary from 250 m/sec to 900 m/sec. Therefore, the strong motion has been simulated at B/C Boundary at Vs30 of 760 m/sec and crustal amplifications suggested by Boore and Joyner (1997) for the Vs30 of 760 m/sec. The near-surface wave attenuation/Fall-off of the high frequency (>1 Hz) Fourier amplitude spectrum (Anderson and Hough 1984)/Kappa values (κ) is taken as 0.03 as used by Chopra et al. (2010) for the estimation of seismic hazard in the adjacent Mainland Gujarat. The Quality factor and stress drop

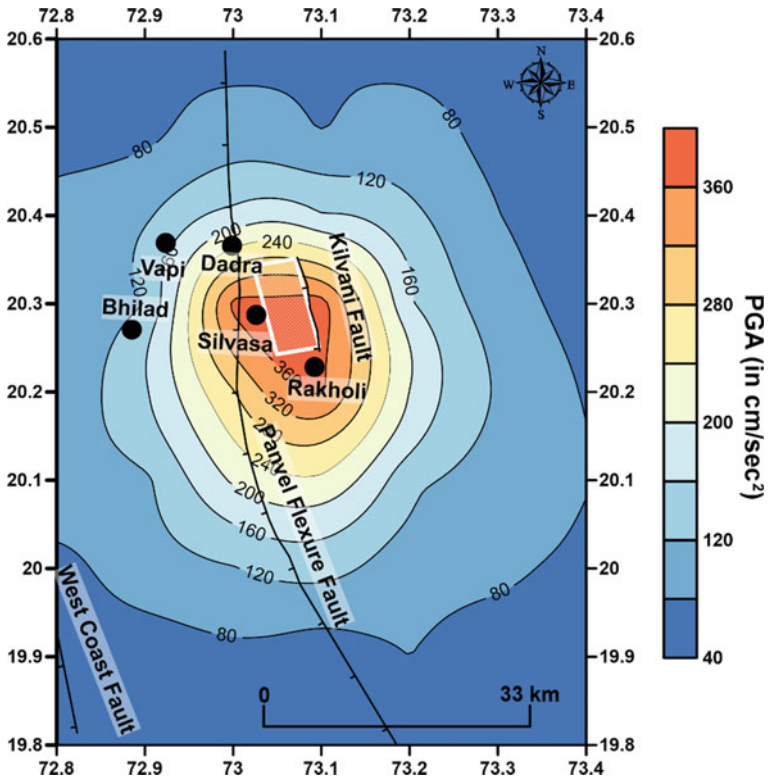

Fig. 1.3 The PGA (in cm/sec^2) distribution map at a Vs of 760 m/sec due to an earthquake of M_w6.2 along the Kilvani Fault

were also considered as suggested by Chopra et al. (2010) for the adjacent Mainland Gujarat area. The input parameters considered for the simulation of ground motion are given in Table 1.1.

Site amplification plays a significant role in the estimation of seismic hazards in any area. In the study area, the Vs30 values proposed by USGS have been used to estimate the site amplification factors at a grid interval of 10 km × 10 km by using the velocity–amplification relationship proposed by Matsuoka and Midorikawa (1994). The PGA distribution map thus prepared at Vs30 of 760 m/sec, the site amplification map (between the Vs of 760 m/sec and the surface Vs) and the PGA distribution map at the surface level have been shown in Figs. 1.3, 1.4, and 1.5, respectively.

Table 1.1 The selected model parameters for the simulation of ground motion

Magnitude (Mw)	6.2	
Fault length and width (km)	(17 km and 11 km)	Wells and Coppersmith (1994)
Strike and dip	170° and 72°	
Slip distribution	Random	
Shear wave velocity	3.6 km/sec	Chopra et al. (2010)
Stress drop	100 bars	Chopra et al. (2010)
Kappa	0.03	Chopra et al. (2010)
Anelastic attenuation Q(f)	$118f^{0.65}$	Chopra et al. (2010)
Geometric spreading	1/R (R≤40 km)	Bodin et al. (2004)
	$1/R^{0.5}$ (40≤R≤80 km)	
	$1/R^{0.55}$ (R≥80 km)	
Duration properties	fc^{-1} (R < 10 km)	Atkinson and Boore (1995)
	fc^{-1} + 0.16R (10≤R≤70km)	
	fc^{-1} - 0.03 (70<R≤130 km)	
	fc^{-1} + 0.04R (130<R<1000 km)	

1.5 Result and Discussions

1.5.1 Faults and Lineament Mapping

During the field geological mapping, a normal fault has been mapped near Kilvani village trending N170°–N350°, with a sharp dip of 72° in the SW direction (Fig. 1.6a). It is evident by the impressive growth of slickensides, the slickensides were occupied by fine-grained white zeolites and calcite. The slickensides zone is very well visible in a depth of 2–4 m in road cuttings (Fig. 1.6a). The slickenlines are suddenly tending towards the south-SW on the surface of fault. The smoothness in touch in the downward direction on slickeside surface and upward direction roughness is observed (Fig. 1.6b), which suggests that the missing western block moved down relative to the block east of the fault (Doblas 1998; Argles 2010). The exposed bedrock along the rock cutting is mainly Basalt, which is found sheared and very closely spaced fractures are formed due to the faulting. The presence of normal fault with a trend N170°–N350° dipping 72° SW suggests the NE-SW extension in the

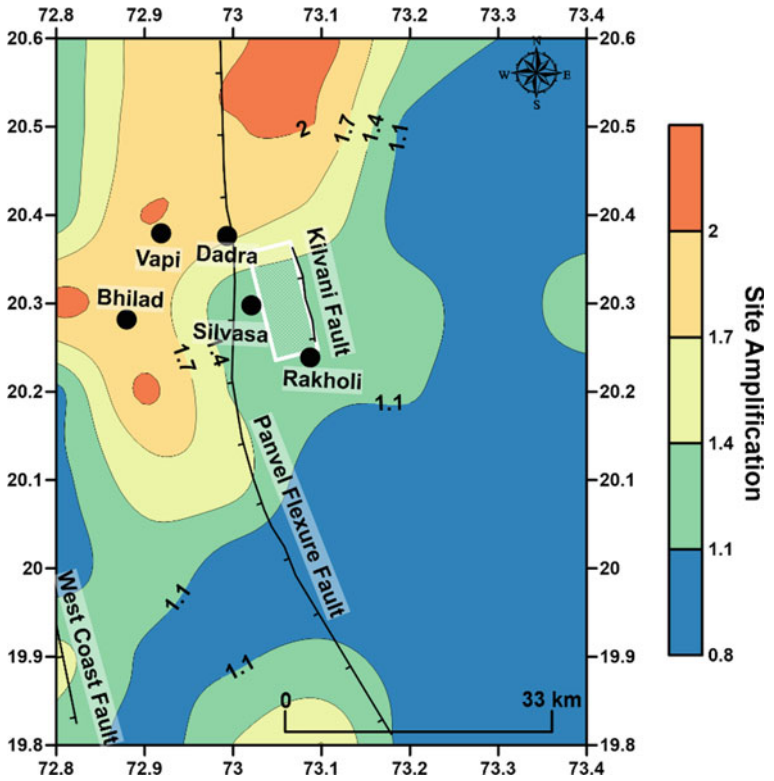

Fig. 1.4 The site amplification map of the study area

study area. The slickensides on striated fault planes were recorded in the expose rock section at Kilvani and Meghwal, (Fig. 1.6). Generally, they present on fresh outcrops showing, thin (~1–5 mm), mineralized (secondary zeolite and quartz, and calcite.) the planes of fault that display primarily a normal slip. Mineralized layers are likely to erode (Doblas 1998; Whiteside 1986; Kranis 2007). The Kilvani fault is the younger fault in the study area as along this fault the displacement in the sediments has been mapped. Though other faults (like the WCF and PF) are also present in the region but along these faults, the signature of displacement or movement has not been found in the study area. The Kilvani Fault also follows the trend of the major faults and the epicentres are occurring along the trend of these faults. Therefore, to estimate the hazard related to seismic event in the area and to estimate the maximum seismic potential, the Kilvani Fault has been considered.

The lineament map has also been generated in the study area, and the results of the analysis depict that these lineaments display maximum resemblance with the trend of the tectonic features present in the area. The lineament density analysis was performed in GIS platform by dividing the study area into four sectors, the results of the lineament density analysis show that the highest density of the lineaments is

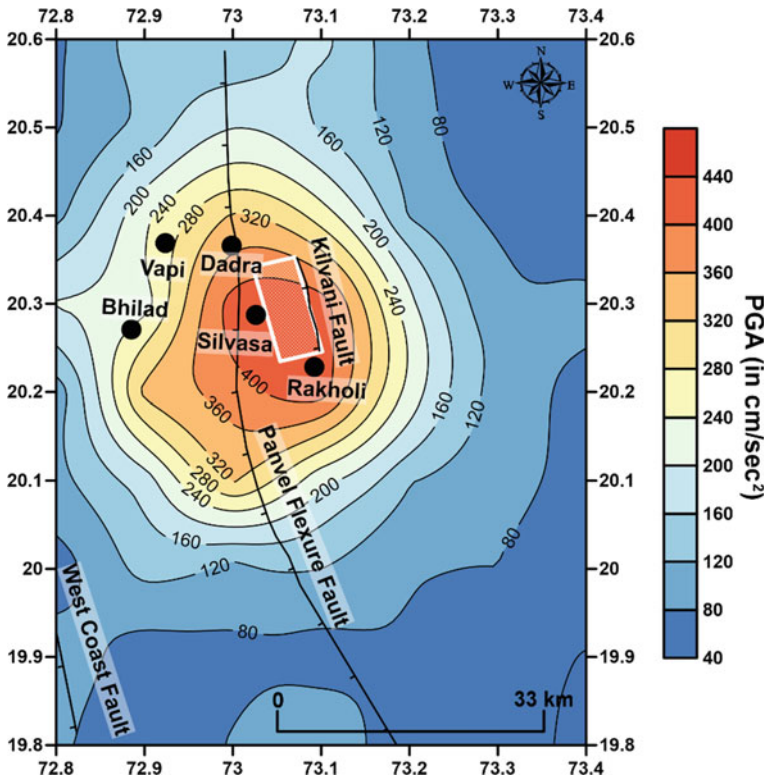

Fig. 1.5 The PGA (in cm/sec^2) distribution map of the surface level due to earthquake of M_w6.2 along the Kilvani Fault

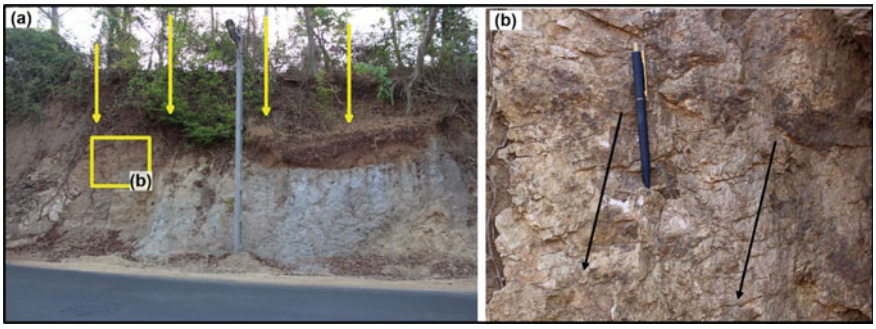

Fig. 1.6 **a** Normal fault near Kilvani village (20°18′1.70"N, 73° 5′53.55"E) road exposures with strike N170°–N350° and dip amount 70° in SW direction, **b** Slickensided fault plane showing the direction of movement by black arrows (After Kumar et al. 2020b)

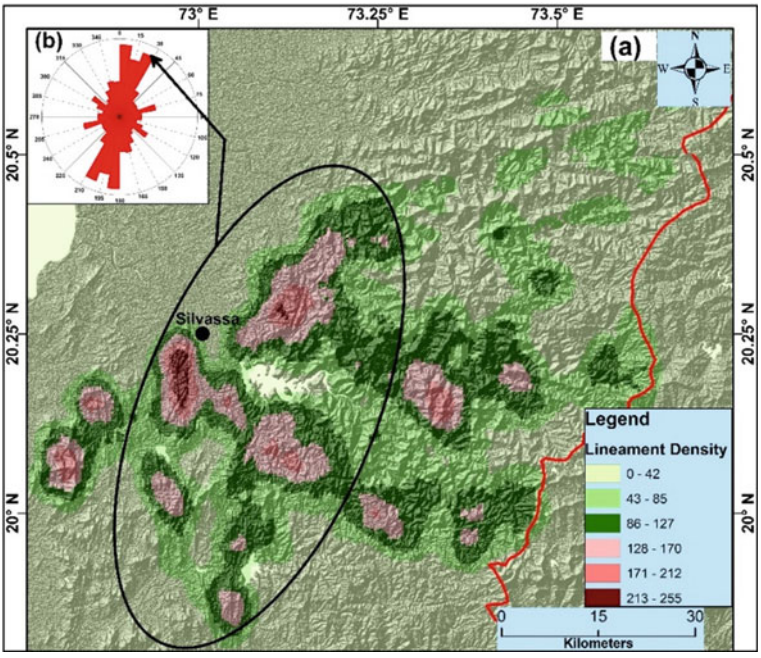

Fig. 1.7 Structural lineament map of the area: **a** lineament density map in which the flat area shows low concentration as compared to flanks, **b** rose diagram of lineaments with a major trend in N-S direction (inset) (After Kumar et al. 2020b)

in the central portion of the study area along the axis of the Kilvani Fault and other tectonic features (Fig. 7b), while the lowest lineament density in alluvial portion. The high lineament density (Fig. 7b) observed in the central portion (in a black circle) was linked with the regional tectonic features present in the study area. Furthermore, the interpretation of the rose diagram and overlay investigation shows that maximum lineaments/linear geological structures are aligned to sub-parallel (N–S direction) to the Kilvani Fault and other tectonic structures (Fig. 7b inset).

1.5.2 Relative Index of Tectonic Activities

The indices like stream length index, valley to floor ratio, hypsometric integral, and basin shape index are calculated, and their collective results were combined to assess the relative index of tectonic activity (RIAT) in the study area. The stream length is an important tool to estimate the relative tectonic activities of any area. The aberration in the profile of river from the steady state may be due to the effect of the lithological, or climatic and tectonic reasons (Hack 1973). The SL index value has been estimated and the area is distributed into 54 sub-basins. Based on the results and the values

classified into three classes; Class I (SL, $\geq$ 600), Class II (300, < SL < 600), and Class III (SL, $\leq$ 300). The 07 numbers of sub-basins come in class-I, a sum of 10 sub-basins comes in class-II and 10 sub-basins comes in Class-III. The results of the study disclose the presence of moderate and high activities in the eastern and northern portions, individually. The central and western portion is moderately least tectonically active along with fairly high stream length index value. The valley to floor ratio index is measured to differentiate among V and U shaped valleys. These are (V-shaped) developed in response to upliftment and flat-floored (U-shaped) wide valleys formed as a reaction to the stability of base level (Bull 1977). The incision by river results into uplift,emt, while low Vf is associated to progressive incision rate and uplift. The < 1 Vf value is related to the V-shaped valleys, linear streams shape with and revealed active upliftment and non-stop downgrade cutting. The > 1 Vf value is associated to flattened or valleys with U shaped, which displays attainment of erosion of base level mainly in response to relative tectonic inactivity (Keller 1986; Keller and Pinter 2022). In the region, the valley to floor width index is calculated in the main streams of sub-basins. Three numbers of classes were classified in this case also; Class I, (Vf $\leq$ 0.5), Class II, (0.5 < Vf < 1.0), and Class III, (Vf $\geq$ 1.0). The findings of the study reveal that the majority of the area comes in Class 1, which shows the V-shape and therefore discloses a remarkably higher degree of tectonic activity. The hypsometric integral index is unbiased of area of the basin and is usually consequent for a precise drainage basin. Usually, the HI outlines the elevational dispersal of an exact area of land, mainly a drainage basin (Strahler 1952). The high value of hypsometric index is possibly related to the current tectonic activity, whereas, the low values signify the mature landscapes, which have been further eroded and less affected by the recent tectonic activities (Strahler 1952). After the results of the analysis, in relations of concavity and convexity of hypsometric curve, the HI may be categorized into three classes, Class 1, (HI $\geq$ 0.5) shape of concave curve; Class 2, (0.4 < HI < 0.5) a shape of concave-convex curve, Class 3, (HI $\leq$ 0.4) the convex shape of curve. The quantity of the breadth of sub-basins varies as of one place to another hence the average value is taken to assess the shape of studied river basin. As per Elias et al., 2019, the index of basin shape (Bs) comprises three classes: (Class I) basin with Elongated shape (Bs $\geq$ 4); (Class II) basin with semi-elongated shape (3 $\leq$ Bs < 4), and (Class III) basin with Circular shape (Bs < 3) (Fig. 1.8). The results of the study reflect that high values of Bs are associated with the basins with elongated shapes, generally connected to relatively enhanced tectonic activities, and low values of Bs entitled to basins with a circular shape generally associated with low tectonic activities.

The eruption of Deccan flood basalt took place at ~65 Ma and covered > 500, 000 km^2 (Chandra 1977; Cox 1988; Acharya et al. 1998; Ramesh and Estabrook 1998). The earlier research in the Deccan province ascribed the viewed variations basically to change in climate, geomorphology, riverine systems, fluctuations in sea levels, and only devoted to the Deccan upland region connection with movements related to neotectonism (Dikshit 1970; Kale and Rajaguru 1987; Watts and Cox 1989; Widdowson and Cox 1996; Renne et al. 2015; Kale et al. 2016). In the present research, an effort is made to evaluate RIAT. The values of the

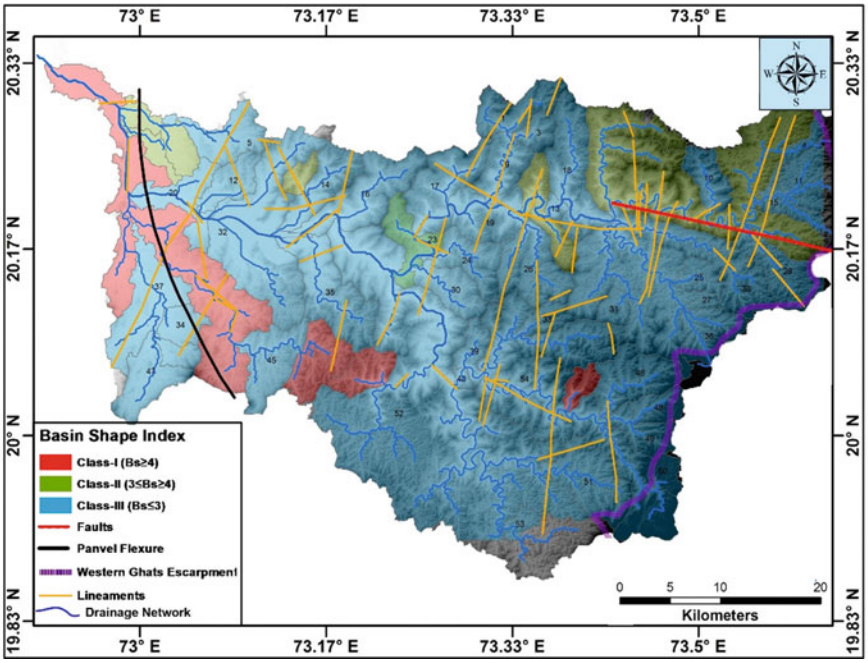

Fig. 1.8 Basin shape index distribution in the sub-watersheds in the study are (after Kumar et al. 2022)

indices computed are added to compute Relative index of Tectonic Activities and then appraised the spatial extent and dispersal of tectonic activities in the study area. The value of RIAT attained by addition of all the indices is grouped in three categories to describe the grade of RIAT in the region, which are given as: $1.3 \leq$ RIAT, $<$ 1.5 in Class II with high activities; 1.57–1.86, class III with moderate activities; and 2.0–2.33 Class IV, with low comparative tectonic activities separately. The distribution of these categories is shown in (Fig. 1.9). The river basins 44,42, 21, 2 fit in to class II (with high activities); the basins 52,43,8,4,3,1 fit into class III (with moderate activities); left all sub-basins fit into class IV (with low activities). The relative index of tectonic activities is high alongside the UGF (Upper Godavari fault), the WGE (Western Ghats escarpment), new lineaments and faults, present in the study area.

In the study area, various types of seismites also mapped from various location in the river sediments during the field investigation. The seismites are primarily found in sandy silt, silty clay and sandy gravels. Major seismites in the area include dykes of intrusive nature and sills of sediments, sediments with slumping structures, clast chunks with suspended nature and bedding with convolute shape.

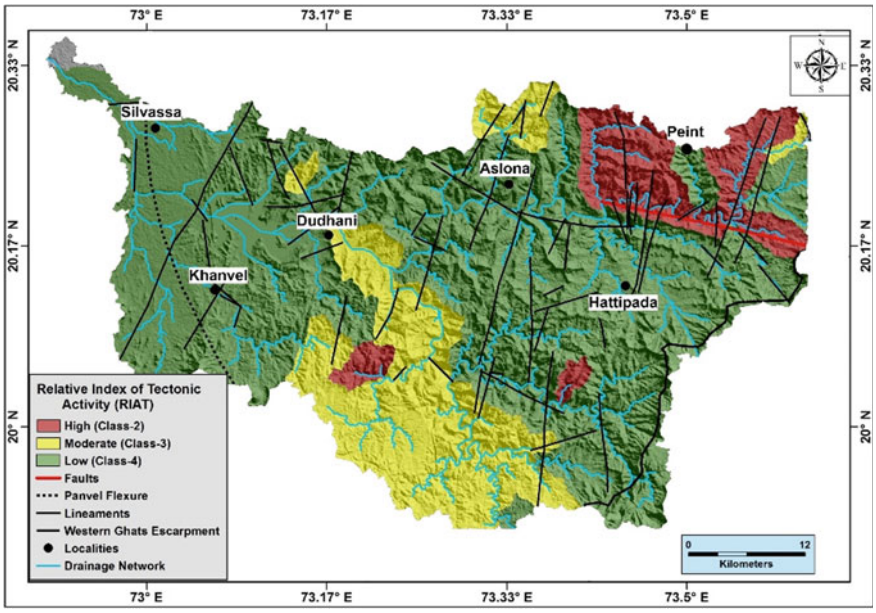

Fig. 1.9 Distribution of relative index of active tectonics (RIAT) in the Darda and Nagar Haveli and surroundings (after Kumar et al. 2022)

1.5.3 Deformation Mechanism

In previous studies in the central regions of Maharashtra the occurrence of SSDS, warping/flexures of sediments, remarkable displacement and deformation in alluvial deposits were documented (Dole et al. 2000, 2002; Rajendran 1997; Kaplay et al. 2013, 2016; Kale et al. 2016). There are various deformation mechanisms, which describe the formation of the seismites. Mills (1983), suggested that the seismites are produced by the disruption of non-lithified and sedimentary layers with water saturation. Researchers like Mills (1983), Lowe (1975), Owen (1987, 2003), Moretti and Sabato (2007) have recommended various deformation mechanisms behind the formation of seismites. The seismites may be formed by the failure in slope due to slumping, liquidization and shear stresses. It might happen if driving force results in reverse density (Allen 1982). The liquefaction or fluidization of the sediments is the most important reason in development of seismites in cohesion-less and water-rich sediment layers (Allen 1982). Normally, the process of the cause and the distortion can be instigated because of the results of exterior instruments like groundwater fluctuations, gravitational and storm currents, and an event of earthquake (Sims 1975; Lowe 1975; Owen 1987, 1996).

1.5.3.1 Trigger Mechanism

There are several probable trigger mechanisms described by various researchers most of them are summarized in this section. The commonly accepted trigger mechanisms are (a) loading of sediment (Moretti and Sabato 2007; Anketell et al. 1970), (b) storm and turbiditic currents (Molina et al. 1998; Dalrymple 1979; Alfaro et al. 2002), (c) sudden collapse in sediments (Waltham and Fookes 2003; Moretti et al. 2001; Moretti and Ronchi 2011), (d) liquefaction of soil through previous fissures (Holzer and Clark 1993; Guhman and Pederson 1992), (v) an earthquake event (Lowe 1975; Seilacher 1969; Sims 1975; Rossetti 1999; Calvo et al. 1998; Alfaro et al. 1999). In the study area, the sediment loading appears to be of least significance for features observed in the alluvial deposits within the study area. Seismites mapped in the study area are present in a large area, which recommends a further regional trigger mechanism in comparison to the limited acts of loading of sediment and storms current, collapse structures, turbiditic currents, and liquefaction via previously existing fissures. Seismic shaking due to the earthquake event could be the most plausible trigger mechanism and it might be the major reason for the development of the seismites within the study area, while present study area is bordered by faults which are active in nature (neotectonically), the Panvel Flexure Fault and its sympathetic faults. The deformed sediments found in the study area may probably be categorized as seismites, based on their extent, nature (river deposits), shapes and dimensions (Owen 1996; Sims 1975; Rossetti 1999; Calvo et al. 1998). The seismites are formed due to earthquake shock after its occurrence and for the development of these features; an area must have undergone to tectonic event and earthquake activities (Moretti and Sabato 2007; Jones and Preston 1987). The ground Shaking done by an earthquake is the widely accepted and famous phenomena behind sediment fluidization. All through the incidence of an earthquake, the pressures in pores are increased for the short time, which results into the loss of contact with grain–grain and short-term loss of strength as of limited pore water expulsion (Allen 1977). In study area, these seismites are qualified for earthquake origin on the basis of the explanations as follows: (a) undeformed beds of soil are present below and above the deformed beds; (b) the size of soil grains of deformed sediments falls in the range of soil liquefaction because of shaking due a seismic ecevnt (Balkema 1997); (c) seismites and their extent, shape, magnitudes, sedimentological properties and facies, are common to the studies on seismites by Rossetti (1999), Sims (1975), Vanneste et al. (1999) and Jones et al. (2000); (d) the presence of active faults in the present study area (Kumar et al. 2020a,b, 2022) and has been experiencing earthquakes with magnitude $M \geq 5$, thus the seismites in the alluvial soil from the area meet with key conditions to be characterized as seismites. To trigger liquefaction in the soil, an earthquake of magnitude 2–3 is enough (Seed and Idriss 1971). For causing liquefaction in the soil, an earthquake magnitude must be >4.5 (Marco and Agnon 1995). The presence of active faults within 15 km to 50 km distance of the study area also affirms the seismites of seismic origin (Fig. 1.10). In view of all the above evidence, it has been postulated that the seismites present in the study area are developed due to the earthquake event of magnitude $M \geq 5$. It has also been proposed that the earthquake,

which might have generated the seismites, possibly will be between magnitude 5 and 7 in the surrounding region.

In an area, if you observe seismic activeness through RIAT, the presence of seismites etc., then it becomes essential to estimate the seismic hazard based on the seismic potential of identified active seismic source(s). In the present study, a displacement of the order of 25 cm (0.25 m) has been estimated along the Kelvani fault. Based on the displacement–magnitude empirical relationship, an earthquake potential of Mw 6.2 has been estimated along this fault. The PGA distribution map of the region based on a scenario earthquake of MW 6.2 along the Kevani fault at Vs of 760 m/sec^2 and surface using site amplification factor estimated through Vs have been simulated using SFFMT. A PGA value of the order of 40 cm/s^2 to 1.360 cm/s^2 has been estimated at Vs 760 m/sec with the maximum value in the western part (towards the dipping direction) of the Kelvani Fault near Silvasa (Fig. 1.3). A site amplification of the order of 0.9–2.15 has been estimated in the study area with a maximum value in the N and NW part (near Vapi) (Fig. 1.4). The higher value of site amplification is estimated in the area covered with the sediments. A surface PGA of the order of 40 cm/sec^2 to 440 cm/sec^2 has been estimated in the study area with a maximum value in the western part of the Kelvani fault (near Silvasa and Rakholi, towards the dip direction) (Fig. 1.5).

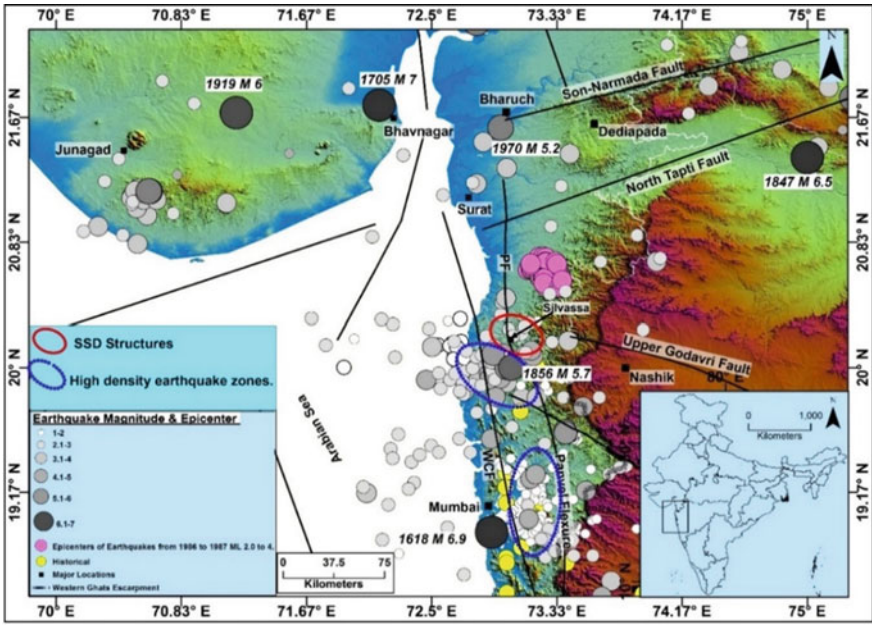

Fig. 1.10 The variation in epicentre distance of seismites (blue ellipse) with their association to 1618, 1856 earthquake (M6.9 and 5.7) affected the study area (after Kumar et al. 2020a)

1.6 Conclusion

The Dadra-Nagar Haveli and the surrounding region, in western India, have been experiencing moderate seismicity (more than 200 earthquakes ($1.0 \leq M \leq 5.7$) since 1856 including two historic events (Magnitude Ms 5 in 1935 and Magnitude Ms 5.7 in 1856). A study is conducted to map the tectonic structures in the region and their associated tectonic-geomorphic features to infer the tectonic behaviour and their impact on seismic hazard in the study area. RIAT of the watersheds of main rivers has been estimated through the geomorphic analysis SL gradient, HI, BS and VF and 03 groups ($1.3 \leq$ RIAT < 1.5 in class II with high activities, $1.5 \leq$ RIAT < 1.8 in class III—with moderate activities, and $1.8 \leq$ RIAT in class IV—with low activities, have been found in the study area indicating it a seismically active region. The study area falls within the Panvel seismic zone with the presence of faults with slickenside bearing planes, shear zones with brittle behaviour, extensional features and deformed dykes suggesting that the study area has faced neotectonic activities and is still active seismically. Through geological fieldwork, the evidence of past major seismic events (>5.5) is also found well preserved in the form of SSDS/seismites in quaternary sediments. The extent and dimension of these seismites indicate that the mechanism to trigger these and forces driven for the source of these structures were shock waves by an earthquake. The maximum moment magnitude of Mw 6.2 has been estimated based on the maximum displacement recorded along the normal active fault mapped in the study area (Kelvani Fault), which trends N170°–N350°, with a sharp dip of 72° in the SW direction. The seismic hazard assessment of the area considering scenario earthquake of Mw 6.2 along this fault located east of Silvasa city has been estimated using the Stochastic Finite Fault Modelling simulation technique. A maximum PGA of the order of 360 cm/sec^2 has been estimated at the EBR with the Vs of 760 m/sec and 440 cm/sec^2 has been estimated at the surface level with a maximum site amplification factor of 2.15 in the area.

References

Acharya HK (1979) Regional variations in the rupture-length magnitude relationships and their dynamical significance. Bull Seismol Soc Am 69(6):2063–2084

Acharya SK, Kayal JR, Roy A, Chaturvedi RK (1998) Jabalpur earthquake of May 22, 1997: constraint from aftershock study. J Geol Soc India 51(3):295–304

Albee AL, Smith JL (1966) Earthquake characteristics and fault activity in southern California. Eng Geol South Calif 1:9–34

Allen JRL (1977) The possible mechanics of convolute lamination in graded sand beds. Jour Geol Soc London 134(1):19–31

Allen JRL (1982) Sedimentary structures, their character and physical basis, vol 1. Elsevier

Allen TI, Wald DJ (2009) On the use of high-resolution topographic data as a proxy for seismic site conditions (VS 30). Bull Seismol Soc Am 99(2A):935–943

Alfaro P, Delgado J, Estévez A, Molina J, Moretti M, Soria J (2002) Liquefaction and fluidization structures in Messinian storm deposits (Bajo Segura Basin, Betic Cordillera, southern Spain). Int J Earth Sci 91(3):505–513

Alfaro P, Estevez A, Moretti M, Soria MJ (1999) Structures sédimentaires de déformation interprétées comme seismites dans le Quaternaire du bassin du Bas Segura (Cordillère bétique orientale). Comptes Rendus de l'Academie de Sciences. Serie IIa. Sciences De La Terre Et Des Planetes 328:17–22

Anderson EM (1951) The dynamics of faulting and dyke formation with applications to Britain. Hafner Pub. Co

Anderson JG, Hough SE (1984) A model for the shape of the fourier amplitude spectrum of acceleration at high frequencies. Bull Seismol Soc Am 74:1969–1993

Anketell JM, Cegła J, Dżułyński S (1970) On the deformational structures in systems with reversed density gradients. In Annales societatis geologorum poloniae, vol 40, no 1, pp 3–30

Argles TW (2010) Recording structural information. In: Coe AL (ed) Geological field techniques. Blackwell Publ, London, pp 163–191

Atkinson GM, Boore DM (1995) Ground motion relations for eastern North America. Bull Seismol Soc Am 85:17–30

Auden JB (1949) Dykes in western India-A discussion on their relationships with the Deccan Traps. Trans Nat Inst Sci India 3:123–157

Balkema AA (1997) Handbook on liquefaction remediation of reclaimed land. Port and Harbour Research Institute

Bansal BK, Gupta S (1998) A glance through the seismicity of peninsular India. J Geol Soc India 52:67–80

Bhattacharya SN, Ghose AK, Suresh G, BaidyaPR, Saxena RC (1997) Source parameters of Jabalpur earthquake of 22 May 1997. Curr Sci 855–863

Bhattacharya HN, Bandyopadhyay S (1998) Seismites in a Proterozoic tidal succession, Singhbhum, Bihar, India. Sed Geol 119:239–252

Biswas SK (1982) Rift basins in western margin of India and their hydrocarbon prospects with special reference to Kutch basin. AAPG Bull 66(10):1497–1513

Biswas SK (1987) Regional tectonic framework, structure and evolution of the western marginal basins of India. Tectonophysics 135(4):307–327

Bodin P, Malagnini L, Akinci A (2004) Ground-motion scaling in the Kachchh basin, India, deduced from aftershocks of the 2001 Mw 7.6 Bhuj earthquake. Bull Seismol Soc Am 94:1658–1669

Bonilla MG, Buchanon JM (1970) Interim report on worldwide historical surface faulting, US Geol Surv Open-file-report 70–34

Boore DM (1983) Stochastic simulation of high-frequency ground motions based on seismo537 logical models of the radiated spectra. Bull Seism Soc Am 538 73(6):1865–1894

Boore DM, Atkinson CM (1987) Stochastic prediction of ground motion and spectral response parameters at hard rock sites in eastern North America. Bull Seism Soc Am 77:440–467

Boore DM, Joyner (1997) Site amplification for generic rock sites. Bull Seism Soc Am 87(2):327–341

Brandes C, Tanner DC (2012) Three-dimensional geometry and fabric of shear deformation-bands in unconsolidated Pleistocene sediments. Tectonophysics 518:84–92

Bull WB (1977) The alluvial-fan environment. Prog Phys Geogr 1(2):222–270

Bull WB (2007) Tectonic geomorphology of mountains: a new approach to paleoseismology. John Wiley & Sons

Bull WB, McFadden LD (2020) Tectonic geomorphology north and south of the Garlock fault, California. In Geomorphology in arid regions, pp 115–138. Routledge

Calvo JP, Rodriguez Pascua M, Martin Velazquez S, Jimenez S, Vicente GD (1998) Microdeformation of lacustrine laminite sequences from Late Miocene formations of SE Spain: an interpretation of loop bedding. Sedimentology 45(2):279–292

Cancani A (1904) Sur l'emploi d'une double ´echelle sismique des intensit´es, empirique et ab571 solue. Gerlands Beitr z Geophys 2:281–283, Cited in Gutenberg and Richter 572 (1942)

Chandra U (1977) Earthquakes of peninsular India-A seismotectonic study. Bull Seismol Soc Am 67(5):1387–1413

Chinnery MA (1969) Earthquake magnitude and source parameters. Bull Seismol Soc Am 59(5):1969–1982
Chopra S, Kumar D, Rastogi BK (2010) Estimation of strong ground motions for 2001 Bhuj (M w 7.6), India earthquake. Pure Appl Geophys 167(11):1317–1330
Chopra S, Kumar D, Rastogi BK, Choudhary P, Yadav RBS (2012) Deterministic seismic scenario in Gujarat, India. Nat Haz 60:1157–2117
Chopra S, Kumar D, Rastogi BK, Choudhury P, Yadav RBS (2013) Estimation of seismic hazard in Gujarat region. India 65:1157. https://doi.org/10.1007/s11069-012-0117-5
Coppersmith KJ (1991) Seismic source characterization for engineering seismic hazard analysis: In Proceedings of 4th international conference on seismic zonation, Vol I, Earthquake engineering research institute, Oakland, California, 3–60
Courtillot V, Besse J, Vandamme D, Montigny R, Jaeger JJ, Cappetta H (1986) Deccan flood basalts at the Cretaceous/Tertiary boundary? Earth Planet Sci Lett 80(3–4):361–374
Cox KG (1988) Inaugural address In: Subbarao KV (ed) Deccan flood basalts. Geol Soc India Mem 10:15–22
Cox RT (1994) Analysis of drainage-basin symmetry as a rapid technique to identify areas of possible Quaternary tilt-block tectonics: an example from the Mississippi Embayment. Geol Soc Am Bull 106(5):571–581
Dalrymple RW (1979) Wave-induced liquefaction: a modern example from the Bay of Fundy. Sedimentology 26:835–844
Darragh RB, Bolt BA (1987) A comment on the statistical regression relation between earthquake magnitude and fault rupture length
Dikshit KR (1970) Polycyclic landscape and the surfaces of erosion in the Deccan Trap country with special reference to upland Maharashtra. Nat Geogr J India 16(3–4):236–252
Doblas M (1998) Slickenside kinematic indicators. Tectonophysics 295(1–2):187–197
Dole G, Peshwa VV, Kale VS (2000) Evidence of a Palaeoseismic event from the Deccan Plateau Uplands. J Geol Soc India 56:547–555
Dole G, Peshwa VV, Kale VS (2002) Evidences of neotectonism in quaternary sediments from Western Deccan Upland Region, Maharashtra. Memoir Geol Soc India 49:91–108
Guhman AI, Pederson DT (1992) Boiling sand springs, Dismal River, Nebraska: agents for formation of vertical cylindrical structures and geomorphic change. Geology 20:8–10
Hack JT (1973) Stream-profile analysis and stream-gradient index. J Res US Geol Surv 1(4):421–429
Hadley DM, Helmberger DV (1980) Simulation of strong ground motions. Bull Seism Soc Am 70:617–630
Hartzell SH (1978) Earthquake aftershocks as green functions. Geophys Res Lett 5:1–4
Hartzell SH (1982) Simulation of ground accelerations for May 1980 Mammoth Lakes, California earthquakes. Bull Seism Soc Am 72:2381–2387
Holzer TM, Clark MM (1993) Sand boils without earthquakes. Geology 21:873–876
Housner GW (1947) Characteristics of strong-motion earthquakes. Bull Seism Soc A 37(1):19–31
Hutchings L (1985) Modeling earthquakes with empirical green's functions (abs). Earthq Notes 56:14
Irikura K, Muramatu I (1982) Synthesis of strong ground motions from large earthquakes using observed seismograms of small events. Proceedings of the 3rd international microzonation conference, Seattle, pp 447–458
Irikura K (1983) Semi Empirical estimation of strong ground motion during large earthquakes. Bull Disaster Prev Res Inst (kyoto Univ.) 33:63–104
Irikura K (1986) Prediction of strong acceleration motion using empirical green's function. In: Proceedings of 7th Japan earthquake engineering symposium, pp 151–156
Irikura K, Miyake H (2011) Recipe for predicting strong ground motion from crustal earthquake scenarios. Pure Appl Geophys 168(1–2):85–104

Jade S, Shrungeshwara TS, Kumar K, Choudhury P, Dumka RK, Bhu H (2017) India plate angular velocity and contemporary deformation rates from continuous GPS measurements from 1996 to 2015. Sci Rep 7:11439. https://doi.org/10.1038/s41598-017-11697-w

Jones ME, Preston RMF (1987) Deformation of sediments and sedimentary rocks. Geological Society, London, Special Publications, no 29

Jones AP, Omoto K (2000) Towards establishing criteria for identifying trigger mechanisms for soft-sediment deformation: a case study of Late Pleistocene lacustrine sands and clays, Onikobe and Nakayamadaira Basins, northeastern Japan. Sedimentology 47(6):1211–1226

Joshi A, Midorikawa S (2004) A simplified method for simulation of strong ground motion using finite rupture model of the earthquake source. J Seismolog 8:467–484

Joshi A, Singh S, Kavita G (2001) The simulation of ground motions using envelope summations. Pure Appl Geophys 158:877–901

Kale VS, Rajaguru SN (1987) Late Quaternary alluvial history of the northwestern Deccan upland region. Nature 325(6105):612–614

Kale VS, Dole G, Upasani D, Pillai SP (2016) Deccan Plateau uplift: insights from parts of Western Uplands, Maharashtra, India. Geological Society, London, Special Publications 445:11–46

Kamae K, Irikura K (1998) Source model of the 1995 Hyogo-ken Nanbu earthquake and simulation of near source ground motion. Bull Seism Soc Am 88:400–412

Kanamori H, Anderson DL (1975) Theoretical basis of some empirical relations in seismology. Bull Seismol Soc Am 65(5):1073–1095

Kanamori H (1979) A semi empirical approach to prediction of long period ground motions from great earthquakes. Bull Seism Soc Am 69:1645–1670

Kaplay RD, Kumar TV, Sawant R (2013) Field evidence for deformation in Deccan Traps in microseismically active Nanded area, Maharashtra. Curr Sci 105(8)

Kaplay RD, Babar MD, Mukherjee S, Kumar TV (2016) Morphotectonic expression of geological structures in the eastern part of the South East Deccan Volcanic Province (around Nanded, Maharashtra, India). Geol Soc London 445:317–335

Keller EA (1986) Investigation of active tectonics: use of surficial earth processes. Active Tecton 1:136–147

Keller EA, Pinter N (1996) Active tectonics, vol 338. Prentice Hall, Upper Saddle River, NJ

Kranis H (2007) Neotectonic basin evolution in central-eastern mainland Greece: an overview. Bull Geol Soc Greece 40(1):360–373

Krishnan MS (1953) The structural and tectonic history of India: Geol Surv India Mem 81:137

Krishnan MS (1982) Geology of India and Burma, 6th Edition, Satish Kumar Jain for CBS Publishers and Distributors 64:536

Kumar N, Mohan K, Dumka RK, Chopra S (2020a) Soft sediment deformation structures in quaternary sediments from dadra and nagar haveli, western India. J Geol Soc India 95(5):455–464

Kumar N, Mohan K, Dumka RK, Chopra S (2020b) Evaluation of linear structures in dadra and nagar haveli, western India: implication to seismotectonics of the study area. J Ind Geophys Union 24(2):10–21

Kumar N, Dumka RK, Mohan K, Chopra S (2022) Relative active tectonics evaluation using geomorphic and drainage indices, in Dadra and Nagar Haveli, western India. Geodesy Geodyn 13(3):219–229

Kuribayashi E, Tatsuoka F (1975) Brief review of liquefaction during earthquakes in Japan. Soils Found 15(4):81–92

Lai SP (1982) Statistical characterization of strong ground motions using power spectral density function. Bull Seism Soc Am 72:259–274

Leeder MR, Alexander J (1987) The origin and tectonic significance of asymmetrical meander-belts. Sedimentology 34:217–226

Lida K (1959) Earthquake energy and earthquake fault. J Earth Sci (7):98–107. Nagoya University

Lowe DR (1975) Water escape structures in coarse-grained sediments. Sedimentology 22:157–204

Marco S, Agnon A (1995) Prehistoric earthquake deformations near Masada, Dead Sea Graben. Geology 23(8):695–698
Matsuoka M, Midorikawa S (1994) GIS-based seismic hazard mapping using the digital national land information. Proceedings of 9th Japan Earthquake
McGuire RK (2001) Deterministic vs probabilistic earthquake hazards and risks. Soil Dyn Earthq Eng 21(5):377–384
Midorikawa S (1993) Semi empirical estimation of peak ground acceleration from large earthquakes. Tectonophysics 218:287–295
Mikumo T, Irikura K, Imagawa K (1981) Near field strong motion synthesis from foreshock and aftershock records and rupture process of the main shock fault (abs.). IASPEI 21st General Assembly, London, Canada
Mills PC (1983) Genesis and diagnostic value of soft-sediment deformation structures—a review. Sed Geol 35(2):83–104
Mohan K (2014) Seismic hazard assessment in the kachchh region of Gujarat (India) through deterministic modeling using a semi-empirical approach. Seismol Res Lett 85(1):117–125
Mohan K, Dugar S, Pancholi V, Dwivedi V, Chopra S, Sairam B (2021) Micro-seismic hazard assessment of Ahmedabad city, Gujarat (Western India) through near-surface characterization/soil modeling. Bull Earthq Eng 19:623–656. https://doi.org/10.1007/s10518-020-01020-w
Mohan K, Rastogi B, Pancholi V, Sairam B (2017) Estimation of strong motion parameters in the coastal region of Gujarat using geotechnical data. Soil Dyn Earthq Eng 92:561–572
Mohan K, Rastogi BK, Pancholi V, Gandhi D (2018) Seismic hazard assessment at micro level in Gandhinagar (the capital of Gujarat, India) considering soil effects. Soil Dyn Earthq Eng 109:354–370
Mohan G, Surve G, Tiwari P (2007) Seismic evidences of faulting beneath and Panvel flexure. Current Sci 93:991–996
Molina JM, Alfaro P, Moretti M, Soria JM (1998) Soft-sediment deformation structures induced by cyclic stress of storm waves in tempestites (Miocene, Guadalquivir Basin, Spain). Terra Nova-Oxford 10(3):145–150
Montessus de Ballore (1911) Seismic history of southern Los Andes south of parallel 16 (In Spanish), Cervantes Barcelona press, Santiago, Chile
Moretti M, Ronchi A (2011) Liquefaction features interpreted as seismites in the Pleistocene fluvio-lacustrine deposits of the Neuquén Basin (Northern Patagonia). Sed Geol 235:200–209
Moretti M, Sabato L (2007) Recognition of trigger mechanisms for soft-sediment deformation in the Pleistocene lacustrine deposits of the Sant'Arcangelo Basin (Southern Italy): seismic shock vs. overloading. Sediment Geol 196(1–4):31–45
Moretti M (2000) Soft-sediment deformation structures interpreted as seismites in middle-late Pleistocene aeolian deposits (Apulian foreland, southern Italy). Sed Geol 135(1–4):167–179
Moretti M, Soria JM, Alfaro P, Walsh N (2001) Asymmetrical soft-sediment deformation structures triggered by rapid sedimentation in turbiditic deposits (Late Miocene, Guadix Basin, Southern Spain). Facies 44(1):283–294
Motazedian D, Atkinson GM (2005) Stochastic finite-fault modeling based on dynamic corner frequency. Bull Seismol Soc Am 95:995–1010
Muguia L, Brune JM (1984) Simulations of strong ground motions for earthquakes in the Mexicali-Imperial valley. Proceedings of workshop on strong ground motion simulation and earthquake engineering applications Pub. 85–02, Earthq. Eng. Res. Inst., Los Altos, California, 21–1–21–19
Naik PK, Awasthi AK (2003) Neotectonic activities in the Koyna River basin–a synopsis. Gondwana Geological Magazine Spl. Publication, 5:157–163
Owen G (2003) Load structures: gravity-driven sediment mobilization in the shallow subsurface. Geol Soc London Spec Publ 216(1):21–34
Owen G (1996) Experimental soft-sediment deformation: structures formed by the liquefaction of unconsolidated sands and some ancient examples. Sedimentol 43:279–293
Owen G (1987) Deformation processes in unconsolidated sands. Geol Soc London Spec Public 29(1):11–24

Purcaru GEORGE, Berckhemer H (1982) Quantitative relations of seismic source parameters and a classification of earthquakes. Tectonophysics 84(1):57–128
Ramesh DS, Estabrook CH (1998) Rupture histories of two stable continental region earthquakes of India. J Earth Syst Sci 107(3):225
Renne PR, Sprain CJ, Richards MA, Self S, Vanderkluysen L, Pande K (2015) State shift in Deccan volcanism at the Cretaceous-Paleogene boundary, possibly induced by impact. Science 350(6256):76–78
Rao BR, Rao PS (1984) Historical seismicity of peninsular India. Bull Seismol Soc Am 74(6):2519–2533
Rao DT, Jambusaria BB, Srivastava S, Srivastava NP, Hamid A, Desai BN, Srivastava HN (1991) Earthquake swarm activity in south Gujarat. Mausam 42(1):89–98
Rao NP, Tsukuda T, Kosuga M, Bhatia SC, Suresh G (2002) Deep lower crustal earthquakes in central India: inferences from analysis of regional broadband data of the 1997 May 21, Jabalpur Earthquake. Geophys J Int 148(1):132–138
Raj R, Bhandari S, Maurya DM, Chamyal LS (2003) Geomorphic indicators of active tectonics in the Karjan River Basin, Lower Narmada Valley, Western India. J Geol Soc India 62:739–752
Rajendran CP (1997) Deformational features in the river bluffs at Ter, Osmanabad district, Maharashtra: evidence for an ancient earthquake. Curr Sci 72(10):750–755
Rossetti DDF (1999) Soft-sediment deformation structures in late Albian to Cenomanian deposits, São Luís Basin, northern Brazil: evidence for palaeoseismicity. Sedimentology 46(6):1065–1081
Saikia CK (1993) Ground motion studies in great Los Angles due to Mw = 7.0 earthquake on the Elysian thrust fault. Bull Seism Soc Am 83:780–810
Saikia CK, Herrmann RB (1985) Application of waveform modelling to determine focal mechanisms of four 1982 Miramichi aftershocks. Bull Seismol Soc Am 75:1021–1040
Schwartz DP, Coppersmith KJ (1986) Seismic hazards: new trends in analysis using geologic data (No. DOE/ER/12018--T10)
Schwartz DP (1988) Paleoseismicity and neotectonics of the Cordillera Blanca fault zone, northern Peruvian Andes. J Geophys Res Solid Earth 93(B5):4712–4730
Seed HB, Idriss IM (1971) Simplified procedure for evaluating soil liquefaction potential. Jour Soil Mech Found Division 97:1249–1273
Seilacher A (1984) Sedimentary structures tentatively attributed to seismic events. Mar Geol 55(1–2):1–12
Seilacher ADOLF (1969) Fault-graded beds interpreted as seismites. Sedimentology 13(1–2):155–159
Sheth HC (1998) A reappraisal of the coastal Panvel flexure, Deccan Traps, as a listric-fault controlled reverse drag structure. Tectonophysics 294:143–149
Sims JD (1973) Earthquake-induced structures in sediments of Van Norman Lake, San Fernando, California. Science 182(4108):161–163
Sims JD (1975) Determining earthquake recurrence intervals from deformational structures in young lacustrine sediments. Tectonophysics 29(1–4):141–152
Singh SK, Bazan E, Esteva L (1980) Expected earthquake magnitude from a fault. Bull Seismol Soc Am 70(3):903–914
Strahler AN (1952) Hypsometric (area-altitude) analysis of erosional topography. Geol Soc Am Bull 63(11):1117–1142
Tandon AN, Chatterjee SN (1968) Seismicity studies in India. MAUSAM, 19(3):273–280
Tocher D (1958) Earthquake energy and ground breakage. Bull Seismol Soc Am 48(2):147–153
Utsu T (1970) Aftershocks and earthquake statistics (1): Some parameters which characterize an aftershock sequence and their interrelations. J Fac Sci Univ, Hokkaido University, Series 7, Geophys 3(3):129–195
Vanneste K, Meghraoui M, Camelbeeck T (1999) Late Quaternary earthquake-related soft-sediment deformation along the Belgian portion of the feldbiss fault, Lower rhine graben system. Tectonophysics 309(1–4):57–79

Waltham AC, Fookes PG (2003) Engineering classification of karst ground conditions. Quarterly Jour Engg Geol Hydrogeol 36:101–118
Watts AB, Cox KG (1989) The Deccan Traps: an interpretation in terms of progressive lithospheric flexure in response to a migrating load. Earth Planet Sci Lett 93:85–97
Whiteside, P (1986) Discussion on 'Large-scale toppling within a sackung type deformation at Ben Attow, Scotland'by G. Holmes and JJ Jarvis. Quart J Eng Geol Hydro 19(4):439–439
Wells DL, Coppersmith KJ (1994) New empirical relationships among magnitude, rupture length, rupture width, rupture area, and surface displacement. Bull Seismol Soc Am 84:974–1002
Widdowson M, Cox KG (1996) Uplift and erosional history of the Deccan Traps, India: Evidence from laterites and drainage patterns of the Western Ghats and Konkan Coast. Earth Planet Sci Lett 137(1–4):57–69
Widdowson M (1997) Tertiary palaeosurfaces of the SW Deccan, Western India: implications for passive margin uplift. Geol Soc London Spec Publ 120(1):221–248
Wyss M (1979) Estimating maximum expectable magnitude of earthquakes from fault dimensions. Geology 7(7):336–340
Yu G (1994) Some aspects of earthquake seismology: slip portioning along major convergent plate boundaries: composite source model for estimation of strong motion and nonlinear soil response modeling. PhD thesis, University of Nevada
Yu G, Khattri KN, Anderson JG, Brune JN, Zeng Y (1995) Strong ground motion from the Uttarkashi earthquake, Himalaya, India, earthquake: comparison of observations with synthetics using the composite source model. Bull Seismol Soc Am 85:31–50
Zeng Y, Anderson JG, Su F (1994) A composite source model for computing realistic synthetic strong ground motions. Geophys Res Lett 21:725–728

Chapter 2
Stress Dissipation in the North-West Himalaya: What We Learnt from Post-seismic Stress Changes

Somak Hajra and Devajit Hazarika

Abstract The Himalaya features a complex subduction system with varying convergence rates throughout its arcuate geometry. The varying rates of convergence result in differential stress generation, and in turn, unequal seismicity and stress dissipation across the arc. As a result, there exist high-risk seismic zones in the seats of previously occurred large earthquakes as well as in the seismic gaps that can potentially hold a future great earthquake. The post-seismic stress drop is the amount of stress released in an earthquake event. The collective stress change for a sequence of events over a time period serves as a significant parameter in determining the rate of seismic activity in a particular region. Comparing the stress changes for different regions helps us identify potentially hazardous zones in terms of incomplete stress dissipation against a background of constant stress accumulation. Numerous studies have been dedicated to the seismogenesis of the northwest (NW) Himalaya. In this chapter, an attempt has been made to disseminate the background knowledge in seismicity and stress scenario prevailing in the NW Himalaya and its implications in understanding potential zones for future great earthquakes. The chapter provides a general introduction to the computational methods employed in utilizing the earthquake data for deciphering tectonic stress. It also provides an overview of the seismicity and stress analysis of the NW Himalaya from west to east covering the Ladakh-Karakoram zone, the Garhwal, and the Kumaon Himalaya. We compile and compare the results in these segments to analyze the potential hazard in these segments independently, relatively, and as a whole.

Keywords Himalaya · Stress drop · Seismic gap · Earthquakes

S. Hajra (✉)
Department of Physics, University of Alberta, Edmonton T6G2M8, Canada
e-mail: somak@ualberta.ca

D. Hazarika
Geophysics Group, Wadia Institute of Himalayan Geology, Dehradun 248001, India
e-mail: devajit@wihg.res.in

Sandeep et al. (eds.), *Geohazards*, Advances in Natural and Technological Hazards Research 53, https://doi.org/10.1007/978-981-99-3955-8_2

2.1 Introduction

The Himalayan orogeny forms one of the youngest continental subduction zones formed by the underplating of the northward bound Indian plate beneath the Eurasian plate. The collision of these two immense plates consequently led to the generation of a significant amount of stress that manifests itself in the form of numerous earthquakes along the entire length of the Himalayan arc. However, the convergence rate is non-uniform in all parts of the Himalaya, thereby leading to differential stress development. As a result, we have seismic gaps that are seismically active regions between two great earthquakes without any damaging event over time (Khattri 1999). The underthrusting of the heavier Indian plate has led to the development of active thrusts in the brittle upper Eurasian crust. The subduction between these two plates is also not smooth as several studies have reported the presence of locking in the form of a ramp structure in the decollement boundary (Main Himalayan Thrust or MHT) between these two plates. All major thrust sheets of the Himalaya, i.e. Himalayan Frontal Thrust (MHT), Main Boundary Thrust (MBT), and Main Central Thrust (MCT) sole down at depth to merge with MHT and accumulate huge strain energy. This ramp structure at mid-crustal depths has been reported in large segments of the north-west (NW) Himalaya such as Satluj (Hazarika et al. 2017), Garhwal (Caldwell et al. 2013), Kumaon (Hazarika et al. 2021) and even in the central Nepal Himalaya (Pandey et al. 1999). The MHT ramp serves as a complex zone of crustal stress accumulation that is often dissipated in the brittle crust in form of devastating earthquakes such as the 1905 Kangra, 1991 Uttarkashi, 1999 Chamoli, and the more recent 2015 Gorkha earthquakes. The entire Himalayan arc is one of the most seismically active belts in the world and the question still persists whether the so-called seismic gaps are simply low-stress zones or dormant phases in the activation process (Fig. 2.1). A large part of the Himalaya is heavily populated, and a great earthquake event poses a significant threat. Several studies related to the tectonics, earthquake sources, and seismogenesis have been carried out to understand the mechanism and pattern of earthquakes in the Himalaya. Many individual studies in the NW part have been aimed at identifying post-seismic stress changes in an attempt to understand the stress regime of the seismic hazard zone. The present study is a compilation, comparison, and summarization of the results of stress drop estimations based on spectral analysis for understanding the potential hazard in these segments independently, relatively, and as a whole.

2.2 Stress Drop Estimation: Concept and Methodology

The physical processes involved in the generation of an earthquake are investigated by different seismological methods, e.g. source mechanism study through waveform inversion technique, stress tensor inversion for regional stress pattern as well as spectral analyses of P and S waves for source parameter study (e.g. stress drop,

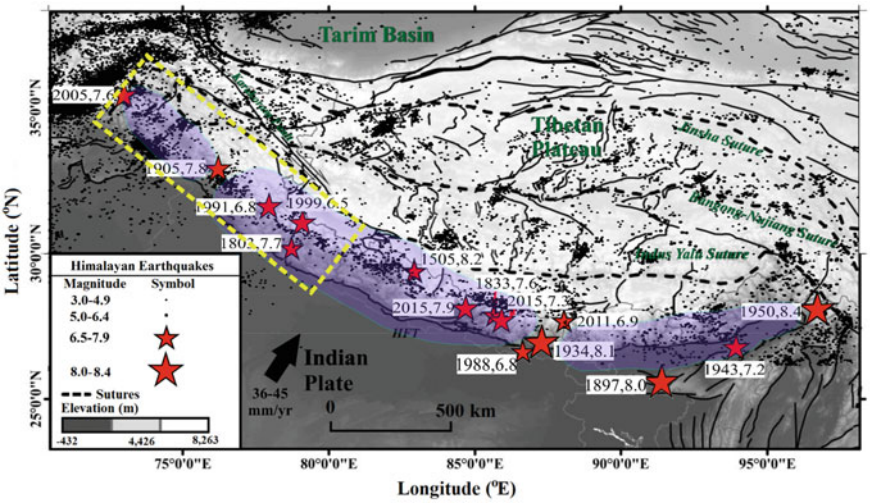

Fig. 2.1 Seismicity after ISC catalog (1964–2020) of the entire Himalayan arc plotted over the topographic map (modified after Hajra et al. 2022b). The strong and great earthquakes in the Himalaya are represented by red stars. The colored zones mark the seismic gaps with the yellow box showing the approximate location of the NW Himalaya

rupture area, rupture length, seismic moment, and moment magnitude). Here, we discuss the spectral analysis method to estimate source parameters. One of the most important source parameters is the stress drop that provides the ambient stress in the vicinity of the earthquake source before and after the occurrence of an earthquake.

For estimating source parameters, the selected P wave or S wave (3–5 s window) is preprocessed (corrected for attenuation, baseline, trend, and mean removal) and integrated to get displacement seismograms and further converted to frequency domain using Fast Fourier Transformation. Two distinct levels of amplitudes can be recognized in the spectra, i.e. a flat level at low frequencies and sharp decay of high-frequency amplitudes (Fig. 2.2). If they are connected by straight lines they intersect at a point termed as corner frequency (fc). The mean amplitude in the low-frequency level is termed as low-frequency spectral level (Ωo). From these two parameters, one can estimate the source parameters. The seismic moment can be estimated following the generalized equation of Keilis-Borok (1960) using P or S spectra:

$$M_0 = \frac{4\pi R^{/} V_{P,S}^3 \rho \Omega_0}{\theta_{P,S} S_{P,S}} \tag{2.1}$$

where R is the hypocentral distance, V_P and V_S are the *P* and *S*-wave velocities, $\rho = 2800\ kg/m^3$ is the density, $\theta_{P,S}$ is the average radiation pattern for the P and S waves, respectively and $S_{P,S}$ is the surface amplification factor for *P* and *S* waves. $\theta_P = 0.52$

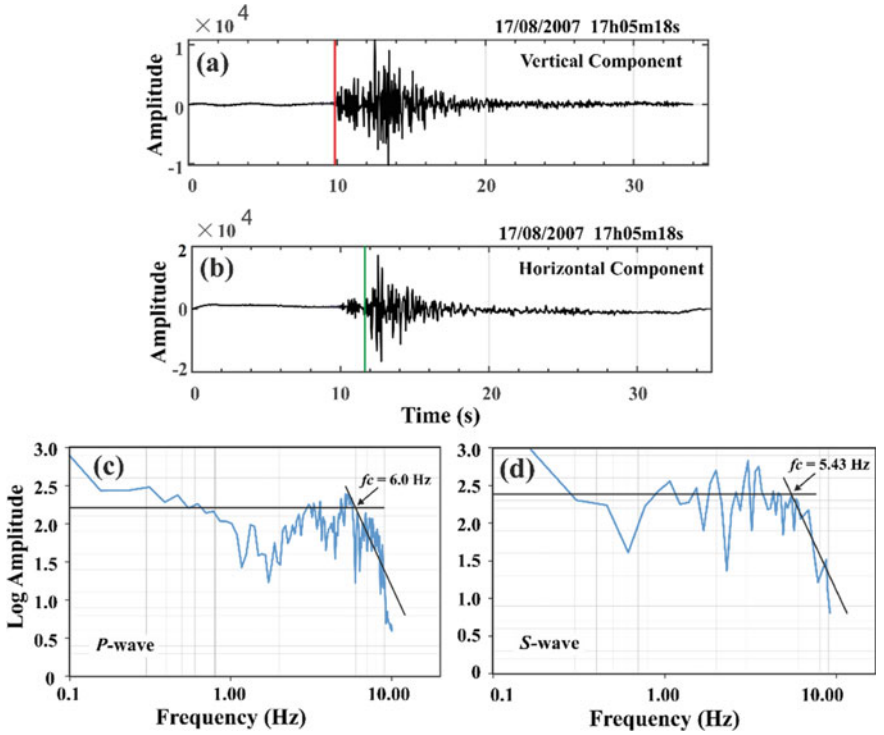

Fig. 2.2 Examples of the **a** vertical and **b** horizontal components of a seismogram. The arrival of P and S waves is marked by red and green lines, respectively. Spectral analysis has been carried out for ~5 s window. The displacement spectra for P and S waves are shown in **c** and **d**. The corner frequency (fc) of respective spectra is correspondingly marked

and $\theta_S = 0.63$ are considered following Boore & Boatwright (1984). The source radius, using P waves (r_p) and S waves (r_s) as well as stress drop can be re-estimated following relations by Brune (1970):

$$r_p = \frac{1.92V_P}{2\pi f_c}(P-\text{wave}),\ r_s = \frac{2.34V_S}{2\pi f_c}(S-\text{wave}),\ \text{and}\ \Delta\sigma = \frac{7M_0}{16r^3} \tag{2.2}$$

The seismic moment magnitude (Mw) is estimated from Mo values using the relationship:

$$logM_0 = 1.5Mw + 9.1 \tag{2.3}$$

After the estimations of source parameters, the scaling relations are developed between important source parameters (M_L, Mw, M_0, $\Delta\sigma$, and fc), which serve as useful inputs for the assessment of earthquake hazards in a region.

2.3 Seismicity and Stress Changes in the NW Himalaya

2.3.1 Spatial Distribution of Seismicity

A strong variation of seismicity along the strike of the Himalaya reflects non-uniform subsurface structure particularly the MHT geometry (Arora et al. 2012). The ramp structure in the MHT is reported as the causal factor for clustered seismicity in the Himalayan Seismic Belt (HSB) around the MCT of the Garhwal Himalaya (Caldwell et al. 2013) and Kumaon Himalaya (Hazarika et al. 2021). The absence of such a ramp and corresponding lack of seismicity M ≥ 5.0 in the HSB of Satluj Valley (Hazarika et al. 2017) indicates the linkage of seismicity with ramp structure on the MHT (Fig. 2.3). The Garhwal-Kumaon region reports the thinnest crust in NW Himalaya varying between 40 and 55 km (Hajra et al. 2019; Hazarika et al. 2018). Most of the crustal shortening and stress accumulation in the MHT ramp is accommodated into the Eurasian crust through the Lesser Himalayan Duplex (Hajra et al. 2021). As such, the Garhwal-Kumaon region shows the classic HSB pattern with the seismicity concentrating in the upper 20 km of the crust marking the decollement ramp near the MCT. A migration or shift of seismicity is observed to the north of Satluj Valley, i.e. near the Kaurik Chango Fault (KCF) zone. The region north of the Himalayan thrust belt, i.e. Trans Himalayan Ladakh Karakoram zone shows unique pattern of seismicity (Parshad et al. 2014; Paul and Hazarika 2022). The Ladakh batholith is free from moderate and large earthquakes whereas ~700 km long Karakoram Fault shows moderate magnitude earthquakes up to crustal depth with dextral strike-slip motion. This Karakoram fault accommodates a large part of strain due to India-Asian collision but surprisingly rarely generates earthquakes of M ≥ 7.0. The absence of earthquakes of M ≥ 7 in the Karakoram Fault Zone poses a vital scientific question that requires knowledge on stress dissipation mechanism. To understand stress dissipation mechanism, a number of studies have been

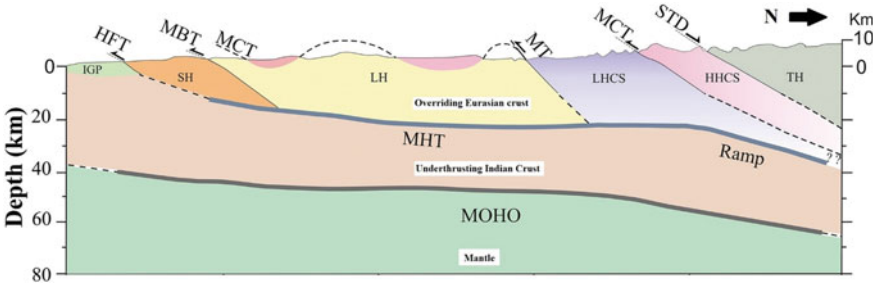

Fig. 2.3 Vertical cross-section across the Satluj Valley showing the merging of thrust sheets (Main Himalayan Thrust-HFT, Main Boundary Thrust-MBT, Main Central Thrust-MCT, Munsiari Thrust-MT, South Tibetan Detachment-STD, etc. with the Main Himalayan Thrust (MHT) (Modified after Hazarika et al. 2017). The MHT shows a ramp beyond the South Tibetan Detachment (STD) in Satluj Valley. The Moho is gradual dipping from south to north

conducted to estimate stress drop. The following section summarizes the observations and corresponding interpretations in the different segments of the Himalaya.

2.3.2 Ladakh Karakoram Zone

The Ladakh Karakoram Trans Himalaya provides a classic example of collision and subduction tectonics through the presence of suture zones (Indus Tsangpo Suture Zone), intra-continental Karakoram Fault (KF) zone, and exhumed blocks such as the Tso-Morari Crystalline (TMC). The TMC exhumation is facilitated by oppositely dipping active boundary faults, Zildat and Karzok. These faults along with the back-thrusting Indus thrust are recognizable active thrusts in the region. Paul and Hazarika (2022) estimated source parameters through spectral analysis of P waves of 51 local earthquake ($1.9 < M_L < 4.3$) data recorded by 10 local broadband seismological stations during 2009–2012 (Fig. 2.4). The study reveals on an average low-stress drop earthquakes in the Ladakh-Karakoram zone. The results show the seismic moment (Mo) within the range of 1.2×10^{12} to 4.3×10^{15} Nm with stress drop values varying from ~0.06 to 64.36 bar. The observation of low-stress drop earthquake has significant implications in explaining seismogenesis in the region. The low-stress drop events in the earthquake cluster of the TMC is explained by the brittle shear failure on the active Zildat and Karzok Faults based on the concept of partial stress drop model (Brune 1970) (see Sect. 2.3.5). According to this model, the complex fault geometry, or asperities on the fault play a significant role. The low-stress drop earthquakes of Karakoram Fault are interpreted as due to the presence of aseismic creeping patches producing low-stress drop earthquakes at the expense of generating large earthquakes. These creeping patches are not able to withstand much stress and release it in the form of micro-earthquakes. Geological studies (e.g. Wallis et al. 2013) investigated the exhumed fault rocks formed in the frictional-viscous transition zone in the KFZ and found evidence of several weakening mechanisms associated with reduced coefficients of friction (<0.4).

2.3.3 The Kangra Earthquake Zone

While the LKZ lies in the Trans Himalaya, the Kangra-Chamba zone lies in the Himalayan fold-thrust belt and was host to the devastating 1905 Kangra earthquake. Most of the earthquakes recorded in the region are $M < 3$ and are mainly confined between MBT and MCT (Sharma and Wason 1994). Alike the LKZ, the seismicity ranges from shallow (~5 km) to deeper (~60 km) crust. The Kangra-Chamba zone exhibits heavy microseismicity distributed in the LH sequence of the previously discussed HSB. The region is highly deformed and the presence of active local faults is also thought to have contributed to the local microseismicity (Fig. 2.5).

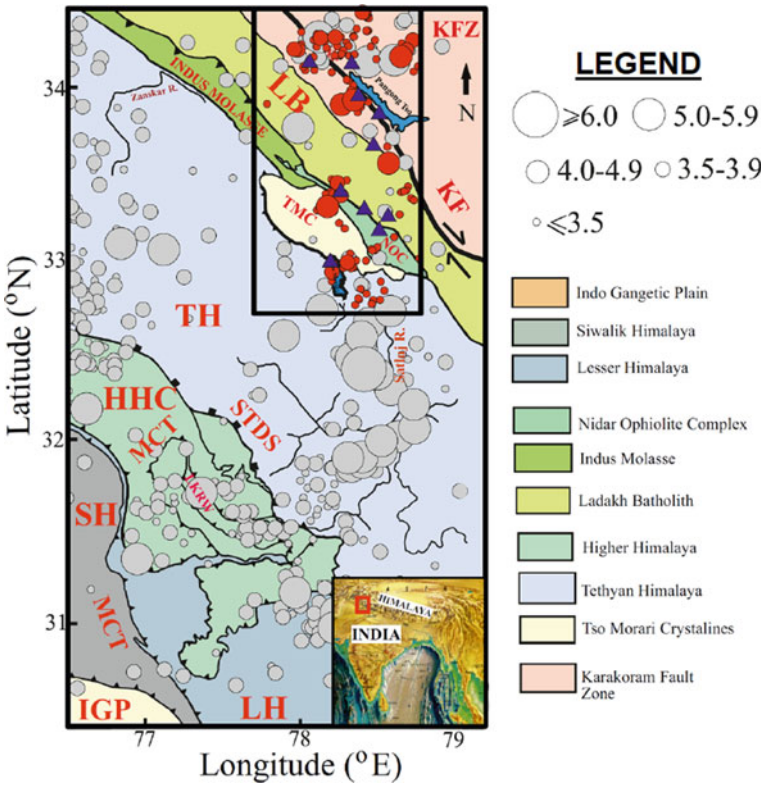

Fig. 2.4 Seismicity map of the LKZ showing the effect of tectonic features and local thrusts (adapted from Paul and Hazarika 2022). The grey and the red circles represent the earthquake epicenters from the reviewed ISC catalog and local study (Hazarika et al. 2017) using broad-band seismological stations shown by blue triangles, respectively. The red circles represent the earthquakes used in source parameter study

Several individual stress drop experiments have been conducted in the vicinity of the Kangra earthquake zone in pockets such as Kishtwar (north-west of the Kangra earthquake zone), Dharamshala, and Bilaspur. The stress drop of reported earthquakes in the Kishtwar zone varies between 5.8 MPa and 13.0 MPa and for the Dharamshala zone between 3.2 MPa and 13.3 MPa (1 bar = 0.1 MPa). The seismic moment of these earthquakes vary between 10^{11} N-m and 10^{16} N-m while the rupture radius is limited between 0.12 and 1.15 km (Sharma et al. 2014). These values are a marked decrease to what is observed in the Ladakh Himalaya. One may argue that the occurrence of a significantly damaging 1905 Kangra earthquake may have drastically reduced the zonal stress. The epicentral zone of the Kangra earthquake zones show intense seismic clustering with stress drop between 10 and 26 bar (Kumar et al. 2013). The adjacent Bilaspur region recorded coincident low- and high-stress drop events ranging between 1 and 51 bars (Kumar et al. 2014). Seismic moments of

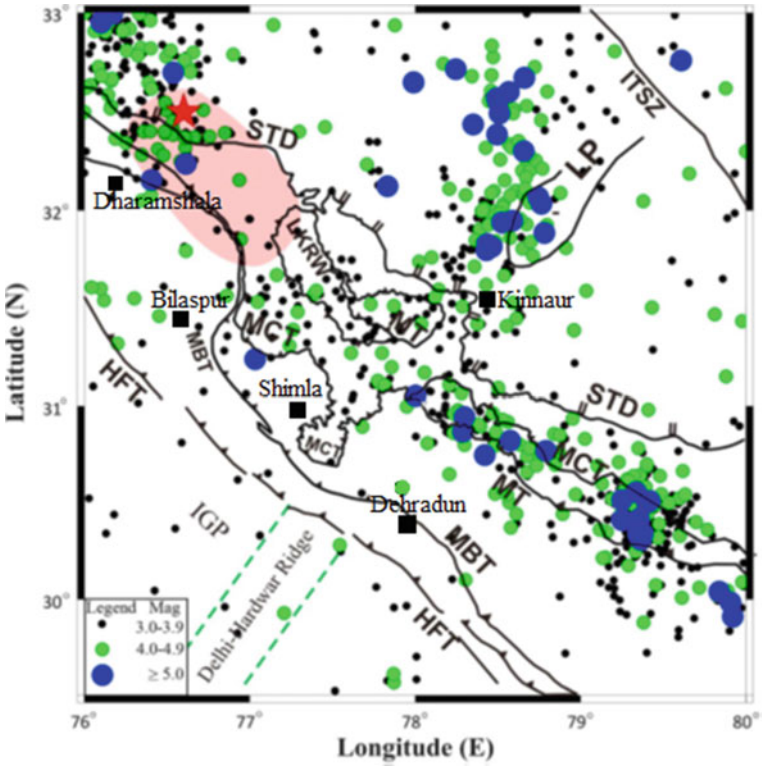

Fig. 2.5 Effect of the Delhi-Hardwar ridge on the seismicity in the vicinity of the 1905 Kangra earthquake zone. The seismicity is for the period of 1960–2015 (*Source* ISC catalog; www.isc.ac.uk) and adapted from Hazarika et al. 2017. The epicenter of 1905 Kangra earthquake and its rupture area is shown by the red star and the shaded area, respectively. The major cities are marked for reference

these events are similar to that in the Kishtwar and vary between 10^{12} and 10^{14} N-m. The source radii of the Bilaspur events are relatively smaller and vary between 187 and 518 m. The Kinnaur region exhibits a diffused seismicity with a northward shift. Kumari et al. (2021) studied the shallow focus microseisms in the Kinnaur and found them to have much lower stress drop (0.03–13 bar) and seismic moment (10^{11}–10^{14}) N-m. This is much low in comparison to the earthquakes in this segment.

2.3.4 The Garhwal and Kumaon Himalaya

The easternmost segment of the NW Himalaya comprises of the Garhwal-Kumaon Himalaya, which is one of the heavily studied segments of the NW Himalaya. This is largely because of its accessibility as well as the occurrence of quite a few recent

notable earthquakes such as the 1991 Uttarkashi, 1999 Chamoli, 2007 Kharsali, and the 2017 Rudraprayag earthquakes. As such, this region has been subjected to seismotectonic and earthquake precursory studies with one of the long-standing multi-parametric observatories in India situated in Ghuttu, Garhwal Himalaya (Shukla et al. 2020). This region has no notable large earthquakes reported over a long period. However, the region has high reported microseismicity, which is credited to the highly brittle crust unable to withstand high seismic stress (Hajra et al. 2022a).

Numerous seismic experiments have been carried out in the Garhwal-Kumaon Himalaya from time to time to study the source characteristics of the local earthquakes (Borkar et al. 2013; Singh et al. 2018; Sivaram et al. 2013; Sharma and Wason 1994). Recent studies such as Hajra et al. (2022b) and Kumari et al. (2021) have carried out an extensive region-wise comparison of these study results over the entire NW Himalaya. Compiled data from different studies carried out in Garhwal-Kumaon show a diverse range of both moment magnitude ($0.8 < Mw < 6.8$) and seismic moment ($10^{10} < Mo < 10^{19}$ N-m). The source radii of the earthquakes in this region vary from 100 m to 13.2 km and the stress drop between 0.01 and 77 bar. Amidst the background of low-stress drop microseisms, there are moderate events in the vicinity of the MHT ramp releasing stress from time to time such as the 1991 Uttarkashi ($M \sim 7$; $\sigma \sim 77$ bar), 1999 Chamoli ($M \sim 6.9$; $\sigma \sim 65$ bar), 2007 Kharsali ($M \sim 4.9$; $\sigma \sim 42$ bar), 2017 Rudraprayag ($M \sim 5.5$; $\sigma \sim 40$ bar) and 2016 Dharchula ($M \sim 5.1$; $\sigma \sim 28$ bar) earthquakes. The upper 10 km of the crust is brittle and inhabited by earthquakes with low-stress drop values between 1 and 10 bar. Beyond 20 km depth, the events are significantly reduced with their σ value decreasing with depth. The mantle shows very few earthquakes and a very low-stress drop. Overall, the region experiences a multitude of low as well as high-stress drop events. Several experiments show that, for the Garhwal Himalaya, the seismic moments vary from 10^{14} to 10^{17} N-m while the source radii vary from 0.4 km to 2.3 km (Kumar et al. 2016). Hajra et al. (2022b) observed that in comparison to Garhwal, earthquakes in the Kumaon Himalaya record lesser value of stress drop and source radii for similar values of seismic moments (Fig. 2.6). This further supports the deformation and incomplete stress dissipation in the Kumaon Himalaya. The stress drop overall is dissimilar for different size of earthquakes suggesting a self-similar nature of earthquake sources (Kumar et al. 2016).

2.3.5 The Complex Stress Picture of the NW Himalaya

Two different models have been postulated to explain the occurrence of low-stress drop events: partial stress drop and low effective stress model (Brune 1970; Brune et al. 1976). The former model considers complex fault geometry or fault barriers. As such, the fault locks soon after the rupture, thereby restricting average slip. This post-earthquake rapid locking in a fault causes low-stress drop as the fault slip cannot reach optimum dynamic stress drop along the entire fault. The latter model attributes low-stress drop events to generating effective stress too low to accelerate the fault.

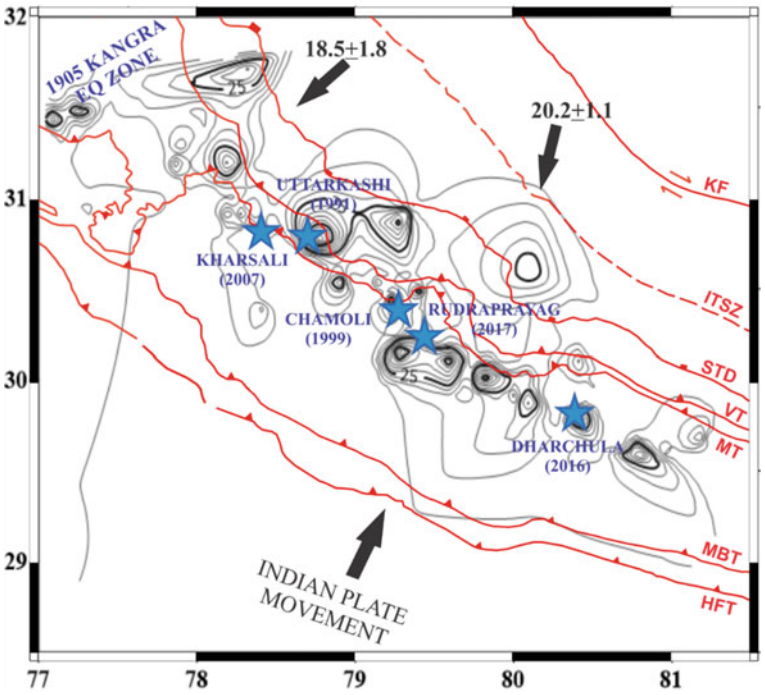

Fig. 2.6 Contour map for 25-year compilation of stress drop for earthquakes in Garhwal-Kumaon Himalaya between 1994 and 2018 (adapted from Hajra et al. 2022b). The notable events during the period have been marked by blue stars. The black arrows at the top represent the zonal convergence rates in mm/year for the NW Himalaya (Stevens and Avouac 2016)

The presence of high pore fluid pressure favors such low effective stress condition. However, this model is not viable as most of the Himalayan segments are highly stressed as observed by GPS studies (Bilham et al. 2001; Stevens and Avouac 2016).

The low-stress drop of shallow events in the TMC Ladakh can be explained by the partial stress drop model caused by complex geometry, asperities and possible presence of creeping patches in the fault zone that are not able to withstand much stress on the associated faults. The microseisms are considered to be point sources and do not represent the entire sizable fault. The average slip in such cases does not reach the total dynamic stress drop of the entire fault surface (Paul and Hazarika 2022). Such fault-weakening mechanisms in the frictional-viscous transition zone of the KF associated with reduced coefficients of friction (<0.4) can promote aseismic creep without generating large earthquakes. Brune's circular model states that the stress drop of earthquakes in a region should be constant irrespective of its size. However, studies in Kangra as well as Garhwal-Kumaon segments Himalaya confirm that the stress drop changes with earthquake size for relatively low magnitude events. For relatively higher-magnitude earthquakes, it appears to follow the Brune's model. This can be explained by the presence of brittle and weak rocks in the upper crust that

hinder stress accumulation. The release of seismic energy is localized close to the major tectonic elements indicating high strains. Hidden faults with stable barriers that are not exposed on the surface are a source of concern. Strain localizations and diffused seismicity in the Satluj Valley are attributed to the arc-perpendicular continuation of ridge structure (Delhi-Hardwar Ridge) into the Himalaya along with the normal Kaurik Chango fault (Arora et al. 2012; Hazarika et al. 2017). Seismic studies have repeatedly emphasized the impact of local structures in the Kangra as well as in the Garhwal Himalaya. Again, the crustal duplex in the Kumaon Himalaya is an indicator of complex strain mechanism. The crustal shortening through the duplex structure involves high wear and tear of the crust subsiding the possibility of accumulating stress in the region. Apart from the role of local structures, the presence of reported intra-crustal fluid is another factor downplaying stress accumulation (Mahesh et al. 2012; Hajra et al. 2021). These rheological implications lead to fault weakening and aseismic slip, which in turn, lead to incomplete stress dissipation.

2.4 Summary and Outlook

The Himalayan orogeny presents mechanisms far more complex than a traditional subduction system with different seismicity patterns and guiding mechanisms in various segments. Large earthquakes in the past have shown the capacity for stress build-up in this part of the crust. However, different inhibiting factors as discussed work against such stress build-up. Occasional moderate to large events have been inadequate in releasing the generated stress. Consequently, with high regional convergence rates, reported slip deficits and strain build-up due to fault locking, the anticipation of future large earthquakes seems natural. Different seismic experiments in the NW Himalaya show incomplete stress dissipation through low-stress drop microseisms. These studies deduce important scaling relations that are in-situ characteristics of the local seismotectonics. These scaling relations provide important contribution to seismic hazard studies. However, these studies have been conducted in pockets of NW Himalaya and a large part of it still remains seismically unexplored. This emphasizes on the need for extensive stress drop analysis to obtain the complete picture for the stress regime. A complete dataset and knowledge in this regard is the only way we can contemplate about prediction/precursory studies countering the possessed seismic risk in the Himalaya.

References

Arora BR, Gahalaut VK, Kumar N (2012) Structural control on along-strike variation in the seismicity of the northwest Himalaya. J Asian Earth Sci 57:15–24

Bilham R, Gaur VK, Molnar P (2001) Himalayan seismic hazard. Science 293(5534):1442–1444

Borkar Y, Kumar A, Gupta SC, Kumar A (2013) Source parameters and scaling relation for local earthquakes in the Garhwal and Kumaun Himalaya, India. Int J Adv Seism 11:1–15

Brune JN (1970) Tectonic stress and seismic shear waves from earthquakes. J Geophy Res 75:4997–5009

Brune JN (1976) The physics of earthquake strong motion. In: Developments in geotechnical engineering, Elsevier, vol 15, pp 141–177

Caldwell WB, Klemperer SL, Lawrence JF, Rai SS, Ashish, (2013) Characterizing the main Himalayan thrust in the Garhwal Himalaya, India with receiver function CCP stacking. Earth Planet Sci Lett 367:15–27

Hajra S, Hazarika D, Bankhwal M, Kundu A, Kumar N (2019) Average crustal thickness and poisson's ratio beneath the kali river valley, Kumaon Himalaya. J Asian Earth Sci 173

Hajra S, Hazarika D, Kumar N, Pal SK, Roy PNS (2021) Seismotectonics and stress perspective of the Kumaun Himalaya: a geophysical evidence of a lesser Himalayan duplex. Tectonophysics 806:228801

Hajra S, Hazarika D, Mondal S, Pal SK, Roy PNS (2022a) Deformation of the upper crust in the Kumaon Himalaya analyzed from seismic anisotropy and gravity lineament studies. Phys Earth Planet Inter 322:106827

Hajra S, Hazarika D, Shukla V, Kundu A, Pant CC (2022b) Stress dissipation and seismic potential in the central seismic gap of the north-west Himalaya. J Asian Earth Sci 239:105432

Hazarika D, Hajra S, Bankhwal M, Verma SK, Yadav DK, Kumar N (2018) Crustal structure beneath multi-parametric geophysical observatory at Ghuttu, Garhwal Himalaya. Him Geol 39(2):233–241

Hazarika D, Hajra S, Kundu A, Bankhwal M, Kumar N, Pant CC (2021) Imaging the Moho and main Himalayan thrust beneath the Kumaon Himalaya: constraints from receiver function analysis. Geophys J Int 224(2):858–870

Hazarika D, Wadhawan M, Paul A, Kumar N, Borah K (2017) Geometry of the main Himalayan thrust and Moho beneath Satluj valley, northwest Himalaya: constraints from receiver function analysis. J Geophy Res Sol Earth 122(4):2929–2945

Keilis-Borok VI, (1960) Investigation of the mechanism of earthquakes. Sov. Res. Geophys 4:29

Khattri KN (1999) Probabilities of occurrence of great earthquakes in the Himalaya. Proc Indian Acad Sci - Earth Planet Sci Lett 108(2): 87–92

Kumar V, Kumar D, Chopra S (2016) Estimation of source parameters and scaling relations for moderate size earthquakes in North-West Himalaya. J Asian Earth Sci 128:79–89

Kumar N, Yadav DK, Mondal SK, Roy PNS (2013) Stress drop and its relation to tectonic and structural elements for the meizoseismal region of great 1905 Kangra earthquake of the NW Himalaya. Nat Haz 69:2021–2038

Kumar A, Kumar A, Gupta SC, Jindal AK, Ghangas V (2014) Seismicity and source parameters of local earthquakes in Bilaspur region of Himachal lesser Himalaya. Arabian J Geosci 7(6):2257–2267

Kumari R, Kumar P, Kumar N (2021) Implications of site effects and attenuation properties for estimation of earthquake source characteristics in Kinnaur Himalaya, India. Pure Appl Geophys 178(11):4345–4366

Mahesh P, Gupta S, Rai SS, Sarma PR (2012) Fluid driven earthquakes in Chamoli region, Garhwal Himalaya: evidence from local earthquake tomography. Geophys J Int 191:1295–1304

Pandey MR, Tandukar RP, Avouac JP, Vergne J, H´eritier T (1999) Seismotectonics of the Nepal Himalaya from a local seismic network. J Asian Earth Sci 17: 703–712

Parshad R, Snehmani RR, Ghangas V, Kumar A, Rana V, Joshi P, Shrivastva PK, Ganju A (2014) Source parameters of local earthquakes in Nubra region, NW Himalaya. Int J Adv Res 2(8): 151–158

Paul A, Hazarika D (2022) Occurrences of low-stress drop earthquakes in the eastern Ladakh-Karakoram zone of the Trans Himalaya and their tectonic implications. J Asian Earth Sci X 7: 100080

Singh R, Paul A, Kumar A, Kumar P, Sundriyal YP (2018) Estimation and applicability of attenuation characteristics for source parameters and scaling relations in the Garhwal Kumaun Himalaya region, India. J Asian Earth Sci 159:42–59

Sivaram K, Kumar D, Teotia SS, Rai SS, Prakasam KS (2013) Source parameters and scaling relations for small earthquakes in Kumaun Himalaya, India. J Seism 17:579–592

Stevens VL, Avouac JP (2016) Millenary Mw> 9.0 earthquakes required by geodetic strain in the Himalaya. Geophy Res Lett 433:1118–1123

Sharma S, Dasgupta A, Kumar A, Bharanidharan B, Mittal H, Sachdeva R (2014) Earthquake activity in Kishtwar-Dharamshala region of north-west Himalaya. Int J 2(8):463–470

Sharma ML, Wason HR (1994) Occurrence of low stress drop earthquakes in the Garhwal Himalaya region. Phys Earth Planet Inter 85:265–272

Shukla V, Chauhan V, Kumar N, Hazarika D (2020) Assessment of Rn-222 continuous time series for the identification of anomalous changes during moderate earthquakes of the Garhwal Himalaya. Appl Rad Iso 166:109327

Wallis D, Phillips RJ, Lloyd GE (2013) Fault weakening across the frictional-viscous transition zone, Karakoram Fault Zone, NW Himalaya. Tectonics 32:1227–1246

Chapter 3
The Crust and Upper Mantle Structure Beneath the Bangladesh and Its Effects on Seismic Hazard

Ritima Das, Utpal Saikia, and Gokul Kumar Saha

Abstract Bangladesh is one of the most densely populated and seismically active region of the world, which is situated on the easternmost part of the India-Eurasia collision zone. It lies at the junction of the three plates—the Indian plate, the Eurasian plate and the Burma plate. With a population over 160 million, the nation Bangladesh is located on a seismically active fold and thrust belt that forms the updip point of an active, oblique subduction zone plunging to the east beneath Myanmar on the eastern edge of the India-Eurasia collision zone. Approximately 15–20 km of sediments have been deposited here during past 55 million years. The process of sedimentation continues till today as the rivers Brahmaputra, Ganges and Meghna flow across the nation Bangladesh and formed the Ganges–Brahmaputra Delta (GBD), the largest delta in the world. The region is mainly an accretionary prism made up mostly of sediments from the cretaceous to the Eocene. Its location on the largest river delta in the world and proximity to the sea puts it at risk for tsunamis and the potential for rivers to overflow their banks in the case of an earthquake. Due to a scarcity of seismic data from Bangladesh, it is still difficult to comprehend the structure of the Bengal Basin and the tectonic forces, which are main sources of its deformation. Understanding the structure beneath Bangladesh is one of the important aspects in order to evaluate its vulnerability towards the earthquake hazard scenario. This study will present an improved 3-D shear wave velocity image of the crust and uppermost mantle beneath Bangladesh region. The shear velocities are obtained from the joint inversion of the receiver function and fundamental mode Rayleigh wave group velocities, which are calculated from the cross-correlation of ambient noise as well as earthquake seismogram. Our findings show that the crust and the

R. Das (✉)
Department of Earth Sciences, Pondicherry University, Pondicherry 605014, India
e-mail: ritima08@pondiuni.ac.in

U. Saikia
Department of Earth & Climate Science, Indian Institute of Science Education and Research- Tirupati, Tirupati 517507, India

G. K. Saha
Department of Earth and Climate Science, Indian Institute of Science Education and Research- Pune, Dr.Homi Bhabha Road, Pune 411008, India

Sandeep et al. (eds.), *Geohazards*, Advances in Natural and Technological Hazards Research 53, https://doi.org/10.1007/978-981-99-3955-8_3

upper mantle structure beneath Bangladesh region is highly varying. The shear wave velocities of the sediments have been observed up to a depth of ~15 km. We can clearly see the subduction pattern in terms of the velocity along the east–west profile from the Indian craton across the Ganga Brahmaputra Delta (GBD) underthrusting the Burma arc of south eastern Asian plate. The findings help us to understand the particular episode of subduction by placing important restrictions on the sedimentary and lithospheric features throughout the system.

Keywords Bangladesh · Bengal Basin · Velocity structure · Earthquake · Seismic hazard

3.1 Introduction

Bangladesh is seismically active due to the ongoing India-Asia collision to the north and the Indo-Burmese subduction to the east. It is surrounded by the Shillong Plateau in the north, Indo-Burma ranges in the east, Indian shield in the west and the Indian Ocean in the south. The rivers Brahmaputra, Ganges and Meghna run across the Bangladesh and form the largest delta in the world: The Ganga–Brahmaputra delta in the south of the nation Bangladesh. In the last 55 million years, for about 15–24 km of sediments have been deposited here (Curray 1994; Maurin and Rangin 2009; Singh et al. 2016). The Shillong Plateau is moving southward to the north at the intersection of the Himalaya and Burma Arcs and may signal the start of the Himalaya's forward jump. The Shillong Plateau has a history of vertical uplift dating back to the Cretaceous and is distinguished by a significant positive E-W trending isostatic anomaly. This is due to regional tectonic stresses from the Himalayan collision zone to the north and the Indo-Burma subduction zone to the east (Verma and Mukhopadhyay 1977). Bangladesh has a population of more than 160 million and is situated on a seismically active fold and thrust belt that serves as the updip point of an active, oblique subduction zone that plunges beneath Myanmar on the eastern side of the India-Eurasia collision zone. During the year 1869–1930, five earthquakes of big magnitude earthquakes (Cachar earthquake; 1869, m = 7.5; Bengal Earthquake 1885, m = 7.0; Great Indian earthquake 1897, m = 8.7; Srimongal earthquake, 1918, m = 7.6; (m: magnitudes in Richter scale) Dhubri Earthquake, 1930, $m_s = 7.1$) (Akhter 2010; USGS catalogue) had been occurred in the surroundings of Bangladesh (Fig. 3.1), which had major affects in the region. All these earthquakes took place within 250 km distance from the city Dhaka of Bangladesh. Recently on April 28, 2021, another earthquake of magnitude $m_w = 6.1$ (USGS catalogue) had been occurred in the Kapili fault of Assam which also affected the region. There are also records of moderate magnitude earthquakes (Fig. 3.1), which occurred in Bangladesh and affected the country. Few among them are May 1997 Sylhet earthquake (m = 5.6), November 1997 Myanmar border earthquake ($m_w = 6.1$) July 1999

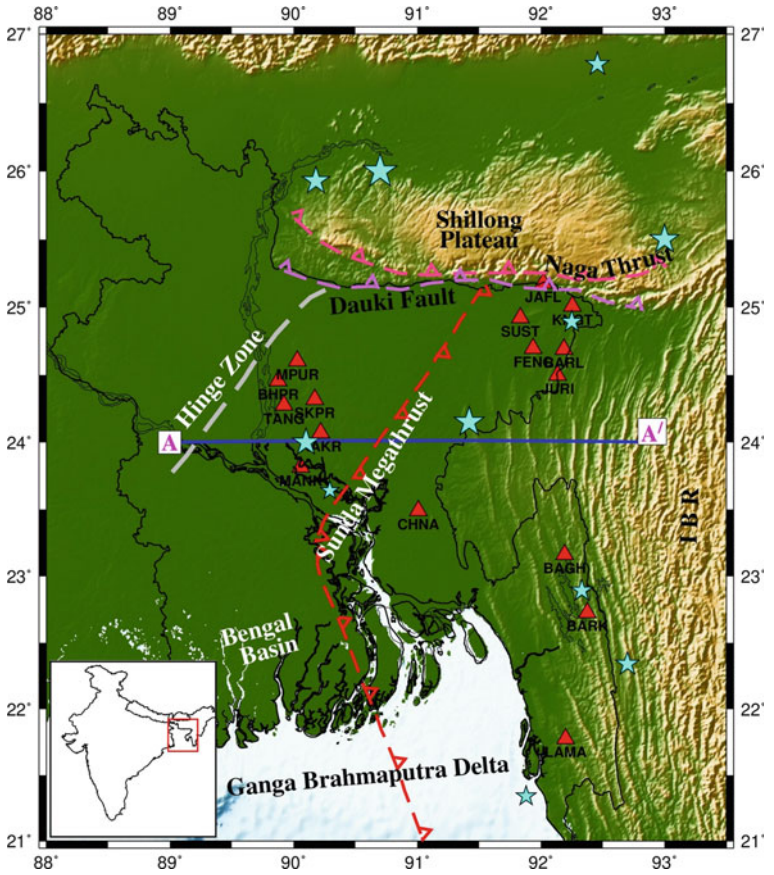

Fig. 3.1 Tectonic map of Bangladesh and its surrounding region. Red triangles are the seismic stations whose data are used for the study. The faults are marked with the dashed lines. Cyan colour stars are the earthquakes (as described in the text) which had major effects on the Bangladesh area. The size of the stars varies according to the magnitude of the earthquake

Moheshkhali Island earthquake (m = 5.1), December 2001 Dhaka city earthquake (m = 4.5), July 2003 Rangamati earthquake ($m_w = 5.7$) (Akhter 2010; USGS catalogue). All these earthquakes resulted in loss of lives, collapse of the buildings and mud-walled houses, serious damage to the cyclone shelter column, brick masonry buildings etc. Despite having the spare records of these earthquakes, the 12–24 mm/year of convergent strain accumulation along with ~8 mm/year of dextral shear beneath the Indo–Burman Ranges (Mallick et al. 2019) show the presence of seismic hazard in the region. A clear understanding of the internal structure of the Earth beneath the region is necessary for properly analysing this risk. The regional-scale seismic velocity structure beneath Bangladesh remains enigmatic despite the region's complicated geology context and high degree of seismic hazards, largely because there are not sufficient local or regional seismic waveform measurements. In order to

better describe the structural settings beneath Bangladesh, we have performed a joint inversion scheme to acquire the shear wave velocity structure beneath the region.

3.2 Geological Background

Bangladesh that shares the geology of the Bengal Basin is situated in the northeastern region of the Indian Subcontinent, between the Indo-Myanmar Ranges to the east and the Indian Shield to the west. The region is encircled in the north with the Himalayan Foredeep, the Shillong Plateau and the Assam Basin (Roy and Chatterjee 2015; Najman et al. 2016). The south of the basin is opened into the Bengal Fan (Najman et al. 2012). Over the last 55 million years around ~15–20 km of sediments has been deposited by the Ganges–Brahmaputra and the Meghna Rivers which flows through the region and formed the largest delta in the world: the Ganges–Brahmaputra Delta (Alam 1989; Steckler et al. 2008; Singh et al. 2016). This delta is constructed with the deposition of fluvial and delta-plain sediments, including the Tipam Sandstone and Dupi Tila Formation (Johnson and Alam 1991). The source of these sediments is mainly drained from the world's largest orogenic system, the Himalayan Range, the closest areas like Shillong Plateau and the Chittagong-Myanmar fold and thrust belt (CMFB). These sediments created a massive sediment accumulation that is currently approaching the Indo-Myanmar Arc subduction zone by advancing the continental margin of the Indian subcontinent by about 400 km (Steckler et al. 2008). The Chittagong-Myanmar fold and thrust belt (CMFB) is a 250 km wide extend in the eastern part of Bangladesh. Over a horizontal distance of 250 km, the height of the CMFB steadily rises from west to east. It begins close to sea level and rises approximately 1,500 m within the Indo-Burman Ranges. Both the Shillong Plateau and the CFMB began to uplift during the end of Miocene, which is around ~5–8 Ma (Johnson and Alam 1991; Alam et al. 2003). The Shillong Plateau is a large, 2-km-high elevated area that is bordered to the south by the steeply descending, deeply ingrained Dauki fault (Johnson and Alam 1991). The GBD is located close to the syntaxis of the Himalayan and Burma arcs, two plate-convergence borders. The Indian plate is overridden by these arcs from the north and the east, which are convex in the direction of the Indian plate. With its large extending foredeeps and thrust-fold belts, India serves as the foreland of both the Himalayan and Burmese convergent borders. Since the Eocene, continents have been colliding along the Himalayan arc. As the Himalayan collision moved forward, it encircled Assam syntaxis and moved down the Burma Arc from north to south (Lee and Lawver 1995; Uddin and Lundberg 1999). The Himalayan and Burmese arc foredeeps show how the lithosphere beneath the subducting plates bent under their weight (Le Dain et al. 1984). On the eastern side of the GBD, the Burma Arc exhibits all the signs of a subduction zone, including a volcanic belt on the Burma overriding platelet up to 25° N, the latitude of the Shillong Plateau (Steckler et al. 2008).

3.3 Seismological Approach for Mapping the Internal Structure Beneath Bangladesh

We have used the method of joint inversion (Julia et al. 2000) of the Rayleigh wave group velocity dispersion along with the receiver functions for the construction of the models. For the surface wave dispersion, we have extracted the values from the surface wave tomography for the entire south Asia using ambient noise and earthquake (Saha et al. 2020, 2021). The receiver functions are constructed from the teleseismic earthquakes recorded in the stations as shown in Fig. 3.1.

3.3.1 Data

In this study, we have used seismic data collected from 16 broadband seismic stations in and around Bangladesh. The data are downloaded from the IU, XI and Z6 network of Incorporated Institutions for Seismology (IRIS) database (Fig. 3.1). The data from the seismograph deployed during 2008–2010 have been used for this study. This data collection was utilised for the construction of the receiver functions. We have used a total of 257 good receiver functions computed from the 16 seismic stations data for this study. We have retrieved the surface wave dispersion values from the entire south Asia using ambient noise and earthquake (Saha et al. 2020, 2021).

3.3.2 Surface Wave Dispersion

For the calculation of group velocity dispersion, we have used the method of multiple filter technique (MFT) developed by Dziewonski et al. (1969), which is later improved by Herrmann (1973), Bhattacharya (1983), Herrmann and Ammon (2004). Both the cross-correlation of data on ambient noise and the data on earthquakes have been used to compute the group velocity dispersions. The continuous vertical component seismograms are used to compute the cross-correlation (Bensen et al. 2008). A total of 18,552 paths recorded at 683 seismic stations have been used to calculate the cross-correlation of the ambient noise. The cross-correlated functions obtained for each pair of stations are then averaged to generate a symmetric signal and stacked to improve the signal to noise ratio (SNR). For the final selection of the data, we have used only those cross-correlation functions whose SNR is greater than 15 and interstation separation is equal to or >3 times the wavelength (Lin et al. 2008). The group velocities were then determined by applying the multiple filter taper analysis to each noise correlation function. After that, from the 417 earthquakes (with magnitude > 5.5) recorded at 209 seismic sites, we included group velocities along 3048 pathways across the area. We have selected regional earthquakes with depths ranging from 10 to 95 km that occurred between 15° S and 40° N and 31° to

130° E. The details of the data are published in Saha et al. (2020, 2021). We could able to construct the 2D group velocity maps from 5 to 70 s period averaged for every 1° x 1° of the study region by using the methodology of Barmin et al. (2001). Saha et al. (2021) give a detailed presentation of the method applied to these sets of data. The resolution test was carried out by creating synthetic data for every checkerboard model in a set that represents the group velocity structures of an imaginary Earth's group velocity structure, computing a solution model using the synthetic data, and comparing the solution velocity models to the synthetic earth models. The resolution of the ray paths used for this analysis for a given time period can be estimated by the distinctness with which the original pattern is reproduced in the inverted model. The cell size of $1^\circ \times 1^\circ$ provides the maximum resolution of the data used in this study from 5 to 70 s period in the study region. Thus, we could get the fundamental mode Rayleigh wave group velocity maps which are well resolved at $1^\circ \times 1^\circ$ by the data used in this study from 5 to 70 s period. The Rayleigh wave group velocities are measured for different frequencies. These frequencies are sensitive to different depths inside the Earth. For a layered Earth model, we can show the relationship between the Rayleigh wave group velocity measurements at different frequencies to the different depth in the Earth by means of the sensitivity kernel. The depth sensitivity increases with the increasing time periods. The 5 s period is sensitive to 5–10 km depth and with increasing time period the depth sensitivity increases to a sensitivity of 70 s period to about 130 km depth. The sensitivity kernel gets more flat with increasing time period, which implies of the larger depth averaging. Saha et al. (2021) show the depth sensitivity kernel of the fundamental mode Rayleigh wave group velocities at different time periods for this study region.

3.3.3 Receiver Function Analysis

The receiver function (RF) is a routinely used method to extract the information of the interior of the Earth. Here, we have used the iterative deconvolution algorithm (Ligorría and Ammon 1999) in time domain for computing the RFs. The RFs are computed with Gaussian width 1.6, which corresponds to the frequency ~0.8 Hz. We have selected the earthquake data recorded for the epicentral distance 30° to 95° and with magnitude greater than 5.5 for the computation of the RFs. The use of the aforementioned distance ranges aids in preventing both complications at a distance larger than 95° brought on by the core-mantle boundary and multiple arrivals in the direct P-wave. Only those seismograms that have a clear P arrival are used which are filtered using a Butterworth high pass filter with a corner frequency of 0.02 Hz after being visually examined corresponding with these events. Using the Taup-Tool-kit (Crotwell et al. 1999), the P arrival on the seismogram is marked in relation to the IASP91 velocity model (Kennett and Engdahl 1991). In order to extract the radial and transverse components, the three component waveforms are then rotated into a great circle and cut 30 s before and 120 s after the predicted P onset. Then by iteratively deconvolving radial components from vertical components in the time domain, these

data are used to construct the receiver functions (Ligorra and Ammon 1999). For further analysis, we have kept only those RFs whose signal to noise ratio (SNR) is greater than 10 and the convolution misfit of the radial component signal power is greater than 80%. The SNR of the receiver function is evaluated using a least squares misfit approach on the original radial waveform. In the misfit criteria, original radial waveform is compared with newly constructed radial waveform.

3.3.4 *Joint Inversion of Surface Wave Dispersion and Receiver Function*

We have used the iterative linearised damped least square method by Julia et al. (2000) for the inversion. For this, we have jointly inverted the surface wave dispersion along with the receiver function to obtain the shear wave velocity structure beneath Bangladesh. The surface wave is sensitive to the absolute S-wave velocity at depth and receiver functions provide constraints on velocity contrast. Through their joint inversion, the complimentary properties of the two datasets are utilised to create a better velocity image (Julia et al. 2000; Bodin et al. 2012). The method states to minimise the following function S

$$S = \frac{1-p}{N_r}\sum_{i=0}^{N_r}\left(\frac{O_{ri}-P_{ri}}{\sigma_{ri}}\right)^2 + \frac{p}{N_s}\sum_{j=0}^{N_s}\left(\frac{O_{sj}-P_{sj}}{\sigma_{sj}}\right)^2$$

where, N_r: Total number of receiver functions.

N_s: Total number of surface wave dispersion.

O_{ri}: Observed receiver function at time t_i.

P_{ri}: Predicted receiver functions at time t_i.

O_{sj}: jth observed surface wave dispersion.

P_{sj}: jth predicted surface wave dispersion.

σ_{ri}: the standard errors in receiver function data set.

σ_{sj}: the standard errors in surface wave dispersion data set.

The influence parameter, or factor p, is an a priori value that modifies the impact of either data set on the minimisation process. The p's value ranges from 0 to 1. We set p to 0.5, which gives the receiver function and dispersion curve fits equal weight. For the initial velocity model, we have considered a half space model with shear wave velocity 4.5 km/s (Vp/Vs = 1.73 and density = 3.3 g/cc) up to a depth of 130 km. We generated the mean dispersion data in a 1° circular bin centred around the station using group velocity maps for the period of 5–70 s. Inversion of the averaged dispersion data is done along with each station's estimated stacked receiver function. The inversion has been performed for all the station of the region. With reference to (Christensen 1996; Rudnick and Gao 2013), the resulting velocity is described

as the upper crust having a corresponding shear velocity of 2.8–3.5 km/s, middle crust having a corresponding shear velocity of 3.5–3.8 km/s, and lower crust having a corresponding shear velocity of 3.8–4.1 km/s.

3.4 Seismic Hazard Scenario and the Velocity Structure Beneath Bangladesh

Tectonic strain can build up within and around the geological structures of Bangladesh. In the past, these structures have released enough energy to cause destructive earthquakes. The great Indian earthquake (1897, m = 8.7) that occurred due to the vertical displacement of the Dauki fault located in the northernmost part of Bangladesh caused an extraordinary shaking of the ground. The Shillong Plateau got pop-up by roughly 20 m in just a few seconds as a result of the earthquake, and debris was blasted miles away from the epicentre. On January 26, 2001, a comparable powerful and exceptional earthquake with a magnitude of 7.5 struck Bhuj, which destroyed major urban areas in Gujarat and took the life of around 25,000 people. Such type of earthquakes is rare but the edges of the Indian peninsula could be severely damaged by this kind of earthquake. Bangladesh is located in the eastern extremity of the Indian peninsula and Kutch Basin located in the western extremity is a mirror image of the Bengal Basin. The eastern and western extremities of the regional geological structures from south to north postulate a geometrical symmetry that would be amenable to identical tectonic behaviour in terms of stress distribution. Keeping this in mind in light of its geological makeup, Bangladesh might be susceptible to large earthquakes. In the easternmost part of Bangladesh, the two tectonic plates (India Eurasia collision) have created a large, nearly flat earthquake-producing fault, which has an estimated seismic potential of Mw 8.2–9.0 earthquake (Steckler et al. 2016; Bürgi et al. 2021). This megathrust underlies the land surface on which over 160 million people reside. In some cases, barely 5 km separate occupied areas from the shallowest part of the megathrust (Bürgi et al. 2021). Bangladesh and the neighbouring nations (India and Myanmar) would suffer terrible consequences from a big earthquake on this system. The dense distribution of the population in the region makes it more vulnerable in terms of the seismic hazard scenario. The 2015 Gorkha Nepal earthquake (M = 7.8) is one of such recent evidence, which demonstrate how bad its impact when an earthquake of such magnitude occurred in densely populated area. It illustrated the serious danger that powerful seismic events pose to society and emphasised the requirement for efficient measures to reduce the risk of earthquakes. Bürgi et al. (2021) mapped the geometry of the decollement below the eastern Bangladesh, which is ~9 km deep in northeast and southeast Bangladesh, but shallow ~5 km in the central-east part with an area of about ~150 × 450 km, which is capable of producing an 8.5 magnitude earthquake. Their study hypothesised that the heavier sediment loads in north and south Bangladesh have twisted the décollement and weighed down the earth's surface. The massive sediment deposit in Bangladesh

is also one of the peculiar reasons of chances of occurring a high-magnitude earthquake. According to recent research, the biggest earthquakes occur in subduction zones with deep sediment deposits (Oleskevich et al. 1999; Heuret et al. 2012).

Most of the previous geophysical studies do not contribute much to the crustal structure beneath the Bengal Basin. Many of the studies are either on the north or further northeast of the Shillong plateau. Regarding the composition of the crust that lies beneath the northern Bay of Bengal, two contrasting viewpoints are prevalent. The Rajmahal and Sylhet Traps lie beneath the onshore Bengal Basin, and the continent-ocean boundary (COB) that runs along that line shows the presence of oceanic crust close to the Bangladesh border (Talwani et al. 2016, 2017; Ismaiel et al. 2019). In contrast, the velocity structure of the northern Bay of Bengal from 19° N to 25° N of the Shillong Plateau (Sibuet et al. 2016, 2017) is suggestive of the continental crust that has thinned to a thickness of approximately 10–20 km due to the insertion of volcanic material in the form of sills and seaward-dipping reflectors (SDRs). In the Sylhet Basin, a continental basin located immediately south of the Shillong Plateau (Johnson and Nur Alam 1991), a thinned continental crust was detected onshore Bangladesh (Kaila et al. 1992) and reached a thickness of 30 km south of the Shillong Plateau (Mitra et al. 2006). Singh et al. (2016) observed thinner crust under the Bengal Basin, and the Shilling Plateau and Bengal Basin show no discernible lateral changes from north to south. They calculated the sedimentary thickness varying from ~3 km to ~17 km across Hinge zone using receiver function modelling. They also reported a thickened crust in the deep Bengal Basin, which is 16–19 km thick with higher velocity might be due to the Kerguelen plume, which was active close to the boundary at the period of rifting. Their study finds similar Moho depth under the Shillong plateau and the Bengal Basin. All the above studies are unable to give a clear picture beneath the Bangladesh, which is essential in order to understand the complete hazard scenario of the region. The location of the ocean/continent boundary is also unknown, despite the fact that the large sediment thickness suggests a thin crust. In order to better understand the variation of velocity anomalies as a function of depth, we have plotted the shear wave velocity obtained from our study of joint inversion of surface wave dispersion with the receiver function along a profile at 24° N latitude from west to east of Bangladesh (Fig. 3.2). The velocity profile shows a clear gradual increase of the sedimentary thickness ~5 km to ~18 km from west to east in Bangladesh. A comparatively high velocity crust has been observed beneath the Bangladesh region. We can observe the subducting structure from west to east at ~45 km depth. This is at the Indo Burma subduction zone where we can observe the high sedimentary deposits of around ~20 km. A large accretionary prism has grown due to subduction of the 20 km thick sediment prism (Steckler et al. 2008). The Bengal Basin is obliquely overthrust from the east by the Indo-Burmese subduction zone. The earthquakes that occurred during last 21 years from 2000 to 2021 in the region are also projected along the velocity profile (Fig. 3.2). The pattern of the earthquake occurrences clearly depicts the subduction structure beneath the region. This clearly shows the vulnerability of the region towards the occurrence of the earthquake. Overall, this study provides significant constraints on the sedimentary and lithospheric features present throughout the system, which aids

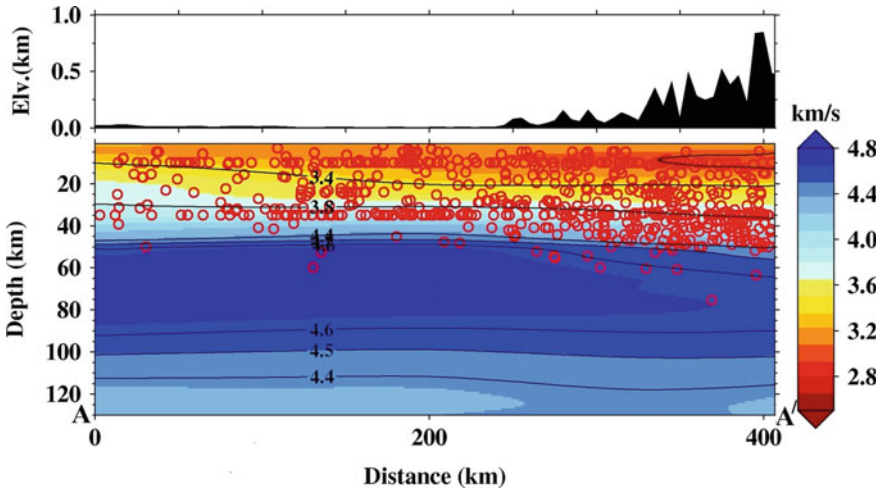

Fig. 3.2 Absolute shear wave velocity variation in the vertical cross-sections along the profile at 24° N (Fig. 3.1). The earthquakes that occurred are projected along the profile. The information of the earthquakes are taken from the catalogue by International Seismological Centre (ISC) (http://www.isc.ac.uk/iscbulletin/search/catalogue/)

in our understanding of the specific event of subduction. Further investigation will be carried out to map the comprehensive structure beneath the entire Bengal Basin along with the Shillong Plateau.

Acknowledgements We thank Dr. Himanshu Mittal and other editorial board for inviting to write the book chapter. A special thanks to the editor Dr. Praveen Kumar and two anonymous reviewers for the constructive comments on improving the chapter. The dataset (which is open to all) used for the study is provided by the IRIS DMC. We have processed the data using Seismic Analysis Code (SAC) and figures are plotted using Generic Mapping Tools (GMT) (Wessel and Smith 1998). The joint inversion has been performed using the computer programs in seismology by Robert Herrmann (http://www.eas.slu.edu/eqc/eqc_cps/CPS/CPS330.html).

References

Akhter SH (2010) Earthquakes of Dhaka. In: Islam MA (ed) Environment of capital Dhaka—plants wildlife gardens parks air water and earthquake celebration series. Asiatic Society of Bangladesh, pp 401–426

Alam M (1989) Geology and depositional history of Cenozoic sediments of the Bengal Basin of Bangladesh. Palaeogeogr., Palaeoclimetol. Palaeoecol 69:125–139

Alam M, Alam M, Curray JR, Chowdhury MR, Gani M (2003) An Overview of the sed-imentary geology of the Bengal Basin in Relation to the Regional Tectonic Framework and Basin-fill History. Sedi. Geology. Sediment Geol Bengal Basin Bangladesh Relat Asia-Greater India Collision Evolut East Bay Bengal 155:179–208. https://doi.org/10.1016/S0037-0738(02)00180-X

Barmin MP, Ritzwoller MH, Levshin AL (2001) A fast and reliable method for surface wave tomography. Pure Appl Geophys 158:1351–1375

Bensen GD, Ritzwoller MH, Shapiro NM (2008) Broadband ambient noise surface wave tomography across the United States. J Geophys Res Solid Earth 113(B5)

Bhattacharya SN (1983) Higher order accuracy in multiple filter techniques. Bull Seismol Soc Am 73:1395–1406

Bodin T, Sambridge M, Tkalćić H, Arroucau P, Gallagher K, Rawlinson N (2012) Transdimensional inversion of receiver functions and surface wave dispersion. J Geophys Res Solid Earth 117(2). https://doi.org/10.1029/2011JB008560

Bürgi P, Hubbard J, Akhter SH, Peterson DE (2021) Geometry of the décollement below eastern Bangladesh and implications for seismic hazard. J Geophys Res Solid Earth 126:e2020JB021519. https://doi.org/10.1029/2020JB021519

Christensen NI (1996) Poisson's ratio and crustal seismology. J Geophys Res 101(B2):3139. https://doi.org/10.1029/95JB03446

Crotwell HP, Owens TJ, Ritsema J (1999) The TauP toolkit: flexible seismic travel- time and ray-path utilities. Seismol Res Lett 70(2):154–160. https://doi.org/10.1785/gssrl.70.2.154

Curray JR (1994) Sediment volume and mass beneath the Bay of Bengal. Earth Planet Sci Lett 125(1–4):371–383

Dziewonski A, Bloch S, Landisman M (1969) A technique for the analysis of transient seismic signals. Bull Seismol Soc Am 59(1):427–444

Herrmann RB (1973) Some aspects of band-pass filtering of surface waves. Bull Seismol Soc Am 63(2):663–671

Herrmann RB, Ammon CJ (2004) Surface waves, receiver functions and crustal structure. Comput Prog Seismol Version 3.30. Saint Louis University

Heuret A, Conrad CP, Funiciello F, Lallemand S, Sandri L (2012) Relation between subduction megathrust earthquakes, trench sediment thickness and upper plate strain. Geophys Res Lett 39:L05304

Ismaiel M, Krishna KS, Srinivas K, Mishra J, Saha D (2019) Crustal architecture and moho topography beneath the eastern Indian and Bangladesh margins–new insights on rift evolution and the continent-ocean boundary. J Geol Soc 176:553–573

Johnson SY, Nur Alam AM (1991) Sedimentation and tectonics of the Sylhet trough, Bangladesh. Geol Soc Am Bill 103:1513–1527. https://doi.org/10.1130/0016-7606(1991)103b1513:SATOTSN2.3.CO;2

Julia J, Ammon CJ, Herrmann RB, Correig AM (2000) Joint inversion of receiver function and surface wave dispersion observations. Geophys J Int 143(1):99–112

Kaila KL, Reddy PR, Mall DM, Venkateswarlu N, Krishna VG, Prasad ASSSRS (1992) Crustal structure of the West Bengal basin, India, from deep seismic sounding investigations. Geophys J Int 111:45e66. https://doi.org/10.1111/j.1365-246X.1992.tb00554.x

Kennett B, Engdahl E (1991) Travel times for global earthquake location and phase identification. Geophys J Int 105429–105465

Le Dain AY, Tapponnier P, Molnar P (1984) Active faulting and tectonics of Burma and surrounding regions. J Geophys Res 89:453–472

Lee TT, Lawver LA (1995) Cenozoic plate reconstruction of Southeast Asia. Tectonophysics 251:85–138

Ligorría JP, Ammon CJ (1999) Iterative deconvolution and receiver-function estimation. Bull Seismol Soc Am 89(5):1395–1400

Lin F, Moschetti MP, Ritzwoller MH (2008) Surface wave tomography of the western United States from ambient seismic noise: Rayleigh and love wave phase velocity maps. Geophys J Int 173:281–298

Mallick R, Lindsey EO, Feng L, Hubbard J, Banerjee P, Hill EM (2019) Active convergence of the India-Burma-Sun- da plates revealed by a new continuous GPS network. J Geophys Res Solid Earth 124:3155–3171. https://doi.org/10.1029/2018JB016480

Maurin T, Rangin C (2009) Structure and kinematics of the Indo-Burmese wedge: recent and fast growth of the outer wedge. Tectonics 28:TC2010. https://doi.org/10.1029/2008TC002276
Mitra S, Priestley K, Gaur VK, Rai SS (2006) Shear-wave structure of the south Indian lithosphere from Rayleigh wave phase-velocity measurements. Bull Seismol Soc Am 96:1551–1559
Najman Y, Allen R, Willett EAF, Carter A, Barfod D, Garzanti E, Wijbrans J, Bickle MJ, Vezzoli G, Ando S, Oliver G, Uddin MJ (2012) The record of himalayan erosion preserved in the sedimentary rocks of the Hatia trough of the Bengal Basin and the Chittagong Hill Tracts, Bangladesh. Basin Res 24:499–519
Najman Y, Bracciali L, Parrish RR, Chisty E, Copley A (2016) Evolving strain partitioning in the eastern Himalaya: the growth of the Shillong plateau. Earth Planet Sci Lett 433:1–9. https://doi.org/10.1016/j.epsl.2015.10.017
Oleskevich DA, Hyndman RD, Wang K (1999) The updip and downdip limits to great subduction earthquakes: thermal and structural models of Cascadia, south Alaska, SW Japan, and Chile. J Geophys Res 104:14965–14991
Roy AB, Chatterjee A (2015) Tectonic framework and evolutionary history of Bay of Bengal Basin in the Indian subcontinent. Curr Sci 109:271–279
Rudnick RL, Gao S (2013) Composition of the continental crust. In: Treatise on geochemistry, second edn, pp 1–51
Saha GK, Prakasam KS, Rai SS (2020) Diversity in the peninsular Indian lithosphere revealed from ambient noise and earthquake tomography. Phys Earth Planet Inter 306:106523
Saha GK, Rai SS, Prakasam KS, Gaur VK (2021) Distinct lithospheres in the Bay of Bengal inferred from ambient noise and earthquake tomography. Tectonophysics 809. https://doi.org/10.1016/j.tecto.2021.228855
Sibuet J-C, Klingelhoefer F, Huang Y-P, Yeh Y-C, Rangin C, Lee C-S, Hsu S-K (2016) Thinned continental crust intruded by volcanics beneath the northern Bay of Bengal. Mar Pet Geol 77:471e486
Sibuet J-C, Klingelhoefer F, Yeh Y-C, Rangin C, Lee C-S (2017) Reply to the comment of Talwani et al. (2017) on the Sibuet et al. (2016) paper entitled "Thinned continental crust intruded by volcanics beneath the northern Bay of Bengal". Marine Petrol Geol 88:1126–1129. https://doi.org/10.1016/j.marpetgeo.2017.07.023
Singh A, Bhushan K, Singh C, Steckler MS, Akhter SH, Seeber L et al (2016) Crustal structure and tectonics of Bangladesh: new constraints from inversion of receiver functions. Tectonophysics 680:99–112. https://doi.org/10.1016/j.tecto.2016.04.046
Steckler MS, Akhter SH, Seeber L (2008) Collision of the Ganges-Brahmaputra Delta with the Burma arc: implications for earthquake hazard. Earth Planet Sci Lett 273:367–378
Steckler MS, Mandal DR, Akhter SH, Seeber L, Feng L, Gale J, Hill EM, Howe M (2016) Locked and Loading megathrust linked to active subduction beneath the Indo-Burman Ranges. Nat Geosci NGEO2760, 10.1038
Talwani M, Desa MA, Ismaiel M, Krishna KS (2016a) The tectonic origin of the Bay of Bengal and Bangladesh. J Geophys Res 121:4836e4851. https://doi.org/10.1002/2015JB012734
Talwani M, Krishna KS, Ismaiel M, Desa MA (2017) Comment on a paper by Sibuet et al. (2016b) entitled "Thinned continental crust intruded by volcanics beneath the northern Bay of Bengal". Mar Pet Geol. https://doi.org/10.1016/j.marpetgeo.2016.12.009
Uddin A, Lundberg N (1999) A paleo-Brahmaputra? Subsurface lithofacies analysis of Miocene deltaic sediments in the Himalayan-Bengal system, Bangladesh. Sediment Geol 123:239–254
U.S. Geological Survey USGS Earthquake Catalog (2019) Retrieved from https://earthquake.usgs.gov/earthquakes/search/
Verma RK, Mukhopadhyay M (1977) An analysis of the gravity field in North-eastern India. Tectonophysics 42 (2e4), 283e317. https://doi.org/10.1016/0040-1951(77)90171-8
Wessel P, Smith WHF (1998) New, improved version of the Generic Mapping Tools released, EOS Trans Am Geophys Un 79:579

Chapter 4
Seismological Data Quality Controls—A Synthesis

Cédric P. Legendre and Utpal Kumar

Abstract Data quality is of utmost importance in assessing seismic hazards and risk mitigation related to geohazards. Erroneous data incorporation may lead to inaccurate observations and judgments. Lack of data or clipped data can be dealt with easily, but errors in the data (e.g., timing, amplitudes) or in the metadata (e.g. location, gain) can induce some strong bias in the estimation of geohazards. As a result, strict and standard quality controls are required to guarantee the accuracy of the assessments. This chapter will discuss some of the common issues with seismological data and offer tips on identifying inaccuracies. Despite recent efforts by the seismological community, there is no uniform framework to identify the errors in seismological data nor to perform some established quality controls. Therefore, we will examine the current state of the art and best practices in seismological quality controls. Some recommendations for new implementations, including some cutting-edge technologies like "Dynamic Time Warping" will be suggested. Missing data (i.e., gaps) are permanent, but all erroneous data do not need to be discarded. In some cases, identifying the problem in the data or metadata allows for reprocessing. The problems with data availability will be examined first, then the challenges with data quality. Finally, a discussion on the metadata errors will be provided.

Keywords Data quality · Data metrics · Seismic network performance · Seismology · Seismic hazard

C. P. Legendre (✉)
Institute of Geophysics, Czech Academy of Science, Boční II/1401, 14131 Praha, Czech Republic
e-mail: legendre@ig.cas.cz

U. Kumar
Berkeley Seismological Laboratory, University of California, 307 McCone Hall #4760, Berkeley, CA 94720-4760, USA
e-mail: utpalkumar@berkeley.edu

Sandeep et al. (eds.), *Geohazards*, Advances in Natural and Technological Hazards Research 53, https://doi.org/10.1007/978-981-99-3955-8_4

4.1 Introduction

A seismic network's primary objective is to provide high-quality data for monitoring earthquakes, analyzing their sources, and studying the structure of the Earth.

While some of the errors in the data and metadata are easy to identify (i.e., missing data gaps), others can be only detected by benchmarking the processed data with the "control" (real data or synthetics). The quality checks are often carried out at three levels: when the data are deployed and collected (seismic records), during the archival process at the data centers, and when it is used for seismic analyses. While some quality controls are not performed routinely, some analyses done at each level are redundant (data availability, timing quality, and other data integrity issues). With the ever-increasing amount of seismic data availability, the accuracy and reliability of the seismic records are essential for conducting further research. Errors in the data and metadata can strongly impact the outcomes of scientific analyses.

With the recent progress in data processing, rigorous quality controls should be used as the norm. However, it requires intense discussions between the data collector, data centers, and users to find a standard to define rigorous quality control.

In this study, we will describe the potential errors in seismic data and offer possible recommendations to spot and fix those inconsistencies. In the first section, we will discuss the data availability. Then, the primary sources of errors occurring in the seismic data will be presented, followed by a discussion on the main source of errors in the metadata. It will be followed by a discussion on detecting errors in seismic data in both raw and processed time-series.

4.2 Data Availability

One of the first and most essential questions is regarding the availability of the data.

No further checks are needed if the data were not recorded or transmitted.

Recent implementations such as Obspy (Beyreuther et al. 2010; Krischer et al. 2015), Pycheron (Aur et al. 2021), the Modular Utility for STAtistical kNowledge Gathering system (MUSTANG, Casey et al. 2018), AutoStatsQ (Petersen 2021), or Integrated Seismic Program (Cabieces et al. 2022) can perform data availability checks routinely.

Information about the data availability is generally provided by the data center hosting the seismic data (i.e., European Integrated Data Archive—EIDA data availability service, Fig. 4.1). However, the data availability tests can also be performed in the case of locally stored data (Herrmann 2013; Ringler et al. 2015).

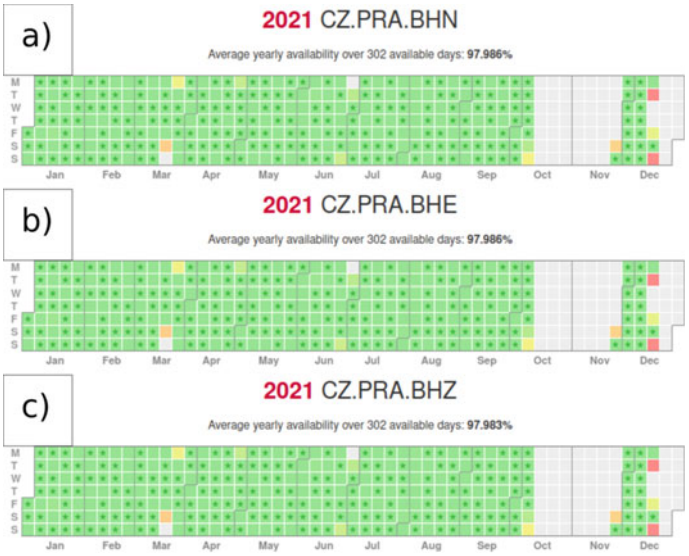

Fig. 4.1 Example of data availability for the station CZ-PRA in the year 2021. The color of each day indicates the amount of data available for this specific day. Green (fully available) to yellow and orange (partially available) to red (no data). Retrieved from https://www.orfeus-eu.org/data/eida/quality/availability/, last accessed 21.10.2022

4.2.1 Waveforms' Availability and Data Integrity Issues

Here, we refer to "available data (and metadata)" as readable waveforms that do not suffer from data integrity issues. Any data that cannot be adequately read will be accounted for as unavailable. It is essential to notice that different channels (Ringler and Evans 2015) may have different availability and quality. Carefully checking all components for the same band and instrument code individually (Ringler and Evans 2015) is of prime importance, as they are recorded independently. Figure 4.1 displays the data availability for the station CZ.PRA from the Czech Regional Seismic Network (Charles University in Prague (Czech) et al. 1973) for the year 2021. For this specific station and channels (BH[ZNE]), the data retrieval is excellent from January to September, but limited data are available in October–November.

There are two main approaches that are frequently used to assess the data availability: first, downloading all the data locally and examining the rate at which data are retrieved on an hourly, daily, or monthly basis. Second, submit numerous random requests for a short period of seismic data (i.e., a few seconds or minutes) and then compare the requests and the retrieved data to perform some statistical analysis.

4.2.2 Gaps/Overlaps

When the data are available, it is essential to check if any gaps or overlaps are present. Overlaps are redundant information, whereas gaps are missing information in the time series. Data centers and users can generally identify gaps and overlaps routinely using data quality tools (e. g. Obspy, Beyreuther et al. 2010; Krischer et al. 2015). For example, Fig. 4.2 displays the data availability in percentage for the station CZ.PRA from the Czech Regional Seismic Network for December 2021.

There are two common ways to deal with gaps. The first approach is simply to discard the data with gaps.

A second option consists of filling the gaps using linear interpolation, filling the missing data with zeros, or a constant value, depending on how much the gap matters.

The reconstruction of missing seismic time series is an important step that has been the focus of recent implementations (Siahkoohi et al. 2018; Yu and Wu 2021; Wei and Li 2022). With recent progress in machine learning, new methodologies arose to reconstruct the time series for the missing data (Jia and Ma 2017; Wang et al. 2020) based on convolutional neural networks.

On another note, the overlaps in the time-series are much easier to identify: data are present but the time-series are redundant (Fig. 4.3), and the correction of overlap is usually done by merging and averaging the duplicated time-series.

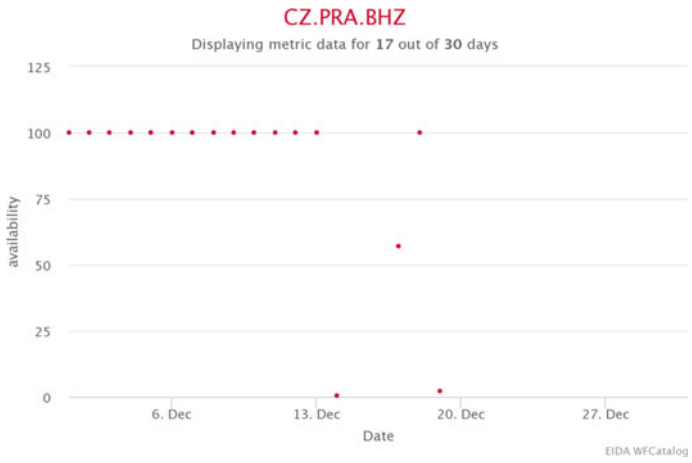

Fig. 4.2 Example of data availability for the station CZ-PRA in December 2021. Retrieved from https://www.orfeus-eu.org/data/eida/quality/availability/, last accessed 21.10.2022

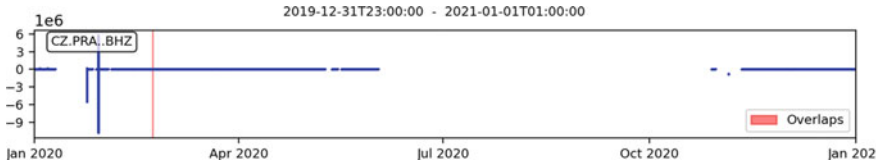

Fig. 4.3 Example of data availability for the station CZ-PRA in 2020. Gaps (missing data) and overlap (marked in red) are computed using Obspy (Beyreuther et al. 2010; Krischer et al. 2015)

4.3 Quality of the Time-Series

Previous tests ensured that the data are available, which is essential but relatively easy to perform. In the following sections, we will discuss the data quality. Reliable data are critical to obtain an accurate result.

4.3.1 Power Spectral Density

A common way to check the data quality is to look at the Power Spectral Density (PSD, McNamara and Buland 2004). PSD estimates the power–frequency distribution and is a common technique for quantifying seismic background noise (McNamara et al. 2009; Anthony et al. 2020). The PSD of ambient background noise for each site is calculated and compared with the global noise model (Peterson 1993).

Figure 4.4 shows an example of PSD computed for the station CZ-PRA for two different epochs: March 2021 and March 2022. The PSD is a strong indicator of the data quality, showing the frequencies for which the noise level is lower than the global model. Figure 4.4a displays an erroneous PSD and some data gaps, while Fig. 4.4b displays a more realistic PSD, suggesting that the data errors have been corrected. Seasonal and temporal changes of the PSD are also significant (Vecsey et al. 2017), as those are relevant for potential errors in the data, as shown in Fig. 4.4a.

Amplitudes of the PSD can also be compared with synthetic waveforms (Petersen 2021), to highlight the potential evaluation of the amplitudes of the seismograms. It is important to note that the Earth model used to generate those synthetic waveforms is of prime importance (Hutko et al. 2017). If the method of forward calculation or the Earth model is unreliable, then the resulting synthetic seismograms will differ vastly from the recorded ground motion (Herrmann and Wang 1985; Monteiller et al. 2021).

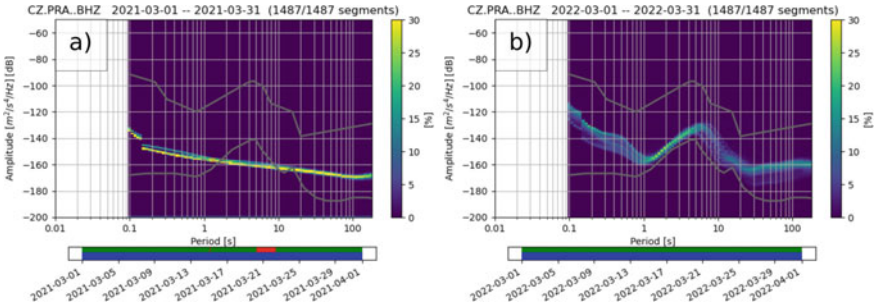

Fig. 4.4 Example of power spectral density (PSD) for the station CZ.PRA in March 2020 & March 2022. Global noise model (Peterson 1993) is indicated with gray lines. PSD is computed using Obspy (Beyreuther et al. 2010; Krischer et al. 2015)

4.3.2 Orientation

One common error in the seismic data is caused by the misorientation of the sensors. Recent studies (Petersen 2021) suggest that more than 4% of the newly deployed seismic stations can have a sensor misorientation higher than 20°. Errors in the orientation of the horizontal components are critical to properly evaluating the source mechanism, as the moment tensor inversions highly depend on the horizontal components (Sipkin 1982; Eulenfeld et al. 2022).

A common way to assess the misorientation of the sensors (Ringler et al. 2013) is to investigate the polarization of P- or Rayleigh-wave by comparing real data and synthetics (Ekström and Busby 2008; Petersen 2021). An example of potential errors in the orientation of the sensors for the KOERI data (Kandilli Observatory And Earthquake Research Institute, Boğaziçi University 1971) has been computed using AutoStatsQ (Petersen 2021), and the results are shown in Fig. 4.5.

4.3.3 Timing Errors

Timing errors are also a critical issue in assessing earthquake early warning. A common way to detect timing errors is to compare synthetic and observed waveforms for numerous teleseismic earthquakes with well-distributed back azimuths (Liu et al. 2017). For each trace, the cross-correlation of the synthetic and observed data will provide a time shift with the highest correlation (VanDecar and Crosson 1990; Rowe et al. 2002). It is important to note that propagating errors in the origin time, the path effects, and the deviations between origin and centroid times can have a significant impact on the measured lag, and should therefore be accounted for. A common approach to minimize these errors is to compute the median time shift at all stations within the network and use it as a reference.

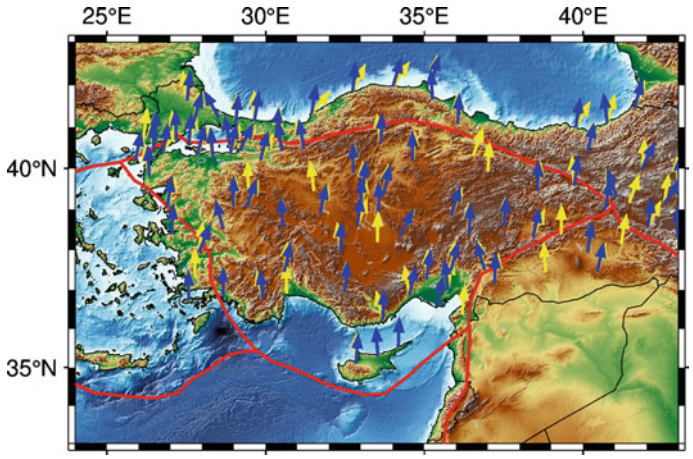

Fig. 4.5 Misorientations of the horizontal components computed using AutoStatsQ (Petersen 2021) for the KOERI data using Rayleigh-wave polarization (blue arrows) and P-wave polarization (yellow arrows), modified from Büyükakpınar et al. (2021)

The resolution of the error in the timing is generally limited by the resolution of the Greens Function database that is used to calculate the synthetics (Hutko et al. 2017). However, a recent study (Kumar et al. 2022b) showed that Dynamic Time Warping could detect subtle changes in the waveforms caused by timing errors.

Comparing waveforms for a local or a teleseismic event at neighboring stations (Kumar et al. 2022b) can potentially highlight timing errors on selected components (Fig. 4.6). It should be possible to precisely quantify any potential lag inside the seismic network by comparing synthetic and observed data at each component individually.

4.3.4 Data—Other Errors

The zero-point of the instrument (the amplitude which would be recorded if there is no motion) is also not included in the preprocessed data. Incorrect demeaning of the time-series is a common source of errors in the raw data. Similarly, the trend (i.e., due to tilt motion during earthquake faulting) from time-series signal has to be accounted for. The seismic waveforms would be clipped when the amplitude exceeds the upper limit of the dynamic range of the seismometer, which could happen during very large earthquakes. Recent implementations (e.g. Obspy, Beyreuther et al. 2010; Krischer et al. 2015) allow correcting for potential offset in the mean or trend of the time-series. Most of the work done on bandpass-filtered data may not need demeaning and detrending, as it is often removed by bandpassing the record.

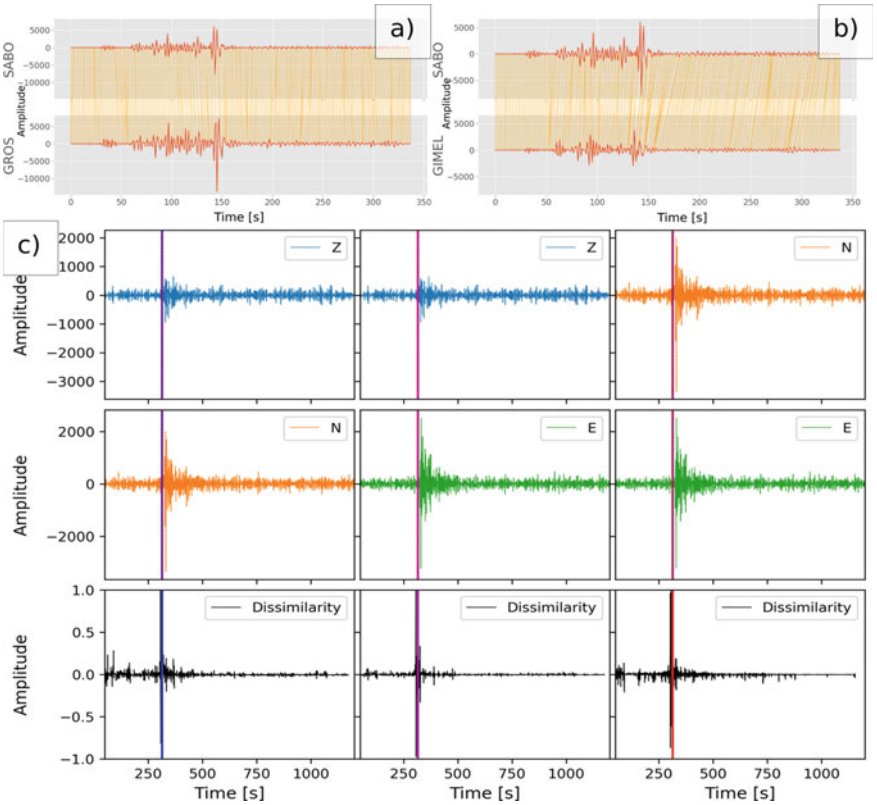

Fig. 4.6 Waveforms at two stations (SL-GROS and CH-GIMEL) compared to the waveforms at the station OX-SABO, for an event occurring in 2016–12-25T14:22:27.03 and a latitude of −43.4053, a longitude of −73.9403, a focal depth of 0 km and a Mw = 7.6. The constant shift between the two seismic traces is highlighted by Dynamic Time Warping. Vertical (top-left and top-middle panels) and horizontal (top-right panel and middle row) velocity components of a seismic record at a single station (CI-LJR) for a magnitude Mw 6.2 earthquake of the Ridgequest sequence (2016). (Bottom row) Dissimilarity functions between pairs of seismograms in the top two rows of the same column. Vertical lines show triggering times, with solid lines on the selected pairs of components (ZN, ZE, and NE) and dashed lines on the others showing the triggering time for other pairs of components

Zhang et al. (2016) developed a method that allows for reconstructing the frequency spectrum of a clipped time-series iteratively under the assumption that the clipped components of the waveform share the same frequency content as the un-clipped components.

4.4 Metadata Quality

The seismic records are generally composed of the data (traces, time-series) and metadata (e.g., StationXML, Hess et al. 2019). A standard format adopted in seismology for the data is the Standard for the Exchange of Earthquake Data (SEED, Ringler and Evans 2015). The SEED format includes both the time-series (i.e., the data only, often in MiniSEED, PC-SUDS, Seisan format) and the metadata. Nowadays, metadata are often represented using the StationXML scheme (Hess et al. 2019). However, other formats (RESP or Poles and Zeros files) are also represented.

The metadata provide information about the type of instrument (sensor, digitizer, data-loggers), instrument characteristics (amplifier, filters and, response), as well as history, geographical coordinates (latitude, longitude, elevation), names (site name, network and station codes), sampling rate, operating time, etc. Errors in the metadata generally lead to errors in the seismic data, as the time-series will not be deconvolved properly. It is therefore of prime importance to identify and fix those errors.

4.4.1 Metadata—Formal Properties

The availability and accuracy of the metadata are critical (Davis and Berger 2012; Zaccarelli et al. 2021). Any change in the instruments should lead to an update of the metadata. It is, therefore, essential to check the availability of the metadata for the operating time of the seismic station and the accuracy of the information provided in the metadata.

The existence of the StationXML file (Hess et al. 2019) is easily detectable. The names of the channels in the StationXML file should match those in the time-series. The StationXML should encompass the whole duration of the entire operating time of the seismic station. Also, the station names and network code in the StationXML file should match those in the time-series. Those errors do not directly affect the time-series's quality, but these entries must be correct to match the proper metadata epoch to the given time-series. Only then could the deconvolution be successful. Finding these formal errors is easy, as they usually appear when the data and metadata entries do not match each other.

Within the StationXML file, the Poles and Zeros (and eventually the complex conjugate pair) and the normalization factor must be present and accurate.

The accuracy of this Poles and Zeros response is also crucial in processing time-series.

4.4.2 Metadata—Geographical Errors

As discussed earlier, the orientation of the components of the seismogram (Fig. 4.5) has to be accurate (Ringler et al. 2013; Petersen 2021). In addition, errors in the location of the seismic station can lead to incorrect interpretations of the seismological results. Sometimes, seismic stations have to be relocated, e.g., due to changes in the instrumentation. Therefore, it is important to check the information regarding the station's geographical coordinates and use the latest available version of the StationXML file (Hess et al. 2019) for the corresponding station. Similarly, the orientation of the horizontal components in the StationXML should be accurate. The dip of the vertical component should be $\pm 90°$.

It is not possible to automatically detect these errors. To do so, an independent comparison between several stations, networks, or synthetic data is required to ensure the reliability of the metadata.

4.4.3 Metadata—Instrumentation Errors

Each seismometer is unique, and each component of the seismometer (sensor, digitizer, data loggers) will affect the processing of the time-series (Pedersen et al. 2020; Chèze et al. 2021).

Setting the instrumentation information properly will ensure an accurate finite impulse response filter, which would lead to errors in the processed seismic data.

Such errors could lead to incorrect amplitudes or lags in the processed time-series that would strongly impact modeling seismic hazards (Kisslinger et al. 1981; Bernardi et al. 2005). Those errors have to be detected first using some measurement method, the assistance of the network operator is then needed to correct and update the metadata.

4.4.4 Metadata—Other Errors

Some other errors can be present in the StationXML file (Hess et al. 2019). Inconsistencies between the epoch among the different channels or between the data and the metadata can be problematic. Some incorrect numbers (e.g., sampling rate, normalization factor, filters, poles, and zeros) can lead to subtle errors in the data. Errors in the instrument response can also originate from the mismatch between the units and numbers (i.e., radians vs. Hertz), leading to erroneous processed data.

If the data were to be used to create geohazard models, any of those errors would also strongly impact the processed data. Erroneous amplitude calculations of the processed time-series would result in inaccuracies in the geohazard models.

4.5 Discussions

4.5.1 Review of Existing Software

Obspy (Beyreuther et al. 2010; Krischer et al. 2015) is a recent open-access Python implementation that deals with seismic data and metadata.

Obspy allows retrieving information on the availability of seismic waveforms and metadata for a given network, station, channel, and client in a selected duration of time. Obspy also allows visualizing data availability of local waveform archive: while reading the time-series, gaps and overlaps are highlighted and can be accounted for (Fig. 4.3). Obspy allows the computation and visualization of Power Spectral Density (Fig. 4.4), as well as the reading and updating of the data and metadata.

Computer Programs in Seismology (Herrmann 2013) is a well-established software used in seismology to perform basic quality controls, such as the existence of different channels and response/poles and zeroes files. Pycheron (Aur et al. 2021), based on the Modular Utility for STAtistical kNowledge Gathering system (MUSTANG, Casey et al. 2018), are open access standalone quality control packages. AutoStatsQ (Petersen 2021) is a toolbox for automated quality control of large seismic networks. It is based on Pyrocko (Heimann et al. 2017, 2019) and is specifically designed to assess quality control. Integrated Seismic Program (Cabieces et al. 2022) is a graphical user interface that allows for time–frequency analysis, computation of synthetic seismograms as well as seismic noise analysis. It is not designed explicitly for quality checks but allows to perform basic tests.

Numerous implementations based on Java (Ringler et al. 2015), Python (i.e., Lou et al. 2013; Vecsey et al. 2017), ForTran (Duret et al. 2007), Matlab (Wüstefeld et al. 2008; Yu et al. 2017) are available as open-access. Most of them are specifically designed to identify one source of errors in the seismic time-series. However, to our knowledge, there is no common standard procedure to assess the data and metadata quality and reliability.

While Dynamic Time Warping generally uses normalized amplitudes, strict controls on the amplitudes are not needed.

Estimation of the earthquake epicenter strongly relies on the accuracy of the timing of the time-series, whereas the estimation of the shake-maps rely on the amplitudes of the seismograms.

Each scientific goal is different and relies on different data processing; therefore, different QC is needed. It is, therefore, essential to establish a standard procedure that would ensure the reliability of the time-series.

4.5.2 Detecting Errors in Processed Data

Assuming the data and metadata are available, the current implementations listed above allow for performing some data quality checks.

Several other options exist to detect errors in the processed data. Investigating the similarity of the waveforms for a teleseismic earthquake recorded at numerous stations can also be a powerful indicator of potential errors in the processed seismic time-series (Kumar et al. 2022b). Clustering the waveforms by the similarity of the time-series (Kumar et al. 2022a) allows to detect stations with potential issues for a specific seismic event, as displayed in Fig. 4.7a. Dynamic Time Warping (Kumar et al. 2022b) can also provide some information about trace similarity and detect the lags and inconsistencies in the time series (Fig. 4.8) efficiently. Similar traces (Fig. 4.8a) would display optimal matching lines that are almost vertical and parallel to each other, while time-series with a constant lag (Fig. 4.8b) would display optimal matching lines that are tilted, but almost parallel to each other. Erroneous amplitudes (Fig. 4.8c) may not be detected using Dynamic Time Warping, as the amplitudes of the time-series are generally normalized before applying Dynamic Time Warping. Traces with a high level of scattering (Fig. 4.8d) would display optimal matching lines that are not parallel to each other. This is an indication that the time series are not similar, potentially caused by incorrect response correction. Dynamic Time Warping is therefore well-suited to be implemented in potential applications of evaluating several aspects of the data quality.

Using the modeling approach by Nolet and Dahlen (2000), an array measurement of surface wave phase velocities based on the two-station method (Kolínský et al. 2011; Legendre et al. 2014) and array beamforming technique (Kolínský et al. 2014) can be computed. The predicted wavefield of the surface-wave fundamental mode Rayleigh waves over a selected region can be computed (Kolínský et al. 2019). The zero-crossings of the ground motion (velocity) close to the envelope maximum of the fundamental mode (Kolínský et al. 2020) can be used as a proxy of the phase wavefront (Kolínský et al. 2021). Any distortion of the wavefront is an indicator of some potential issue with the processed data (Fig. 4.7b). Stations with incorrect data

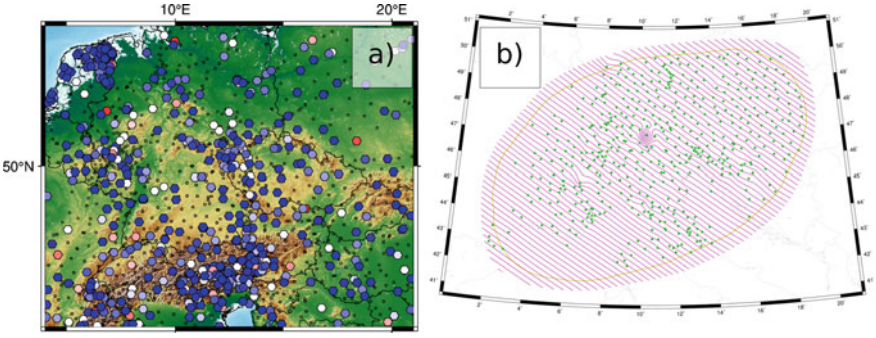

Fig. 4.7 Dynamic Time Warping similarity among all stations providing data computed using *dtwhaclustering* package (Kumar et al. 2022a). Phase wavefront for a Rayleigh surface wave fundamental mode, period of 100 s, propagating across the AlpArray Seismic Network (Hetényi et al. 2018). Incorrect metadata entry at one of the stations shows up as a distortion of the wavefield. After correcting the issue, the wavefield was smooth over the whole network

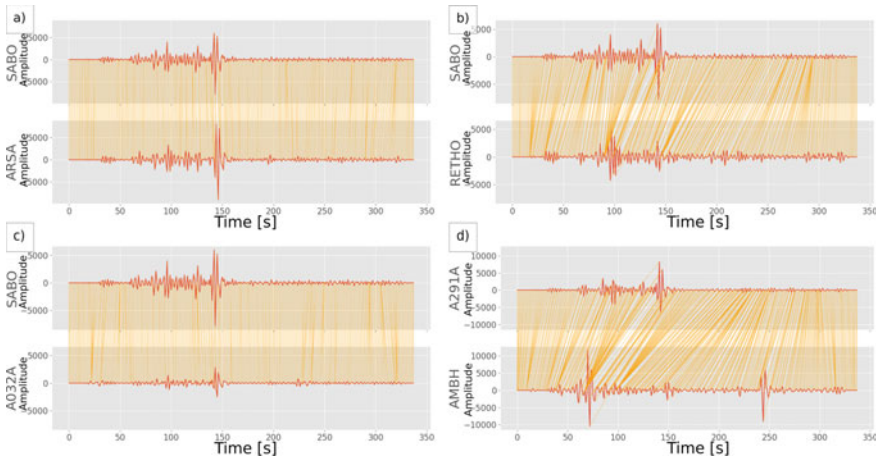

Fig. 4.8 Dynamic Time Warping (Kumar et al. 2022b) can provide useful information about **a**- traces with high similarity (stations OX-SABO / OE-ARSA), **b**- traces with time lags (stations X-SABO / GR-RETHO), **c**- traces with amplitude differences (stations OX-SABO / Z3-A032A) and **d**- inconsistencies in the time series (stations HU-AMBH / Z3-A291A). All the velocity waveforms are retrieved for an event occurring at 2016-12-25T14:22:27.03 and for a latitude of −43.4053, a longitude of −73.9403, a focal depth of 0 km, and a Mw = 7.6)

display inconsistent arrival times compared with respect to the wavefront computed at neighboring stations. A simple visual inspection allows the detection of distortion of the wavefront, which is an essential step in identifying the errors in the data or metadata at specific stations. In the case of the AlpArray network illustrated in Fig. 4.7b, the outlying station had incorrect metadata entry and after identification of the problem, the metadata was corrected, and the test was performed again to prove that the wavefronts were all smooth then.

4.5.3 Implications for Seismic Hazard

Geohazards are broad and encompass a wide range of hazards from atmospheric phenomena (i.e., tornadoes, typhoons/hurricanes, Canitano et al. 2021), oceanic phenomena (e.g., tsunami—Kato et al. 2018), geologic phenomena (i.e., faults, volcanoes—Milkov 2005; Legendre et al. 2015c) and geophysical phenomena (i.e., earthquakes—Wu and Kanamori 2005).

Here, we will focus mainly on the geohazards that use seismic measurements as the primary data source, and the potential effects of erroneous seismic data. Evaluating local seismic response (Rivera et al. 2008; Alam et al. 2021) is of high importance for engineering purpose. Errors in the metadata (i.e., finite impulse response filter) could lead to very strong discrepancies in the results.

The behavior of seismic waves (Legendre et al. 2017b; Mittal et al. 2019a) is fundamental in geohazard assessment. Any error in the seismic data would lead to inconsistent observations. Seismological data are inverted for 1D, 2D, or 3D models encompassing isotropic velocities (Legendre et al. 2012, 2015a) and anisotropic components (Legendre et al. 2015b). Those models are then used to generate synthetic seismograms (Hutko et al. 2017) that will be compared with recorded seismic data. Similarly, understanding the structure of the crust and upper mantle employing tomography can provide some constraints on the location and the vertical extension of volcanoes (Kumar et al. 2021; Kumar and Legendre 2022). Errors in the seismic data would have a very strong impact on the reliability of the results. Seismic data quality is, therefore, of utmost importance to ensure the reliability of further computation.

The understanding of the earthquake ground shaking (Legendre et al. 2017a; Mittal et al. 2019a) is based on the amplitudes of the seismograms at any specific time. Any errors in the amplitudes caused by errors in the metadata (i.e., gain factor, amplifier) would generate some drastic errors in the assessment of seismic hazard.

Hazard Maps are generally produced using decades of data recorded at numerous stations to evaluate the georisk. Any errors in the seismic data would lead to errors in the maps. As those maps have direct influence on the society (e.g. urbanization, insurance), it is of prime importance to ensure that the errors are minimized (Molchan 1997; Mogren 2021).

Ground motion simulations (Sandhu et al. 2020) are rely heavily on the response spectra. Any error in the metadata would induce some bias in the ground motion simulation (Arora et al. 2020).

Horizontal-to-vertical spectral ratio (Mittal and Kumar 2015; Molnar et al. 2018, 2022) requires accurate amplitudes of all three components of the time-series. Any inconsistencies in the time-series would have a strong impact on the result.

Earthquake early warning systems (Gasparini et al. 2007; Mittal et al. 2019b; Böse et al. 2022) are heavily relying on data accuracy. Any errors (i.e., timing, location, amplitudes) in the seismic data and metadata would generate large uncertainties in the reliability of the detection of potentially damageable earthquakes.

The near-surface site conditions (Gadylshin et al. 2022d, a, c; Parolai et al. 2022) are essential for mitigating seismic risks assessed at the local and regional scale. Similarly, information about shallow structures (Wege et al. 2022d, a, c) is critical to estimate geotechnical properties. Foti et al. (2018) showed that earthquake data can be used to estimate near-surface site conditions. Any errors in the processed data, as well as in the metadata, would lead to inaccuracies in the result.

Techniques of Artificial Intelligence, such as machine learning (Kong et al. 2019; Li et al. 2018), pattern recognition (Roden et al. 2015; Di et al. 2019), and deep learning (Jiao and Alavi 2020; Mousavi and Beroza 2022) are emerging in geosciences and in analyzing geohazards. They all require high-quality data to be trained efficiently (Maity et al. 2014; Mousavi et al. 2019). Errors in the time-series would have a very strong impact on the reliability of the outcome.

Knowledge about the crustal and lithospheric structures is also of prime importance in regions with a high population density and seismicity (e.g. in Turkey, as shown in Legendre et al. 2020, 2021) also rely on high-quality seismological data.

Hazard maps (Frankel et al. 2000; Stein et al. 2012) can be used for land-use planning, mitigation, and emergency response. Those maps also heavily dependent on the input from seismological studies, for which high-quality measurements are required.

4.6 Conclusion

Here, we demonstrated that data quality is of utmost importance to ensure the reliability of seismological studies and assessment of geohazards.

The errors in the data and metadata can be categorized into three categories.

First, the lack of data or metadata (i.e., gap) or redundancy of those information (i.e., overlap).

In the second category, the errors can be spotted directly without any processing of the data (i.e., inconsistent names, non-zero mean).

In the third category, the errors require deconvolving the time-series from the instrumental response to be identified (i.e., inconsistent amplitudes).

Most of the errors in the time-series can be accounted for, either by the data collector, the data centers, or the users.

Users have different expectations regarding data quality and will require very precise information (e.g. lag, amplitude) while some other criteria would be neglected (i.e., normalization of the time-series using Dynamic Time Warping).

It is therefore important to find common rules to define what a rigorous quality control is, and at which stage it should be performed.

4.7 Data Availability

Data for this study has been retrieved from:

- AlpArray Seismic Network (AlpArray Seismic Network 2015),
- Austrian Seismic Network (ZAMG—Zentralanstalt für Meterologie und Geodynamik 1987),
- Czech Regional Seismic Network (Charles University in Prague (Czech) et al. 1973),
- German Regional Seismic Network (Federal Institute for Geosciences and Natural Resources 1976),
- Hungarian National Seismological Network (Kövesligethy Radó Seismological Observatory (Geodetic And Geophysical Institute, Research Centre For Astronomy And Earth Sciences, Hungarian Academy Of Sciences (MTA CSFK GGI KRSZO)) 1992),
- Kandilli Observatory And Earthquake Research Institute (Kandilli Observatory And Earthquake Research Institute, Boğaziçi University 1971),

- North-East Italy Seismic Network (Istituto Nazionale di Oceanografia e di Geofisica Sperimentale—OGS 2016),
- Seismic Network of the Republic of Slovenia (Slovenian Environment Agency 1990),
- Southern California Seismic Network (California Institute of Technology and United States Geological Survey Pasadena 1926),
- Switzerland Seismological Network (Swiss Seismological Service (SED) At ETH Zurich 1983).

4.8 Code Availability

All measurements have been performed using Obspy (Beyreuther et al. 2010; Krischer et al. 2015), AutoStatsQ (Petersen 2021), Dynamic Time Warping (Kumar et al. 2022b) or the *dtwhaclustering* package (Kumar et al. 2022a).

Acknowledgements C.L is funded by the Institute of Geophysics, Czech Academy of Sciences.

Data from the AlpArray Seismic Network (AASN) were made freely available to the public as part of the AlpArray initiative (www.alparray.ethz.ch). We acknowledge the operation of the temporary AlpArray Seismic Network under FDSN network code Z3 (Hetényi et al. 2018) and AlpArray Seismic Network (AlpArray Seismic Network 2015), used in this study.

The facilities of IRIS Data Services, and specifically the IRIS Data Management Center, were used for access to waveforms, related metadata, and/or derived products used in this study. IRIS Data Services are funded through the Seismological Facilities for the Advancement of Geoscience (SAGE) Award of the National Science Foundation under Cooperative Support Agreement EAR-1851048. The facilities of Observatories and Research Facilities for European Seismology (Haslinger et al. 2022, ORFEUS) and European Integrated Data Archive (Strollo et al. 2021, EIDA) were used for access to waveform and metadata required in this study. Individual figure panels were generated with the Generic Mapping Tools (Wessel et al. 2019). Individual figure panels were combined using Inkscape (Inkscape Project 2022).

References

Alam Z, Sun L, Zhang C, Su Z, Samali B (2021) Experimental and numerical investigation on the complex behaviour of the localised seismic response in a multi-storey plan-asymmetric structure. Struct Infrastruct Eng 17(1):86–102

AlpArray Seismic Network (2015) AlpArray Seismic Network (AASN) temporary component. AlpArray Working Group. https://doi.org/10.12686/alparray/z3_2015

Anthony RE, Ringler AT, Wilson DC, Bahavar M, Koper KD (2020) How processing methodologies can distort and bias power spectral density estimates of seismic background noise. Seismol Res Lett 91(3):1694–1706

Arora S, Joshi A, Kumari P, Kumar P, Sah SK, Lal S, Singh NP (2020) Strong ground motion simulation techniques—a review in world context. Arab J Geosci 13(14):1–12

Aur KA, Bobeck J, Alberti A, Kay P (2021) Pycheron: a python-based seismic waveform data quality control software package. Seismol Res Lett 92(5):3165–3178

Bernardi F, Braunmiller J, Giardini D (2005) Seismic moment from regional surface-wave amplitudes: applications to digital and analog seismograms. Bull Seismol Soc Am 95(2):408–418
Beyreuther M, Barsch R, Krischer L, Megies T, Behr Y, Wassermann J (2010) ObsPy: a python toolbox for seismology. Seismol Res Lett 81(3):530–533
Böse M, Andrews J, O'Rourke C, Kilb D, Lux A, Bunn J, McGuire J (2022) Testing the shakealert earthquake early warning system using synthesized earthquake sequences. Seismological Research Letters
Büyükakpınar P, Aktar M, Petersen GM, Köseoğlu A (2021) Orientations of broadband stations of the KOERI seismic network (Turkey) from two independent methods: P-and Rayleigh-wave polarization. Seismol Res Lett 92(3):1512–1521
Cabieces R, Olivar-Castaño A, Junqueira TC, Relinque J, Fernandez- Prieto L, Vackár J, Rösler B, Barco J, Pazos A, García-Martínez L (2022) Integrated seismic program (ISP): a new python GUI-based software for earthquake seismology and seismic signal processing. Seismol Soc Am 93(3):1895–1908
California Institute of Technology and United States Geological Survey Pasadena (1926) Southern California seismic network. International Federation of Digital Seismograph Networks. https://doi.org/10.7914/SN/CI
Canitano A, Mouyen M, Hsu Y-J, Linde A, Sacks S, Lee H-M (2021) Fifteen years of continuous high-resolution borehole strainmeter measurements in eastern Taiwan: an overview and perspectives. GeoHazards 2(3):172–195
Casey R, Templeton ME, Sharer G, Keyson L, Weertman BR, Ahern T (2018) Assuring the quality of IRIS data with MUSTANG. Seismol Res Lett 89(2A):630–639
Charles University in Prague (Czech), Institute of Geonics, Institute of Geophysics, Academy of Sciences of the Czech Republic, Institute of Physics of the Earth Masaryk University (Czech), & Institute of Rock Structure and Mechanics (1973) Czech regional seismic network [Data set]. International Federation of Digital Seismograph Networks. https://doi.org/10.7914/SN/CZ
Chèze J, Maron C, Rivet D, Peix F, Brunel D, Martin X, Delouis B (2021) METEOR: online seismic metadata builder. Seismol Res Lett 92(2A):1141–1147
Davis P, Berger J (2012) Initial impact of the global seismographic network quality initiative on metadata accuracy. Seismol Res Lett 83(4):697–703
Di H, Gao D, AlRegib G (2019) Developing a seismic texture analysis neural network for machine-aided seismic pattern recognition and classification. Geophys J Int 218(2):1262–1275
Duret F, Mooney W, Detweiler S (2007) New codes for ambient seismic noise analysis. In AGU Fall Meeting Abstracts 2007:S43B-1306
Ekström G, Busby RW (2008) Measurements of seismometer orientation at USArray transportable array and backbone stations. Seismol Res Lett 79(4):554–561
Eulenfeld T, Dahm T, Heimann S, Wegler U (2022) Fast and robust earthquake source spectra and moment magnitudes from envelope inversion. Bull Seismol Soc Am 112(2):878–893
Federal Institute for Geosciences and Natural Resources (1976) German Regional Seismic Network (GRSN). Bundesanstalt für Geowissenschaften und Rohstoffe. https://doi.org/10.25928/mbx6-hr74
Foti S, Hollender F, Garofalo F, Albarello D, Asten M, Bard P-Y, Comina C, Cornou C, Cox B, Di Giulio G et al (2018) Guidelines for the good practice of surface wave analysis: a product of the InterPACIFIC project. Bull Earthq Eng 16(6):2367–2420
Frankel A, Mueller C, Barnhard T, Leyendecker E, Wesson R, Harmsen S, Klein F, Perkins D, Dickman N, Hanson S et al (2000) USGS national seismic hazard maps. Earthq Spectra 16(1):1–19
Gadylshin K, Cheverda V, Tverdokhlebov D (2022a) Reconstruction of the near-surface model for the conditions of eastern siberia using full waveform inversion. In Doklady earth sciences, vol 502, pp 37–40. Springer
Gasparini P, Manfredi G, Zschau J et al (2007) Earthquake early warning systems. Springer
Haslinger F, Basili R, Bossu R, Cauzzi C, Cotton F, Crowley H, Custódio S, Danciu L, Locati M, Michelini A et al (2022) Coordinated and interoperable seismological data and product services

in Europe: the EPOS thematic core service for seismology. Annal Geophys 65(2):DM213–DM213
Heimann S, Kriegerowski M, Isken M, Cesca S, Daout S, Grigoli F, Juretzek C, Megies T, Nooshiri N, Steinberg A et al (2017) Pyrocko-an open-source seismology toolbox and library
Heimann S, Kriegerowski M, Isken M, Nooshiri N, Steinberg A, Sudhaus H, Vasyura-Bathke H, Dahm T (2019) Pyrocko-A versatile software framework for seismology. In Geophysical research abstracts, vol 21
Herrmann R, Wang C (1985) A comparison of synthetic seismograms. Bull Seismol Soc Am 75(1):41–56
Herrmann RB (2013) Computer programs in seismology: an evolving tool for instruction and research. Seismol Res Lett 84(6):1081–1088
Hess D, Carothers L, Beaudoin B, Falco N (2019) Recent advances to PASSCAL software for managing and archiving seismic data. In Geophysical research abstracts, vol 21
Hetényi G, Molinari I, Clinton J, Bokelmann G, Bondár I, Crawford WC, Dessa J-X, Doubre C, Friederich W, Fuchs F et al (2018) The AlpArray seismic network: a large-scale European experiment to image the Alpine orogen. Surv Geophys 39(5):1009–1033
Hutko AR, Bahavar M, Trabant C, Weekly RT, Fossen MV, Ahern T (2017) Data products at the IRIS-DMC: growth and usage. Seismol Res Lett 88(3):892–903
Inkscape Project (2022b) Inkscape (1.2.1) [Internet] (2022b)
Istituto Nazionale di Oceanografia e di Geofisica Sperimentale-OGS (2016) North-East Italy seismic network [Data set]. FDSN. https://doi.org/10.7914/SN/OX
Jia Y, Ma J (2017) What can machine learning do for seismic data processing? An interpolation application. Geophysics 82(3):V163–V177
Jiao P, Alavi AH (2020) Artificial intelligence in seismology: advent, performance and future trends. Geosci Front 11(3):739–744
Kandilli Observatory And Earthquake Research Institute, Boğaziçi University (1971) Kandilli observatory and earthquake research institute (KOERI). Int Federation Digital Seismogr Netw. https://doi.org/10.7914/SN/KO
Kato T, Terada Y, Tadokoro K, Kinugasa N, Futamura A, Toyoshima M, Yamamoto S-I, Ishii M, Tsugawa T, Nishioka M et al (2018) Development of GNSS buoy for a synthetic geohazard monitoring system. J Disaster Res 13(3):460–471
Kisslinger C, Bowman JR, Koch K (1981) Procedures for computing focal mechanisms from local (SV/P) z data. Bull Seismol Soc Am 71(6):1719–1729
Kolínský, P., Bokelmann, G., Group, A. W (2019) Arrival angles of teleseismic fundamental mode Rayleigh waves across the AlpArray. Geophys J Int 218(1):115–144
Kolínský P, Bokelmann G, AlpArray Working Group (2021) On the wobbles of phase-velocity dispersion curves. Geophys J Int 224(3):1477–1504
Kolínský P, Málek J, Brokešová J (2011) Shear wave crustal velocity model of the western Bohemian Massif from Love wave phase velocity dispersion. J Seismolog 15(1):81–104
Kolínský P, Schneider FM, Bokelmann G (2020) Surface wave diffraction pattern recorded on AlpArray: Cameroon volcanic line case study. J Geophys Res Solid Earth 125(7):e2019JB019102
Kolínský P, Valenta J, Málek J (2014) Velocity model of the Hronov-Poříčí Fault Zone from Rayleigh wave dispersion. J Seismolog 18(3):617–635
Kong Q, Trugman DT, Ross ZE, Bianco MJ, Meade BJ, Gerstoft P (2019) Machine learning in seismology: turning data into insights. Seismol Res Lett 90(1):3–14
Krischer L, Megies T, Barsch R, Beyreuther M, Lecocq T, Caudron C, Wassermann J (2015) ObsPy: a bridge for seismology into the scientific Python ecosystem. Comput Sci Discov 8(1):014003
Kumar U, Legendre C, Huang B (2021) Crustal structure and upper mantle anisotropy of the Afar triple junction. Earth Planets Space 73(1):1–17
Kumar U, Legendre C, Lee J-C, Zhao L, Chao BF (2022a) On analyzing GNSS displacement field variability of Taiwan: hierarchical agglomerative clustering based on dynamic time warping technique. Comput Geosci 105243

Kumar U, Legendre CP (2022) Crust-mantle decoupling beneath Afar revealed by Rayleigh-wave tomography. Sci Rep 12(1):1–8
Kumar U, Legendre CP, Zhao L, Chao BF (2022b) Dynamic time warping as an alternative to windowed cross correlation in seismological applications. Seismol Soc Am 93(3):1909–1921
Kövesligethy Radó Seismological Observatory (Geodetic And Geophysical Institute, Research Centre For Astronomy And Earth Sciences, Hungarian Academy Of Sciences (MTA CSFK GGI KRSZO)) (1992) Hungarian national seismological network. Deutsches GeoForschungsZentrum GFZ. https://doi.org/10.14470/UH028726
Legendre C, Chen Q-F, Zhao L (2014) Lithospheric structure beneath the East China sea revealed by Rayleigh-wave phase velocities. J Asian Earth Sci 96:213–225
Legendre C, Meier T, Lebedev S, Friederich W, Viereck-Götte L (2012) A shear wave velocity model of the European upper mantle from automated inversion of seismic shear and surface waveforms. Geophys J Int 191(1):282–304
Legendre C, Tseng T, Mittal H, Hsu C-H, Karakhanyan A, Huang B (2017a) Complex wave propagation revealed by peak ground velocity maps in the Caucasus Area. Seismol Res Lett 88(3):812–821
Legendre C, Tseng T, Zhao L (2020) Surface-wave phase-velocity maps of the Anatolia region (Turkey) from ambient noise tomography. J Asian Earth Sci 193:104322
Legendre C, Zhao L, Chen Q-F (2015a) Upper-mantle shear-wave structure under east and southeast Asia from automated multimode inversion of waveforms. Geophys J Int 203(1):707–719
Legendre CP, Deschamps F, Zhao L, Chen Q-F (2015b) Rayleigh-wave dispersion reveals crust-mantle decoupling beneath eastern tibet. Sci Rep 5(1):1–7
Legendre CP, Tseng T-L, Chen Y-N, Huang T-Y, Gung Y-C, Karakhanyan A, Huang B-S (2017b) Complex deformation in the Caucasus region revealed by ambient noise seismic tomography. Tectonophysics 712:208–220
Legendre CP, Zhao L, Huang W-G, Huang B-S (2015c) Anisotropic Rayleigh-wave phase velocities beneath northern Vietnam. Earth Planets Space 67(1):1–16
Legendre CP, Zhao L, Tseng T-L (2021) Large-scale variation in seismic anisotropy in the crust and upper mantle beneath Anatolia, Turkey. Commun Earth Environ 2(1):1–7
Li Z, Meier M-A, Hauksson E, Zhan Z, Andrews J (2018) Machine learning seismic wave discrimination: application to earthquake early warning. Geophys Res Lett 45(10):4773–4779
Liu Y, Teng J, Xu T, Wang Y, Liu Q, Badal J (2017) Robust time-domain full waveform inversion with normalized zero-lag cross-correlation objective function. Geophys J Int 209(1):106–122
Lou, X., Van Der Lee S, Lloyd S (2013) AIMBAT: a python/matplotlib tool for measuring teleseismic arrival times. In AGU fall meeting abstracts, vol 2013, pp IN51B–1547
Maity D, Aminzadeh F, Karrenbach M (2014) Novel hybrid artificial neural network based autopicking workflow for passive seismic data. Geophys Prospect 62(4-Vertical Seismic Profiling and Microseismicity Frontiers):834–847
McNamara D, Hutt C, Gee L, Benz HM, Buland R (2009) A method to establish seismic noise baselines for automated station assessment. Seismol Res Lett 80(4):628–637
McNamara DE, Buland RP (2004) Ambient noise levels in the continental United States. Bull Seismol Soc Am 94(4):1517–1527
Milkov AV (2005) Global distribution of mud volcanoes and their significance in petroleum exploration as a source of methane in the atmosphere and hydrosphere and as a geohazard. Mud Volcanoes, geodynamics and seismicity, pp 29–34
Mittal H, Kumar A (2015) Stochastic finite-fault modeling of M w 5.4 earthquake along Uttarakhand–Nepal border. Nat Hazards 75(2):1145–1166
Mittal H, Wu Y-M, Lin T-L, Legendre CP, Gupta S, Yang BM (2019a) Time-dependent shake map for Uttarakhand Himalayas, India, using recorded earthquakes. Acta Geophys 67(3):753–763
Mittal H, Wu Y-M, Sharma ML, Yang BM, Gupta S (2019b) Testing the performance of earthquake early warning system in northern india. Acta Geophys 67(1):59–75
Mogren S (2021) Geo-hazard assessment of the NEOM area, Northwest Saudi Arabia, using seismological and potential field data. Arab J Geosci 14(2):1–12

Molchan GM (1997) Earthquake prediction as a decision-making problem. Pure Appl Geophys 149(1):233–247
Molnar S, Cassidy J, Castellaro S, Cornou C, Crow H, Hunter J, Matsushima S, Sánchez-Sesma F, Yong A (2018) Application of microtremor horizontal-to-vertical spectral ratio (MHVSR) analysis for site characterization: state of the art. Surv Geophys 39(4):613–631
Molnar S, Sirohey A, Assaf J, Bard P-Y, Castellaro S, Cornou C, Cox B, Guillier B, Hassani B, Kawase H et al (2022) A review of the microtremor horizontal-to-vertical spectral ratio (MHVSR) method. J Seismol 1–33
Monteiller V, Beller S, Plazolles B, Chevrot S (2021) On the validity of the planar wave approximation to compute synthetic seismograms of teleseismic body waves in a 3-D regional model. Geophys J Int 224(3):2060–2076
Mousavi SM, Beroza GC (2022) Deep-learning seismology. Science 377(6607):eabm4470
Mousavi SM, Sheng Y, Zhu W, Beroza GC (2019) Stanford EArthquake Dataset (STEAD): a global data set of seismic signals for AI. IEEE Access 7:179464–179476
Nolet G, Dahlen F (2000) Wave front healing and the evolution of seismic delay times. J Geophys Res Solid Earth 105(B8):19043–19054
Parolai S, Lai CG, Dreossi I, Ktenidou O-J, Yong A (2022) A review of near-surface QS estimation methods using active and passive sources. J Seismol 1–40
Pedersen HA, Leroy N, Zigone D, Vallée M, Ringler AT, Wilson DC (2020) Using component ratios to detect metadata and instrument problems of seismic stations: examples from 18 yr of GEOSCOPE data. Seismol Res Lett 91(1):272–286
Petersen G (2021) Source studies of small earthquakes in the AlpArray: CMT inversion, seismotectonic analysis and methodological developments. PhD thesis, Universität Potsdam Potsdam
Peterson JR (1993) Observations and modeling of seismic background noise. Technical report, US Geological Survey
Ringler AT, Evans JR (2015) A quick SEED tutorial. Seismol Res Lett 86(6):1717–1725
Ringler AT, Hagerty M, Holland J, Gonzales A, Gee LS, Edwards J, Wilson D, Baker AM (2015) The data quality analyzer: a quality control program for seismic data. Comput Geosci 76:96–111
Ringler AT, Hutt CR, Persefield K, Gee LS (2013) Seismic station installation orientation errors at ANSS and IRIS/USGS stations. Seismol Res Lett 84(6):926–931
Rivera D, Meli R, Sánchez R, Orozco B (2008) Evaluation of the measured seismic response of the Mexico City Cathedral. Earthq Eng Struct Dynam 37(10):1249–1268
Roden R, Smith T, Sacrey D (2015) Geologic pattern recognition from seismic attributes: Principal component analysis and self-organizing maps. Interpretation 3(4):SAE59–SAE83
Rowe CA, Aster RC, Borchers B, Young CJ (2002) An automatic, adaptive algorithm for refining phase picks in large seismic data sets. Bull Seismol Soc Am 92(5):1660–1674
Sandhu M, Sharma B, Mittal H, Yadav R, Kumar D, Teotia S (2020) Simulation of strong ground motion due to active Sohna fault in Delhi, national capital region (NCR) of India: an implication for imminent plausible seismic hazard. Nat Hazards 104(3):2389–2408
Siahkoohi A, Kumar R, Herrmann F (2018) Seismic data reconstruction with generative adversarial networks. In 80th EAGE conference and exhibition 2018, vol 2018. European Association of Geoscientists & Engineers, pp 1–5
Sipkin SA (1982) Estimation of earthquake source parameters by the inversion of waveform data: synthetic waveforms. Phys Earth Planet Inter 30(2–3):242–259
Slovenian Environment Agency (1990) Seismic network of the Republic of Slovenia. Int Fed Digital Seismogr Netw. https://doi.org/10.7914/SN/SL
Stein S, Geller RJ, Liu M (2012) Why earthquake hazard maps often fail and what to do about it. Tectonophysics 562:1–25
Strollo A, Cambaz D, Clinton J, Danecek P, Evangelidis CP, Mar- mureanu A, Ottemöller L, Pedersen H, Sleeman R, Stammler K et al (2021) EIDA: the European integrated data archive and service infrastructure within ORFEUS. Seismol Res Lett 92(3):1788–1795
Swiss Seismological Service (SED) At ETH Zurich (1983) National seismic networks of Switzerland. ETH Zürich. https://doi.org/10.12686/sed/networks/ch

VanDecar J, Crosson R (1990) Determination of teleseismic relative phase arrival times using multi-channel cross-correlation and least squares. Bull Seismol Soc Am 80(1):150–169
Vecsey L, Plomerová J, Jedlička P, Munzarová H, Babuška V, Group AW et al (2017) Data quality control and tools in passive seismic experiments exemplified on the Czech broadband seismic pool MOBNET in the AlpArray collaborative project. Geosci Instrument Methods Data Syst 6(2):505–521
Wang Q, Shen Y, Fu L, Li H (2020) Seismic data interpolation using deep internal learning. Explor Geophys 51(6):683–697
Wege S, Legendre CP, Chi W-C, Wang TK, Kunath P, Liu C-S (2022d) Field and synthetic waveform tests on using large-offset seismic streamer data to derive shallow seabed shear-wave velocity and geotechnical properties. Earth Space Sci 9(6):e2021EA002196
Wei Q, Li X (2022) Big gaps seismic data interpolation using conditional Wasserstein generative adversarial networks with gradient penalty. Explor Geophys 53(5):477–486
Wessel P, Luis J, Uieda L, Scharroo R, Wobbe F, Smith W, Tian D (2019) The generic mapping tools version 6 (6.3.0). Geochem Geophys Geosyst 20(11):5556–5564
Wu Y-M, Kanamori H (2005) Rapid assessment of damage potential of earthquakes in Taiwan from the beginning of P waves. Bull Seismol Soc Am 95(3):1181–1185
Wüstefeld A, Bokelmann G, Zaroli C, Barruol G (2008) SplitLab: a shear-wave splitting environment in Matlab. Comput Geosci 34(5):515–528
Yu C, Zheng Y, Shang X (2017) Crazyseismic: a MATLAB GUI-based software package for passive seismic data preprocessing. Seismol Res Lett 88(2A):410–415
Yu J, Wu B (2021) Attention and hybrid loss guided deep learning for consecutively missing seismic data reconstruction. IEEE Trans Geosci Remote Sens 60:1–8
Zaccarelli R, Bindi D, Strollo A (2021) Anomaly detection in seismic data–metadata using simple machine-learning models. Seismol Res Lett 92(4):2627–2639
ZAMG - Zentralanstalt für Meterologie und Geodynamik (1987) Austrian seismic network. International Federation of Digital Seismograph Networks. https://doi.org/10.7914/SN/OE
Zhang J, Hao J, Zhao X, Wang S, Zhao L, Wang W, Yao Z (2016) Restoration of clipped seismic waveforms using projection onto convex sets method. Sci Rep 6(1):1–10

Chapter 5
Use of Geophysical Techniques in Seismic Hazard Assessment and Microzonation

Sumer Chopra, Pallabee Choudhury, Rakesh Nikam, Peush Chaudhary, Harsh Limbachiya, and Vishwa Joshi

Abstract Seismic hazard assessment is a process that involves extensive geological, geophysical and geotechnical studies of a region where such studies are required. In such an endeavour, we need to model three main contributing factors, source, path and site effects. The passive geophysical techniques play a significant role in providing important inputs for modelling source, path and site effects. The main advantages of geophysical techniques are that they are mostly non-destructive, efficient, cost-effective and well-proven in the last 50 years. Geophysical techniques such as Gravity and Magnetotelluric (MT) contribute largely to the detection and characterization of possible local seismic faults, both, exposed and blind, in other words, characterization of the source. It is found that near surface shear-wave velocity helps in estimating the local site effect. Mostly, shallow geophysical surveys like multi-channel analysis of surface waves (MASW) or down-hole/up-hole/cross-hole surveys constrain the shear-wave velocity. Time-domain electromagnetic (TDEM), resistivity imaging and microtremor techniques are becoming popular in constraining structures up to few hundred of metres. The MASW surveys are implemented for obtaining 1D and 2D models of shear-wave velocities at a site in microzonation and site-specific studies. The microtremor is another geophysical technique that was earlier used to map predominant periods of a site under investigation, is now actively used to obtain 1D and 2D structures up to a few hundred metres by modelling horizontal-to-vertical ratio (HVSR) curves. The use of geophysical methods in resolving the dips of major active faults and segregation of major lithological units in the Kachchh rift is provided as case study. The integrated geophysical approach is also discussed in resolving the depth of engineering bed layer in Ahmedabad.

Keywords Seismic microzonation · Multi-channel analysis of surface waves · Microtremor · Time-domain electromagnetic · Magnetotelluric

S. Chopra (✉) · P. Choudhury · R. Nikam · P. Chaudhary · H. Limbachiya · V. Joshi
Institute of Seismological Research, Gandhinagar, Gujarat, India
e-mail: sumerchopra@isr.res.in

Sandeep et al. (eds.), *Geohazards*, Advances in Natural and Technological Hazards Research 53, https://doi.org/10.1007/978-981-99-3955-8_5

5.1 Introduction

Earthquakes are considered to be one of the most destructive natural hazards that cause huge losses in terms of lives, property and economy within few minutes of its occurrence. Inspite of many advances in the current scientific knowledge, it is not possible to predict or forecast earthquakes in terms of size, time and space. Therefore, it is necessary to undertake the alternative measures to mitigate the effect of earthquakes. The assessment of seismic hazard with reasonable prediction of the level of ground motions expected at a site is necessary to reduce losses and building safe environ. The seismic hazard assessment is a complex exercise and involves modelling of source, path and site to model ground motions that are expected at a site of interest during large earthquakes. In the first two decades of the twenty-first century, two earthquakes of M ~9 have occurred (2005 Sumatra; 2011 Tohuku) with many large earthquakes (2010 Haiti; 2008 Sichuan; 2005 Muzafarabad; 2003 Bam; 2001 Bhuj; 2015 Gorkha; 2005 Nias; 2018 Sulawesi) that are responsible for extensive destruction to infrastructure and massive loss of lives.

There are three major steps involved in the assessment of seismic hazard at micro-level, termed as seismic microzonation. The first part consists of evaluation of the expected input motion, the second part is the estimation of local site effects through ground response analysis and finally preparation of microzonation maps depicting hazard, vulnerability and risk. This requires collection and analysis of a large amount of seismological, geological and geotechnical data. The concept of seismic microzonation is based on the fact that the intensity of ground shaking in certain frequency bands gets modified by the pile of unconsolidated sediments, or in a larger sense, local geological conditions alter the characteristics of ground motions. The damage pattern of many large earthquakes has demonstrated that local site condition plays an important role in modifying ground motions at a site. The role of local site effect on the pattern of damage has been noticed during 1985 Mexico, 1989 Loma Prieta, 1994 Northridge, 1995 Kobe earthquakes and 2001 Bhuj earthquake. The damage and loss of lives observed in these earthquakes have been directly related to local site conditions (Singh et al. 1988; Chang et al. 1996; Faccioli et al. 2002). During 2001 Bhuj earthquake, extensive damage is noticed in Ahmedabad, which is around 250 km from the epicentre (Jain et al. 2001). More recent example is 2015 Gorkha earthquake (Parameswaran et al. 2015).

The estimation of local site effect is a challenging problem among geoscientists involved in seismic microzonation. The geophysical surveys in the past 50 years have taken leaps and bound with the improvement in the resolution. Mostly, integrated geophysical techniques are performed to map sub-surface shallow and deep structures. The seismic, gravity, magnetic, resistivity and magneto-telluric (MT) surveys are generally used to map structures, folds and faults, which may help in identifying potential sources of large earthquakes. The most important parameter to quantify local site effect is the shear-wave velocity (V_S), which provides information about stiffness of the strata. The V_S is an important parameter for ground response analysis and ground motion prediction equations for estimating and is a proxy to local site

effect. The shallow geophysical surveys like multi-channel analysis of surface waves (MASW) or down-hole/up-hole/cross-hole surveys are used to measure shear-wave velocity. The microtremor is another geophysical technique that was earlier used to map predominant periods of a site under investigation, is now actively used to obtain 1D and 2D structures up to a few hundred metres by modelling horizontal-to-vertical ratio (HVSR) curves. The chapter describes the use of all these geophysical techniques for seismic hazard assessment.

5.2 Geophysical Techniques in Seismic Hazard Assessment

A number of geophysical techniques are available to map the subsurface from few tens of meters to tens of kilometres. The most important parameter that is required to measure the strength of the subsurface materials is the shear-wave velocity (V_S), which is an important parameter to characterize a site. Many geophysical tools are available to map V_S in the subsurface. The resolution and depth depend on the type of method adopted. The characterization of the source is also an important activity towards the assessment of seismic hazard and electromagnetic surveys like magnetotelluric (MT) and time domain electromagnetic (TDEM) may help in mapping shallow and deep faults and their orientations. These all techniques are described and discussed in subsequent paragraphs.

5.2.1 Multi-channel Analysis of Surface Waves

The multi-channel analysis of surface waves (MASW) is a non-invasive and the most popular geophysical method used in seismic hazard and microzonation studies. This technique was introduced by Park et al. (1999). It provides information about the stiffness of the ground in terms of shear-wave velocity (V_S). In this method, surface waves are generated by a sledge hammer, which are recorded on geophones spread along a profile. The propagation velocities are analysed and V_S is obtained. The information up to 25–30 m can be obtained from MASW (Park et al. 2007). Here, the dispersive properties of the surface waves are used to get 1D information beneath the ground. This is used to characterize the sites in terms of most commonly obtained parameter, V_{S30} (shear-wave velocity to 30 m depth). The V_{S30} is actively used in many ground prediction models as a site proxy. The MASW survey is successfully used to study damage pattern of large earthquakes, like 1956 Anjar and 2001 Bhuj earthquakes (Rastogi et al. 2011; Sairam et al. 2018). In these studies, the damages in Anjar town and Ahmedabad metropolitan city are analysed using MASW surveys in damaged and non-damaged sites. It is found that the damage regions have low V_{S30} as compared to non-damaged sites. Nowadays, passive MASW is also becoming popular, whereby information up to few hundreds of metres can be obtained. Here,

surface waves generated from natural sources like tides, winds, oceans etc. or anthropogenic sources, which generate energy in low frequencies, are used to map subsurface (Park et al. 2007). Other applications of MASW that are useful in assessing hazard are mapping bedrock, voids, shallow structures, estimating elastic moduli and soil properties.

5.2.2 Microtremor

Along with source and path effects, local site effects, also referred to as surface and subsurface geological and topographical conditions, have a significant impact on ground shaking and the damage it causes to engineered structures. It is well known that site-specific factors, including irregular surface topography to a lesser extent, can significantly affect the amplitude, frequency content and duration of the ground motion, which can have a significant impact on how severe the earthquake's damage is. Before taking site effects into account, the estimation of the seismic risk at a location of interest is not comprehensive.

The local site effect can be estimated using various methodologies, depending to the level of accuracy required and studying zoning level. The site responses can be estimated directly by carrying out geophysical surveys at points of interest. However, such geophysical surveys are both time-consuming and expensive. Thus, indirect, non-invasive methods were explored for rapidly estimating site responses. The use of the single-station spectral ratios technique is most popular for obtaining credible first-order estimates of predominant frequency and local amplification factors (Nogoshi and Igarashi 1971; Nakamura 1989; Lermo and Chavez-Garcia 1994; Panou et al. 2005; Langston et al. 2009; Parolai et al. 2010; Chopra et al. 2013). Popularly known as horizontal to vertical spectral ratio (HVSR) technique, this method estimates site response using spectral ratios of horizontal to vertical component records of ambient vibrations, termed as microtremors (Fig. 5.1a). The microtremors are short period vibrations that result from coastal effects, atmospheric loading, wind interaction with structures and vegetation and cultural sources. The bedrock overlying thick sediments reflects in the form of a peak in the HVSR spectrum (Fig. 5.1b). The frequency of this peak depends on the thickness of the sediments above bedrock. As the thickness of the sediments increases, the peak shifts from high to low frequency. The method is quite simple and cost-effective and has the ability to cover large areas. This made the method quite popular and it is now widely used in seismic hazard assessment and microzonation. Among various geophysical and geotechnical methods currently in use for microzonation, the Horizontal-to-Vertical Spectral Ratio (HVSR) method using microtremors has achieved high acceptability in the last decade (Bard 1999).

The analysis of the microtremor recording for site effect estimation has gained more interest in recent years, and it is commonly thought that both single station HVSR technique and multi-station (array) measurements may allow obtaining dynamical characteristics of the subsoil from the ambient vibration measurements (Wathelet et al. 2008; Bard 1999; Okada 2003). The HVSR curve can be modelled to

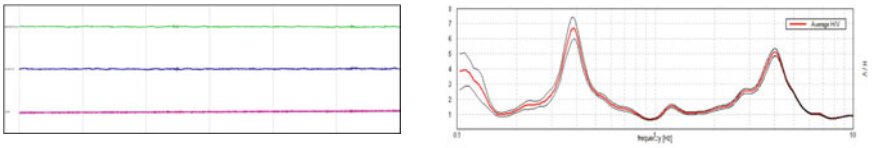

(a) (b)

Fig. 5.1 **a** A sample three-componet microtremor record from a site along with **b** HVSR curve

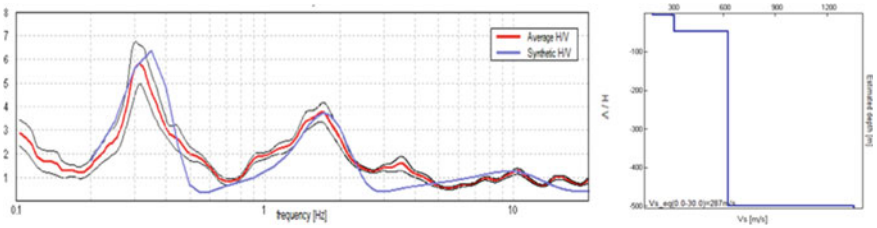

Fig. 5.2 Forward modelling of HVSR curve and 1D shear-wave velocity model at a site

obtain subsurface information and major stratigraphic boundaries in terms of shear-wave velocity (Fig. 5.2). In earthquake engineering field, the shear-wave velocity of the subsurface structure is considered as the key parameter for its influence on local ground motion behaviour. A theoretical H/V curve is fitted to the field H/V curve using either forward modelling or inversion technique to obtain the subsurface information. The constraints to initial model are provided by geotechnical data or some known information about local geology. For inversion, the ellipticity curve (Fig. 5.3) is extracted from the HVSR curve by applying the frequency-time analysis and thereby optimizing the horizontal and vertical amplitude components in the signal (Fäh et al. 2001, 2003). An initial model is assumed consisting of a number of layers. Each layer is defined with the P- and S-wave velocities, Poisson ratio and density. The neighbourhood algorithm may be used for the inversion to minimize the misfit between the observed and the modelled curve (Sambridge 1999; Wathelet et al. 2008).

5.2.3 Magnetotelluric Method

The magnetotellurics (MT) is a passive geophysical technique for imaging the electrically conductive structure of the Earth from the near-surface to the upper mantle and beyond by utilizing the naturally occurring electromagnetic field. The time-varying electric and magnetic fields are measured simultaneously in the orthogonal direction at the Earth's surface and their ratio (transfer function) provides the properties of the Earth (Tikhonov 1951; Cagniard 1953). The penetration depth of the

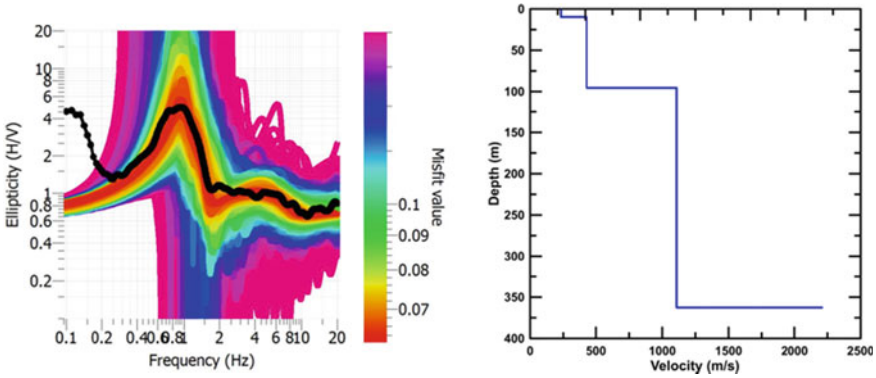

Fig. 5.3 Inversion of HVSR curve (black line shows observed HVSR and red is the best fit) and 1D shear-wave velocity model at a site

electromagnetic waves depends on the Earth's conductivity and the sounding period of the electromagnetic waves. The decay of the electromagnetic field is exponential as they diffuse in the medium and is given by the skin depth relationship. The conductive structures deeper than this skin depth are insensitive to electromagnetic waves. The period range used in the MT measurements is about ~10^{-4} to ~10^{5} s, while the resistivity range for most Earth materials is about 10^{-1} to 10^{5} Ω.m. This provides a skin depth ranging from shallow to the deep upper mantle. This broad range of depth penetration makes the MT method superior to other active EM and geophysical methods and can be used where the target range varies from shallow to deep. The time-varying electromagnetic waves are generated by different natural phenomena. For frequencies higher than 1 Hz, meteorological activity such as lightning discharges is the main source while the interaction between the solar plasma and the Earth's magnetic field generates frequencies lower than 1 Hz. For data acquisition, magnetometers or Induction coils are used that sense the magnetic fields, while for sensing electric fields non-polarizing electrodes (such as Pb-$PbCl_2$) are used. The Induction coil and electrodes are connected to the main recording unit. The recorded MT data are subjected to processing (elimination of bad data points), analysis (dimensionality and directionality) and finally inversion (1D/2D/3D). Various inversion techniques are proposed for 1D inversion (Constable et al. 1987), 2D inversion (deGrooth-Hedlin and Constable 1990; Rodi and Mackie 2001) and 3D inversion (Siripunvaraporn et al. 2005; Egbert and Kelbert 2012; Kelbert et al. 2014). The final resistivity section, obtained after inversion, reflects the geological features/process of the study region.

The MT method is a proven method and is used worldwide not only for academic (tectonic studies, geological and fault mapping, hazard, earthquake studies etc.) but also for commercial (Hydrocarbons, Minerals, Geothermal, Groundwater survey etc.) purposes. Recently, it has been used for seismic hazard estimation also (Aizawa et al. 2017; Mohan et al. 2018a, b; Lu et al. 2019; Rastogi et al. 2023). MT is used to characterize the fault, which is required for estimating the associated seismic hazard.

The geometry of the fault plays a critical role in the seismic hazard; therefore, it is highly important to image the actual geometry of the fault system. However, since the prediction of any earthquake precisely is not possible, the hazard and risk associated with it can be calculated to minimize the loss during the earthquake. In the present scenario, where urbanization is rapidly expanding and multiple high-rise buildings and mega structures are constructed, MT is highly useful for subsurface mapping followed by the associated seismic hazard.

In Kachchh intraplate region of Gujarat, MT has been successfully used to constrain the dip of an active Kachchh Mainland fault (KMF). The dip of KMF is an enigma as various researchers proposed different dips associated with KMF (Biswas 2005; Mandal et al. 2007, 2016; Rastogi et al. 2014; Pande, 2003). The KMF is a major fault having an extension of more than 150 km. This fault is segmented by the various transverse faults. KMF is seismically active (Morino et al. 2008) and a major source of seismic hazard for western India (Rastogi et al. 2013; Chopra et al. 2012; Mohan 2014). To characterize the KMF, a MT study has been carried out by Mohan et al. (2010, 2015) in the eastern part and Mohan et al. (2018) in the western part. In the eastern part, MT data were recorded along two distinct profiles. The final inverted resistive section shows the south-dipping nature of the KMF fault (Fig. 5.4a). In the western part, MT data along a single profile across KMF is acquired. The resistivity section of this profile (Fig. 5.4b) shows that the nature of KMF is north-dipping. Hence, it is observed that the same fault has a different dip direction as evidenced by the MT method. It is observed that transverse faults are capable of changing the dip of the fault (Nicholson et al. 1986; Ron et al. 1986; Lamb 1989). The geometry of the fault such as discontinuities and dip influence the earthquake magnitudes (King and Nabelek 1985; Wesnousky 2008). According to Fialko (2006), the rupture that takes place along the dipping fault segment can produce 2–3 times larger ground shaking compared to the footwall. Similarly, the distribution of strain on several adjacent faults instead of a primary fault influences the resulting ground motion (Lozos 2016). According to Mohan et al. (2018b), the estimated peak ground acceleration (PGA) has a strong dependency on the dip of the fault, which again affects the associated seismic hazard assessment across a fault. In addition to this, identification of the blind faults (having no expression on the surface) is also a challenge for estimation of the hazard and risk. The conductor C2 (in Fig. 5.4b) named as Ulat-Kotda fault is identified with the MT method. This fault shows no expression on the Earth's surface. Thus, MT method is highly useful for mapping the fault geometry and identification of blind faults. Since faults are the main source of seismic hazard, hence a detailed mapping is required for hazard and loss estimation where MT surveys help in delineating faults and their orientation.

5.2.4 Time Domain Electromagnetic Method

The time domain electromagnetic method (TDEM) is a nondestructive, cost-effective and time-consuming technique, which is widely used to image shallow subsurface

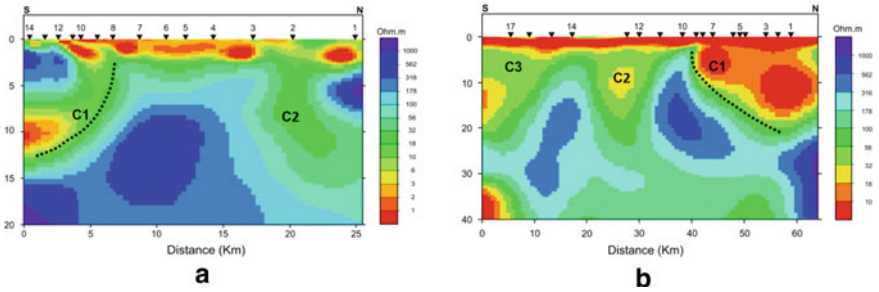

Fig. 5.4 Resistivity section across the KMF **a** Eastern part. C1: KMF, C2: SWF **b** Western part. C1: KMF, C2: Ulat-Kotda fault, C3: KHF (modified after Mohan et al. 2018a)

structures, fault zone studies, paleo-channel identification, liquefaction zone identification, mineral exploration and aquifer mapping. The TDEM method can reach several hundred metres depth depending upon the lithological conductivity of the terrain and is the most effective and sensitive method for detecting conductive ores, seawater intrusion, paleo-channels and liquefaction zones. During the survey, when the current is passed through a transmitter wired loop, which is interrupted or switched off at a specific time, the current rapid decays and dissipates into the ground, generating induced eddy current by the time-varying secondary magnetic field. These secondary magnetic field amplitude and decay rate are recorded at the surface and analysed in terms of how electrical resistivity varies with depth (McNeill 1994).

The TDEM method is successfully employed to map subsurface characteristic of the Kachchh Mainland Fault (KMF) in Kachchh region of Gujarat (Nikam et al. 2022). A total 26 TDEM sites were acquired that spread over three profiles across the KMF fault zone (Fig. 5.5a). The resistivity sections of the three profiles decipher information up to depth of 250 m. The resistivity sections across the KMF indicate heterogeneous structure of the fault zone. The shallow subsurface geometry of the KMF zone shows a sharp resistivity contrast between the Mesozoic rocks and the Quaternary alluvium overlain on Tertiary rocks (Fig. 5.5b). This shows that the TDEM technique can identify the subsurface geometry of the faults and earthquake-related structures (Pavankumar et al. 2018). This study has a big impact on how future seismic hazard risk and hazard mitigation models for the Kachchh region are developed.

5.2.5 Electrical Resistivity Tomography (ERT)

The DC electrical resistivity method involves delivering an electric current between a pair of outer electrodes and measuring the potential difference between a pair of inner electrodes to determine the electrical resistance. In homogenous ground, the electrode separation determines the depth of current penetration, and changing the

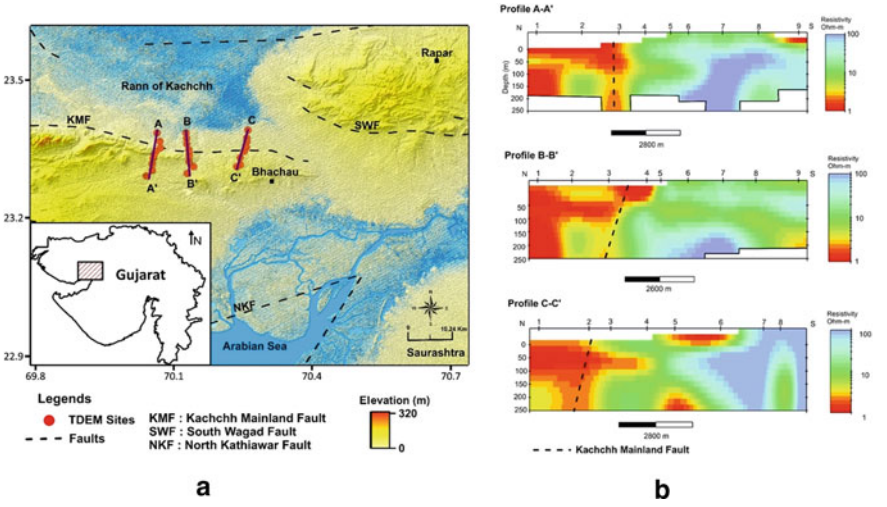

Fig. 5.5 **a** Tectonic map of the Kachchh, Gujarat **b** Geoelectric resistivity sections across the three N-S profiles (modified after Nikam et al. 2022)

electrode separation reveals the ground's stratification. There are a few techniques for arranging electrodes, including the Wenner method, the Schlumberger technique, pole-pole, dipole–dipole and pole-dipole techniques. A new development in the electrical resistivity method is the use of 2-D Electrical Resistivity Tomography (ERT). The ERT is used to map the true resistivity variation of the sub-surface litho-units continuously along the line of the profile, in which multiple electrodes are maintained in a straight line with a consistent spacing between the inner electrodes. In lithological studies, the ERT is widely used in sub-surface geological formations. The ERT technique is widely used in mineral exploration, geo-engineering projects and structural studies like faults, folds and dykes. In general, the ERT technique is used for shallow and intermediate depth applications down to approximately 250 m. The automated acquisition of large amount of data in optimal time and cost, presentation of images of sub-surface litho units along the entire spread length with high resolution due to mapping of same location a number of times for different electrode spacing are some of the major advantages of ERT. The ERT is an important technique to delineate the sub-surface geometry of buried sand bodies like paleo-channels (Sinha et al. 2013). The electrical resistivity data were first analysed in terms of physical factors, such as resistivity and formation thickness, and then these parameters were integrated with the available lithological data to understand the underlying stratigraphy. In general, loose sediment having low resistivity and compact sediments shows high resistivity, this resistivity contrast is useful for basement analysis.

The eastern part of the Kachchh region is seismically active zone. After 2001 Bhuj earthquake (Mw7.7), thrust movement of western extension of the E-W South Wagad Fault (SWF) have been reported near Chobari village (McCalpin and Thakkar 2003). In this sedimentary terrain, the Tertiary sandstone is present beneath the

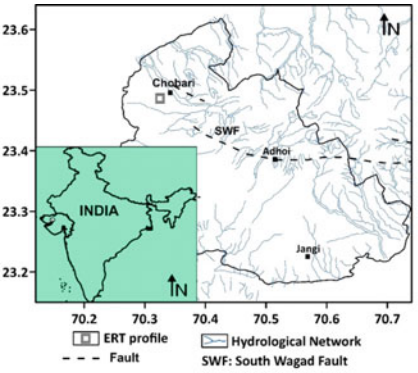

(a)

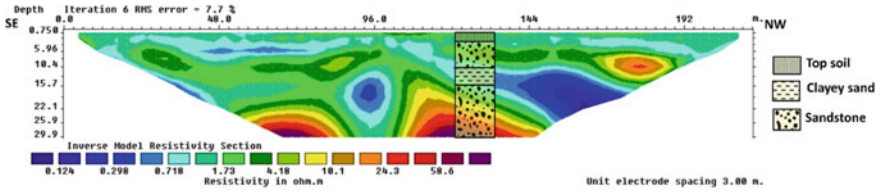

(b)

Fig. 5.6 **a** Geomorphological map study area, and **b** Two-dimensional resistivity section

thick alluvium (Fig. 5.6b). Some clayey sand layers were also identified. The ERT survey is performed and Wenner—Schlumberger combined electrodes arrangement were used. The ERT profile is 216 m long with 3 m interval electrode spacing. The resistivity section is correlated with available borehole data of this region (Fig. 5.6b). The resistivity section of the profile shows that the top layer (0–4 m) is of loose soil with resistivity in the range 1–2 Ωm. Beneath this, the sandstone layer is present, having thickness of 8 m with resistivity in the range 2–70 Ωm. The clayey sand layer is present between two sandstone layers having a thickness of 6 m with resistivity > 1Ωm. Below that, sandstone layer is present. This information is useful for the basement studies.

5.2.6 Borehole Logging

In this method, the seismic waves are generated inside or outside a borehole and are measured by geophones kept near the borehole or inside the borehole depending upon the method. In down-hole survey, the source is kept near the borehole and the geophone is lowered in the borehole at successive depths after every shot to obtain

the V_S. Whereas in up-hole survey, the geophone is kept near the borehole and source in the borehole. In cross-hole survey, two or more boleholes are used where one is used for source, and other is used for recording seismic waves using geophones. In suspension logging, both source and receivers are inside the boreholes. Among all these logging methods, down-hole and cross-hole surveys are more popular. The borehole logging method has more vertical resolution than the surface-based methods like MASW. It is also useful in detecting low-velocity layers under a high-velocity layer.

5.3 Discussions

The assessment of seismic hazard at a site involves basically modelling of source, path and site effects. It is seen that various geophysical techniques are useful in mapping structures to constrain the sources (Table 5.1). The length and width of a fault play an important role in estimating the maximum magnitude expected from a fault whereas its dip has implications in severity of ground motions. It has been observed that sites located on the hanging wall of a causative fault are more prone to damage as they experience more accelerations in comparison to sites located on the footwall side. It is observed that MT survey is very useful in constraining the widths and dips of faults, capable of generating large earthquakes. The estimation of V_S is an integral part of any seismic microzonation project. Here geophysical techniques like MASW, microtremor and velocity logging can be used. In assessing seismic hazard in urban areas, non-invasive techniques are useful and in old city areas where finding space for carrying out drilling or other invasive geophysical surveys are difficult, microtremor surveys are very useful in estimating V_S. Mohan et al. (2021) used geophysical techniques to constrain the engineering bed layer (EBL) for seismic microzonation studies of Ahmedabad city in Gujarat, India. Here, geophysical techniques like MASW, PS-Logging, Deep Seismic Studies (DSS) and microtremor were used to map the distribution of EBL in the city. A comparison of various geophysical techniques is provided in Table 5.1. The assessment of seismic hazard with reasonable level of accuracy is a challenging problem and an integrated approach using a variety of geophysical surveys can reduce the uncertainties involved in the exercise.

Table 5.1 Comparison of various geophysical techniques used for seismic hazard assessment

Method	Parameter measured	Penetration depth	Resolution	Application in seismic hazard	Time for survey
Multi-channel analysis of surface waves (MASW)	Shear-wave velocity	25–30 m	Good	• 1D and 2D shear-wave velocity distribution • Site characterization	1–2 h per site
Microtremor	Shear-wave velocity	100–500 m	Good	• Identification of major stratigraphic boundaries • Basement mapping	1–2 h per site
Magnetotelluric	Resistivity	10–50 km	Good to fair	• Identification of buried faults • Mapping of faults • Width and dip of fault	24–72 h depending upon depth of interest
Borehole logging	Primary and Shear-wave velocity	100 m	Very good	• 1D shear-wave velocity distribution • Identifying various layers • Site characterization	2 days for drilling boreholes and around 2 h for measurement
Time domain electromagnetic and electrical resistivity tomography	Resistivity	200–750 m	Good	• Near surface fault identification • Identification of soil layers • Identification of paleochannels	2 h per site

References

Aizawa K, Asaue H, Koike K, Takakura S, Utsugi M, Inoue H, Yoshimura R, Yamazaki KI, Komatsu S, Uyeshima M, Koyama T (2017) Seismicity controlled by resistivity structure: the 2016 Kumamoto earthquakes, Kyushu Island, Japan. Earth, Planets and Space 69(1):1–10

Bard P-Y (1999) Microtremor measurements: a tool for site effect estimation? In: Irikurak K, Kudok K, Okadah H, Sasatanit T (eds) The effects of surface geology on seismic motion. Balkema, Rotterdam p, pp 1251–1279

Biswas SK (2005) A review of structure and tectonics of Kutch basin, western India, with special reference to earthquakes. Curr Sc 88(10):1592–1600

Cagniard L (1953) Basic theory of the magneto-telluric method of geophysical prospecting. Geophysics 18(3):605–635

Chang SW, Bray JD, Seed RB (1996) Engineering implications of ground motions from the northridge earthquake. Bull Seismol Soc Am 86(1B):270–288
Chopra S, Kumar D, Rastogi BK, Choudhury P, Yadav RBS (2012) Deterministic seismic scenario for Gujarat region, India. Nat Haz 60(2):517–540
Chopra S, Kumar D, Rastogi BK, Choudhury P, Yadav RBS (2013) Estimation of site amplification functions in Gujarat region, India. Nat Haz 65(2):1135–1155
Constable SC, Parker RL, Constable CG (1987) Occam's inversion: a practical algorithm for generating smooth models from electromagnetic sounding data. Geophys 52(3):289–300
deGroot-Hedlin C, Constable S (1990) Occam's inversion to generate smooth, two-dimensional models from magnetotelluric data. Geophys 55(12):1613–1624
Egbert GD, Kelbert A (2012) Computational recipes for electromagnetic inverse problems. Geophy J Int 189(1):251–267
Faccioli E, Vanini M, Frassine L (2002) Complex site effects in earthquake ground motion, including topography. In 12th European conference on earthquake engineering, Elsevier Science Ltd. Paper No 844, p 23
Fäh D, Kind F, Giardini D (2001) A theoretical investigation of average H/V ratios. Geophys Jour Int 145(2):535–549
Fäh D, Kind F, Giardini D (2003) Inversion of local S-wave velocity structures from average H/V ratios, and their use for the estimation of site-effects. J Seismol 7(4):449–467
Fialko Y (2006) Interseismic strain accumulation and the earthquake potential on the southern San Andreas fault system. Nature 441(7096):968–971
Jain SK, Murty CVR, Dayal U, Arlekar, JN, Chaubey SK (2001) The republic day earthquake in the land of M K Gandhi, The Father of the Nation, an EERI publication
James M, Thakkar M (2003) 2001 Bhuj-Kachchh earthquake: Surface faulting and its relation with neotectonics and regional structures, Gujarat, Western India. Annal Geophys 46:2003. https://doi.org/10.4401/ag-3463
Kelbert A, Meqbel N, Egbert GD, Tandon K (2014) ModEM: a modular system for inversion of electromagnetic geophysical data. Comput Geosci 66:40–53
King G, Nábělek J (1985) Role of fault bends in the initiation and termination of earthquake rupture. Science 228(4702):984–987
Kühn D, Ohrnberger M, Dahm T (2011) Imaging a shallow salt diapir using ambient seismic vibrations beneath the densely built-up city area of Hamburg, Northern Germany. J Seismol 15:507–531
Lamb S (1989) Rotations about vertical axes in part of the New Zealand plate-boundary zone, theory and observation. In Paleomagnetic Rotations and Continental Deformation Springer, Dordrecht, pp 473–488
Langston CA, Shu-Chioung CC, Lawrence Z, Bodin P, Horton S (2009) Array observations of microseismic noise and the nature of H/V in the Mississippi embayment. Bull Seismol Soc Am 99(5):2893–2911
Lermo J, Chavez-Garcia FJ (1994) Are microtremors useful in site response evaluation? Bull Seismol Soc Am 83:1574–1594
Lozos JC (2016) A case for historic joint rupture of the San Andreas and San Jacinto faults. Sci Adv 2(3):e1500621
Lu R, Liu Y, Xu X, Tan X, He D, Yu G, Cai M, Wu X (2019) Three-dimensional model of the lithospheric structure under the eastern Tibetan Plateau: implications for the active tectonics and seismic hazards. Tectonics 38(4):1292–1307
Mandal P (2016) Variations of seismic velocities in the Kachchh rift zone, Gujarat, India, during 2001–2013. Tectonophysics 672:68–86
Mandal P, Chadha RK, Raju IP, Kumar N, Satyamurty C, Narsaiah R, Maji A (2007) Coulomb static stress variations in the Kachchh, Gujarat, India: Implications for the occurrences of two recent earthquakes (M w= 5.6) in the 2001 Bhuj earthquake region. Geophy J Int 169(1):281–285
McNeill JD (1994) Principles and application of time domain electromagnetic techniques for resistivity sounding. Technical Note TN-27, Geonics Ltd., Ontario

Mohan K (2014) Seismic-hazard assessment in the Kachchh region of Gujarat (India) through deterministic modeling using a semi-empirical approach. Seismol Res Lett 85(1):117–125

Mohan K, Chaudhary P, Patel P. Chopra S (2018a) can dip reversal happen along a major fault?-A magnetotelluric study in Kachchh, Western India. In AGU fall meeting abstracts, vol 2018, pp T23B–0373

Mohan K, Chaudhary P, Patel P, Dugar S, Chopra S (2018b) Kachchh Mainland fault: Characterization and associated Seismic hazard. In National conference and field workshop on Recent studies on the Geology of Kachchh basin

Mohan K, Rastogi BK, Chaudhary P (2015) Magnetotelluric studies in the epicenter zone of 2001, Bhuj earthquake. Jour Asian Eart Sc 98:75–84

Mohan K, Sastry RS, Harinarayana T, Rastogi BK (2010) New findings in the epicenter zone of 2001, Kachchh Earthquake using magnetotelluric studies. In As abstract in the proceedings of 7th Annual Meeting of Asia Oceania Geoscience Society (AOGS) during 5–9 July 2010

Mohan K, Dugar S, Pancholi V, Dwivedi V, Chopra S, Sairam B (2021) Micro-seismic hazard assessment of Ahmedabad city, Gujarat (Western India) through near-surface characterization/soil modeling. Bull Earthq Eng 19:623–656

Morino M, Malik JN, Ansari K, Bhuiyan C, Mishra P, Kaneko F (2008) Active low-angle reverse fault and wide Quaternary deformation identified in Jhura trench across the Kachchh Mainland Fault, Kachchh, Gujarat, India. Active Fault Res 29:71–78

Nakamura Y (1989) A method for dynamic characteristic estimation of subsurface using microtremors on the ground surface. Railway Tech Res Inst Q Rep 30:25–33

Nicholson C, Seeber L, Williams P, Sykes LR (1986) Seismic evidence for conjugate slip and block rotation within the San Andreas fault system, southern California. Tectonics 5(4):629–648

Nikam R, Chopra S, Kumar GP et al (2022) Investigation of hydrological characteristics of the Kachchh Mainland Fault (KMF) Zone, Gujarat, Western India using time domain electromagnetic study. J Earth Syst Sci 131:248

Nogoshi M, Igarashi T (1971) On the amplitude characteristics of microtremor (part 2). J Seismol Soc Jpn 24:26–40

Okada H (2003) The microtremor survey method, geophysical monograph No. 12, Soc. Exploration Geophysicists, Tulsa, OK

Pande P (2003) Seismotectonic framework of the region and source mechanism of Kutch earthquake-2001. Geol Survey of Ind Spl Publ 76:225–233

Panou AA, Theodulidis N, Hatzidimitriou P, Stylianidis K, Papazachos CB (2005) Ambient noise horizontal-to-vertical spectral ratio in site effects estimation and correlation with seismic damage distribution in urban environment: the case of the city of Thessaloniki (Northern Greece). Soil Dyn Earthq Eng 25:261–274

Parameswaran RM, Natarajan T, Rajendran K, Rajendran CP, Mallick R, Wood M, Lekhak HC (2015) Seismotectonics of the April–May 2015 Nepal earthquakes: an assessment based on the aftershock patterns, surface effects and deformational characteristics. J Asian Eart Sc 111:161–174

Park CB, Miller RD, Xia J (1999) Multichannel analysis of surface waves. Geophysics 64(3):800–808

Park CB, Miller RD, Xia J, Ivanov J (2007) Multichannel analysis of surface waves (MASW)—active and passive methods. Lead Edge 26(1):60–64. Kansas Geological Survey, Lawrence, USA

Parolai S, Bindi D, Ansal A, Kurtulus A, Strollo A, Zschau J (2010) Determination of shallow S-wave attenuation by down-hole waveform deconvolution: a case study in Istanbul (Turkey). Geophy J Int 181(2):1147–1158

Pavankumar G, Chaudhary I, Nagar M, Chauhan A, Prizomwala SP, Mahesh P, Chopra S (2018) Transient electromagnetic investigations in a tectonic domain of the Kachchh Intraplate Region, Western India: A morphotectonic study of the Kachchh mainland fault. Tectonics. https://doi.org/10.1029/2017TC004884

Rastogi BK, Aggrawal SK, Rao N, Choudhury P (2013) Triggered/migrated seismicity due to the 2001 M w7. 7 Bhuj earthquake, Western India. Nat Haz 65(2):1085–1107
Rastogi BK, Mandal P, Biswas SK, Talwani P (2014) Seismogenesis of earthquakes occurring in the ancient rift basin of Kachchh, Western India. Intraplate earthquakes, pp 126–161
Rastogi BK, Mohan K, Sairam B, Singh AP, Pancholi V (2023) Geotechnical, geological and geophysical investigations for seismic microzonation and site-specific earthquake hazard analysis in Gujarat. Advances in earthquake geotechnics. Springer, Singapore, pp 73–91
Rastogi BK, Singh AP, Sairam B et al (2011) The possibility of site effects: the anjar case, following past earthquakes in Gujarat, India. Seismol Res Lett 82:59–68
Rodi W, Mackie RL (2001) Nonlinear conjugate gradients algorithm for 2-D magnetotelluric inversion. Geophysics 66(1):174–187
Ron H, Aydin A, Nur A (1986) Strike-slip faulting and block rotation in the Lake Mead fault system. Geology 14(12):1020–1023
Sairam B, SinghAP PV, Pancholi V, Chopra S, Dwivedi VK, Kumar MR (2018) Influence of local site effects in the Ahmedabad mega city on the damage due to past earthquakes in Northwestern India. Bull Seismol Soc Am 108(4):2170–2182
Sambridge M (1999) Geophysical inversion with a neighbourhood algorithm-I. Searching a parameter space. Geophys J Int 138(2):479–494
Singh SK, Lermo J, Domínguez T, Ordaz M, Espinosa JM, Mena E, Quaas R (1988) The Mexico earthquake of September 19, 1985-A study of amplification of seismic waves in the valley of Mexico with respect to a hill zone site. Earthq Spec 4(4):653–673
Sinha R, Yadav G, Gupta S, Singh A, Lahiri S (2013) Geo-electric resistivity evidence for subsurface palaeochannel systems adjacent to Harappan sites in northwest India. Quat Int 308–309:6–75
Siripunvaraporn W, Egbert G, Lenbury Y, Uyeshima M (2005) Three-dimensional magnetotelluric inversion: data-space method. Phy Eart Planet Inter 150(1–3):3–14
Tikhonov AN (1951) Determination of the electrical characteristics of the deep strata of the Earth's crust. Dokl Acad Nauk SSR 73:295–297 (in Russian)
Wathelet M, Jongmans D, Ohrnberger M et al (2008) Array performances for ambient vibrations on a shallow structure and consequences over V s inversion. J Seismol 12:1–19
Wesnousky SG (2008) Displacement and geometrical characteristics of earthquake surface ruptures: Issues and implications for seismic-hazard analysis and the process of earthquake rupture. Bull Seismol Soc Am 98(4):1609–1632

Chapter 6
Earthquake Response and Its Implications Towards the Structural Design Codes for Himalayan Range and Adjoining Regions of India

Babita Sharma and Manisha Sandhu

Abstract It is impossible to prevent earthquakes but it is possible to mitigate the related effects and to reduce the loss of life, injuries and damages associated with the disastrous earthquakes. Eventually, earthquakes may generate many more disasters such as liquefaction, landslides, earth ruptures and most prominently ground vibrations which in turn may accompany the collapse of non-earthquake-resistant buildings resulting in massive loss of life and property. Therefore, it is essential to substantiate the effects of earthquakes along with the existing structural design codes. The assessment of the earthquake response analysis for the earthquakes that occurred beneath NW, Central and NE Himalayan regions of India symbolised the normalised spectral amplifications for various categories of the sites exposed on hard rock, sediments and alluvium. It has been observed that the hard strata prominently exhibit a lower spectral acceleration than that of the alluvium sites for NW, Central and NE Himalayan regions for different kinds of site conditions and regional geological formations. The comparison of spectral acceleration and corresponding predominant period with that of the design code given by the Bureau of Indian Standard (BIS) design code demonstrates the efficacy of the BIS code which may be strictly implemented for both urban as well as rural Himalayan and adjoining regions of India as the estimated response curves from actual earthquakes for all the sites fall within the structural limits proposed by BIS code. As a conclusive remark, it is stated that BIS-based structural design codes may provide safety to the structures in case of earthquake shaking in and around the Himalayan region of India. It is also inferred that the use of an appropriate building design code that considers the constraints of the response spectrum and related predominant period may have the potential to reduce the loss of life and property in case of Himalayan disastrous earthquakes.

B. Sharma (✉)
National Centre for Seismology, Ministry of Earth Sciences, New Delhi, India
e-mail: babita.s@nic.in

M. Sandhu
Department of Geophysics, Kurukshetra University, Kurukshetra, India

Sandeep et al. (eds.), *Geohazards*, Advances in Natural and Technological Hazards Research 53, https://doi.org/10.1007/978-981-99-3955-8_6

Moreover, it is also imperative to design an earthquake risk resilient society to mitigate imminent plausible seismic hazards originating in the detachment zone of the Himalayan Frontal Thrust system.

Keywords Response analysis · Spectral acceleration · Ground motion · BIS · Earthquake risk resilient

6.1 Introduction

It is evidently known that the Indian plate is moving in a north-east direction and colliding with the Eurasian plate. Himalayan mountains are formed due to this collision activity and also the collision of the Indian plate with the Eurasian plate is accountable for the formation of various tectonic active faults along the Himalayan belt. All the major to great earthquakes in India and its neighbouring regions occur along these active faults. Bureau of Indian Standards (BIS 2002) has differentiated the whole of India into four seismic zones such as Zone II, Zone III, Zone IV and Zone V. Out of these zones, the areas that fall under Zone V are assumed to be the most seismically prone areas in the country whereas the areas fall under zone II are of the least risk. Largely Zone V is comprised of entire north-eastern Indian states, few parts of Jammu and Kashmir, Himachal Pradesh, Uttarakhand, Rann of Kutch in Gujarat, few parts of North Bihar and Andaman & Nicobar Islands. These areas are primarily under the threat of earthquakes occurring in the Himalayan and adjoining areas. On the other hand, the Zone IV parts of Jammu & Kashmir, Himachal Pradesh, Uttarakhand, Delhi Territory, parts of Uttar Pradesh Sikkim, Bihar, West Bengal, parts of Gujarat and small portions of Maharashtra. The entire areas of the country coming under zone V and IV; are liable to high seismic hazards (Fig. 6.1a), making the areas coming in these zones under the threat of devastation due to the major to great earthquakes.

The Himalayan belt, which is also the inter-plate region of the Indian subcontinent, encompasses an approximately 2500 km long Himalayan belt from west to east (Fig. 6.1b). The Himalayan mountains formed due to the north-east ward movement of Indian plate which collides with the Eurasian plate. During this activity, several tectonic features were formed along the Himalayan belt. The Himalayan orogeny is divided into a number of such tectonic features as the Main Central Thrust (MCT); Main Boundary Thrust (MBT), and the Main Himalayan Thrust (MHT) (Robinson et al. 2003; Kayal 2010). MHT is comprised of a ramp-like structure having a low dip angle and also shows lateral variations along the Himalayan arc (Herman et al. 2010). The lesser Himalayan thrust belt lies in between the MBT and MCT (Schelling and Arita 1991) due to which the crustal deformation is undergoing in the central Himalayan region along MHT (Cattin and Avouac 2000; Zhao et al. 1993; Nakata 1989). Here many prominent and very destructive earthquakes have occurred in the past named as the 1897 Shillong Earthquake (M 8.1), 1905 Kangra Earthquake (M 7.8), 1934 Bihar-Nepal Earthquake (M 8.4), and 1950 Assam Earthquake

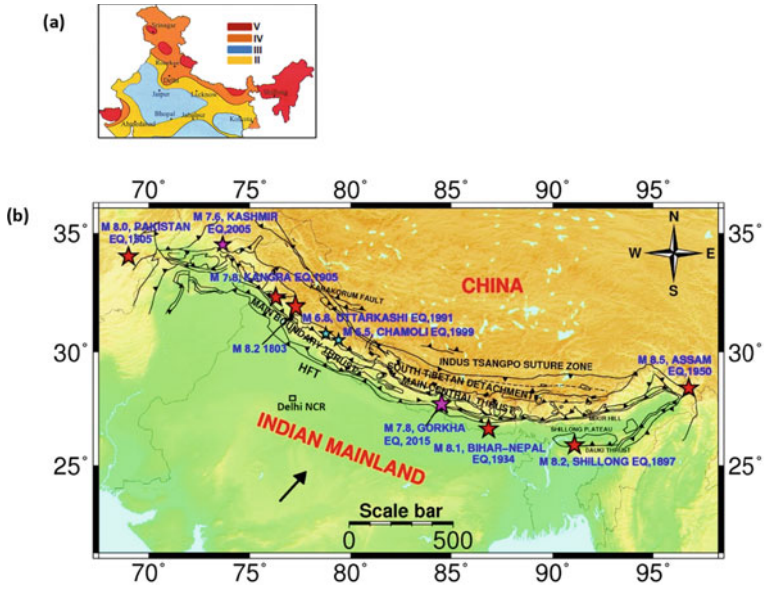

Fig. 6.1 The seismic zonation map (BIS 2002) of the Himalayan and the adjoining areas (**a**), The ongoing movement of the Indian plate along with the main tectonic features present in the Himalayan range and the prominent earthquakes of this area have also been shown (**b**)

(M 8.7). These earthquakes were devastating in the Himalayan and the surrounding areas (Gansser 1964; DeCelles et al. 2001). Also, an earthquake with Mw 7.9 also occurred in the year of 2015 in Nepal and this earthquake was considerably felt in India, especially in the Indo-Gangetic plain areas (seismo.gov.in; Sharma et al. 2017).

It is very important to study the strong ground motions of the earthquakes recorded along the Himalayan belt. These earthquake ground motions carry vital information about the subsurface of the earth and hence are required to estimate various ground motion parameters such as source, path and site effects. The seismic analysis depends not only on peak ground acceleration (PGA), but also rely on the predominant period of spectra. Therefore, the response spectrum is always used by construction engineers in the seismic analysis of buildings. The normalised spectral acceleration and velocity response spectra were computed from recorded ground motions of large earthquakes in the western USA (Housner 1959) and were utilised later by engineers. The peaks in ground motion response spectra depend on the numerous site conditions. The peak values of ground acceleration, velocity and displacement are associated with the acceleration response spectra for dominating frequencies (Newmark and Hall 1969; Hayashi et al. 1971; Seed et al. 1976; Mohraz 1976). Similar studies using Chi–Chi and Northridge earthquakes were carried out by Su et al. (2006). Likewise, in Indian scenario response analysis is carried by several researchers (Raghukanth and Iyengar 2007; Sharma et al. 2016, 2017; and Mittal et al. 2006). In these studies,

it was emphasised that the comparison of the BIS code with that of the spectral acceleration actually gives the idea of the behaviour of the earthquakes, which intern is important to accurately measure the risk in case of seismic hazards, especially in the Himalayan region.

6.2 Importance of Response Spectrum

There are importantly two aspects; one is the frequency content and the other is the shape of the response spectra because it is merely the presentation of the soil conditions in the form of the site characterisation. The impact of energy in the case of an earthquake in a computed frequency range is the main reason for the higher amplitude in the response spectrum. It is important to note that the high-frequency content is not found at the larger distances and loose sediments tend to show the effect of the amplified ground motions. Response spectrum can be used at various damping ratios as also shown in Fig. 6.2a for 2, 5 and 10% damping ratio. In case of the 2001 Bhuj earthquake that occurred in the western part of India, it was observed that the damage to the buildings was not uniform throughout the city of Ahmedabad located in Gujarat. Here, the taller buildings with foundations on thick soft layers experienced more damage than the same types of buildings constructed on stiffer soils. Reverse kind of observation on the other hand for one/two story buildings exposed to more destruction even constructed on stiffer soils. This showed that the same earthquake exhibits completely variable motions towards two different formations. More importantly, the interaction between the structural response and the nature of ground motion have always a reliable significance in the assessment of seismic hazard.

In case of the seismic hazard assessment, the Peak Ground Acceleration (PGA) and the duration of ground motion are significantly important. The strong ground motions are always depending on three factors such as the source, path and site effects, whereas there is dependency of the site characteristics on the magnitude, epicentral distance, and thickness of the soil column at a site. An earthquake with a comparatively high magnitude may be associated with less hazard than an earthquake with a small magnitude but having a longer duration. Moreover, seismic design codes utilise the response spectra of earthquakes which in turn may be utilised in the structural seismic analyses for strengthening construction design practices in urban and rural areas. An example is provided in Fig. 6.2b, where the three types of response spectra with different kinds of soils are shown.

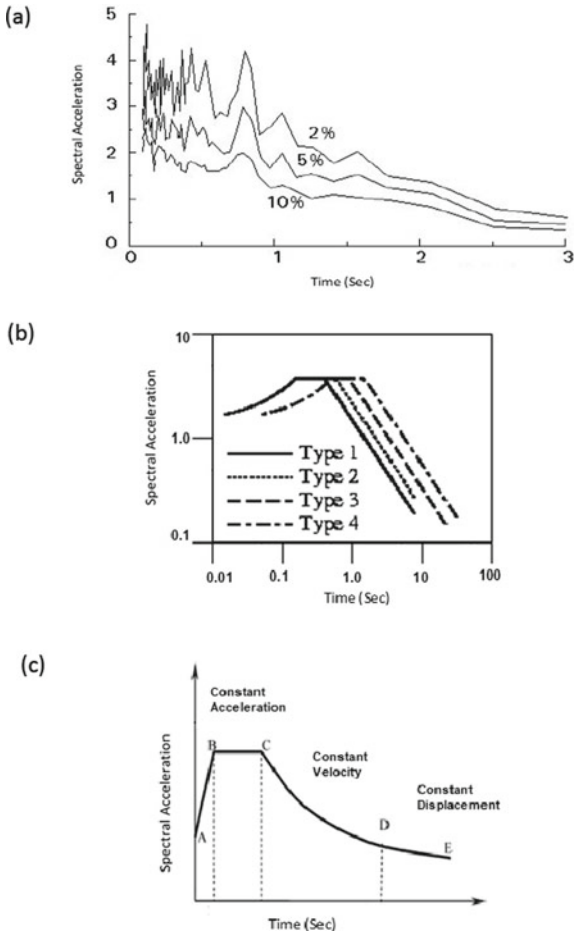

Fig. 6.2 A typical acceleration response spectrum for three damping ratios, i.e. 2%, 5% and 10% (**a**), Response spectrum type 4 response simulated sample functions (**b**). The relevance of the Spectral acceleration versus time plot (**c**)

6.3 Contribution of Response Spectrum in Construction Design Practices

The PGA and the duration of the earthquake waveforms serve as vital information for designing the parameters for construction codes. It depends upon the nature of earthquake activity, and their recurrence times for a particular region. If such information is not available then, the simulated ground motions may be used for the purpose. The data of major to great earthquakes is required to get a precise code of design which may be used for the safe construction design to build a seismic resilient society. Therefore, the response spectra and their corresponding predominant periods are important parameters to get an idea of the seismic source and site conditions for different earthquakes in a region. Figure 6.2c shows the typical shape of elastic design spectra along with the importance of the acceleration, velocity and displacement on

a response spectrum. According to the BIS code developed by the Bureau of Indian standard (BIS 2002), the response spectrum is used to satisfy various parameters such as the seismic source, the local soil conditions and the damping ratios of the structure considered. The shaking in an earthquake is usually represented in the form of acceleration response spectra which is the primary input used in the current seismic code.

6.4 Seismic Activity and Ground Motion Analysis

Strong motion data recorded for earthquakes that occurred in NW, Central and NE Himalayas, show considerable and continued seismic activity. The network of strong motion accelerographs (SMA) is sponsored by the Ministry of Earth Sciences and installed by IIT, Roorkee, all over the Himalayan belt. These instruments are triaxial force-balanced accelerometers with three component recorders and 18 bit digitizers. The sampling rate is 200 sps and the recording was kept in trigger mode along with a compact flash card (Mittal et al. 2006; Kumar et al. 2012; Mittal et al. 2012). The case study presented herewith is related to NW, Central and NE Himalayan regions using the earthquakes recorded by this network.

Out of the total 300 stations, 35 instruments are installed in different parts of Uttarakhand (Fig. 6.3a) and a total of 50 earthquakes were recorded in Uttarakhand which are used to estimate the response spectrum. Only Pre-Cambrian sites are considered in this case. Figure 6.3b presents the seismotectonics of the Ganga basin adjacent to the Central Himalayan region along with the stations. Here the SMA stations are installed in UP and Bihar states. In this case, only the sites corresponding to the quaternary alluvium are considered as the whole Indo-Gangetic plain is comprised of the recent alluviums of quaternary ages. In the NE Indian region, the considered earthquakes and stations recorded these earthquakes, are shown in Fig. 6.3c. In case of the NE Indian region, three kinds of sites are considered. Consideration of three kinds of overall geological formations in terms of Pre-Cambrian, tertiary and quaternary periods; have been considered in the present study. Here, Pre-Cambrian are the earliest of the geologic ages and are considered hard rocks, whereas the tertiary period rocks are sedimentary in nature corresponding to the Cenozoic era while the Quaternary period formations are related to recent alluviums.

The acceleration response spectrum for 5% damping is estimated using baseline corrected strong motion recordings of earthquakes from NW, Central and NE Himalayan regions. All the earthquakes used in the analysis are having magnitude >3. After that, the rotation of horizontal components is done to get N–S and E–W components. After that, the SMA data has been bandpass filtered from the frequency band of 0.01 to 25 Hz. Duhamel integral approach is used on the corrected data to estimate the response spectrum for 5% damping and the geometric mean of two horizontal components is estimated. The response spectrum is then normalised and the stations with the same geology are assembled to estimate the average for its associated geological formation. Figures 6.4a, b; 6.5a, b and 6.6a, b depict the normalised

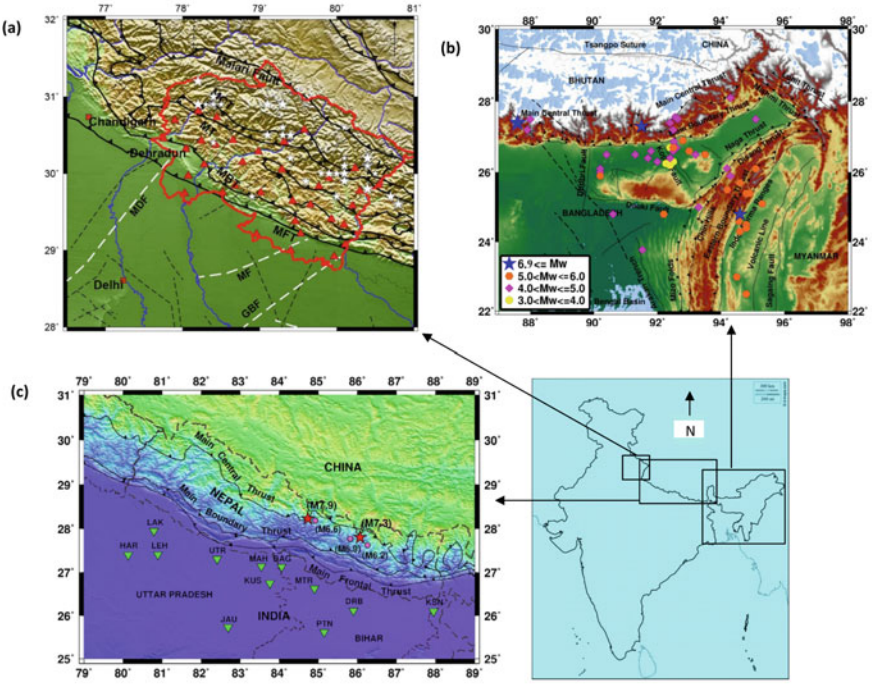

Fig. 6.3 Study areas (Three inset regions) as per the India map in the bottom right and their enlarged portions in detail: For NW Himalayan region stations and earthquakes considered (**a**), for Central Himalayan region stations and earthquakes considered (**b**) and for NE Himalayan region earthquakes considered; the details of the station is given in Sharma et al. (2016) (**c**)

Spectral Acceleration (SA) plots with Period for NW, Central and NE Himalayan regions respectively using horizontal as well as the vertical components of the Strong motion data corresponding to these three different Indian regions.

6.5 Assessment of Comparative Outcomes

The SMA data is very important as it can be used to simulate the strong ground motions for the worst-case scenarios (Sharma et al. 2013, 2015, 2016, 2017, 2020), for estimating the attenuation characteristics (Sharma et al. 2015; Sharma and Rastogi 2014) and also for estimating the response spectrum. The small as well as the large earthquake data may be used to estimate the response analysis which in turn may be compared with that of the BIS code to test the efficacy of the existing BIS code. The response spectra integrated in the present study using the records from horizontal and vertical components by SMA stations for NW, Central and NE Himalayan regions.

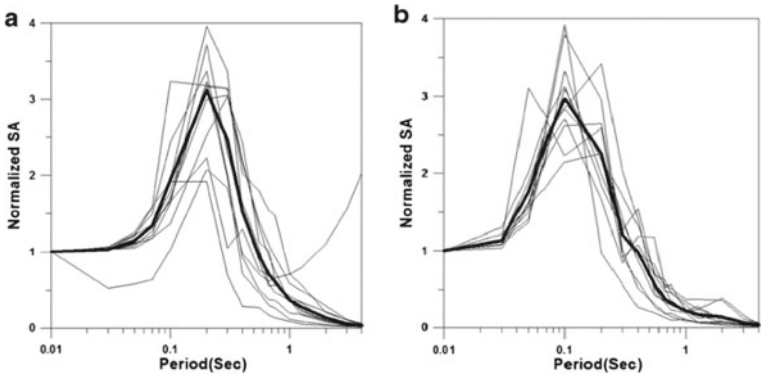

Fig. 6.4 Normalised spectral acceleration versus Period plots using the recorded strong motion data for the NW Himalayan region; Horizontal component (**a**) and Vertical component (**b**)

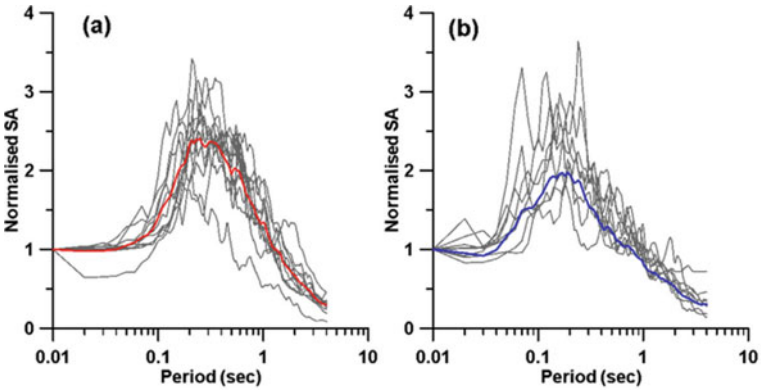

Fig. 6.5 Normalised spectral acceleration versus Period plots using the recorded strong motion data for the Central Himalayan region; Horizontal component (**a**) and Vertical component (**b**)

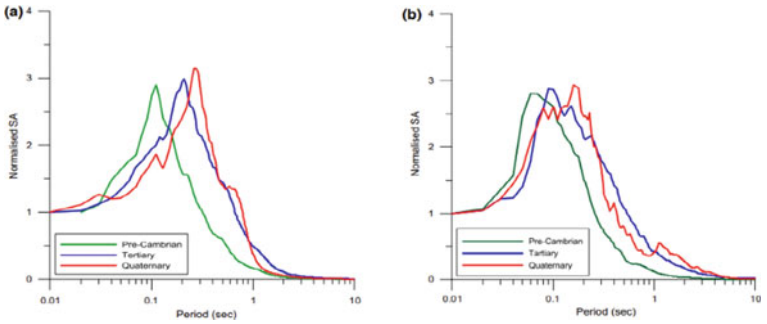

Fig. 6.6 Normalised spectral acceleration versus Period plots using the recorded strong motion data for the NE Himalayan region; Horizontal component (**a**) and Vertical component (**b**)

The average response spectra for all regions corresponding to both horizontal components are compared with that of the Bureau of Indian Standard code (Fig. 6.7). As an outcome, the average response spectrum estimated using the horizontal components of the strong motion data is found to fall within the limit of the average response spectra given by BIS-2002 for the country. The similar shape for the variation of the three study areas is associated with alluvial sediments of NE Brahmaputra quaternary sediments and Indo-Gangetic alluviums (Fig. 6.7). Also, the BIS code is compatible with the Pre-Cambrian formations of NW and NE Indian regions along with the Tertiary formations of the NE Indian region. The 2015 Nepal Earthquake and the 2016 Manipur Earthquake had devastating consequences for the communities in their respective regions, leading to significant loss of life and property. The reason for this was primarily the poor construction practices used by the people in the corresponding affected regions. It also validates that the existing BIS code was not followed in constructing the buildings in these parts because of which these areas experienced considerable damage to life and property. It is essential to follow the BIS guidelines in order to reduce the risk during earthquake shaking especially for critical structures such as schools, hospitals, bridges. etc. The knowledge of site conditions and the geological exposures at various locations may be improved with the help of geophysical and geotechnical investigations derived from Seismic microzonation. This may help to find out the necessary input for safer construction designs in the urban and rural areas of the country. This huge loss from the seismic hazard may be reduced in case of damaging earthquakes, especially in the Himalayan region of India (Mishra 2012, 2014a, b). The normalised response spectra calculated for three different Himalayan parts are having comparatively more amplification for the horizontal components than those of the vertical components. These results are obvious as with that of the standardized observation. Also, it is stated that there is a considerable variation in the estimates of site effects on different kinds of formations such as sediments and rock formations (Fig. 6.8). For this reason, the reliability of the used data set must be authenticated and the applied techniques also must be effective as per the norms and conditions. This has been well-taken care in the analysis to get the appropriate comparative results for the three different Himalayan regions. In case of the NE and NW Himalayan regions, the amplification factor is a little higher as per the computed results (Fig. 6.7). BIS code based on the different recording time histories of earthquakes always gives modifications such as the last modification was given in 2016. The improved code must be implemented in the earthquake-prone areas for new and old buildings to construct and retrofit.

Thus, we can conclude that the BIS code may be applicable for Himalayan Border states, especially in NW, Central and NE Indian regions, as response curves for normalised spectral acceleration for Precambrian, Tertial and quaternary period formations lie in the structural limits proposed by BIS (2002) code (Fig. 6.7). However, this code is improved and improved guidelines are widely in circulation through the construction authorities. As earthquake prediction is not possible precisely in time and space and loss of lives during an earthquake are generally

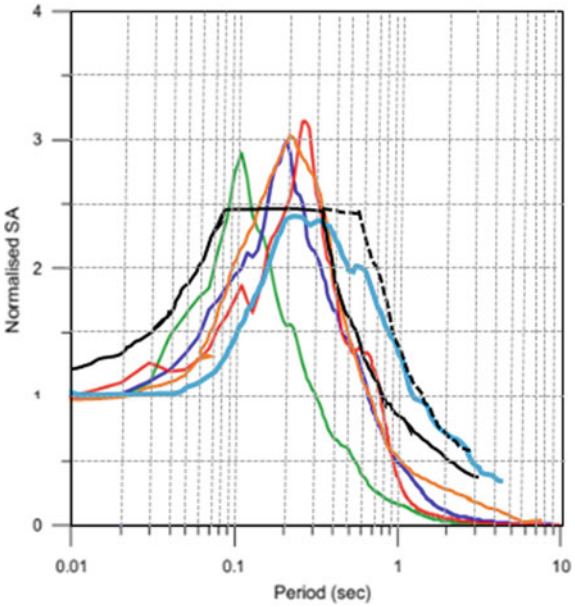

Fig. 6.7 Comparative analysis of the normalised spectral acceleration for three different Indian regions with that of the BIS code (Green line: Pre-Cambrian rocks of NE Indian region, Dark blue line: Tertiary formations of NE Indian region, Red line: Quaternary formations of NE Indian region; Light blue line: Quaternary formations of Indo-Gangetic plain; Orange line: Pre-Cambrian formations of NW Himalayan region; Black solid line: BIS code for rocks and Black dash line: BIS code for soil

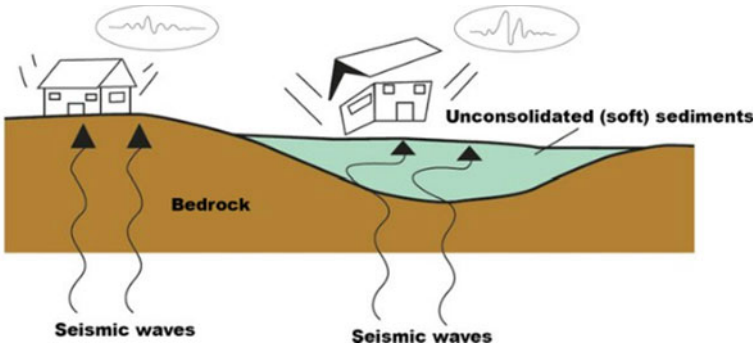

Fig. 6.8 Difference of site amplification phenomenon on the bedrock and unconsolidated (soft) sediments (after, Ciaccio and Cultrera 2014; Darvasi and Agnon 2019)

due to the damage/collapsed buildings, it is, therefore, required to properly plan the construction practices as per the BIS code in order to mitigate the seismic disaster. The Bureau of Indian Standards (BIS) has published criteria for the construction of earthquake-resistant structures. The design of structures should be as per the BIS code. Also, the structures like hospitals, schools, bridges, nuclear power plants, etc. should be earthquake resistant. However, it is not possible to reconstruct all of the poorly built structures, but for such poorly built structures, BIS has prepared retrofitting guidelines. Further, losses due to earthquakes can be considerably reduced through proper planning and implementation of pre- and pos—disaster preparedness and management strategies by working on the possible earthquake effects for various seismic zones.

6.6 Conclusions

There are several threatening social consequences of earthquakes which are in terms of huge losses to life and property. This may be direct economic losses as still we are not able to predict earthquakes. Thus, the earthquake preparedness for a seismic resilient society is the need of the hour that may be associated with the follow-up of the proper structural design practices. To reduce the seismic risk, it is very essential to assess the seismic hazard accurately because earthquakes are one of the deadliest natural disasters that induce huge loss of life and property all over the world, especially in the Himalayan regions of India as a lot of population is residing in the Indo-Gangetic and Brahmaputra plain areas. These areas are always under threat of earthquakes occurring in the adjacent Himalayan regions. The earthquake data of the Himalayan regions may be used to estimate several parameters such as PGA, response spectrum, predominant periods, etc. Following are the concluding points to make out of the study:

- The available data for Himalayan regions is used to estimate the response spectrum in the NW, Central and NE Indian shows compatibility with that of the BIS code.
- The BIS code is applicable and may be used in construction practices for Himalayan Border states, especially in NW, Central and NE Indian regions, as response curves for normalised spectral acceleration for Precambrian, Tertial and quaternary period formations lie in the structural limits proposed by BIS code.
- BIS code based on the different recording time histories of earthquakes always give modifications such as the last modification was given in 2016. The improved code must be implemented in the earthquake-prone areas for new and old buildings to construct and retrofit.
- Further, losses due to earthquakes can be considerably reduced through proper planning and implementation of pre- and post-disaster preparedness and management strategies by working out the possible earthquake effects for various seismic zones.

Acknowledgements BS is grateful to Secretary, Ministry of Earth Sciences (MoES) and Director, National Centre for Seismology (NCS), MoES for always encouraging attitude and providing a positive environment to carry out research work. MS is thankful to the Chairman, Department of Geophysics, Kurukshetra University for constant inspiration.

References

BIS (2002) Criteria for earthquake resistant design of structures, part I—general provisions and buildings. Bur Indian Stand. IS 1893 [part I]

Cattin R, Avouac JP (2000) Modeling mountain building and the seismic cycle in the Himalaya of Nepal. J Geophys Res 105:13389–13407. http://dx.doi.org/ https://doi.org/10.1029/2000JB900032

Ciaccio MG, Cultrera G (2014) Terremoto e rischio sismico. Ediesse, Italy

Darvasi Y, Agnon A (2019) Calibrating a new attenuation curve for the Dead Sea region using surface wave dispersion surveys in sites damaged by the 1927 Jericho earthquake. Solid Earth 10:379–390. https://doi.org/10.5194/se-10-379-2019

DeCelles PG, Robinson DM, Quade J, Ojha TP, Garzione CN, Copeland P, Upreti BN (2001) Stratigraphy, structure, and tectonic evolution of the Himalayan fold-thrust belt in western Nepal. Tectonics 20(4):487–509

Gansser A (1964) Geology of the Himalayas. Wiley-Interscience, New York

Hayashi S, Tsuchida H, Kurata E (1971) Average response spectra for various subsoil conditions. In: Proceedings of third joint meeting, U.S. Japan panel on wind and seismic effects. UJNR, Tokyo

Herman F, Copeland P, Avouac JP, Bollinger L, Maheo G, Le Fort P, Rai S, Foster D, Pecher A, Stuwe K, Henry P (2010) Exhumation, crustal deformation, and thermal structure of the Nepal Himalaya by inversion of thermochronological and thermobarometric data and modeling of the topography. J Geophys Res 115:B06407. https://doi.org/10.1029/2008JB006126

Housner GW (1959) Behavior of structures during earthquakes. J Eng Mech Division Proc ASCE 85(EM4):109–129

Kayal JR (2010) Himalayan tectonic model and the great earthquakes: an appraisal. Geomat Nat Hazards Risk 1:51–67

Kumar A, Mittal H, Sachdeva R, Kumar A (2012) Indian national strong motion network. Seism Res Lett 83(1):29–36

Mishra OP (2012) Applications of information technology in disaster risk management with reference to South Asia Disaster Knowledge Network (SADKN) and digital vulnerability Atlas of South Asia. In: 5th Asian Ministerial conference on disaster risk reduction (5th AMCDRR), 22–25 October 2012 at Yogyakarta, Indonesia

Mishra OP (2014a) Intricacies of the Himalayan seismotectonics and seismogenesis: need for integrated research. Curr Sci 106(2):176–187

Mishra OP (2014b) Seismological research in India (2007–2011). Proceeds Indian Nat Sci Acad (PINSA) 76(3):361–375

Mittal H, Gupta S, Srivastava A, Dubey RN, Kumar A (2006) National strong motion instrumentation project: an overview. In: 13th symposium on earthquake engineering. Indian Institute of Technology, Roorkee, Dec 18–20. Elite Publishing, New Delhi, pp 107–115

Mittal H, Kumar A, Ramhmachhuani R (2012) Indian national strong motion instrumentation network and site characterization of its stations. Int J Geosci 3:1151–1167. https://doi.org/10.4236/ijg.2012.326117

Mohraz B (1976) A study of earthquake response spectra for different geological conditions. Bull Seismol Soc Am 66:915–935

Nakata T (1989) Active faults of the Himalayas of India and Nepal. Spec Pap Geol Soc Am 232:243–264

Newmark NM, Hall WJ (1969) Seismic design criteria for nuclear reactor facilities. In: Proceedings of fourth world conference earthquake engineering, vol B-4. Santiago, pp 37–50

Raghukanth STG, Iyengar RN (2007) Estimation of seismic spectral acceleration in peninsular India. J Earth Syst Sci 116:199–214

Robinson DM, DeCelles PG, Garzione CN, Pearson ON, Harrison TM, Catlos EJ (2003) Kinematic model of the Main Central Thrust in Nepal. Geology 31(4):359–362

Schelling D, Arita K (1991) Thrust tectonics, crustal shortening and the structure of the Far Eastern Nepal Himalaya. Tectonics 10:851–862

Seed HB, Ugas C, Lysmer J (1976) Site dependent spectra for earthquake-resistant design. Bull Seismol Soc Am 66:221–243

Sharma B et al (2017) Comparison of average response spectrum for the main earthquake of 25th April 2015 (Mw 7.9) with BIS-2002 code, 2017. J Asian Earth Sci 133:12–23

Sharma B (2014) A comparative attenuation study of seismic waves in terms of seismic Albedo for Chamoli, Kachchh and Koyna regions of India. Int J Eng Sci Invent 3(6):33–40

Sharma B, Chingtham P, Sutar AK, Chopra S, Shukla HP (2015) Frequency dependent attenuation of seismic waves for Delhi and surrounding area, India. Ann Geophys 58(2). http://dx.doi.org/https://doi.org/10.4401/ag-6636

Sharma B, Chopra S, Kumar V (2016) Simulation of strong ground motion for 1905 Kangra earthquake and a possible mega thrust earthquake (Mw 8.5) in western Himalaya (India) using Empirical Green's Function technique. Nat Hazards 80(1):487–503

Sharma B, Chopra S, Sutar AK, Bansal BK (2013) Estimation of strong ground motion from a great earthquake in central seismic gap region using empirical green's function method. PAGEOPH. https://doi.org/10.1007/s00024-013-0647-0

Sharma B, Rastogi BK (2014) Spatial distribution of scatterers in the crust of Kachchh region, Western India by inversion analysis of coda envelopes. Disaster Adv 7(5):84–93

Su F, Anderson JG, Zeng Y (2006) Characteristics of ground motion response spectra from recent large earthquakes and their comparison with IEEE standard 693. In: Proceedings of 100th anniversary earthquake conference, commemorating the 1906 San Francisco Earthquake. San Francisco

Zhao W, Nelson KD, Che J, Quo J, Lu D, Wu C, Liu X (1993) Deep seismic reflection evidence for continental underthrusting beneath southern Tibet. Nature 366:555–559

Chapter 7
Liquefaction Potential Index (LPI): A Parameter to Assess Liquefaction Hazard

Supratim Chanda, Neeraj Kumar, and D. Kushwaha

Abstract This chapter focusses on the evaluation and assessment of earthquake induced liquefaction hazard of ground using Liquefaction Potential Index (LPI) technique. In this study, the reclaimed ground site of Jaigarh Port in Maharashtra is considered where, reclamation process was carried out with Dredged Soil using hydraulic fill method. As a consequence, loose clean non-plastic fines in saturated condition are prone to be liquefied under periodic shaking. Moreover, the engineering essence is not just limited to identifying this sudden loss of strength of ground, rather to assess the severity of the phenomenon. Therefore, the need of indexing is required based on field assessments like Standard Penetration Test (SPT) or other means. LPI technique quantifies and predicts some of ground's failure potential in terms of strength and stiffness during strong ground motion. The procedure to compute LPI is a well-established numerical technique. In past, many researches kept footprints on this vital area, which was later extended and modified with time to time. In case of residential area and shallow depth, liquefaction severity can be measured by the concept of Liquefaction Severity Number (LSN). The chapter provides insight of various techniques to assess liquefaction potential through practical examples and field study.

Keywords Liquefaction · SPT · Hazard · LPI · Reclaimed fill · Microzonation

7.1 Introduction

Liquefaction is a catastrophic natural phenomenon as noted from the past experiences, mainly responsible for failure of foundation beneath the buildings. The residential and industrial structures which are designed and build as per codal provisions to resist the seismic forces, have shown better performance than non-engineered structures. But in the past, it was reported in many studies that buildings have

S. Chanda · N. Kumar (✉) · D. Kushwaha
Central University of Haryana, Mahendergarh, Haryana 123031, India
e-mail: neerajlohchab@cuh.ac.in

Sandeep et al. (eds.), *Geohazards*, Advances in Natural and Technological Hazards Research 53, https://doi.org/10.1007/978-981-99-3955-8_7

collapsed due to foundation failure, even though the super structure is intact and safe. Now a days, rapid development one can encounter more and more hazardous ground situation due to scarcity of land. For safe design of foundation system against liquefaction, or taking economical decision on ground improvement techniques to be implemented at site; quantitative studies and measures of hazard level is need of the hour. In this context Liquefaction Potential Index (LPI) was first introduced by Iwasaki et al. (1978, 1982) as an effective measure of liquefaction hazard of ground under strong shaking force. Since then, this concept has been widely used by many researchers with or without modifications (Dixit et al. 2012; Tonkin and Taylor 2013; Chung and Rogers 2017). Past studies have shown that LPI has a good correlation in terms of predicting the overall liquefaction hazard of a ground (Lees et al. 2015). In the complex scenario, when the strata vary with depth as well as spatially with the presence of cohesive and granular type soils, single factor of safety against such event is inappropriate. In typical Indian scenario present study is confine on using the easily available SPT data from the site related investigation.

7.2 Criteria of Ground Mobility

Mobility of ground or liquefaction in particular is an implication of strong ground motion which causes loss of substantial amount of strength and stiffness of sub-soil. Loose clean fine sand in saturated condition is susceptible to such hazard. Many researches have organized creative researches to understand this major nonlinear characteristic of ground (Hazen 1920). Qualitative studies based on plasticity index, grain size distribution, liquid limit and moisture content were documented as Chinese criteria or its modifications and by others like Seed and Idriss (1982), Boulanger and Idriss (2006), Bray et al. (2004).

The landmark study was carried out by Seed and Idriss (1971) to evaluate potential liquefaction based on field test like SPT, CPT (Cone Penetration Test) etc. Later many researchers have modified their methods according to suitability of site and ground, but basics were kept same (Youd and Idriss 2001; Idriss and Boulanger 2010). Semi-empirical approach is used by them to find the factor of safety against liquefaction (F_L) and formulated the Eq. (7.1).

$$F_L = \frac{CRR}{CSR} \tag{7.1}$$

where "CRR" stands for cyclic resistance ratio of ground and "CSR" stands for cyclic stress ratio (Youd and Idriss 2001; Idriss and Boulanger 2010; Chanda et al. 2023).

7.3 Stratigraphy and Seismicity of the Location

The site under investigation is located at Jaigarh in Ratnagiri of Western ghat hilly regions in Maharashtra. This region is located at high seismic zone IV with expected ground acceleration 0.24 g as per past recorded earthquakes and as prescribed in the Indian Standard IS-1893:2002 (Part 1) with possible magnitude (M_w) 6.5 in Richter scale (Umesh 1977). The ground is located at sea shore with high water table. The formation level was achieved through filled dredged geomaterial. Bore log studies reveal the top layer is loose, silty sand and sometimes gravels are encountered. Beyond 10.0 m depth basalt rock was encountered. Figure 7.1a, b depicts the reclaimed land near Arabian sea in different year, 2011 and 2014.

7.4 Evaluation of LPI and LSN

7.4.1 Liquefaction Potential Index (LPI)

The ground with different layers has different factor of safeties against liquefaction for each layer as represented in Eq. 7.1. In order to take a decision, one needs a single parameter to judge the condition of a site. Hence an "*Averaging*" like parameter or "*Expected*" value over different layers of geomaterial was defined as Liquefaction Potential Index (LPI). Iwasaki et al. (1978, 1982) demarcated such parameter as in Eq. (7.2).

$$\mathrm{LPI} = \int_0^{20} F.w(z)dz \tag{7.2}$$

In the above integral equation "z" represents the depth from top formation layer (assumed 0.0 m as top of ground or lower limit) or natural ground level. The upper limit of the integral is considered up to 20.0 m depth below natural ground level (as vulnerability to liquefaction decreases with increase of depth due to larger effective stress). "w(z)" is weighting function equals to (10–0.5z). The severity number "F" is defined as follows.

$$\begin{aligned} \mathrm{F} &= 1 - \mathrm{F_L} \quad \text{for, } \mathrm{F_L} \leq 1.0 \\ &= 0 \quad \text{for, } \mathrm{F_L} > 1.0 \end{aligned} \tag{7.3}$$

where "F_L" is factor of safety against liquefaction as defined in Eq. (7.1). For the purpose of calculation, the integration in Eq. (7.2) will be evaluated numerically as a discreate summation. The above concept of LPI is generally satisfactory instead a few cases where it overestimates situations. Maurer et al. (2015) based on Ishihara (1985), has proposed slightly modified version of it. But, in present study the work

Table 7.1 Iwasaki hazard level

Liquefaction potential index (LPI)	RD level, Iwasaki et al. (1986)
LPI = 0	Very low
0 < LPI < 5	Low
5 < LPI < 15	High
LPI > 15	Very high

is confine to Iwasaki. After validation in site performance in Japanese earthquakes, Iwasaki (1986) has proposed the following hazard level as shown in the Table 7.1. More or less when LPI is less than 5.0, liquefaction is unlikely in a site and hazard level is severe if LPI is greater than 15.

7.4.2 Liquefaction Severity Number (LSN)

Liquefaction Severity Number (LSN) proposed by Tonkin and Taylor (2013) is used in liquefaction and its consequences in shallow depth foundation and inhabited land from volumetric settlement point of view.

$$\mathrm{LSN} = 1000 \int \frac{\varepsilon_{\mathrm{V}}}{\mathrm{Z}} dz \tag{7.4}$$

where ε_v is volumetric strain during densification in the subjected layer by Zang et al. (2002), Lee (2007) and "z" is depth in meter of the said layer below ground level. Site observations in Canterbury earthquake has been summarized in Table 7.2 (Tonkin and Taylor 2013; Bhattacharyya et al. 2019).

Table 7.2 Tonkin and Taylor hazard level

LSN Range	PREDOMINANT Performance
0–10	Little or no liquefaction, minor effects
10–20	Minor effect, sand boils
20–30	Moderate level liquefaction, sand boils, few damage in structures
30–40	Moderate to severe liquefaction, settlements of foundation cause structural damage
40–50	Major expression of liquefaction, undulation and damage to ground surface, severe total and differential settlement of foundation
>50	Severe damage, extensive evidence of liquefaction, damage to services

7.5 Case Studies and Results

The subsoil of reclaimed land in Jaigarh port under consideration was investigated through twelve boreholes (as shown in the Fig. 7.2). Standard Penetration Test (SPT) was carried out to encounter subsoil in different layers of strata and recorded the penetration number to co-relate to other parameters of interest. One sample calculation of "LPI" is tabulated in Table 7.3. The below results reveal that silty sand and silty clay layers of roughly 6.0–13.0 m depth from formation level are prone to liquefaction and contributes to the LPI.

The expected vulnerability level can now be integrated up to 20.0 m to find it. Here the same is noted to be above 6.0 and location is turned to be highly liquefiable as per scaling in Table 7.1.

Box-and-whisker plots in Fig. 7.3a, b of LPI's and LSN's of different borehole locations for different earthquake magnitude (M_w) is shown as a decision-making guideline for the site and further action needed like ground improvements. It is quite evident from these plots that the median values of LPI's in this site are apart from each other for different earthquake magnitude as expected.

Though the LSN medians are closed to each other. Hence overall performance of the second one shall be carefully used to reach any conclusion. LSN parameter can be used for shallow depth foundation and its effect on volumetric changes in the subsoil.

Another very useful pictorial presentation as Microzonation (contour plot) of LPI is shown below in Fig. 7.4. Here based on each borehole locations, we have determined the Liquefaction Potential Index values. Then by using grid method, the contour for respective LPI is approximately plotted.

Easily one can assess that locations near BH-2 and BH-9 are most hazardous with LPI greater than 25. Near the virgin land the soil has negligible liquefaction hazard. Adjacent to berth and shoreline also experience zero LPI, possibly due to shore protection and improved ground with boulder work.

Fig. 7.1 **a** Jaigarh reclamation in 2011. **b** Jaigarh Port in 2014

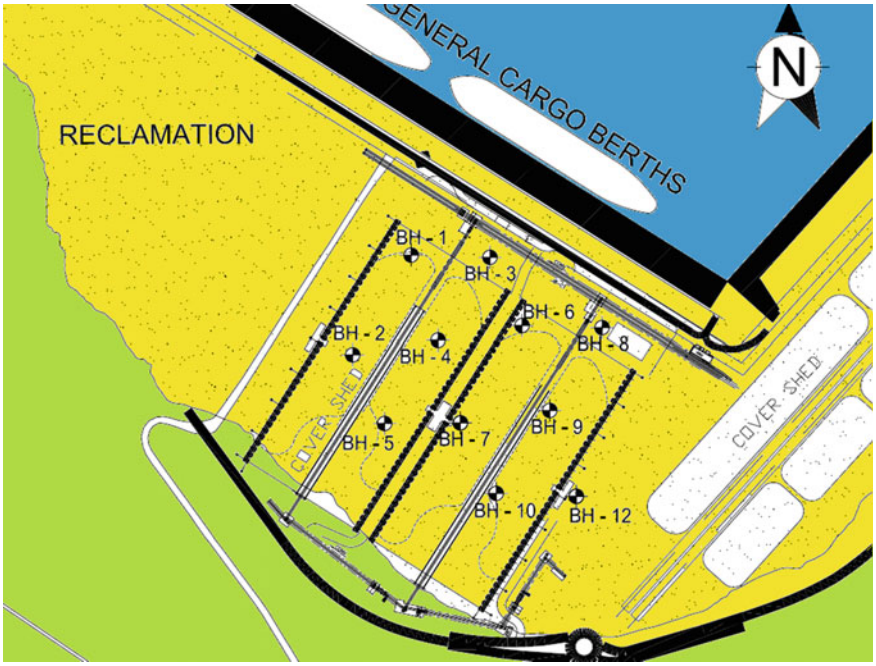

Fig. 7.2 Bore hole locations plan

7.6 Discussions on Reclaimed Ground

DMG (1999), has classified the lithological characteristics of high hazard zones for liquefaction. Soil deposits of Holocene period where water table is within 10.0 m from ground in a moderate seismic zone has a high chance of liquefaction. For the cases of filled-up or reclaimed ground, uncompacted or poorly compacted geomaterials near Port areas are likely to be liquefied with a very high hazard level. Mostly the reclamation in Jaigarh Port were done by dredged geomaterial using hydraulically filled technique. This makes the new formation, i.e., loosely filled with silty fine sands of non-plastic nature. Hence the ground is primarily not usable instantly. The site shall be dynamically compacted or properly improved with surcharge with calculated timeline prior to any heavy construction over it.

Table 7.3 Example of LPI calculation

Liquefaction potential index analysis							
Conclusion:		As per Iwasaki et al. (1982) Hazard level is =				High	
Location	BH01		Liquefaction potential index (LPI) = $\Sigma\, w(z_i)F(z_i)\Delta z$ =				6.32
Depth from formation (m)	z_i of mid layer (m)	*F.O.S* (F_L)	Soil type	F(z)	$w(z_i)$	Δz	$w(z_i)F(z_i)\Delta z$
1.50	0.75	2.13	***Silty Sand***	0.00	9.63	1.50	0.00
3.00	2.25	2.39		0.00	8.88	1.50	0.00
4.50	3.75	1.29		0.00	8.13	1.50	0.00
6.00	5.25	0.58		0.42	7.38	1.50	4.69
7.50	6.75	0.99	***Silty Clay***	0.01	6.63	1.50	0.15
9.00	8.25	0.96		0.04	5.88	1.50	0.37
10.50	9.75	0.94		0.06	5.13	1.50	0.47
12.00	11.25	0.90		0.10	4.38	1.50	0.64
13.50	12.75	1.00		0.00	3.63	1.50	0.00
15.00	14.25	1.05	***Silty Clay***	0.00	2.88	1.50	0.00
16.50	15.75	1.01		0.00	2.13	1.50	0.00
18.00	17.25	1.18		0.00	1.38	1.50	0.00
19.50	18.75	1.25		0.00	0.63	1.50	0.00
21.00	20.25	1.37		0.00	0.00	1.50	0.00
22.50	21.75	1.37		0.00	0.00	1.50	0.00
24.00	23.25	1.59		0.00	0.00	1.50	0.00
25.50	24.75	2.64	***Rock***	0.00	0.00	1.50	0.00
27.00	26.25	2.48		0.00	0.00	1.50	0.00
28.50	27.75	2.95		0.00	0.00	1.50	0.00
30.00	29.25	2.74		0.00	0.00	1.50	0.00
31.50	30.75	2.56		0.00	0.00	1.50	0.00
33.00	32.25	2.44		0.00	0.00	1.50	0.00
34.50	33.75	2.32		0.00	0.00	1.50	0.00

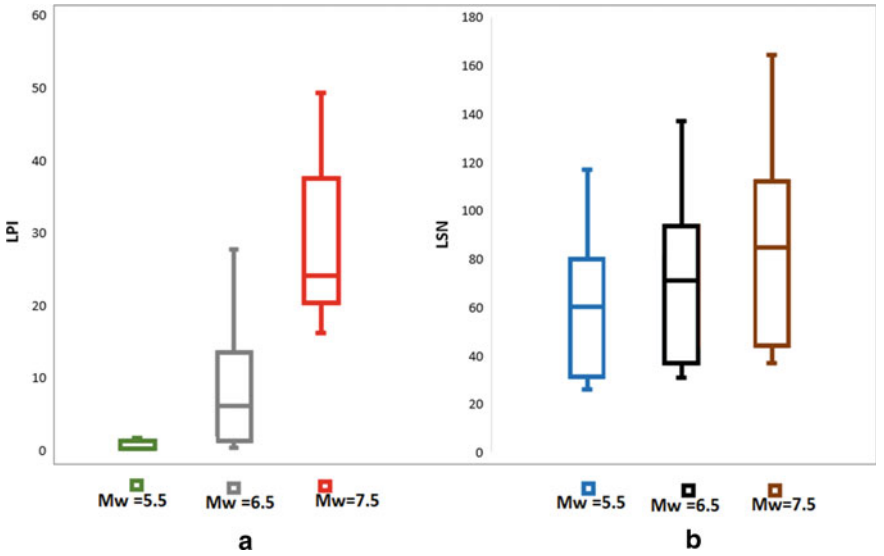

Fig. 7.3 **a** Comparison of LPI's of different earthquake magnitude. **b** Comparison of LSN's of different earthquake magnitude

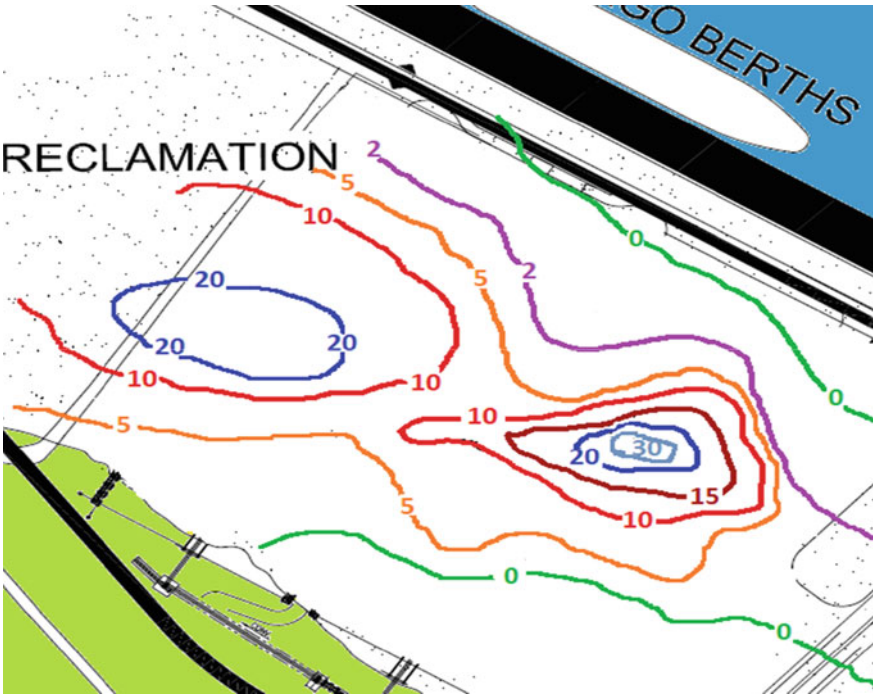

Fig. 7.4 Liquefaction Potential Index Contour Map plotted for $M_w = 6.5$

7.7 Conclusion

Liquefaction hazard can be classified in many ways. The easiest way is calculation of factor of safety of ground layer wise, as given in Eq. 7.1. If the Factor of Safety is less than 1.0, that is Cyclic Stress Ratio (CSR) exceeds Cyclic Resistance Ratio (CRR) of ground, the layer is liquefiable for concerned ground acceleration. Another possible way of qualitative assessment may be by Chinese criteria and many of its variations based on plasticity and liquid limit. Even if SPT values are beyond 30 in a layer, one can well assume it as non-liquefiable from past experiences as in Seed and Idriss (1971). Here an attempt has been made to quantify overall ground safety against liquefaction vide liquefaction potential index and similar methodologies.

7.8 Further Reading

All the previous discussions were based on deterministic analytical approach. Hazard level of any natural disasters though can better be explained in stochastic framework. Following probability-based Eq. (7.5) of Juang et al. (2003) may be used in this regard.

$$P_L = \frac{1}{1 + \left(\frac{F_L}{0.96}\right)^{4.5}} \tag{7.5}$$

There are many others who have made important contribution in this direction and still lot of progress is required to study other aspects to liquefaction.

Acknowledgements We thankfully acknowledge the support obtained time to time from Manoj Kumar, Chief Civil Engineer of Grafix Engineering Consultant Pvt Ltd., New Delhi.

References

Bhattacharya S, Orense RP, Lombardi D (2019) Seismic design of foundations. Thomas and Telford (ICE Publishing), Westminster, London, Concepts and Applications

Boulanger R, Idriss IM (2006) Liquefaction susceptibility criteria for silts and clays. J Geotech Environ Eng, ASCE 132(11):1413–1426

Bray JD, Sancio RB, Durgunoğlu HT et al (2004) Subsurface characterization at ground failure sites in Adapazari, Turkey. J Geotech Environ Eng, ASCE 130(7):673–685

Chanda S, Kumar M, Kumar N, Shukla RP (2023) Study of liquefaction potential at Jaigarh port using standard penetration test data and consequences: a case study. In: Proceedings of 17th symposium on earthquake engineering, vol 3. SEE 2022. Lecture notes in civil engineering, vol 331. Springer, Singapore. https://doi.org/10.1007/978-981-99-1579-8_14

Chandra U (1977) Earthquakes of peninsular India—a seismotectonic study. Bull Seism Soc Am 67(5):1387–1413

Chung J, Rogers DJ (2017) Deterministic and probabilistic assessment of liquefaction hazards using the liquefaction potential index and liquefaction reduction number. J Geotech Environ Eng, ASCE 143(10): 04017073-1–9

Dixit J, Dewaikar DM, Jangid RS (2012) Assessment of liquefaction potential index for Mumbai city. Natural Hazards Earth Syst Sci 12:2759–2768

DMG Special publication 117: Guidelines for analyzing and mitigating liquefaction in California. Southern California, USA (1999)

Hazen A (1920) Hydraulic fill dams. Trans Am Soc Civ Eng 83:1717–1745

Idriss IM, Boulanger RW (2010) SPT Based liquefaction triggering procedures: Report No. UCD/CGM-10–02, Department of Civil and Environmental Engineering, College of Engineering, University of California at Davis, pp 1–259

Ishihara K(1985) Stability of natural deposits during earthquakes. In: 11th international conference on soil mechanics and foundation engineering. Rotterdam, Netherlands, pp 321–376

Iwasaki T, Tokida K, Tatsuko F, Yasuda S (1978) A practical method for assessing soil liquefaction potential based on case studies at various site in Japan. In: Proceedings of the 2nd international conference on microzonation, national science foundation. Washington, DC, pp 885–896

Iwasaki T, Tokida K, Tatsuoka F, Watanabe S, Yasuda S, Sato H (1982) Microzonation for soil liquefaction potential using simplified methods. In: Proceedings of the 3rd international conference on microzonation, national science foundation. Washington, DC, pp 1319–1330

Iwasaki T (1986) Soil liquefaction studies in Japan: state of the art. Soil Dyn Earthquake Eng 5(1):2–68

Indian Standard IS– 1893:2002 (Part 1): Criteria for earthquake resistant design of structures—Part 1: General provision and building, Bureau of Indian Standards, New Delhi (2016)

Juang CH, Yuan H, Lee DH, Lin PS (2003) A simplified CPT-based method for evaluating liquefaction potential of soils. J Geotech Geoenviron Eng 129(1):66–80

Lee CY (2007) Earthquake-induced settlements in saturated sandy soils. Asian Res Publishing Netw (ARPN) 2(4):6–13

Lees JJ, Ballagh RH, Orense RP, Van Ballegooy S (2015) CPT-based analysis of liquefaction and re-liquefaction following the Canterbury earthquake sequence. Soil Dyn Earthquake Eng 79(B): 304–314

Maurer BW, Green RA, Cubrinovski M, Bradley BA (2015) Evaluation of the liquefaction potential index for assessing liquefaction hazard in Christchurch, New Zealand. J Geotech Geoenviron Eng, ASCE 140(7). https://doi.org/10.1061/(ASCE)GT.1943-5606.0001117

Seed H, Idriss I (1971) Simplified procedure for evaluating soil liquefaction potential. J Soil Mech Found Div, ASCE 97(SM9): 1249–1273

Seed HB, Idriss IM (1982) Ground motions and soil liquefaction during earthquakes, earthquake engineering research institute. Oakland, CA, USA

Tonkin and Taylor (2013) Liquefaction vulnerability study, earthquake commission. Wellington, New Zealand

Youd TL, Idriss IM (2001) Liquefaction resistance of soils, summary report from the 1996 NCEER and 1998 NCEER/NSF workshops on evaluation of liquefaction resistance of soils. J Geotech Geoenv Eng 127(4):297–313

Zhang G, Robertson PK, Brachman R (2002) Estimating liquefaction-induced ground settlements from the CPT. Can Geotech J 39:1168–1180

Chapter 8
Radon Time Series Data for Earthquake Precursory Studies in Taiwan: An Overview

Vivek Walia, Arvind Kumar, and Ching-Chou Fu

Abstract One of the main causes of human catastrophes worldwide is earthquakes. However, according to studies on earthquake prediction, it is important to stress that there are currently no reliable, detectable, and systematic precursory phenomena that precede large earthquakes. Taiwan is a highly seismic zone because it is thought to be a result of the collision between the Philippine Sea plate and the Eurasian plate. Recently, detailed research on the changes in soil-gas radon composition in Taiwan's southwestern and northeastern regions near the geologic fault zone was carried out. Temporal soil-gas radon fluctuations along several faults were continually investigated at the installed monitoring stations. According to the current investigations, some earthquakes with a magnitude of ≥ 5 that were noted in the area throughout the study period were linked to the patterns of soil-gas anomalies. The data has been processed using a variety of filters to lower the noise level, which helps to filter out the high-frequency noise and daily volatility brought on by various parameters. The data and working hypotheses were combined using AMP (Apache, MySQL, and PHP), a well-known and well-liked open-source web application solution, to make a website that could effectively show and help us manage the real-time database. Based on the observed aberrant patterns from monitoring stations, we were able to propose the region for impending earthquakes from the proposed tectonic-based model for earthquake precursory studies in Taiwan.

Keywords Precursors · Radon · Earthquakes · Database · Real-time

V. Walia (✉) · A. Kumar
National Center for Research on Earthquake Engineering, NARLabs, Taipei, Taiwan
e-mail: vivekwalia68@gmail.com; walia@narlabs.org.tw

C.-C. Fu
Institute of Earth Sciences, Academia Sinica, New Taipei, Taiwan

Sandeep et al. (eds.), *Geohazards*, Advances in Natural and Technological Hazards Research 53, https://doi.org/10.1007/978-981-99-3955-8_8

8.1 Introduction

For the past 50 years, geochemical precursors have been considered research-oriented for studies on earthquake prediction. Examples of precursors include changes in water level, radon (222Rn), methane (CH_4), carbon dioxide (CO_2), and dissolved ions in water. Potential hydrogeological and geochemical precursory signals have been shown to exist hours to months before some big earthquakes at "sensitive" monitoring sites among many non-sensitive locations. One of the most seasoned and tested geochemical precursors among them is radon (Walia et al. 2009; Nicoli et al. 2019; Fu et al. 2017). 222Rn in soil and groundwater has shown the highest sensitivity among potential earthquake precursors due to its radioactive nature and deep origin. Radon studies have been carried out in a lot of nations throughout the world, including Italy, Germany, Japan, India, and others. Radon monitoring in soil and groundwater can reveal clues about seismic occurrences through spatial and temporal changes. While temperature, relative humidity, rainfall, pressure, and other meteorological conditions also affect the amount of radon that is released from the soil from below to the surface (Arora et al. 2017; Kumar et al. 2015). Because both meteorological and seismic events can cause radon emissions to be disrupted. It is frequently impossible to tell the difference between radon anomalies or patterns caused by seismic events and those merely caused by changes in meteorology. While some oddities are hidden, others are wrongly believed to be signs of earthquake precursors. It is vital to employ computational and statistical tools in order to reduce the influence of meteorological conditions on radon emission (Torkar et al. 2010; Kumar et al. 2015; Arora et al. 2017). It is well recognized that the distribution of soil-gas compositional differences can be used to infer fault zone mapping (Al-Taminmi and Abumurad 2001; Guerra and Lombardi 2001; Fu et al. 2005, 2009) and as the predecessors for earthquakes (Segovia et al. 1989; Woith and Pekdeger 1992; Walia et al. 2005, 2006; Yang et al. 2005, 2006). According to studies on the degassing of the subsurface conducted by a variety of authors (King et al. 1993; Baubron et al. 2001; Yang et al. 2003), gases can move to the surface by advection, diffusion, and dispersion as they are carried by hot fluids rising to the surface and move along preferred paths like faults and fractures. The rate of migration and soil-gas concentration are influenced by a variety of factors, such as granulation, microcracks, surface wind, uranium distribution in the soil and bedrock, soil porosity and humidity, etc. A fault can be considered a weak region made up of fluids, gouges, and highly fragmented materials. Active faults increase the soil's permeability, which encourages gas escapes at the surface.

Taiwan is considered a seismically active region because it is thought to be the result of the collision of two tectonic plates, the Philippine Sea plate and the Eurasian plate. Taiwan is surrounded by active subduction zones to the south and east. While an oceanic lithosphere of the Eurasian plate is subducting beneath the Philippine Sea plate along the Manila Trench, the oceanic component of the Philippine Sea plate is subducting northwestward beneath the Eurasian plate to the east (Fig. 8.1c). These ongoing collisions are typically considered to be the main contributor to the tectonic stress in the region. On Taiwan's most recent tectonic map, which was

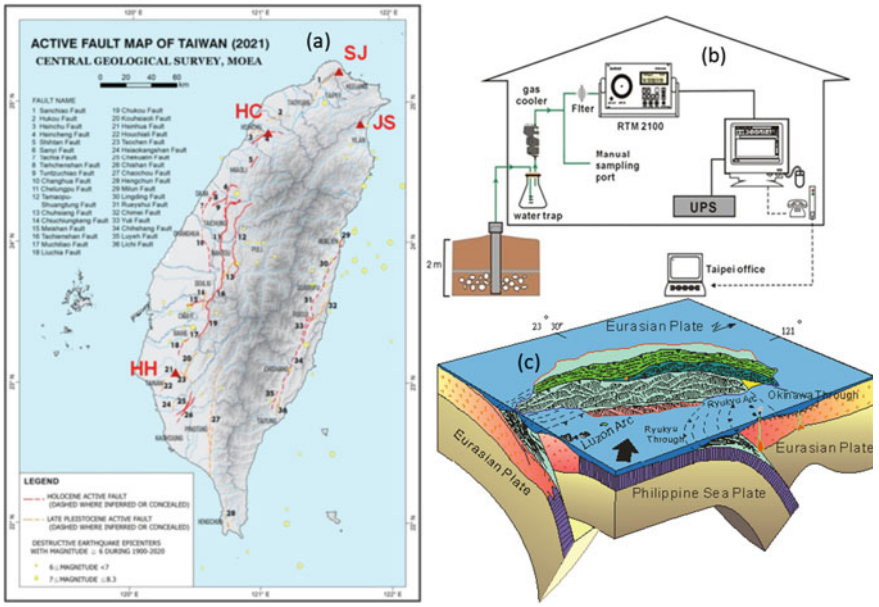

Fig. 8.1. **a** Taiwan's active fault map with locations of monitoring stations, **b** a sketch plan for a continuous monitoring station, and **c** a 3D tectonic model of Taiwan (Walia et al. 2009)

released by the Central Geological Survey of Taiwan, MOEA, 36 active faults have been identified (Fig. 8.1a). Our institute has set up four radon monitoring stations to investigate temporal radon changes in the soil-gas composition. These are located along a number of fault lines in the following places: Hsinchu (HC), Tainan (HH), Ilan (at Jaosi (JS)), and Yangmingshan area (SJ) (along the Shanchiao fault). The soil-gas radon time series data used in this inquiry were provided by the San-Jie (SJ) monitoring station in northern Taiwan (Fig. 8.1a).

8.2 Continuous Monitoring Station Setup

Figure 8.1a shows the soil-gas radon monitoring locations maintained by our institute, the National Center for Research on Earthquake Engineering (NCREE), Taipei. 2 m holes were drilled and covered with PVC pipes to create a monitoring stations. To stop any unwanted materials from entering, a little mesh is put to the bottom of the PVC pipe. Rainwater cannot seep into the hole because PVC sheets spanning the entire length of the PVC pipe roughly 1 mat the bottom stops the rainwater. To decrease the effect of environmental effects, several stones were also put to the bottom before closing in the holes on all sides. The top surface is ultimately cemented, and housing is built on it to keep the required instruments. The automated monitoring system's schematic layout is shown in Fig. 8.1b. After passing through the gas cooler and

water trap, the soil gas was fed into the alpha spectroscopy (SARAD RTM2100) through an internal pump for radon and thoron detection. Due to a two-stage filter, only radon gas types 222 and 220 can travel through the chamber, keeping out radon and its offspring. Every 15 min, radon levels were tested. A count-sum that is much more than the background noise can be produced in the 15-min time frame. All of the data is transmitted to the central processing center through the Internet. With the exception of minor delays brought by equipment failure or power supply outages, data for the years after 2006 are continually accessible. The station operation went in phases. Seismic parameters (such as earthquake parameters, the strength at a monitoring station, etc.) and other meteorological parameter data from the Central Weather Bureau of Taiwan (www.cwb.gov.tw) were used.

8.3 Real-Time Monitoring

The data has been synoptically evaluated for earthquake precursory anomaly patterns in light of precipitation and other metrological parameters reported elsewhere (Kumar et al. 2020). To assist in determining the origins of precursory signals in almost real-time, a set of criteria was created. A real-time database has periodically been built, and any necessary modifications have been done. In the past, manual real-time databases were developed. Both its efficiency and the data processing system for seismic precursory research were improved. An operating system's efficiency simply hinges on how quickly it responds and how soundly its logic holds up in seismic precursory investigations. As a result, it's imperative to work on effectively minimizing "reaction time," which can be accomplished by applying particular information technology tactics. Figure 8.2a shows the algorithm that was used to build a real-time database in Taiwan. First, seismic and metrological data from the central weather bureau, as well as radon data from the monitoring stations, have been transmitted via the internet to the NCREE server. After that, the open-source programming language "R" was used to complete the data computing tasks. A low-pass filter has been used to reduce the noise level during this stage. The filter will remove high-frequency noise and daily volatility caused by a variety of variables, including environmental influences, measurement uncertainty for earth tides, and background noise. After normalizing the data using "Visual Signal," the probability distribution of variance in the data will be evaluated. The working approach was modified to "programmed data operation and visualization," which not only allows for real-time operation, but also expedites batch processing. In the subsequent step, information will also be linked to the well-known and popular open-source "AMP" web application solution stack (Apache, MySQL, and PHP). The Apache HTTP server, also referred to as Apache, is a web server application that significantly supported the early growth of the World Wide Web (www). MySQL, also referred to as "My Sequel," is the second-most used open-source software in the world. The server-side scripting language PHP, on the other hand, was developed for web development but may also be applied to other computing activities; uploads seismic parameters, meteorological parameters, and

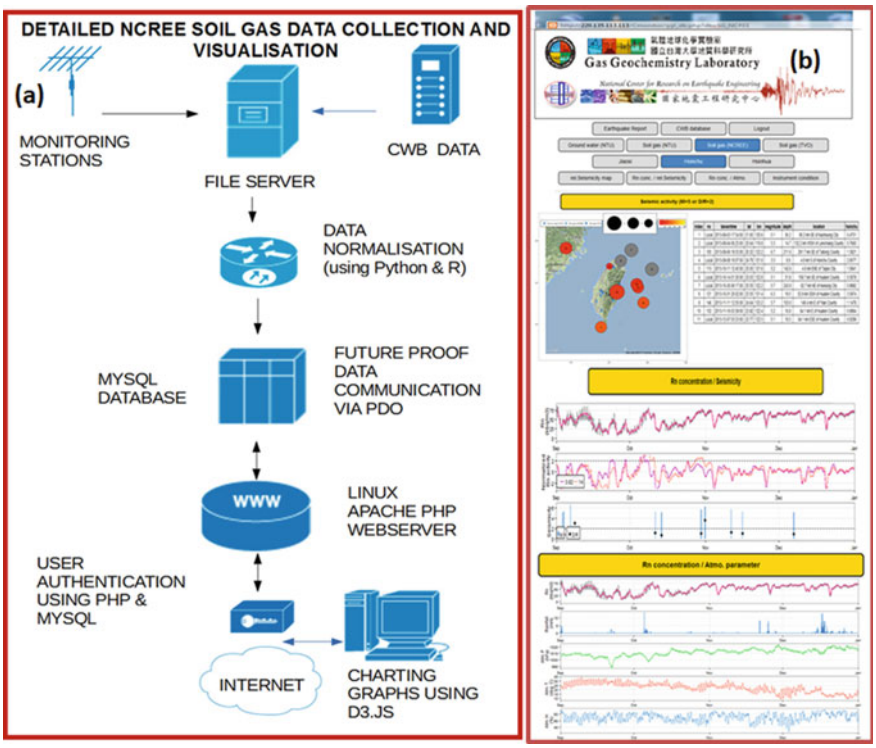

Fig. 8.2. **a** The algorithm used to create the real-time database; **b** a screenshot of the database showing a monitoring station in Taiwan with various parameters (Kumar et al. 2020)

monitoring station data simultaneously from the Central Weather Bureau of Taiwan (www.cwb.gov.tw). Seismic parameters include magnitude, position, depth, intensity, epicentral distance, and others. Figure 8.2b displays a screen picture of the real-time database for data from one of the monitoring stations, including seismic and meteorological features.

8.4 Tectonic-Based Model for Taiwan

We examined and compared data from a network of monitoring stations linked to a number of large earthquakes and their aftershocks for temporal patterns of radon abnormalities (Fig. 8.1). Based on long-term radon monitoring data from the existing monitoring stations, we are able to divide the monitoring stations into two distinct tectonic zones, i.e., the North and South parts of Taiwan (Fig. 8.3). (Walia et al. 2009). The tectonic activities stress variation along the Okinawa Trough and Ryukyu Trough, which are in the North and Central, Eastern part of Taiwan (Fig. 8.1c), as

well as localized earthquakes having magnitude <5 located within a radius of about 50 km from the monitoring stations, have been observed to be more disruptive to soil-gas radon variations. While tectonic activity along the Luzon Arc and other tectonic activity in the Southern part of Taiwan are more likely to be the cause of soil-gas radon fluctuations in the South zone. As a result, from the continuous monitoring time series that have been recorded, we have seen that the Southern monitoring stations collectively give the precursory signal of earthquakes happening in the South-Southeastern part of Taiwan, whereas in the Northern zone stations, the majority of the soil-gas anomalies are associated with precursory signals that are observed for the earthquakes that are felt in the North or Northeastern part of Taiwan. We are currently in the process of providing an interpretative tectonic-based model that divides Taiwan into two distinct tectonic zones based on these observations. The suggested model has been reported and examined elsewhere (Walia et al. 2009, 2013). Data from the network of continuous monitoring stations that NCREE and NTU have run together over the past few years were recorded and fit the suggested model well (Walia et al. 2009, 2013). We tried it for certain earthquakes that occurred in the area in prior studies and are close to identifying the area for imminent earthquakes with a magnitude of ≥5 based on the particular monitoring stations' aberrant signals (Fu et al. 2017; Walia et al. 2013). It has been discovered that earthquakes with a magnitude of ≥5 that recorded a local intensity of two or more at the specific monitoring stations listed by CWB (http://www.cwb.gov.tw) and had an epicentral distance and focal depth of <100 km and <40 km, respectively, had shown precursory signals and fit the proposed model very well.

8.5 Precursory Study for Meinong Earthquake

On 6 February 2016, 03:57:26.1 (GMT 5 February 2016, 07:57:26.1), an earthquake with ML 6.6 on the Richter scale rocked the Meinong district of Kaohsiung City, Taiwan, and can be associated with earthquakes in the second category occurring on active faults in Western Taiwan. According to the Central Weather Bureau's Seismological Center, the epicenter was located at 22.92°N and 120.54°E (27.1 km Northeast of Pingtung County) and had a comparatively shallow depth of 14.6 km (modified from a focal depth of 16.7 km, as previously reported). The earthquake was felt throughout Taiwan. The Broadband Array in Taiwan for Seismology (BATS) and United States Geological Survey (USGS) reported the focal mechanism of this seismic event as a thrust mechanism with two nodal planes striking in the North–South (NS) and the Northwest-Southeast (NW–SE) directions as suggested by both the agencies (Wu et al. 2016).

The majority of the Southern monitoring stations, which are found in the South and Southeast of Taiwan, have shown precursory signals, and the local intensity for the Meinong earthquake was observed to be ≥3 (Fig. 8.3) as reported in Fu et al. (2017). In contrast, no precursory signals were observed at the Northern monitoring stations for the Meinong earthquake. Pingtung (PT), the monitoring station located

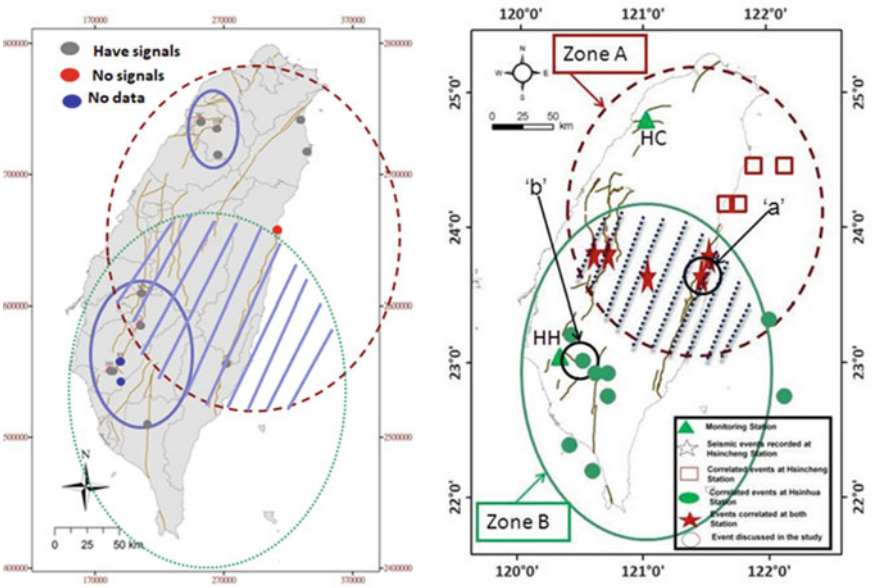

Fig. 8.3. Proposed tectonic-based model for Taiwan and distribution of events recorded at monitoring stations along Hsincheng (HC) and Hsinhua faults (HH) (Walia et al. 2009, 2013)

in the southernmost part, measured a local intensity of 5 and an epicentral distance for the Meinong earthquake of roughly 31 km. Figure 8.4a displays radon time series data for the time window from 15 December 2015 to 15 March 2016 at the PT station. According to data from the previous year, under typical normal circumstances, radon values range from 15 to 20 kBq m^{-3} (Yang et al. 2011). Prior to the Meinong earthquake, radon levels began to rise on January 23, 2016, about 14 days before it struck its maxima on January 25, 2016, when it crossed the +2 level in standard deviation, approximately 12 days before the main seismic event, respectively. More than a few anomalies were recorded between 12 January 2016 and 6 February 2016 that exceeded the standard deviation plus 2. Even though there was a significant earthquake with a magnitude of 6.7 on February 6, 2016, it was found to be quite a distance from the PT monitoring station and does not meet the prior selection criteria. Otherwise, radon levels began to rise on January 13, 2016, reaching their peak on January 16, 2016, and one significant earthquake, at a magnitude of 5.8, occurred in Southeast Taiwan on January 19, 2016. This earthquake was located 86 km from the PT station and meets the criteria. Between February 6 and February 18, 2016, co- and post-seismic subtle variations were also seen, and these high concentration spikes may not be directly related to pre-seismic events.

Since November 2006, radon levels have been continually monitored at the established Hsinhua (HH) monitoring station in the Tainan region along the Hsinhua Fault for earthquake precursory investigations (Walia et al. 2009, 2013; Kumar et al. 2015). Figure 8.4b displays time series radon data from the HH station for the period

between December 15, 2015 and March 15, 2016. The epicenter of the Meinong earthquake, with an observed local intensity of 5, is located at a distance of approximately 26 km from the HH monitoring station. After the station and the surrounding area had hourly rainfall or cumulative daily rainfall of more than 20 and 70 mm, respectively, time series radon data began to rise as of 3 January 2016. First, heavy rainfall that was observed was attributed to this change. However, in the case of Taiwan, it might not be applicable. Some research (Sibson 1977; Quattrocchi 1999; Jimenez and Garcia-Fernandez 2000) claimed a strict correlation between increased pore pressure brought on by rainfall and earthquake triggering. However, in the case of Taiwan, significant rainfall might not be the primary factor in the occurrence of earthquake triggering. The average duration of any radon value shift caused by heavy rain at HH station is seven to ten days; however, in this case, the radon value did not return to the threshold value (around 40 kBq m^{-3}).On January 6, 2016, the radon levels nearly surpassed a +2 standard deviation. According to Kumar et al. (2015) and Walia et al. (2013), the observed radon rise is determined to represent a long-term trend, which is typically not the case in older data. It is discovered that the HH monitoring station is the one that is closest to the Meinong earthquake's epicenter among all currently operational stations. According to Huang et al. (2016), earthquakes like the Meinong earthquake may be caused by faults at shallower depths when there is a moderate lower crustal and high fluid pressure and focused stress. These fluids tend to migrate upward via a crack system in the crust when there is an increase in stress because they have a higher pressure at the bottom. The gradual buildup of stress in the area before the approaching Meinong earthquake may be the cause of the long-term increase in radon readings at the HH monitoring station. It can also be explained by the fact that the Hsinhua District (Tainan) CWB real-time strong ground motion station recorded the biggest peak ground acceleration of 401 cm/s^2 in the East-West direction.

The Chihshang monitoring (CS) station, which is situated in Taitung County in Southeast Taiwan, is approximately 75 km from the Meinong earthquake's epicenter. Figure 8.4c displays the radon time series data for the CS station from December 15, 2015 to March 15, 2016. At this site, a local intensity of approximately 3 was observed. Radon levels began to rise on January 23, 2016, peaking between January 29 and 30, around 8 days before the Meinong earthquake. Although it was not definitely attained, the threshold value (passing the +2 level in standard deviation) was discovered to be extremely close to it. The late pattern of the radon rising at this monitoring site suggests that for this earthquake, the stress distribution was closer on the western side. Additionally, it was noticed that Taiwan's western region had a higher local intensity than its eastern region (Wu et al. 2016; Lee et al. 2016). The Western region also saw greater ground acceleration as a result of the Meinong earthquake. The surface sliding of the Chihshan Fault may have also affected soil radon emission during this observation period, as emission at the CS station was somewhat reduced (Fu et al. 2009). It might be argued that no appreciable increases in soil radon were noticed following two substantial earthquakes that occurred in Southeastern Taiwan on January 13 and January 19, 2016, with magnitudes of 5.3 and 5.8, respectively.

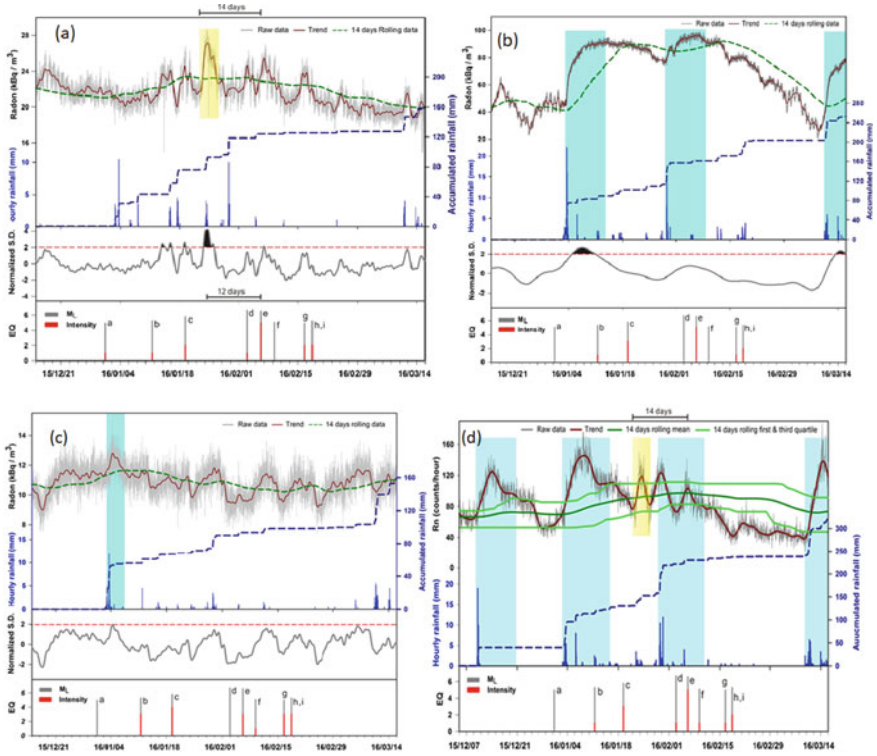

Fig. 8.4. Soil-gas radon time series data along with seismic events and hourly rainfall data related to Meinong Earthquake at **a** Pingtung (PT) station, **b** Hsinhua (HH) station, **c** Chihshang (CS) station, and **d** Chunglun-T1 (CL-T1) station. The brown and green lines show the trend data and the 14-day rolling average of radon, respectively, while the gray line represents the raw data. The soil-gas annual average and the anomaly threshold value (+2) are shown by horizontal dashed lines. The light blue shadows show radon concentrations impacted by this time's strong rains. The length of the soil radon anomalies for the Meinong earthquake is indicated by the yellow shadow (Fu et al. 2017)

Figure 8.6 displays the radon time series data from the Chunglun-T1 (CL-T1) station from December 5, 2015 to March 15, 2016. The Meinong earthquake, with a local intensity of 5, was detected at the CL-T1 monitoring station, which is located around 51 km from the epicenter. A similar pattern of anomalies has been seen in CL-T1 monitoring as it has in the HH monitoring station (Fig. 8.4d). Similar to HH station, the significant increases in radon readings on December 10, 2015, January 3, 2016, and March 10, 2016, can also be linked to severe rainfall (examples include total daily rainfall >30 mm or hourly rainfall >10 mm). The blue bar in Fig. 8.4d depicts the period's precipitation effect. The significant rainfall effect at CL-T1 station, which lasted for 10–12 days and was specifically recorded as daily precipitation if it exceeded 30 mm, is responsible for the change in radon readings. On January 23, 2016, roughly 14 days before the Meinong earthquake, an increase

in radon readings was seen at the CL-T1 station during this period of heavy rainfall. The observed outcome agreed with the PT station. A few days after the seismic event of magnitude 6.6, when the aftershocks started to diminish, the radon values at all monitoring sites in the Southern zone returned to the baseline levels.

8.6 Conclusion

It can be concluded that the various tectonic settings of the region under consideration interfere with the transmission of stress/strain for a certain earthquake. Results from the data produced by our Taiwanese monitoring sites point to this conclusion. Therefore, it may be argued that pre-earthquake strain accumulation in one zone was not transported to another zone and that this may be the reason for missing precursory signals if an abnormality was identified at one zone monitoring station but not at the other zone station. On the other hand, we anticipate anomalies in both monitoring stations if the upcoming earthquake happened in the common zone. It is crucial to locate the earthquake preparation zone in order to correlate any imminent earthquake with geochemical monitoring. The tectonic-based hypothesis fitted well for certain earthquakes of magnitude ≥ 5. Therefore, a number of monitoring stations were established to cover all quadrant characteristics of precursors and to get around the obstacle of pre-earthquake strain transfer in different tectonic zones. This was done in order to have good monitoring results and to have useful data with respect to temporal variations of pre-earthquake signals. For the first time, Real-Time Database for Geochemical Earthquake Precursory Research has been developed and tested utilizing open-source software. The purpose of this is to enhance the data processing for studies on earthquake precursors. We can examine how the data has changed both before and after seismic occurrences thanks to the system. The ability to keep an eye on the sensor that is set up in the monitoring stations is another advantage of this system. It will let us know if a particular station's sensor is malfunctioning by withholding its data, which will encourage us to fix the sensor as quickly as possible to reduce data gaps. Before using any statistical or mathematical techniques on the time series, the data must be continuous. As a result of ongoing radon monitoring, it has been discovered that large earthquakes are preceded by some precursory signals in radon concentrations. Four stations in Southern Taiwan observed significant variations in soil radon levels two weeks before the Meinong earthquake. The idea states that variations in soil radon concentrations at various sites simultaneously display precursory signals that can aid in predicting the general location of approaching large earthquakes. The opening or closing of cracks can cause strain field changes that happened during the buildup of stress prior to seismic activity, which can disrupt the migration of gas and fluid. Therefore, measurements of soil radon can be thought of as a strong and effective tool for investigating earthquake precursory studies in Taiwan.

References

Al-Taminmi MH, Abumurad KM (2001) Radon anomalies along faults in North of Jordan. Radiat Meas 34:397–400

Arora BR, Kumar A, Walia V, Yang TF, Fu C-C, Liu T-K, Wen K-L, Chen C-H (2017) Cleaning soil gas radon at hsinchu, Taiwan for contamination from meteorological and hydrological parameters: a step forward to identify earthquake precursors. J Asian Earth Sci 149:49–63

Baubron J-C, Rigo A, Toutain J-P (2001) Soil gas profiles as a tool to characterize active tectonic areas: the Jaut Pass example (Pyrenees, France). Earth Planet Sci Lett 196:69–81

Fu C-C, Yang TF, Walia V, Liu T-K, Lin S-J, Chen C-H, Hou CS (2009) Variations of soil-gas composition around the active Chihshang fault in a plate suture zone, Eastern Taiwan. Radiat Meas 44:940–944

Fu C-C, Walia V, Yang TF, Lee L-C, Liu TK, Chen C-H, Kumar A, Lin S-J, Lai T-H, Wen K-L (2017) Preseismic anomalies in soil-gas radon associated with 2016 M6.6 Meinong earthquake, Southern Taiwan. Terrestrial, Atmospheric and Ocean Sci 28(5): 787–798

Fu C-C, Yang TF, Walia V, Chen C-H (2005) Reconnaissance of soil gas composition over the buried fault and fracture zone in Southern Taiwan. Geochem J 39:427–439

Guerra M, Lombardi S (2001) Soil–gas method for tracing neotectonic faults in clay basins: the Pisticci field (Southern Italy). Tectonophysics 339:511–522

Huang MH, Tung H, Fielding EJ, Huang HH, Liang C, Huang C, Hu JC (2016) Multiple fault slip triggered above the 2016 Mw 6.4 MeiNong earthquake in Taiwan. Geophys Res Lett 43:7459–7467

Jimenez MJ, Garcia-Fernandez M (2000) Occurrence of shallow earthquakes following periods of intense rainfall in Tenerife, Canary Islands. J Volcanol Geother Res 103:463–468

King CY, Zhang W, King BS (1993) Radon anomalies on three kinds of faults in California. Pure Appl Geophys 141:111–124

Kumar A, Walia V, Lin S-J, Fu C-C (2020) Real-time database for geochemical earthquake precursory research. Nat Hazards 104(2):159–1369

Kumar A, Walia V, Arora BR, Yang TF, Lin S-J, Fu C-C, Chen C-H, Wen K-L (2015) Identifications and removal of diurnal and semi-diurnal variations in radon time-series data of Hsinhua monitoring station in SW Taiwan using singular spectrum analysis. Nat Hazards 79(1):317–330

Lee SJ, Yeh TY, Lin YY (2016) Anomalously large ground motion in the 2016 ML 6.6 Meinong, Taiwan, earthquakes: A synergy effect of source rupture and site amplification. Seismol Res Lett 87:1319–1326

Nicoli L, Massimiani G, Segantin S, Zucchetti M (2019) Detection of radon emissions during 2016/2017 earthquakes in abruzzo (Italy). Fresenius Environ Bull 28(2):672–680

Quattrocchi F (1999) In search of evidences of deep fluid discharges and pore pressure evolution in the crust to explain the seismicity style of Umbria-Marche 1997–98 seismic sequence (Central Italy). Ann Geophys 42(4):609–636

Segovia N, De La Cruz-Reyna S, Mena M, Ramos E, Monnin M, Seidel JL (1989) Radon-in-soil anomaly observed at Los Azufres geothermal field, Michoacan: a possible precursor of the (MS =8.1) Mexico earthquake. Nat Haz 1:319–329

Sibson RH (1977) Fault rocks and fault mechanisms. J Geol Soc Land 133:191–214

Torkar D, Zmazek B, Vaupotič J, Kobal I (2010) Application of artificial neural networks in simulating radon levels in soil gas. Chem Geol 270(1–4):1–8

Walia V, Virk HS, Yang TF, Mahajan S, Walia M, Bajwa BS (2005) Earthquake prediction studies using radon as a precursor in N-W Himalayas, India: a case study. Terrestrial, Atmospheric Ocean Sci 16(4):775–804

Walia V, Virk HS, Bajwa BS (2006) Radon precursory signals for some earthquakes of magnitude occurred in N-W Himalaya. Pure Appl Geophys 163:711–721

Walia V, Yang TF, Lin S-J, Kumar A, Fu C-C, Chiu J-M, Chang H-H, Wen K-L, Chen C-H (2013) Temporal variation of soil gas compositions for earthquake surveillance in Taiwan. Radiat Meas 50:154–159

Walia V, Yang TF, Lin S-J, Hong W-L, Fu C-C, Wen K-L, Chen C-H (2009) Continuous temporal soil-gas composition variations for earthquake precursory studies along Hsincheng and Hsinhua faults in Taiwan. Radiat Meas 44:934–939

Woith H, Pekdeger A (1992) Radon in soil gas: a contribution to the joint German-Turkish earthquake prediction research project. Mém. Expl. Cartes Géologiques Et Minières De La Belgique 32:181–188

Wu YM, Liang W-T, Mittal H, Chao W-A, Lin C-H, Huang B-S, Lin C-M (2016) Performance of a low-cost earthquake early warning system (P-Alert) during the 2016 ML 6.4 Meinong (Taiwan) earthquake. Seismo Res Lett 87(5). https://doi.org/10.1785/0220160058

Yang TF, Chou CY, Chen C-H, Chyi LL, Jiang JH (2003) Exhalation of radon and its carrier gases in SW Taiwan. Radiat Meas 36:425–429

Yang TF, Walia V, Chyi LL, Fu C-C, Wang C-C, Chen C-H, Liu TK, Song SR, Lee CY, Lee M (2005) Variations of soil radon and thoron concentrations in a fault zone and prospective earthquakes in SW Taiwan. Radiat Meas 40:496–502

Yang TF, Fu C-C, Walia V, Chen C-H, Chyi LL, Liu T-K, Song SR, Lee M, Lin CW, Lin C-C (2006) Seismo-geochemical variations in SW Taiwan: multi-parameter automatic gas monitoring results. Pure Appl Geophys 163:693–709

Yang TF, Liu TK, Kuo MCT (2011) Observation and research on active faults by geochemical method (II). Cent Geol Survey Open-file report 100–08:378pp

Chapter 9
Spatial Prediction of Earthquake-Induced Landslide Susceptible Zones—A Case Study from Indian Himalaya

Sandeep Kumar, Parveen Kumar, Sameeksha Kaushik, Yaspal Sundriyal, and Vikram Gupta

Abstract Earthquake-induced landslide hazard is the most serious threat in seismotectonically active mountains like the Himalayas. It has frequently been noted that the damage caused by earthquake-induced landslides is significantly greater than the earthquake itself. Therefore, assessing the susceptible zones of earthquake-induced landslides in seismically active areas is essential. In this study, the probabilistic hazard assessment of the earthquake-induced landslides has been conducted for the Goriganga Valley, Kumaun Himalaya. Numerous studies indicate that a great earthquake of magnitude 8 M_w or higher could strike this area at any time. Hence, mapping earthquake-induced landslides using an improved Newmark's model has been conducted for earthquakes of magnitude 8 M_w. The inclusion of arias intensity to estimate the permanent displacement of the slope for future scenario earthquakes make this work unique from others. The model provides the permanent displacements of potential slopes, which is the function of shear strength parameters of jointed rock mass, the inclination angle of valley slopes, and the arias intensity of the area. It provides the spatial distribution of possible slope failures in the area. It has been noted that ~25% of the study area is susceptible to earthquake-induced landslides when subjected to direct shaking of an earthquake of magnitude 8 M_w. The results of this work provide great insight to planners and civil engineers for hazard mitigation and assessment of the study region.

Keywords Earthquake-induced landslides · Earthquake · Arias intensity · Himalaya · Improved Newmark's method

S. Kumar · S. Kaushik · Y. Sundriyal (✉)
Geology Department, HNB Garhwal University, Srinagar, India
e-mail: ypsundriyal@gmail.com

P. Kumar · V. Gupta
Wadia Institute of Himalayan Geology, Dehradun, India

Sandeep et al. (eds.), *Geohazards*, Advances in Natural and Technological Hazards Research 53, https://doi.org/10.1007/978-981-99-3955-8_9

9.1 Introduction

Earthquake-induced landslides are utmost disastrous geohazards in the world. These mainly occur in seismo-tectonically active terrains and are commonly caused by numerous factors like local geology, geomorphological, hydrology, and anthropogenic. Several times, earthquake-induced landslides have been observed to cause more damage than the ground shaking of their triggering earthquake (Keefer 1984; Cruden 1991). These landslides affect the immense loss of lives and colossal damage to building structures. Therefore, these landslides are critical geohazards in the seismo-tectonically active mountains such as the Himalaya (Owen et al. 2008; Roback et al. 2018).

These landslides are typically evaluated using physical-based models that incorporate seismological data. In earlier studies, peak ground acceleration is the most commonly used seismic parameter for modeling earthquake-induced landslides (Jibson et al. 2000; Strom and Wang 2022). But recently, an earthquake's aris intensity is more reliable for modeling the earthquake-induced landslide for better results (Gupta and Satyam 2022; Sepulveda 2022). To evaluate seismogenic landslides, Newmark (1965) has introduced the method which deliberates the landslide will happen when ground acceleration caused by seismic event is greater than the critical acceleration of the slope, and displacement of the hill slope may be computed using the ground acceleration history of the earthquake. The estimated slope displacement can be employed to determine slope instability during the ground shaking caused by the earthquake (Jibson et al. 2000).

Many studies have been conducted on earthquake-induced landslides using peak ground acceleration values after the occurrence of the earthquake (Jibson et al. 2000; Wang and Lin 2010; Huang et al. 2020; Zang et al. 2020; Strom and Wang 2022). Kumar et al. (2021) proposed the landslide susceptibility map for the Kumaon region by considering the peak ground acceleration (PGA), whereas in the present work, arias intensity is considered for better evaluation. Arias intensity has weightage over PGA for slope failure studies as it comprises both amplitude and duration information, so the present work gives upgraded results for better assessment of hazard. This study was conducted using a simulated earthquake of magnitude 8.0 M_w in the catchment of the Goriganga River, which is situated in the Kumaon region of the Indian Himalayas. The study region, which is a seismically active portion of the Himalayan arc, is situated in the central seismic gap flanked by the rupture zones of two significant earthquakes, the 1934 Bihar Nepal earthquake and the 1905 Kangra earthquake (Khattri and Tyagi 1983).

9.2 Study Area

The study area is located between latitudes of 29°44′58″N and 30°35′13″N and longitudes of 80°02′25″E and 80°22′25″E. It covers the area of the Goriganga River

catchment, which is one of the major tributaries of the Kali River. The region covers an area of ~2200 km^2 and lies in the Kumaun region of the Indian Himalayas (Fig. 9.1).

The region straddles the Tethyan Sedimentary Sequence (TSS), the Higher Himalayan gneisses, and the Lesser Himalayan meta-sediments geologically

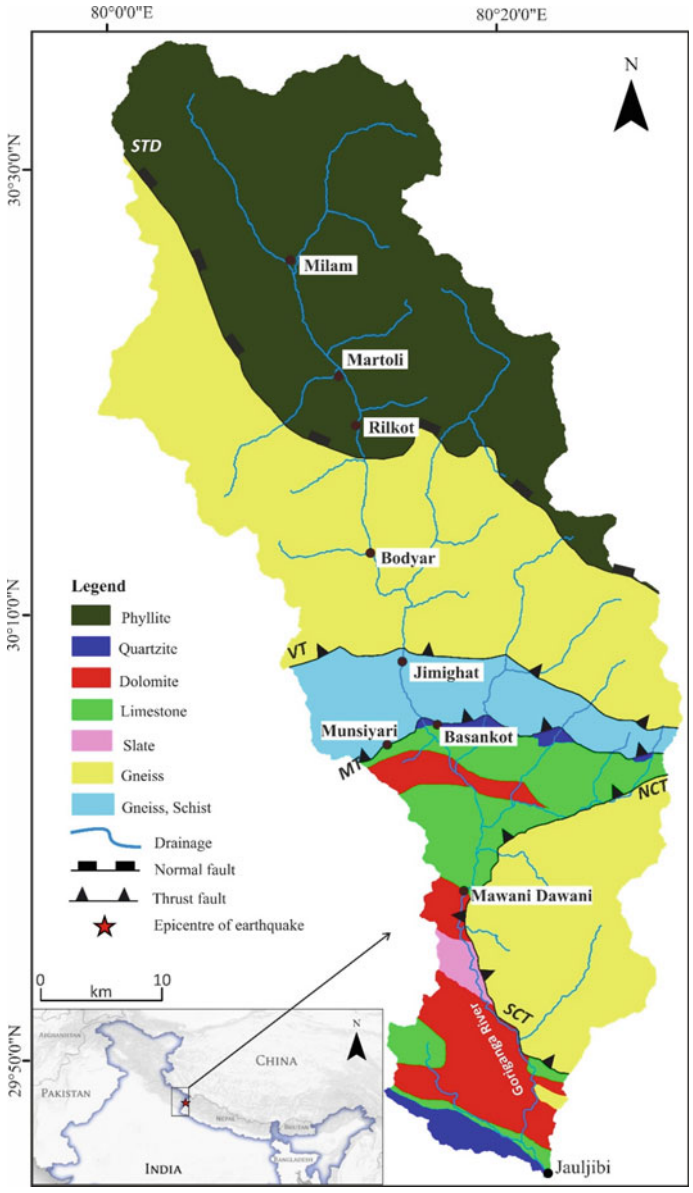

Fig. 9.1 The geological settings of the study area (Adopted from Kumar et al. 2021)

(Fig. 9.1). The major geological faults, South Tibetan Detachment (STD) in the northern research region and Vaikrita Thrust (VT) in the central study area separate these geological segments from one another (Validya 1980). The rocks of the Lesser Himalayan metasedimenteries are comprised of dolomite, limestone, slate, gneisses, quartzite, and schistose gneiss well exposed along the Munsiyari Thrust. These rocks are grouped in the Rautgara Formation, the Gangolihat Formation, the Manthali Formation, the Berinag Formation, and the Munsiyari Formation. The rocks of the Lesser Himalaya comprise the augen gneisses of high-grade metamorphism, and they are known as Chiplakot Crystallines, which are confined by the South Chiplakot Thrust (SCT) in the South and the North Chiplakot Thrust (NCT) in the North (Valdiya 1980). The rocks of the Higher Himalaya are overlain over the Lesser Himalayan metasedimentaries and are comprised of high-grade metamorphic rocks, which are mainly gneisses and are characterized as the Vaikrita Group of rocks. The rocks of TSS lie over the rocks of the Higher Himalaya and exhibit the rocks of phyllites (Valdiya 1980). Two local faults are well exposed in the southern parts of the study area, which are the Baram Fault and the Rauntis Fault, having the strike of NNW-SSE and NW-SE, respectively (Luirei et al. 2006).

Geomorphologically, the region has a rugged topography with a relief of about 6833 m and the characteristics of steep to very steep slopes. While fluvial topography predominates downstream from Bodyar village, glacial formations are more prominent upstream. In the studied region, a number of geomorphic features may be seen, including terraces, waterfalls, hot springs, and triangular facets. Climatically, the region has a humid environment and experiences an annual rainfall of ~2,000 mm. Seismically, the area is susceptible to high-magnitude earthquakes and lies in the seismic zone V on the seismic zoning map of India (Khattri and Tyagi 1983).

9.3 Methodology

The improved Newmark method (Zang et al. 2020) has been used for the spatial prediction of earthquake-induced landslide-susceptible zones. Newmark earlier introduced the Newmark method (1965) and later, it is reformed by Zang et al. (2020) by utilizing the joint characteristics of the rock mass to estimate the shear strength of unloading joints on the slope. This method includes the calculation and integration of the static factor of safety, the critical acceleration of slopes, and the arias intensity to estimate the Newmark permanent displacement of slopes, which are depicted in the flowchart of methodology (Fig. 9.2).

The basic internal friction angle, the unit weight, the joint roughness coefficient, the joint wall compressive strength, and the inclination of slope have all been used to calculate the static factor of safety in the first stage. The thickness of the jointed rock blocks, which is assumed to be 3 m in the study, has also been taken into consideration. The details of geotechnical parameters are described in Table 9.1. The inclination of slopes is calculated using a high-resolution digital elevation model (DEM) of the ALOS PALSAR with a resolution of 12.5 × 12.5 m.

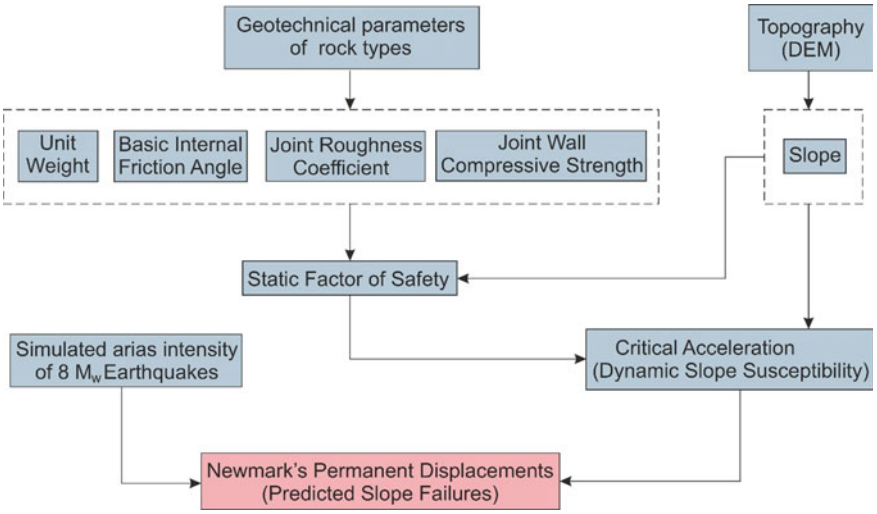

Fig. 9.2 Flowchart of methodology

Table 9.1 The geotechnical factors of the jointed rock mass assigned to rocks presented in the study area

Rock types	γ (kN/m3)	Source	Φ (deg.)	References	JRCn	JCSn (MPa)	Reference
Phyllite	28.3	Rock Mechanics Database Provided by Colorado School of Mines	28°	Duncan (1969)	3.3	68.6	Kumar et al. (2021)
Gneiss	26.5		29°	Coulson (1972)	5.1	105.4	
Schistose gneiss	26.8		26°	Coulson (1972)	4.4	104.9	
Quartzite	26.9		44°	Duncan and Scheerman-Chase (1965)	6.2	105.9	
Limestone	21.5		31°	Duncan (1969)	5.7	57.7	
Dolomite	25.9		32°	Coulson (1972)	3.6	104.4	
Slate	26.5		25°	Barton (1971)	1.5	78.6	

Further, the static factor of safety is estimated using the geotechnical and topographical parameters. It defines the stability of slopes in the absence of external forces. It is described by the following equation (Barton 1973) (Fig. 9.3):

$$F_s = \frac{\tan[JRC_n\left(\frac{JCS_n}{\gamma t \cos\alpha}\right) + \Phi_b]}{\tan\alpha} \tag{9.1}$$

In the second stage, the critical accelerations of slopes were calculated by using the estimated values of the static factor of safety and the inclination of slopes. It is

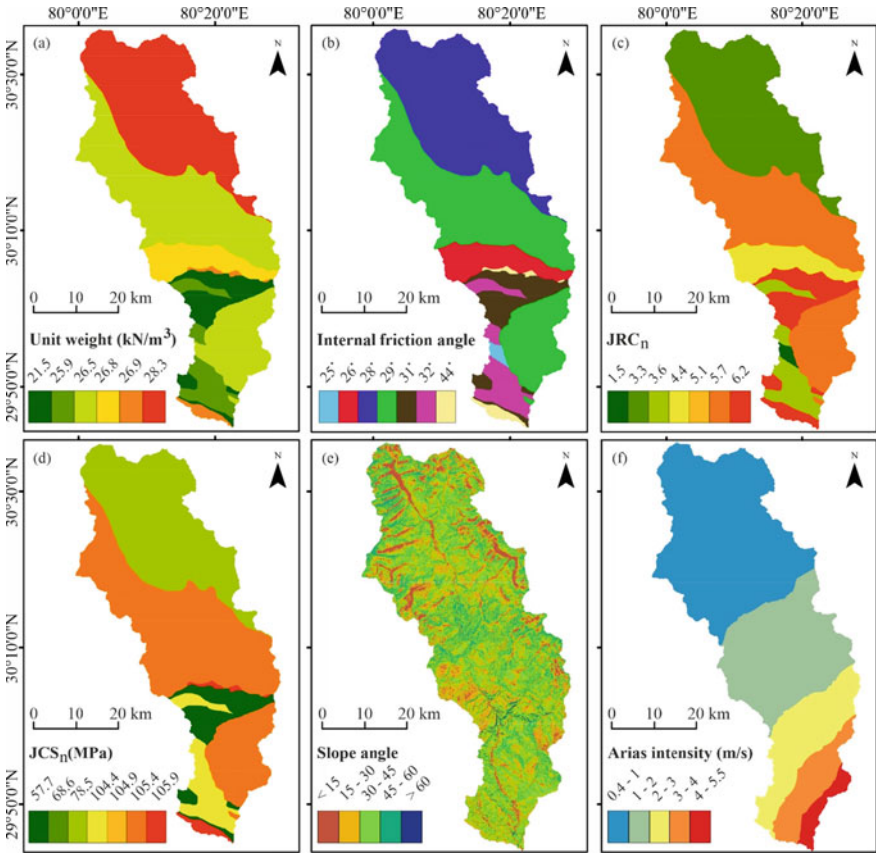

Fig. 9.3 Geotechnical, topographical, and seismic parameters of the study area **a** Unit weight (γ), **b** Internal friction angle (Φ_b), **c** Joint roughness coefficient (JRC_n), **d** Joint wall compressive strength (JCS_n), **e** Slope angle, and **f** Arias intensity of earthquake 8 M_w

expressed in the following equation (Newmark 1965):

$$a_c = (F_s - 1)g\sin\alpha \tag{9.2}$$

In the third stage, The Arias Intensity (I_a) distribution map for the present study area is prepared for the probable future earthquake of magnitude 8.0 M_w. The scenario earthquake of magnitude 8.0 M_w is simulated at the location of the epicenter (29.698° N & 80.754° E) of the 04 April 2011 Indo-Nepal earthquake (5.4 M_w) (Sandeep et al. 2019). The I_a map is prepared by dividing the study area into 0.1° × 0.1° grids, and the waveform is simulated at each grid point. These waveforms recorded at each grid are used to compute the arias intensity values by using the following expression (Arias 1970):

$$I_a = \frac{\pi}{2g} \int_0^{t\max} [a(t)]^2 dt \tag{9.3}$$

where I_a is the arias intensity from the record, a(t) is the acceleration of ground motion at time t, t_{max} is the total duration of the ground motion, and g is the acceleration due to gravity. Arias intensity is expressed in the unit of m/sec.

In the final stage, Newmark permanent displacement of slopes is calculated by computing the slope models of the critical acceleration and the arias intensity of the probable earthquake 8.0 M_w utilizing the following formula (Hsieh and Lee 2011):

$$\log D_n = 0.788 \log I_a - 10.166 a_c + 5.95 a_c \log I_a + 1.799 \pm 0.294 \tag{9.4}$$

where D_n is the Newmark's permanent displacement (cm), I_a is the simulated arias intensity (m/sec), and a_c is the critical acceleration (g). It describes the spatial distribution of potential landslide zones under the ground shaking of an earthquake.

9.4 Results and Discussion

Newmark's analysis was carried out by computing the static factor of safety and critical acceleration using Eqs. 9.1 and 9.2, respectively. It has been noted that the values of F_s and a_c of slopes vary with the strength of rock mass and slope angles in the area. Slopes made up of low-strength rock material and steep inclination exhibit low values of static factor of safety and critical acceleration, indicating a high probability of their failure (Jibson et al. 2000). Many studies have found this type of results in different parts of the world like Northridge province, California (Jibson et al. 2000), Chi-Chi province, Taiwan (Wang and Lin 2010), Hong Kong province (Huang et al. 2020), Ludian province, China (Zang et al. 2020), Kumaun Himalaya, India (Kumar et al. 2021), Central Asia (Strom and Wang 2022). The slopes having the values of static factor of safety (Fs) ~1 are highly susceptible to failure, and the values >1 are less subject to failure (Jibson et al. 2000; Kumar et al. 2021).

According to this study, the study area's Bogdyar, Martoli, Rilkot, and Milam villages in the north, Basankot, Jimighat, and Mandkani villages in the center, and Porthi village in the middle, all have a poor static factor of safety values (Fig. 9.4a). These regions feature weak rock types such as slates, gneisses (Schistose), and phyllites as a result. In comparison to other locations in the study region, these places also have steeper slopes with rock materials that are strongly jointed and fractured. Additionally, the research area's northern Milam, Rilkot, Martoli, and Bodyar villages, the middle region between the Vaikrita and Munsiyari thrusts, and southern Porthi village all show low critical acceleration values, indicating that these locations are very vulnerable under dynamic conditions (Fig. 9.4b). Low-strength rock materials and steep terrain in these areas are the primary contributors to this (Jibson et al. 2000;

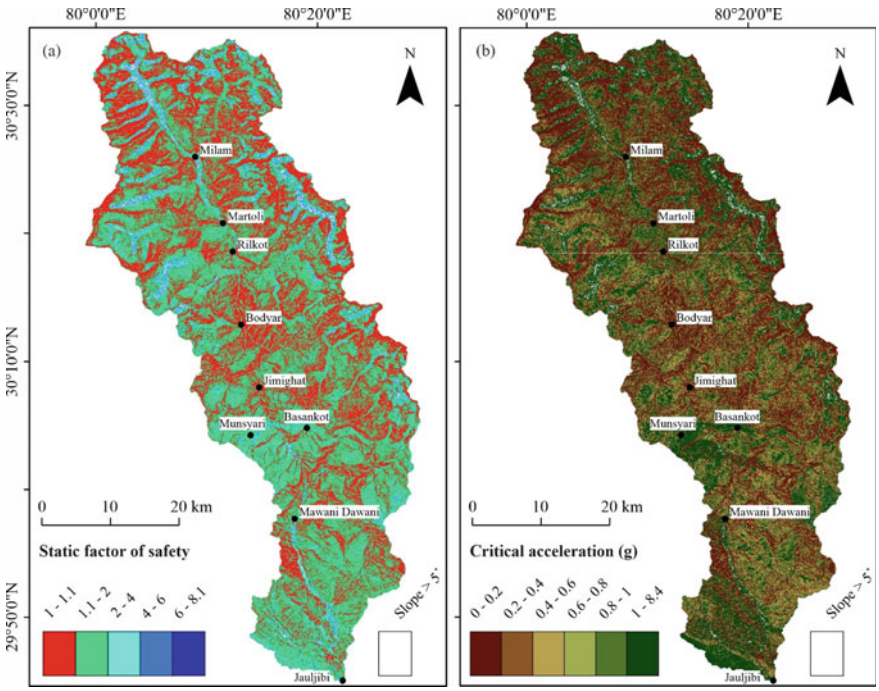

Fig. 9.4 The maps show the **a** static factor of safety, and **b** critical acceleration of the slopes for the study area

Kumar et al. 2021). The critical acceleration map (Fig. 9.4b) depicts the spatial distribution of dynamic slope stability in the study region. The slopes are dynamically unstable when their critical acceleration is less than the ground acceleration caused by an earthquake event. It defines the probability of slope failures under dynamic conditions (Jibson 2000).

Finally, the Newmark permanent displacement depicts the distribution of predicted slope failures in an area (Jibson et al. 2000; Kumar et al. 2021). In this study, Newmark analysis was conducted using Eq. 9.4 exhibits the displacement of susceptible slopes up to 209 cm in the area (Fig. 9.5).

Further, the Newmark permanent displacement map is classified into six classes. The area with Newmark's permanent displacement greater than 40 cm indicates the high chances of earthquake-induced landslide occurrences (Kumar et al. 2021). Slopes with Newmark displacement of less than 40 cm comprise high-strength material with gentle to moderate slope inclinations. However, slopes having a Newmark displacement greater than 40 cm are weak lithology with a number of discontinuities and are made up of steep inclinations. Similar results have also been documented in other parts of the globe when earthquakes shake them (Keefer 1984; Jibson et al. 2000; Wang and Lin 2010; Zang et al. 2020; Kumar et al. 2021; Kumar and Gupta

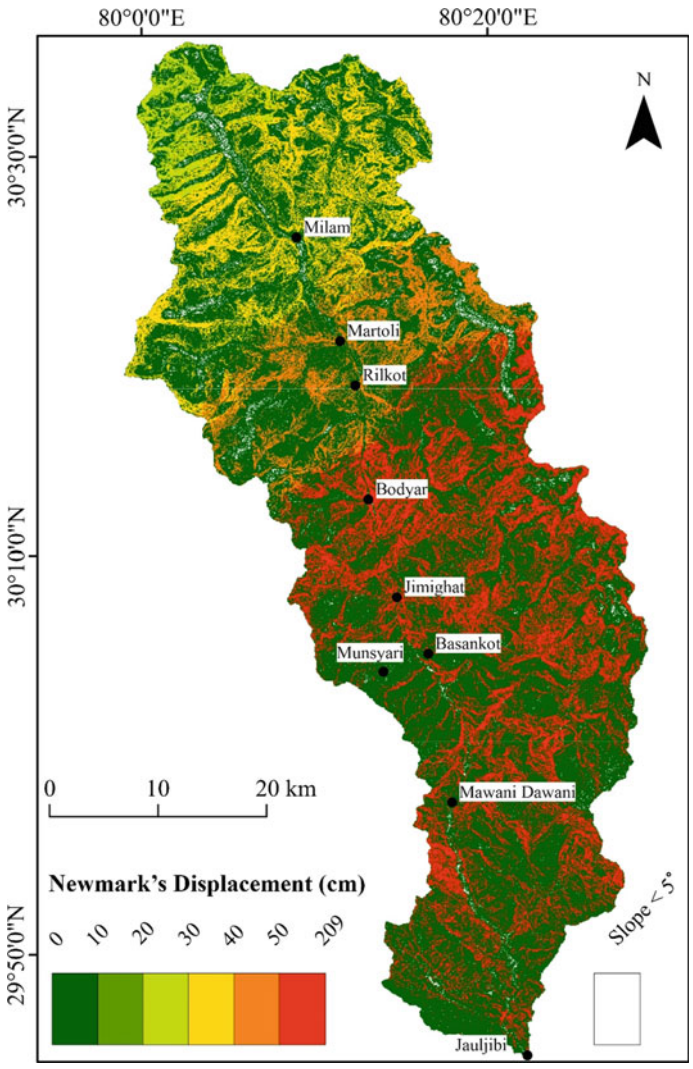

Fig. 9.5 Newmark's permanent displacements during the ground shaking of an earthquake magnitude of 8.0 (M_w)

2021; Gupta et al. 2021, 2022; Gupta and Satyam 2022). Because the simulated earthquake's epicenter lies in the southeast of the research region, the regions with high susceptibility zones are primarily found in the south, southeast, and central portions of the study area (Fig. 9.1). As a result, this region displays high arias intensity ratings, which indicate strong ground shaking during an earthquake. These values decrease as you leave the epicenter (Wilson and Keefer 1984; Keefer 1984).

9.5 Conclusions

The current study utilizes Newmark's technique to evaluate the susceptible zones for the earthquake-induced landslides under the shaking of ground due to earthquake 8.0 M_w. The incorporation of the arias intensity for estimating Newmark permanent displacement makes this work more significant than the previous work done in this region. Along with I_a, the shear strength properties of unloading jointed rock materials are considered to produce more accurate results in the form of earthquake-induced landslide-susceptible zones. The high earthquake-induced landslide susceptible zones cover ~25% of the study area. Low landslide-sensitive zones are found along gentle to moderate slopes with rock of high strength. However, high and very high landslide-susceptible zones are chiefly restricted by steep slopes and weak lithology. This work provides significant inputs for detailed hazard assessment of the Kumaon region.

Acknowledgements The Authors from Geology Department, Hemwati Nandan Bahuguna Garhwal University (A Central University) are thankful to the Department of Science and Technology (DST), India for providing financial support vide project no. DST/CCP/MRDP/187/2019(G) dated 29/06/2020, and we are grateful to the Vice-Chancellor for providing full cooperation. The author PK and VG sincerely acknowledged the Director, Wadia Institute of Himalayan Geology, Dehradun.

References

Arias A (1970) Measure of earthquake intensity. Massachusetts Inst. of Tech., Cambridge. Univ. of Chile, Santiago de Chile

Barton N (1971) A relationship between joint roughness and joint shear Strength. Rock Fract Int Symp Rock Mech Nancy, Fr paper1–8

Barton N (1973) Review of a new shear-strength criterion for rock joints. Eng Geol 7:287–332

Coulson JH (1972) Shear strength of flat surfaces in rock. Proc 13th Symp on Rock Mech Urbana, vol Ill, pp 77–105

Cruden DM (1991) A simple definition of a landslide. Bull Int Assoc Eng Geol—Bull L'association Int Géologie L'ingénieur 43:27–29

Duncan N (1969) Engineering geology and rock mechanics, vols 1 and 2

Duncan N, Sheerman-Chase A (1965–1966) Planning design and construction-rock mechanics in civil engineering works. Civ Eng Public Work Rev 61: 213–215

Gupta K, Satyam N (2022) Co-seismic landslide hazard assessment of Uttarakhand state (India) based on the modified Newmark model. J Asian Earth Sci: X 8:100120

Gupta V, Kumar S, Kaur R, Tandon RS (2022) Regional-scale landslide susceptibility assessment for the hilly state of Uttarakhand, NW Himalaya, India. J Earth Syst Sci 131(1):2

Gupta V, Paul A, Kumar S, Dash B (2021) Spatial distribution of landslides vis-à-vis epicentral distribution of earthquakes in the vicinity of the main central thrust zone, Uttarakhand Himalaya India. Curr Sci 120(12):1927–1932

Hsieh SY, Lee CT (2011) Empirical estimation of the Newmark displacement from the Arias intensity and critical acceleration. Eng Geol 122(1–2):34–42

Huang D, Wang G, Du C et al (2020) An integrated SEM-Newmark model for physics-based regional coseismic landslide assessment. Soil Dyn Earthq Eng 132:106066

Jibson RW, Harp EL, Michael JA (2000) A method for producing digital probabilistic seismic landslide hazard maps. Eng Geol 58:271–289

Joshi SA, Sah SK et al (2019) Modeling of 2011 IndoNepal earthquake and scenario earthquakes in the Kumaon Region and comparative attenuation study using PGA distribution with the Garhwal Region. Pure Appl Geophys 176: 4687–4700.https://doi.org/10.1007/s00024-019-02232-1

Keefer DK (1984) Landslides caused by earthquakes. Geol Soc Am Bull 95(4):406–421

Khattri KM, Tyagi AK (1983) Seismicity patterns in the Himalayan plate boundary and identification of the areas of high seismic potential. Tectonophysics 96:281–297

Kumar S, Gupta V (2021) Evaluation of spatial probability of landslides using bivariate and multivariate approaches in the Goriganga valley, Kumaun Himalaya, India. Nat Hazards 109(3):2461–2488

Kumar S, Gupta V, Kumar P, Sundriyal YP (2021) Coseismic landslide hazard assessment for the future scenario earthquakes in the Kumaun Himalaya, India. Bull Eng Geol Env 80(7):5219–5235

Luirei K, Pant PD, Kothyari GC (2006) Geomorphic evidences of neotectonic movements in Dharchula area, northeast Kumaun: a perspective of the recent tectonic activity. J Geol Soc India 67:92–100

Newmark NM (1965) Effects of earthquakes on dams and embankments. Geotechnique 15:139–160

Owen LA, Kamp U, Khattak GA et al (2008) Landslides triggered by the 8 October 2005 Kashmir earthquake. Geomorphology 94:1–9

Rathje EM, Saygili G (2009) Probabilistic assessment of earthquake-induced sliding displacements of natural slopes. Bull New Zeal Soc Earthq Eng 42:18–27

Roback K, Clark MK, West AJ et al (2018) The size, distribution, and mobility of landslides caused by the 2015 Mw7.8 Gorkha earthquake, Nepal. Geomorphology 301:121–138

Sepúlveda SA (2022) Earthquake-induced landslide susceptibility and hazard assessment approaches. In: Coseismic landslides. Springer, Singapore, pp 543–571

Strom A, Wang G (2022) Some earthquake-induced rockslides in the central Asia region. In: Coseismic Landslides. Springer, Singapore, pp 143–168

Valdiya KS (1980) Geology of kumaun lesser Himalaya. Wadia Inst Himal Geol Rajpur Road Dehradun Himachal times Press, p 280

Wang KL, Lin ML (2010) Development of shallow seismic landslide potential map based on Newmark's displacement: the case study of Chi-Chi earthquake, Taiwan. Environ Earth Sci 60:775–785

Wilson RC, Keefer DK (1984) Dynamic analysis of a slope failure from the 6 August 1979 Coyote Lake, California, earthquake. Int J Rock Mech Min Sci Geomech Abstr 21:220–221

Wu JH, Tsai PH (2011) New dynamic procedure for back-calculating the shear strength parameters of large landslides. Eng Geol 123:129–147

Yang Q, Zhu B, Hiraishi T (2021) Probabilistic evaluation of the seismic stability of infinite submarine slopes integrating the enhanced Newmark method and random field. Bull Eng Geol Environ 1–19

Zang M, Qi S, Zou Y et al (2020) An improved method of Newmark analysis for mapping hazards of coseismic landslides. Nat Hazards Earth Syst Sci 20:713–726

Chapter 10
Tsunamis in the Past and Recent Years over Indian Coasts: A Review

Babita Dani, Vaibhava Srivastava, A. P. Singh, and R. Bhatla

Abstract The deadliest tsunami prior to 2004 in South Asia was on November 27, 1945, of Mw8.1, which originated off the Makran coast of Pakistan in the Arabian Sea and caused deaths as far as Mumbai. Tsunami characteristics associated with the west coast of India are studied in detail here to understand the tsunamigenic hazard along coastal regions of Gujarat, India. After the deadly tsunami of 2004 in the Indian Ocean, many scientists and geologists over the world started studying the two possible tsunamigenic earthquake zones [i.e., Makran Subduction Zone (MSZ) and Andaman-Sumatra Subduction Zone (ASSZ)] in detail to assess the cause, vulnerability (of coastal areas), and proper preparedness and mitigation against such natural hazards. Therefore, a detailed study of these vulnerable subduction zones is much needed because it is beneficial in planning the protection measures to counter inundation and damages caused due to tsunamis and also in the proper execution of an early warning system. A much needed and reliable catalog of tsunamis in the Indian Ocean and tsunamis that affected the west coast of the Indian region and vicinity have been assessed to study the tsunami hazard. In view of this, the present study deals with the study of seismic gaps in the subduction zones along MSZ and ASSZ that could give rise to large tsunamis in future. And also, tsunami travel times, wave height, run-up, and possible inundation scenarios have been summarized.

B. Dani (✉) · V. Srivastava
Department of Geology, Institute of Science, Banaras Hindu University, Varanasi, India
e-mail: babitadanibhu@gmail.com; babita.dani1@bhu.ac.in

V. Srivastava
e-mail: vsrivastavabhu@gmail.com

A. P. Singh
National Centre for Seismology, Ministry of Earth Sciences (MoES), New Delhi 110003, India
e-mail: ajay.pratap@gov.in

R. Bhatla
Department of Geophysics, Institute of Science, Banaras Hindu University, Varanasi, India

DST-Mahamana Centre of Excellence in Climate Change Research, Institute of Environment and Sustainable Development, Banaras Hindu University, Varanasi, India

R. Bhatla
e-mail: rbhatla@bhu.ac.in

Sandeep et al. (eds.), *Geohazards*, Advances in Natural and Technological Hazards Research 53, https://doi.org/10.1007/978-981-99-3955-8_10

Keywords Tsunamigenic earthquakes · MSZ and ASSZ · Tsunami hazard · Indian coasts

10.1 Introduction

A series of fast-moving devastating long ocean waves has been called a tsunami after the Japanese term meant for harbor waves. These waves may be generated by underwater earthquakes, landslides, volcanic eruptions, meteorological events, and asteroid impacts. Meteorological or 'meteotsunamis' are those tsunamis which are generated from atmospheric disturbances however, more than 85% of all types of tsunamis are generated world over from earthquakes (Bernard and Meinig 2011), and those capable of generating tsunamis are therefore referred as tsunamigenic earthquakes. The water above the deformed area is displaced from its equilibrium position as a result of the tsunamigenic earthquake. Waves are thus formed as displaced water mass, which attempts to recover its equilibrium under the influence of gravity. The key factor that governs the extent of a tsunami is the degree of vertical seafloor deformation which depends on the magnitude of the earthquake, focal depth (the depth below the seabed at which the earthquake occurs), fault characteristics (fault length and width), and secondary faulting. Generally, an earthquake should have a moment magnitude (Mw) > 6.5 and be relatively shallow, between 20 and 100 km below the seafloor, for a tsunami to occur. A shallower depth delivers the strongest impulse but a deeper earthquake distributes the impulse over a larger area causing less impact (Pattiaratchi 2020). Tsunamis may cause violent floods at adjacent and distant coastlines with devastating impacts on coastal communities. The effects of a tsunami depend on the characteristics of the seismic event that generated the tsunami, the distance from its point of origin, its size (magnitude), and at last, the configuration of the bathymetry (that is the depth of water in oceans) along the coast that the tsunami is approaching (Patel et al. 2016). These impacts include loss of life, property damage, and loss of biodiversity, and may pose possible threats to the environment like sea water inundation into the land, causing salinization problems for soil and groundwater, sediment deposition, and may induce salt injuries in crops. In the recent past, eastern coastline of India was hit by a tsunami resulting from an earthquake (Sumatra–Andaman Earthquake) on 26 December 2004 causing severe loss of life, properties, and the environment. It was centered in the ocean near the coast of Sumatra, Indonesia. Around two lakh people, mainly on the shores of the Indian Ocean, died from this disaster. Hundreds of thousands of people in Indonesia, Sri Lanka, Thailand, India, Somalia, and other nations, were killed or injured by it (Singh et al. 2012). These incidents have compelled scientist all over the world to ponder over these menaces seriously, which has devastating effects, particularly in coastal regions. The tsunamigenic earthquakes in the Arabian Sea are not as frequent compared to those in the Andaman Sea. However, the western coast of India (which was last hit by a significant tsunami generated due to earthquake in the MSZ in 1945) is equally at risk for the damage of this kind in future. Therefore, awareness in this

regard is quite necessary for the preparedness and mitigation of possible tsunami hazards as a strong backbone of the Indian economy is associated with most of its coasts.

In the past, we have witnessed many catastrophic natural hazards of this kind and have learned a few lessons that can be applied to lessen the impacts thereof. For instance, an integrated early warning and mitigation system can be implemented immediately that enables Indian Ocean countries to identify and prepare for tsunamis and other coastal hazards. The vulnerability and risk of people are higher in densely populated coastal zones and small islands. Therefore, prioritizing investments in disaster preparedness, evacuation planning, and mitigation is crucial for governments to address these challenges effectively. Enhance decision-making while responding to tsunami warning center alerts by developing efficient means of communicating and responding to the hazard. Organizations at all levels (international, regional, and national) should cooperate and coordinate better, recognizing the significance of proper funding strategies. The importance of integrating communities at the forefront of the reconstruction effort. Maintaining public awareness of the threats of earthquakes and tsunamis, including how to comprehend their genesis and how to prepare for such events through educational outreach and training Kontar et al. (2014).

10.2 Historical Records of Tsunami on Indian Coasts

Recent tsunamis in the Indian Ocean (off the west coast of Northern Sumatra, Indonesia on 26 December 2004) and associated Pacific Ocean (South Pacific: 29 September 2009, Chile: 27 February 2010 and 1 April 2014, Japan: 11 March 2011, Solomons: 6 February 2013, etc.) and 16th June 1819 and 1945 Makran earthquake in the Arabian Sea, have proven the vulnerability of coastal areas for such natural hazards. 26 December 2004, the Indian Ocean tsunami has run-up up to 30 m high (resulting in more than 200,000 dead) and affecting 12 countries and three continents. Tsunamis are rare in the Indian Ocean as the seismic activity is much less than what exists in the Pacific. The historical records state there have been seven records of tsunamis set off by earthquakes near Indonesia, Pakistan, and one at the Bay of Bengal (Jordan 2008). As far as Indian coasts are concerned, it is necessary to have a historical background of the earthquakes and tsunamis of the past. The available records of the tsunamis and the locations of the tsunamigenic sources are summarized in Table 10.1. For India, there are two tsunamigenic earthquake sources namely Makran Subduction Zone (MSZ) in the Arabian Sea and Andaman-Sumatra Subduction Zone (ASSZ) in the Eastern Indian Ocean. It is obvious that the east coast of India is affected by tsunamis generated along ASSZ and the west coast from MSZ (Fig. 10.1). Therefore, a thorough investigation of these susceptible subduction zones is vital since it helps in the proper design and implementation of an early warning system as well as the protection measures to prevent inundation and tsunami damage.

Table 10.1 Available records of the tsunami sources on the western and eastern coasts of India

S. No.	Year	Tsunami source	Location (Long., Lat.)	Reference
1	326BC	Earthquake	67.30, 24.00 (Indus delta /Kutch region)	Lisitzin (1974)
2	1008	Earthquake	a.60.00, 25.00 b.52.3, 27.7 (Iranian Coast)	Murty et al. (1999) Ambraseys and Melville (1982)
3	1524	Earthquake	Gulf of Cambay	Bendick and Bilham(1999)
4	1819	Landslide	Rann of Kachchh	Macmurdo (1821)
5	1845	Volcanic and landslide	Rann of Kachchh	Nelson (1846)
6	1897	Earthquake	62.30, 25.00 (Gwadar, Pakistan)	Patel et al. (2013)
7	1945	Earthquake	63.00, 24.50 (Makran, Pakistan)	Murty et al. (1999), Jaiswal et al.,(2009)
8	900 AD	Earthquake	79.53,10.46 (Nagapattinam, Tamilnadu, Sunda-Andaman arc)	Rastogi and Jaiswal (2006)
9	1762	Earthquake	92, 22 Bay of Bengal (Bangladesh)	Mathur (1988)
10	1842	Earthquake	90, 21.5 (North of Bay of Bengal)	Oldham (1883)
11	1847	Earthquake	93.667, 7.333 (Little Nicobar Island)	Berninghausen (1966), Heck (1947)
12	1868	Earthquake	92.73, 11.67 (Andaman Islands)	NGDC/NOAA
13	1874	Earthquake	Sunderbans (Bangladesh)	NGDC/NOAA
14	1881	Earthquake	92.43, 8.52 (West of Car Nicobar)	Berninghausen (1966), Ortiz and Bilham (2003)
15	1882	Earthquake	81.14, 8.34 (Sri Lanka/Indonesia)	Berninghausen (1966)
16	1883	Volcanic	Krakatau, Indonesia	Berninghausen (1966)
17	1884	Earthquake	West of Bay of Bengal	Murty et al. (1999)
18	1935	Earthquake	94, 5.5 (Andaman-Nicobar)	NGDC/NOAA
19	1941	Earthquake	Andaman Islands	Bilham et al. (2005)

(continued)

Table 10.1 (continued)

S. No.	Year	Tsunami source	Location (Long., Lat.)	Reference
20	2004	Earthquake and Landslide	3.31, 95.85 (west coast of Sumatra and Andaman-Nicobar/ Indonesia)	NGDC/NOAA

Note **Serial number 1–7 (on western coast) and 8–20 (on eastern coast)**

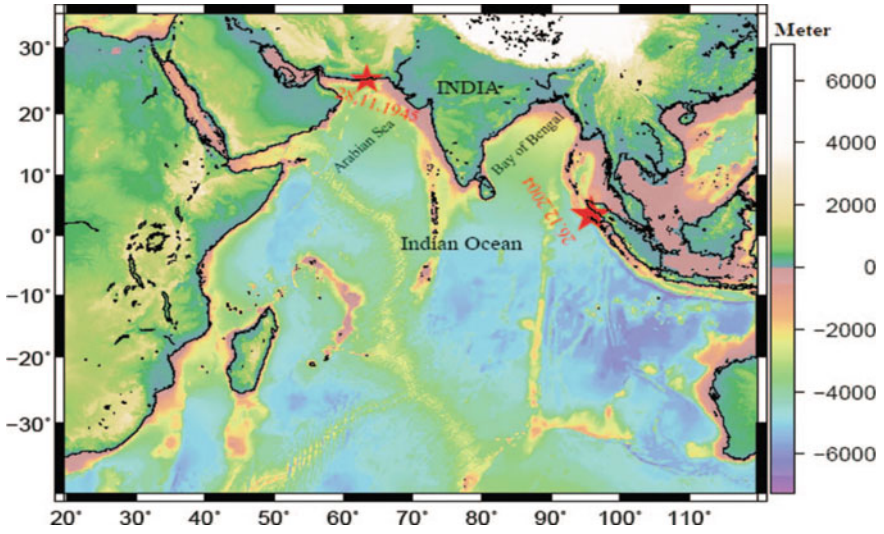

Fig. 10.1 Possible Tsunamigenic sources for India (*Source* Singh et al. 2012)

10.3 Tsunamis in the Western Coast of India: Makran Subduction Zone and Tsunami

The presence of three very active tectonic plates (the Arabian, Eurasian, and Indian plates) and a long strike-slip fault in the Arabian Sea (Fig. 10.2) makes the Makran coast extremely vulnerable to earthquakes and tsunamis. Most of the tsunamis have been recorded on the eastern and southern segments of the Arabian Sea (Katariya et al. 2014). The Makran Subduction Zone is divided into two segments the eastern and western segment, which exhibits strong variation in seismicity (Hoffmann et al. 2013). Byrne et al. (1992) described that five of the great earthquakes in the Makran region ruptured the Eurasian-Arabian plate in four different rupture segments of lengths of about 200 km each in 1483 (58–60°E), 1851, 1864 (61–63°E), 1765 (65–67°E), and 1945 (63–65°E). Out of all these earthquakes, only the 1945 earthquake is known to have caused a large tsunami, followed by a large aftershock in 1947 immediately to the south. Some other historical tsunami events that have affected the western coast of India are given in Table 1. Also, in the past, the western coasts such as Gujarat were affected by tsunamis generated along Makran Subduction Zone.

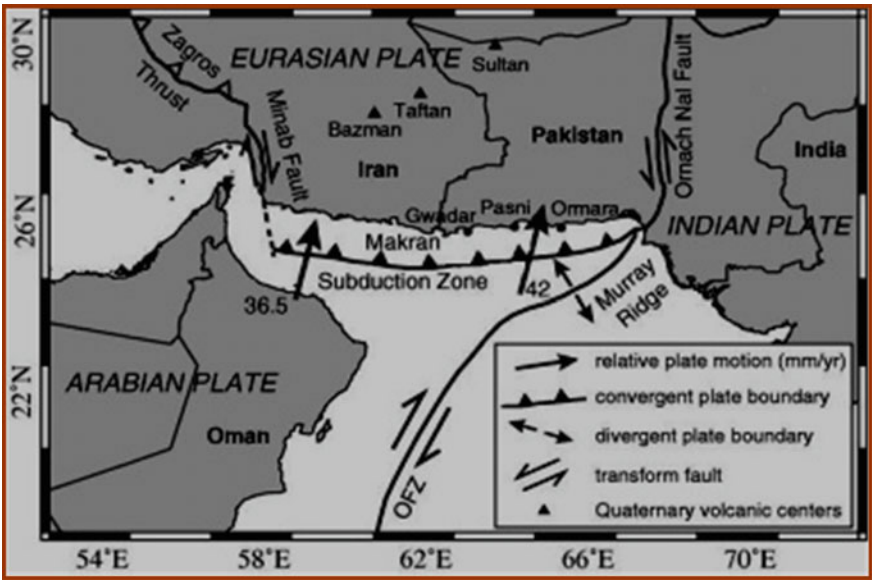

Fig. 10.2 General map of MSZ and its seismo-tectonic settings modified after Byrne et al. 1992 (*Source* Patel et al. 2010)

On the 16th of June, 1819, a tsunami struck the Gujarat coast with a height of the order of 2.3 m in the Kachchh region which was reported during the Kachchh Earthquake (Jaiswal et al. 2009). The 27th November 1945 Tsunami generated due to an earthquake of magnitude 8.1 (Mw) in the MSZ happens to be one of the most devastating tsunamis in the Arabian Sea. The tsunamis generated from the MSZ source area affected the northern Arabian Sea with serious devastation along the western coastlines of India and Lakshadweep islands (Pararas-Carayannis 2005, 2008). The tsunami took away the lives of many and caused huge destruction along the coastal areas of Pakistan, Iran, Oman, and India. The height of the tsunami wave was around 13 m (40 feet) along the Makran coast of Pakistan. Many fishing villages and port facilities were destroyed. The collective impact of the earthquake and the tsunami caused more than 4000 deaths. Karachi was also struck by waves of about 6.5 feet in height. The waves completely devastated the lives of people at Khudi (Shahid 2005). The tsunami wave of a height of 11–11.5 m struck the Gulf of Kachchh region of Gujarat (represented in Fig. 10.3). A massive destruction and loss of life have occurred. The height of the tsunami wave was around 2 m at some places like Mumbai Harbor, Versova, Haji Ali, Juhu, and Danda. Total of 15 people died at Versova, Haji Ali, Danda, and Juhu (Pararas-Carayannis 2005). An attempt was made by Patel et al. (2010) for numerical simulation of the tsunami generation from the MSZ and its propagation into the Arabian Sea to study its consequences on the Porbandar city of Gujarat, India, and found it to have a larger vulnerability than any other port of western Gujrat. Rashidi et al. (2018) evaluated the tsunami wave

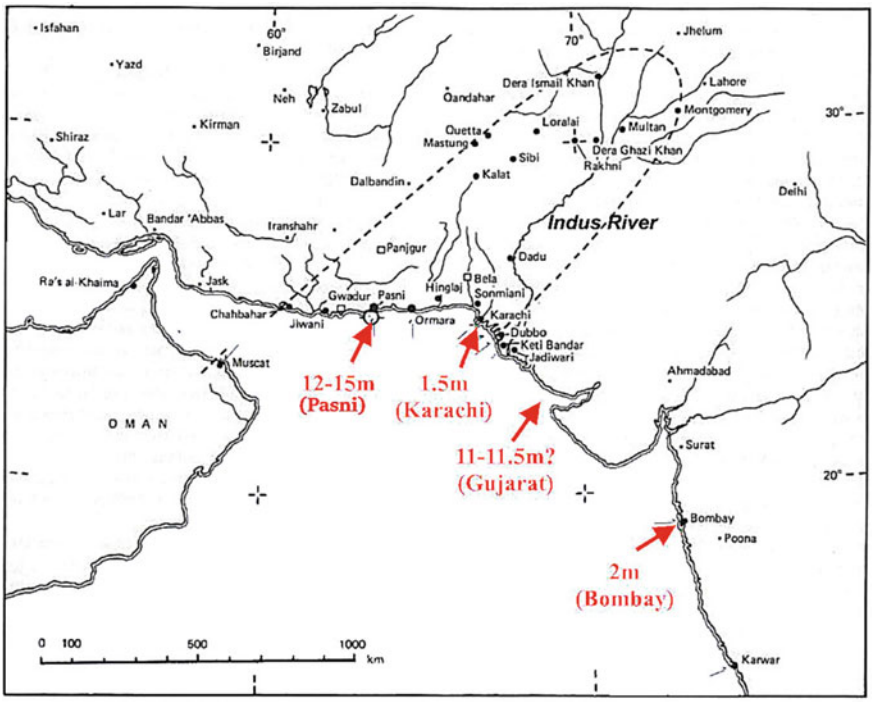

Fig. 10.3 Reported maximum Tsunami Heights along west coast of India in published literatures (*Source* Patel et al. 2016)

energy generated by bottom motion for a tsunamigenic source model distributed along the full length of the MSZ. The MSZ, an approximate 1000 km section of the Eurasian-Arabian plate, is located offshore of Southern Iran and Pakistan (Fig. 10.2). The whole rupture of the plate boundary is divided into 20 segments with a width of around 200 km and a co-seismic slip of about 10 m but with different lengths. Also, found that the total tsunami wave energy displays only 0.33% of the seismic energy released from the earthquake source.

Hoechner (2016) has also illustrated that the Makran Subduction Zone is capable of generating destructive earthquakes and tsunamis though it is seismically inactive for the last few decades. The instrumental and historical seismicity at the subduction plate boundary were analyzed and various synthetic earthquake catalogs were generated spanning 3 lakhs years with varying magnitude-frequency relations. For every event in the catalogs, they computed estimated tsunami heights and presented the resulting tsunami hazard all along the coastlines of Pakistan, Iran, Oman, and India. In the available literature, we have found some works related to the vulnerability of tsunami hazards on the western coast of India. Hazard mapping for Tsunami and strategy for Tsunami evacuation for Diu and Okha and the western coast of Gujarat state on the Indian subcontinent have been shown (Patel et al. 2014, 2017a, b). They

have developed tsunami hazard maps by analyzing the coastal inundation characteristics of Gujarat. Devi and Shenoi (2012) have summarized the tsunami-related research work carried out in India during the past four years all focusing on the numerical modeling of tsunami generation, propagation, run-up, and inundation to establish tsunami warnings. They suggested that numerical modeling can be a tool for providing a proper understanding of the future occurrence of tsunamis. These studies were useful for making public policy and for decision makers in developing disaster management strategies (Patel et al. 2014, 2017a, b). Various scientific studies aimed at understanding the physical processes of tsunami generation, propagation, and inundation for issuing tsunami warnings. For this purpose, the numerical modeling can be an appropriate tool (Patel et al. 2010). It is important to have an improved understanding of the seismo-tectonics and seismicity of the Makran region so as to know the potential of tsunamigenic earthquake occurrence. Also, there is a need to know the sources of past earthquakes through the use of paleo tsunami, tsunami risk assessment, creating evacuation maps, and hazard reduction strategy (Katariya et al. 2014). Byrne et al. (1992) evaluated the source parameters for 14 earthquakes at Makran including the great (Mw8.1) earthquake of 1945. Using the uplift data, dislocation modeling was applied to the 1945 event. They determined the loci of seismic and aseismic slip along the plate boundary and also assessed the effects of the large forearc and accretionary wedge on the style of plate boundary slip.

10.4 Tsunamis on the Eastern Coast of India: Andaman-Sumatra Subduction Zone and Tsunami

The Indian Ocean is the most probable source area for future destructive tsunamis (Jordan 2008; Rastogi and Jaiswal 2006; Singh et al. 2012). The earthquake of 26 June 1941 has been the only strongest ever recorded in the history of the Andaman and Nicobar Islands, generating a disastrous tsunami, until the great earthquake of 26 December 2004. On the basis of the recorded instrumental data, the Sumatra–Andaman region was not supposed to have a high risk of tsunami (Berninghausen 1966; Jankaew et al. 2008). However, after the 2004 Indian Ocean tsunami, many geologists and researchers all over the world instigated to study the geological evidence of tsunamis in this region (Monecke et al. 2008; Satake and Atwater 2007). Paleo-records of tsunamis can help to identify the risk zones based on the study of the past records of tsunami hazards improving risk assessment (Dominey-Howes 2002). Over 562 tsunamis dues to earthquakes have been reported between 810 BC and 2012. Out of these 562, 253 events are with a magnitude less than 6. The number of events with magnitude ranging from 3 to 3.9, 4 to 4.9, and 5 to 5.9 is 14, 93, and 146, respectively. Around 246 earthquakes are reported to have occurred having a magnitude over 5.9, of which 14 events are reported to have a magnitude of 7.9. They have occurred in 825–835, 1663, 1762, 1797, 1833, 1861, 1897, 1903, 1928, 1950, 1969, 2004, 2005, and 2007 (Alam and Dominey-Howes 2016). In the past, the

Sumatra–Andaman region experienced around 348 earthquakes between 1900 and 1980 (Bapat 1982). The Bay of Bengal region faced some great historic earthquakes including the 19 August 1868 (Newcomb and McCann 1987), the 31 December 1881, and the 26 June 1941 events which originated along the Andaman Trench. On 31 December 1881, an earthquake below the Andaman Islands generated a tsunami of a height of 0.8 m, which was recorded by eight tide gauges in the Bay of Bengal. The results of Waveform and amplitude modeling of this tsunami shows an uplift of 10–60 cm of the Car Nicobar Island as it was generated by an earthquake of 7.9 Mw along the India-Andaman plate boundary. As a result, the 40 km of the northern segment is detached from the southern 150 km long segment by a 100 km region toward the west of the Andaman (Ortiz and Bilham 2003).

Based on the statistical information, Pararas-Carayannis (2005) reported that, in the Andaman Sea Basin, most of the earthquakes with even higher magnitudes than 7.1, did not generate any destructive tsunamis so far. For example, two earthquakes, on 23rd August 1936 and 17th May 1955, had magnitudes of 7.3 and 7.2, respectively, but both of them did not generate any large tsunami event. Earthquakes mostly in the Andaman Sea are linked with strike-slip faulting (this involves horizontal tectonic movements). This can be a possible reason for the low occurrence of tsunamis due to earthquakes in the Andaman Sea basin. In the past, an earthquake in 1941 was the only known event for large-scale destruction. Similarly, the 26th December 2004 earthquake had split the Great Sunda Arc into smaller segments throughout the northern Sumatra region. This event includes both thrust and bookshelf faulting which is one of the rare cases. This could be the possible reason why the December 2004 earthquake generated an extreme tsunami) Pararas-Carayannis 2005). Kumar et al. (2007) assessed the damage caused by tsunami due to the 26 December 2004 tsunami based on the pre-event and post-event satellite images. This tsunami occurred due to the Indonesian earthquake (Mw9.3) on Car Nicobar Island and it was found that the maximum wave height was 15 m in the south-eastern parts of the island and a minimum of 0.7 m with a distance from the coastline of 400 m and 368.58 m, respectively. The run-up levels were wide-ranging from 2 to 19 m, and the inundation distance from the coast extended from 295.87 to 1202.57 m on the island. Most of the infrastructural, commercial, and residential complexes have been severely damaged; 2.5 and 1 m of sand was deposited at Aukchung and Arong beaches, respectively. Near Malacca Beach, coastal subsidence of 0.75 to 1.25 m has been reported. Many other islands (Car Nicobar, Aukchung, Kimus, and Malacca villages) also underwent coastal modification and erosion.

Paris et al. (2004) investigated sediment transport and deposition during the December 26, 2004 tsunami inflow and outflow in the Lhok Nga Bay, located 10 km west of the city of Banda Aceh (North-West Sumatra, Indonesia). Side-scan sonar data of the near-shore area are used to study the morphometry and distribution of boulders offshore. Entrainment of finer sediments offshore is inferred by estimating the movable grain sizes based on the simulated current velocities of the tsunami waves. Most of the sediments deposited on land came from offshore, from fine sands to coral boulders. All rocky outcrops offshore were affected by the tsunami (down to 25 m deep). A study has been made by Warek (2013) covering tsunami generation,

propagation, and inundation using 8 earthquake scenarios along the New Britain Trench and Ramu-Markham fault zone in the south-eastern region of Papua New Guinea based on the TUNAMI-N2 numerical modeling. All earthquake scenarios consisted of Mw8.6 and Mw8.7 as mega earthquakes, the remaining were of Mw8.1 magnitude. The result of the surface deformation shows an average of 1 m raise, while half a meter for subsidence in all scenarios. Tsunami heights and travel times were obtained at coastal points from the computed waveforms. From the computation of the earthquake scenario, Mw8.7 the tsunami heights of 3–4 m were observed at coastal areas of Finch, Woodlark Island, and Kiriwina Island. Tsunami travel times were observed to be 10 min to nearby coastal areas in the computation of all earthquake scenarios. The results of the inundation model at the required area revealed that Salamaua was inundated around 3 m. The bathymetry and coastal topography of Lae City may have been the advantage to lessen the effect of a tsunami on Lae City. The historical records state there have been seven records of tsunamis set off by earthquakes near Indonesia, Pakistan, and one at the Bay of Bengal. Bhaskaran et al. (2005) has also worked on the 26th December 2004 Indian Ocean tsunami and they provided a Tsunami Travel Time atlas for the Indian Ocean in their work. This tsunami was triggered by an earthquake of magnitude 9.0 off the coast of Sumatra, Indonesia. Kumar et al. (2008) developed a comprehensive atlas providing expected time of arrival (ETA) for various coastal destinations in the Indian Ocean rim was developed. Application of computing tools like Artificial Neural Network (ANN) for the prediction of ETA can be immensely useful in a real-time mode. The major advantage of using ANN in a real-time tsunami travel time prediction is its efficacy in producing ETA at a much faster time and also simultaneously preserving the consistency of prediction. Overall, it can be mentioned that modern technology can prevent or help in minimizing the loss of life and property provided we integrate all essential components in the warning system and put it to the best possible use. Recently, the Indian Ocean Tsunami Warning and Mitigation System, also known as IOTWS, has been constructed. When the tsunami struck the Indian Ocean in 2004, there were no tsunami early warning systems were setup. The very first tsunami early warning system was developed in Japan after the Sanriku Tsunami in 1933. The Indian Tsunami Early Warning System (ITEWS), which has its headquarters in Hyderabad and is run by INCOIS, was founded in 2007. The ITEWS system consists of a real-time network of seismic stations, tidal gauges, and a tsunami warning center that operates around-the-clock to monitor tsunamis, detect earthquakes that could cause them, and alert vulnerable areas in time (Kumar et al. 2008; Mokhtari 2020).

10.5 Tsunami Hazard and Bathymetry

10.5.1 Gujrat Coast

Tsunami wave propagation depends mainly on the bathymetry. Other geomorphological parameters, the presence of coral reefs, mangroves, and vegetation also determines the extent of tsunami on the maximum length of inland impacts. For the accurate assessment of the wave propagation and arrival times of tsunami at different places, it is essential to have a proper understanding of the nearshore bathymetry (precise water depths), the alignment and elevation of seashores, and the distance from the epicenter of the earthquake. For the estimation of future tsunami hazards, the study of possible inundation area is very important (Satake 1988). Kurian et al. (2006) studied how the run-up and height of tsunami wave are regulated with the help of the bathymetry near the eastern part of south India and Kerala for the December 2004 tsunami case. Singh et al. (2008) also studied the patterns of possible inundation taking into account the coastal geomorphic characteristics and the offshore bathymetry of different areas from the coastal parts of Gujarat (i.e., Saurashtra, Gulf of Kachchh, and south Gujarat). Thus, the understanding of the mechanism of coastal geomorphic assemblage related to response against tsunamis, not only capable of guiding toward disaster risk reduction activities, but also to the studies on past tsunamis. The sandy beaches and ridges absorb tsunami energy and act as barriers suggested by Shukla et al. (2010).

Figure 10.4, shows the bathymetry of the Makran coast and western coast of India along Gujarat. The mainland area is narrow in the offshore region of Kachchh, while it is broader in the offshore region of south Gujarat. Resulting in the different patterns of inundation due to the propagation of tsunami waves in these two regions. It was observed that the low-lying nearshore topography region is more likely to be inundated. This type of different geomorphic settings can show varied inundation scenarios of tsunami effects. The Gulf of Kachchh is more expected to be impacted by the tsunami generated along the already mentioned source region (Patel et al. 2010, 2016). The nearshore topography is very low (1–5 m msl) here and there exist vast intertidal areas. The nearshore bathymetry is steep up to ~5 m, due to this the waves can be amplified here. Thus, these regions are more vulnerable to be flooded due to tsunami. Mandvi coast is economically very important and is situated in the middle of the Gulf of Kachchh shielded with sand dunes and linear beaches. Usually, the dunes are 5–10 m in height and help in protecting the backshore areas from inundation. However, these dunes are made up of coarse-grained detrital sand which can be easily weathered by the strong tsunami waves. The Gulf of Kachchh has ecological importance as it has a Marine National Park which promotes coral reefs, mangroves, and those elegant species that can be affected by a small rise or drop in the water level (Patel et al. 2016). According to Patel et al. (2010), with an increase in the depth of water, the arrival time decreases; therefore, considering the bathymetry, they concluded that the western coast of Gujarat is having larger

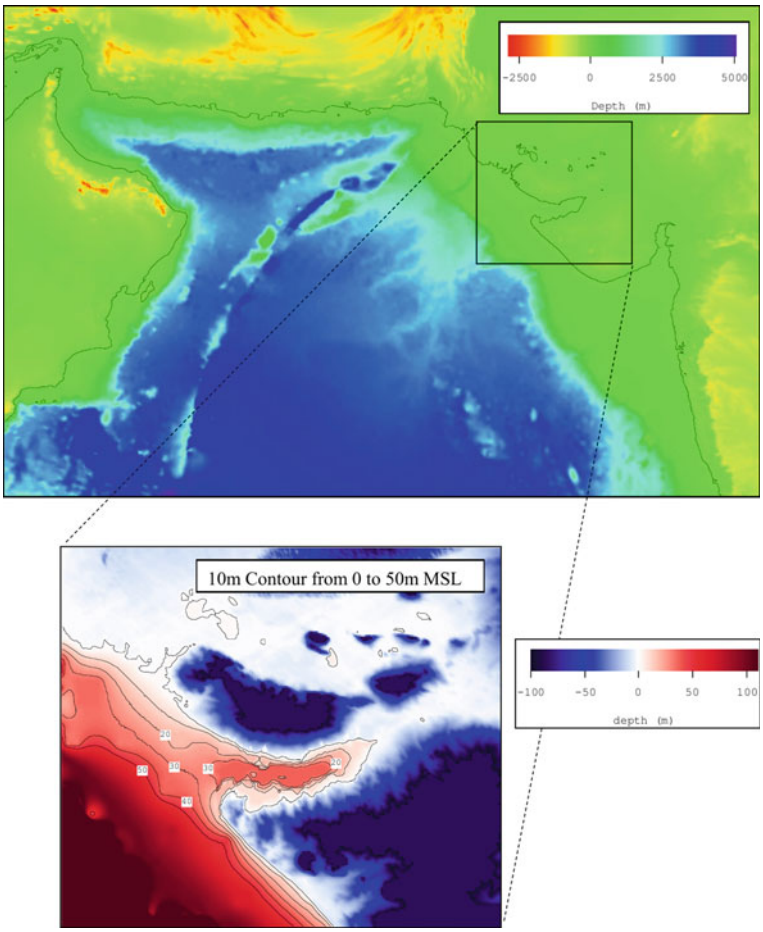

Fig. 10.4 Bathymetry map for the Gujrat coast

vulnerability to tsunami. Hence, it can be summarized as the Gujarat coast of India is extremely susceptible to tsunami attack in the near or far future.

10.5.2 The Role of Coastal Vegetation

The role of coastal vegetation has been extensively known as a natural barrier that can help in reducing the energy of tsunami waves. Although, a vegetation barrier is not sufficient to stop a tsunami completely, and its usefulness depends on the structure of coastal vegetation and the magnitude of tsunami. Patel et al. (2017a, b) evaluated the aftermath of the 2004, Indian Ocean Tsunami, data after the tsunami has emerged

from field studies in several affected countries indicating that mangrove forests have played a critical role in saving human lives and property. The presence of sand dunes, coral reefs, and mangrove forest can all acts as a natural coastal defense which can help to reduce the effect of tsunami wave intensity that may cause serious destruction in a coastal area. The trees of mangroves have shown very successful results among the sea and ocean shore evolution with respect to time. In many extreme conditions mangrove trees have been proven as boundaries of protection against tsunamis. Anthropogenic activities like tourism, shrimp farming, and industrial developments have damaged these mangrove forests and coral reefs, which has made the coastal areas even more vulnerable to catastrophic natural disasters like tsunamis. It is necessary to plan the proper management of coastal vegetation and forests to sustain their buffering function against tsunamis. For a sustainable and continuing vegetation bioshield, an Integrated Coastal Vegetation System has been proposed which includes the utilization of resources obtained from the forest, public participation and awareness program. Although, many governmental and non-governmental organizations have already established various projects related to the coastal vegetation but due to lack of maintenance many of them have failed (Tanaka 2009).

10.6 Discussions

Past and recent witnessed devastation due to tsunamis in the Indian Ocean have proven the vulnerability of its coastal areas to such an extreme natural hazard. Based on the studies and understanding of the historical seismicity at a subduction plate boundary, many scientists concluded that coastal areas of India are highly vulnerable to tsunamis in the future also. Since India has a 1600 km long coastline and has massive capital and infrastructure investments in its coastal areas. Therefore, awareness in this regard is necessary for the preparedness and mitigation of possible tsunami hazards as a strong backbone of the Indian economy is associated with most of its coasts. After the 2004 Indian Ocean tsunami, scientists and researchers all over the world started studying the historical seismicity of subduction zone areas that could give rise to tsunamigenic conditions to identify the risk zones. This paper summarizes the past and recent tsunamis that occurred in the Indian Ocean causing devastating impacts (loss of life, property damage, and impacts on the environment) and also reported works on the numerical modeling of tsunami wave generation, run-up, height, and inundation to find out the possible future risks. Conclusions of the previous studies show that the earthquake of Eastern Makran in 1945 is an interplate thrust event. Due to this event, the subduction zone ruptured in approximately 1/5th of its length. Nine other minor earthquake events occurred in eastern Makran having the same thrust mechanisms located near the tectonic plate boundary. These events were the shallowest (around 70–80 km of the plate boundary) and it was found that during and between great earthquakes this segment along with the overlying accretionary wedge remained aseismic. But the western Makran segment has no historical record of shallow events that could have produced large destructive earthquakes.

It is possible that this segment is either completely aseismic or its sub-segments are presently locked. It is probably possible that both seismic and aseismic slippage is taking place. Although, the seismicity of the Makran region is relatively low compared to the neighboring regions, which have been devastated regularly by large earthquakes (Jacob and Quittmeyer 1979) and the MSZ is seismically inactive for the past few decades but its ability to generate destructive earthquakes and tsunamis in the future cannot be ignored. The presence of distinct late Holocene marine terraces along parts of coastal areas of the eastern and western Makran shows that both sections of the arc are proficient in generating large earthquakes (Byrne et al. 1992). If that theory is true, then western Makran could give rise to future great earthquakes or can rupture in a number of segments in rather smaller-magnitude events. Unlike the eastern part of Makran, western Makran experiences mostly aseismic slip. Earthquakes in western Makran occur mostly at intermediate depths within the down going plate. But, Byrne et al. (1992) suggested that the plate boundary in western Makran has no clear record of historic great events, nor has modern instrumentation detected any shallow thrust events at least for the past 25 years which is contradictory and there needs more study to find out whether which hypothesis is correct. Knowledge of the velocity structure and nature of the state of consolidation or lithification of rocks at depth in the interior portion of the forearc of western Makran can help to ascertain whether that portion of the plate boundary moves aseismically or ruptures in large to great earthquakes. Although, a few great earthquakes occurred occasionally mostly in the eastern part of the Makran Subduction Zone.

In addition to the risk from tidal waves, and coastal erosion the Arabian Gulf region is also vulnerable to earthquake and tsunami hazards. Since, the Arabian Plate is constantly subducting under the Eurasian Plate at a rate of 4 cm/year, the country like Iran and the adjacent region including the Arabian Gulf are prone to high-level seismic activity which is explained by Byrne et al. (1992). Kumar in 2009 reported that, in the past, a number of tsunamigenic earthquakes have been recorded to occur in this region. There is ample scientific proof to consider that this region is expected to be hit in the future also. Arabian Gulf countries are developing some reclaimed islands and constructing offshore settlements. Long-term (100 ± 25 years) sustainability of these developments was examined and assessed in sight of probable geological hazards that have struck this region in the past and likely to occur in the future too. All these construction projects are challenging and require caution against these unpredictable yet extremely hazardous natural events over which humans have absolutely no control. They suggested that since the Arabian Gulf countries have amply of land and long coastline, new townships should be planned and established on the onshore coastal areas. In spite of the developments on the offshore reclaimed islands, the onshore investments would comparatively be safer. Using a hydrodynamic numerical simulation Patel et al. (2010) focused on the run-up height of tsunami waves, arrival time and inundation, and the impacts of different fault parameters. They stated that the time of arrival of the tsunami increases and run-up height decreases, when the distance between the epicenter and location increases. Similarly, the arrival time of a tsunami decreases, and run-up height increases, when the width, length, and dip angle increase. Rashidi et al. (2018) pointed out that with

an increase in magnitude by one unit, the associated tsunami wave energy goes 1000 times more. Considering both static and dynamic bottom motions, he also stated that once the sea floor deformation stops the total tsunami energy decreases with time representing that it is not constant.

10.7 Conclusions

The western and eastern coasts of India have experienced many tsunami events in the past and are highly vulnerable to Tsunamigenic earthquakes in the future also. Based on the past and recent literature study in the MSZ and ASSZ, it is found that tsunamigenic earthquakes can occur and cause great destruction in the near future. Coastal areas of the western part of India are highly vulnerable to Tsunamigenic earthquakes along the MSZ, which may have severe impacts on various coastal communities and mangroves. The presence of sand dunes, coral reefs, mangrove forest, and vegetation can all acts as a natural barrier and can efficiently determine the extent of inland tsunami impacts. Since, this area is highly susceptible to earthquakes and tsunamis due to the existence of three very active tectonic plates, viz., the Arabian, Eurasian, and Indian tectonic plates, therefore, this region should be monitored very closely. As it is clear from the past records of tsunami events reported by many scientists that the subduction zone of Makran poses a gap area that is seismically inactive for many long years but can be a possible source of future great earthquakes that could generate tsunamigenic conditions along the western Indian coast. Therefore, a detailed study of these vulnerable subduction zones is much needed because it is beneficial in planning the protection measures to counter inundation and damages caused due to tsunami and also in the proper execution and implementation of an early warning system. It was also observed that proper awareness, planning, management, and community participation are needed for the preparedness and a sustainable and long-lasting mitigation for possible tsunami hazards.

Acknowledgements The corresponding author would like to thank for the funding support from the University Grants Commission, New Delhi, in the form of Senior Research Fellowship.

Author Contributions All authors have contributed to the study conception and design. The first draft of the manuscript was written by *Babita Dani* and all authors commented on previous versions of the manuscript. All authors read and approved the final manuscript.

Declarations

Conflict of Interest The authors declare no conflicts of interest.

References

Alam E, Dominey-Howes D (2016) A catalogue of earthquakes between 810BC and 2012 for the Bay of Bengal. Nat Hazards 81:2031–2102. https://doi.org/10.1007/s11069-016-2174-7

Ambraseys NN, Melville CP (1982) A history of Persian earthquakes. Cambridge University Press, Cambridge (NY), p 219

Bapat A (1982) Tsunamis and earthquakes in the Bay of Bengal. Tsunami Newsletter, Int Tsunami Inf Center, Honolulu 15(3):36–37

Bendick R, Bilham R (1999) A search for buckling of the SW Indian coast related to Himalayan collision. In: Macfarlane A, Sorkhabi RB, Quade J (eds) Himalaya and tibet: mountain roots to mountain tops. Geol Soc. America Spl. Pap., 328: 313–322

Berninghausen WH (1966) Tsunamis and Seismic Seiches reported from regions adjacent to the Indian Ocean. Bull Seism Soc Am 56(1):69–74

Bernard EN, Meinig C (2011) History and future of deep-ocean Tsunami measurements.https://doi.org/10.23919/OCEANS.2011.6106894

Bhaskaran PK, Dube SK, Murty TS, Gangopadhyay A, Chaudhuri A, Rao AD (2005) Tsunami travel time atlas for the Indian ocean. Indian Institute of Technology, Kharagpur, India, 286 pages with CD

Bilham R, Engdahl R, Feld N, Sayabala SP (2005) Partial and complete rupture of the Indo-Andaman plate boundary 1847–2004. Seism Res Lett 76(3):299–311

Bilham R (1999) Slip parameters for the Rann of Kutch, India, 16 June, 1819 earthquake quantified from contemporary accounts. In Stewart IS, Vita-Finzi C (eds) Coastal tectonics, Geol Soc London, vol 146, pp 295–318

Byrne DE, Sykes LR, Davis DM (1992) Great thrust earthquakes and aseismic slip along the plate boundary of the Makran subduction zone. J Geophys Res 97(B1):449–478

Devi EU, Shenoi SSC (2012) Tsunami and the effects on coastal morphology and ecosystems: a report. Proc Indian Natn Sci Acad 78(3):513–521

Dominey-Howes D (2002) Documentary and geological records of tsunamis in the Aegean Sea region of Greece and their potential value to risk assessment and disaster management. Nat Hazards 25:195–224

Hoechner A, Babeyko AY, Zamora N (2016) Probabilistic tsunami hazard assessment for the Makran region with focus on maximum magnitude assumption. Nat Hazards Earth Syst Sci 16:1339–1350

Hoffmann G, Rupprechter M, Balushi NA, Grützner C, Reicherter K (2013) The impact of the 1945 Makran tsunami along the coastlines of the Arabian Sea (Northern Indian Ocean)—a review. Z Geomorphol 57(4):257–277

Jaiswal RK, Singh AP, Rastogi BK (2009) Simulation of the Arabian Sea Tsunami propagation generated due to 1945 Makran earthquake and its effect on western parts of Gujarat (India). Nat Hazards 48:245–258

Jankaew K, Atwater BF, Sawai Y, Choowong M, Charoentitirat T, Martin ME, Prendergast A (2008) Medieval forewarning of the 2004 Indian Ocean tsunami in Thailand. Nature 455:1228–1231

Jordan BR (2008) Tsunamis of the Arabian Peninsula, a guide of historic events. Sci Tsunami Haz 27(1):32

Katariya BK, Patel VM, Patel DM, Patel KA, Aparnathi M (2014) Tsunamigenic earthquake along the Makran Subduction: "A Case Study of 1945 Makran earthquake." Int J Sci Res Dev 2(3):2321–613

Kontar YA et al (eds) (2014) Tsunami events and lessons learned: environmental and societal significance, advances in natural and technological hazards research, vol 35. Springer. https://doi.org/10.1007/978-94-007-7269-4

Kumar A, Chingkhei RK, Dolendro TH (2007) Tsunami damage assessment: a case study in Car Nicobar Island, India. Int J Remote Sens 28(13–14):2937–2959

Kumar A (2009) History of earthquakes and tsunamis in the Arabian Gulf: potential hazard for reclaimed island communities. WCCE – ECCE – TCCE Joint Conference: Earthquake & Tsunami.

Kumar BP, Kumar R, Dube SK, Rao AD, Murty T, Gangopadhyay A, Chaudhuri A (2008) Tsunami early warning system—an Indian ocean perspective. J Earthquake Tsunami 2(3):197–226

Kurian NP, Pillai A, Rajith K, Mural BT, Kalaiarasan P (2006) Inundation characteristics and geomorphological impacts of December 2004 tsunami on Kerala coast. Curr Sci 90:240–249

Lisitzin E (1974) Sea level changes. Elsevier Oceanographic Series, vol 8. New York, p 273

Macmurdo C (1821) Account of the earthquake which occurred in India in June 1819. Edinburgh Philos J 4:106–109

MacMurdo J (1823) Papers relating to the earthquake which occurred in India in 1819. Trans Literary Soc Bombay 3:90–116

Mokhtari M (2020) Introductory chapter: the lessons learned from past tsunamis and todays practice. Tsunami—Damage Assessment and Medical Triage. https://doi.org/10.5772/intechopen.94909

Murty TS, Bapat A, Prasad V (1999) Tsunamis on the coastlines of India. Sci Tsun Haz 17(3):167–172

Mathur SM (1998) Physical geology of India. National Book Trust of India, New Delhi

Monecke K, Finger W, Klarer D, Kongko W, McAdoo BG, Moore AL, Sudrajat SU (2008) A 1000-year sediment record of tsunami recurrence in northern Sumatra. Nature 455:1232–1234

Nelson C (1846) Notice of an earthquake and a probable subsidence of the land in the district of Cutch, near the mouth of Koree, or the eastern branch of the Indus in June 1845. Q J Geol Soc London 2:103

Newcomb KR, McCann WR (1987) Seismic history and seismotectonics of the Sunda Arc. J Geophys Res 92(B1):421–439

Oldham RD (1883) A catalogue of Indian earthquakes from the earliest time to the end of A.D. 1869. Mem Geol Surv India 19(3): 163–215

Oldham RD (1884) Notes on the earthquake of 31st December 1881. Records of Geol Surv India 19:47–53

Ortiz M, Bilham R (2003) Source area and rupture parameters of the 31 December 1881 Mw=7.9 Car Nicobar Earthquake estimated from tsunamis recorded in the Bay of Bengal. J Geophys Res- Solid Earth 108(4), ESE 11, 1–16.https://doi.org/10.1029/2002JB001941

Pararas-Carayannis G (2005) The great earthquake and Tsunami of 26 December 2004 in Southeast Asia and the Indian Ocean. http://drgeorgepc.com/Tsunami2004Indonesia.html

Pararas-Carayannis G (2008) Future tsunami disasters in the Indian Ocean. In: The 14th world conference on earthquake engineering. Beijing, China. Tsunami Society

Paris R, Fournier J, Poizot E, Etienne S, Morin J, Lavigne F, Wassmer P (2010) Boulder and fine sediment transport and deposition by the 2004 tsunami in Lhok Nga (western Banda Aceh, Sumatra, Indonesia): a coupled offshore–onshore model. Mar Geol 268(1–4):43–54

Patel VM, Patel HS, Singh AP (2010) Tsunami propagation in Arabian Sea and its effect on Porbandar, Gujarat, India. J Eng Res Stud 1(2):206–217

Patel VM, Dholakia MB, Singh AP (2013) Tsunami risk 3D visualizations of Okha coast, Gujarat (India). Int J Eng Sci Innov Technol 2(2):2319–5967

Patel DM, Patel VM, Permar AS, Katariya B, Dadhich G (2014) Tsunami evacuation system for western coast of Gujarat in Okha city. In: International conference on multidisciplinary research & practice 1(8): 411–414. ISSN: 2321-2705

Patel VM, Dholakia MB, Singh AP (2016) Emergency preparedness in the case of Makran tsunami: a case study on tsunami risk visualization for the western parts of Gujarat, India. Geomat Nat Haz Risk 7(2):826–842

Patel DM, Shah K, Yagnik P, Avadh R, Sardhara S (2017a) Literature review on tsunami evacuation system on coast of Diu. Int J Innov Res Sci Technol 3(09), 108–111. ISSN: 2349-6010

Patel DM, Prajapati G, Prajapati R, Raval H (2017b) A review on: resilience of tsunami by mangrove belt in Surat city. Int J Innov Res Sci Technol 3(09):34–39. ISSN: 2349-6010

Pattiaratchi C (2020) Influence of ocean topography on tsunami propagation in western Australia. J Mar Sci Eng 8: 629. https://doi.org/10.3390/jmse8090629
Quittmeyer RC, Jacob KH (1979) Historical and modern seismicity of Pakistan, Afghanistan, northwestern India, and southeastern Iran. Bull Seismol Soc Am 69(3):773–823
Rastogi BK, Jaiswal RK (2006) A catalog of tsunamis in the Indian Ocean. Sci Tsunami Haz 25(3):128
Rashidi A, Shomali ZH, Dutykh D, Khah NKF (2018) Evaluation of tsunami wave energy generated by earthquakes in the Makran Subduction Zone. Ocean Eng, ISSN 0029–8018(165):131–139
Satake K (1988) Effects of bathymetry on tsunami propagation: application of Ray tracing to tsunamis. Pageoph 126(1):27–36
Satake K, Atwater B (2007) Long-term perspectives on giant earthquakes and tsunamis at subduction zones. Annu Rev Earth Planet Sci 35:349–374
Shukla SB, Prizomwala SP, Ukey V, Bhatt N, Chamyal LS (2010) Coastal geomorphology and tsunami hazard scenario along the Kachchh coast, western India. Ind J Geo-Marine Sci 39(4):549–556
Shahid S (2005) Tsunami disaster in South Asia. Pak J Meteorol (Pakistan Meteorological Department) 2(3):3–9
Singh AP, Bhonde U, Rastogi BK, Jaiswal RK (2008) Possible inundation map of coastal areas of Gujarat with a tsunamigenic earthquake. Ind Miner 61(3–4); 62(1–4): 59–64
Singh AP, Murty TS, Rastogi BK, Yadav RBS (2012) Earthquake generated tsunami in the Indian ocean and probable vulnerability assessment for the east coast of India. Mar Geodesy 35:49–65
Singh VS (2008) Impact of the earthquake and tsunami of December 26, 2004, on the groundwater regime at Neill Island (south Andaman). J Environ Manage 89:58–62
Tanaka N (2009) Vegetation bioshields for tsunami mitigation: review of effectiveness, limitations, construction, and sustainable management. Landscape Ecol Eng 5:71–79
Warek M (2013) Tsunami Propagation and Inundation Modellings along South-East Coast of Papua New Guinea (*Conference Paper*)
Websites: NOAA (National Oceanic and Atmospheric Administration, U.S. Department of Commerce) and National Geophysical Data Center (https://ngdc.noaa.gov)

Chapter 11
Instrumentation of India's First Regional Earthquake Early Warning System and Site Characterization of Its Stations

Pankaj Kumar, Kamal, M. L. Sharma, R. S. Jakka, and Pratibha

Abstract The Earthquake Early Warning System Laboratory, Centre of Excellence in Disaster Mitigation & Management, Indian Institute of Technology Roorkee has developed India's first Earthquake Early Warning System (EEWS). For this, Uttarakhand, a Himalayan state of the Republic of India, was selected for setting up the regional EEWS. Seismic sensors have been installed in the central seismic gap region, an area where strong and higher magnitude earthquakes are predicted and likely to occur in the future. A total of 169 sensors have been installed in this seismically active region. The control room has been set up in the Earthquake Early Warning System Laboratory. The data is streamed to the laboratory through dedicated VPNoBB network of BSNL and SWAN. The server does the processing of the data in real time. Warning of the earthquakes that occurred in the instrumented region is issued through two modes. Under first mode, sirens have been installed in the Government-owned buildings of Dehradun, Haldwani, and District Emergency Operation Center in all 13 districts of Uttarakhand. In the second mode, earthquake warning are issued through the mobile app 'Uttarakhand Bhookamp Alert', which has now been renamed now as 'Bhukamp Disaster Early Vigilante (BhuDEV)'. This app was launched to the public on 4th August, 2021 by the honorable Chief Minister of Uttarakhand. In this article, site classification for the instrumented field sites is performed. It is vital for analyzing the seismic hazard of an area and understanding the damage patterns caused by earthquakes. In the present study, 169 sites of the seismic network array of EEWS for Uttarakhand are classified on the basis of geological settlement at the locations of the stations.

P. Kumar (✉)
Centre of Excellence in Disaster Mitigation and Management, IIT Roorkee, Roorkee, India
e-mail: pkumar@dm.iitr.ac.in

Kamal
Department of Earth Sciences, IIT Roorkee, Roorkee, India

M. L. Sharma · R. S. Jakka
Department of Earthquake Engineering, IIT Roorkee, Roorkee, India

Pratibha
Department of Mathematics, IIT Roorkee, Roorkee, India
e-mail: pratibha@ma.iitr.ac.in

Sandeep et al. (eds.), *Geohazards*, Advances in Natural and Technological Hazards Research 53, https://doi.org/10.1007/978-981-99-3955-8_11

Keywords Earthquake early warning system · Site classification · Geological conditions · Uttarakhand · Seismic gap

11.1 Introduction

The Himalayas originated from the closure of the Tethys Ocean and arose in the form of mountains during the late Cretaceous to Tertiary period ~50 Million years ago (Patriat and Achache 1984). The buoyant crust of the Indian plate was detached from the underlying mantle, and subsequent deformation raised the Himalayan mountains (Gupta and Bhatia 1981). The dynamical processes of the Himalayan region have produced several complex tectonic clusters and continuously building up convergent stresses over the past ~50 million years (Chaudhary and Sharma 2017). The Indian tectonic plate has been steadily pushing the Asian plate northward at an average rate of ~50 mm/yr since its collision (Jade et al. 2017; Paudyal and Panthi 2010; Steckler et al. 2008). The process of collision and underthrusting of the Indian plate beneath the Asian plate and the conjunction region of these plate boundaries makes this region one of the most seismically active regions of the world (Bhatia et al. 1999; Gansser 1964). The collision and subduction of these plate boundaries has resulted in the formation of the ~2500 km long curving mountain range of the Himalayas from Nanga Parbat with an elevation of 8215 m above Mean Sea Level (MSL) (Hobusch 2016) in the W-NW to Namcha Barwa of altitude of 7755 m above MSL in E-NE (Gupta et al. 1982, Neate 1989). Underthrusting causes continuous deformation from sector to sector and numerous faults and folds along the entire Himalayan arc (Jade et al. 2017; Waldia 1984). The most significant tectonostratigraphic subdivisions are Main Central Thrust (MCT), Main Boundary Thrust (MBT), Main Frontal Thrust (MFT), and Indus-Tsangpo Suture Zone (ITSZ) (DiPietro and Pogue 2004; Gupta and Gahalaut 2014; Malik et al. 2008; Zhang et al. 1999). The MCT and MBT dip towards the north while the ITSZ dips towards the south (Khatri and Tyagi 1983). MCT was active at in early age and is considered to be the oldest thrust system while MBT is now considered as a dynamic thrust system. The southernmost and youngest fault system is the MFT. The entire thrust system subdivides the Himalayas into four important regions, namely the Tethys Himalaya, the Great Himalaya, the Lesser Himalaya and the Outer Himalaya (Gade and Raghukant 2017). Tectonic plate movements create stress at the junction of fault plate boundaries and thus, stress is generated. Earthquakes result from the catastrophic failure of rocks and the release of accumulated stress (Gupta et al. 2001).

The Indian Himalayas covers an area of ~0.5 Million Km^2 and is equivalent to ~16.2% of the country's total land mass. The Himalayas form the northern boundary of the country (ENVIS Centre on Himalayan Ecology 2020). Most of the upper Himalayas are covered with snow-clad peaks and glaciers, while the middle Himalayas are covered with dense forests. The Himalayan mountain range extends over 12 states, viz., Jammu-Kashmir, Ladakh, Himachal-Pradesh, Uttarakhand, Sikkim, Arunachal-Pradesh, Meghalaya, Nagaland, Manipur, Tripura, and the

hilly regions of two states, namely Assam and West Bengal. The Indian Himalayas are home to a thin and scattered population compared to the national demographics. However, the growth rate is much higher than the national average. A vast area of the Himalayan foothills and its surrounding plains is highly vulnerable to seismic hazards and has seen many devastating earthquakes (Sharma 2003).

During earthquakes, it is evidenced that some structures are majorly affected while nearby few structures do not exhibit significant damages. This is due to the variation of site response characteristics within the region and geotechnical irregularities in the underlying complex surface layers, and, in addition, to improper building designs and malpractice of building codes (Fukushima et al. 2007; Humar et al. 2001; Inaba et al. 2000). The holistic approach is required to perform a seismic hazard study of the vulnerable region. It includes deterministic, probabilistic seismic hazard analysis, geophysical evidence, deformations studies, paleo seismic studies, parametric studies, geotechnical investigations, etc. The site-specific ground response analysis to know the behavior of surface layers concerned with the earthquake shakings during the earthquake events. The site response analysis plays a vital role in mitigating earthquake hazards. For this purpose, drilling at the site of interest will lead to a better understanding of the response of subsurface layers to seismic vibrations. Exploratory drilling is undoubtedly the most reliable way to understand the dynamic properties of underground layers, but it requires significant expenditure in terms of finance, manpower and time (Nakamura 1989).

A parameter commonly known as the time-averaged shear wave velocity (V_{s30}), measured from the soil surface to a depth of 30 m, is an accepted criterion for classifying sites. This is implemented by various building codes, including the National Earthquake Hazard Reduction Program (NEHRP) (BSSC 2004), the Universal Building Code (UBC 1994) and the New Zealand Seismic Code (New Zealand Standards 2004). The site response in ground motion prediction equations (GMPE) is considered in the form of $V_{s30.}$ The V_{s30} values can be estimated either directly from V_s soil profile or using proxies (Xie et al. 2016). Various methods are available to evaluate local site effects or site amplification. These include established techniques such as the traditional spectral ratio technique (Borchardt 1970), the generalized inversion technique (Field and Jacob 1995) and the receiver function method (Langston 1979). Additionally, there are other approaches, such as the Nakamura method, which involves computing the spectral ratio of the horizontal and vertical components of the recorded micro-shocks or ambient noise (Nakamura 1989) and the Coda-wave approach (Phillips and Aoki 1986).

For the sites for which ground motion data are not available, the PGA is estimated from the developed GMPEs. PGA estimation is used to analyze the behavior of the buildings that are expected to be exposed to earthquakes of various magnitudes. Thus, it plays a vital role in the designing of engineering structures. The accuracy in the estimated PGA depends on the consideration of several factors, such as the magnitude of the earthquake, the representation of seismic wave propagation, the distance from the source to the site and the simple representation of site effects in terms of V_{S30}. Irregularities in the subsurface layers have shown that they have a substantial influence on the ground motions recorded by seismic sensors. Improper

modeling of site effects confounds estimates of surface ground motion (Zhao et al. 2006). In this paper, site classification of seismic recording stations in Uttarakhand Himalaya has been carried out and studied.

11.2 Seismic Gaps in the Study Region

Several large earthquakes, e.g., M_w 8.1, 1897 Shillong (Gupta and Singh 1989), M_w 7.8, 1905 Kangra (Ambraseys and Douglas 2004), M_w 8.2, 1934 Bihar-Nepal (Singh and Gupta 1980), M_w 8.6, 1950 Assam-Tibet (Gupta and Singh 1989) and M_w 7.8, 2015 Nepal (Martin et al. 2015) have occurred in the Himalayan region (Fig. 11.1). No major earthquake (M 8 or greater) has happened in the Himalayas since 1950. Several researchers have determined in their research findings that a major earthquake is long due in the Himalayas (Arjun et al. 2014; Kumar et al. 2022a, b; Sharma and Arora 2005), which can be more devastating than previous earthquakes (Wyss et al. 2018). The Himalayas and its foothill regions are exposed to rapid population growth, unmanaged urban sprawling and infrastructure (Bansal and Verma 2013). There hasn't been a strong earthquake in the Uttarakhand region since March 29, 1999, when one with a magnitude of 6.6 occurred in Chamoli region. Semsic hazard studies have concluded that the return period of a strong earthquake in this region is ~30 years (Sharma 2003). So there may be a strong earthquake in Uttarakhand in the coming times. The recurrence of the earthquakes reflects seismic quiescence in the Himalayan region (Srivastava 2004; Gupta 2015). The duration of the seismic quiescence is large in the cases of large-magnitude earthquakes, and it may extend up to centuries or more (Srivastava 1992). Preliminary space–time analysis and studies of seismic activity in the Himalaya reveal three major seismic gaps, namely, the Kashmir gap in the west of the 1905 Kangra earthquake, the central seismic gap between the 1905 Kangra earthquake and the 1934 Bihar-Nepal earthquake, and the Assam gap between the 1897 Shillong and 1950 Assam-Tibet earthquakes (Khatri 1987). Later, Srivastava et al. (2015) further investigated the seismic activities in the Himalayan region by considering patterns of seismicity, local tectonics, global positioning system observations, microearthquakes, paleoseismicity and other related data sets. He delineated two types of seismic gaps of differentiating features throughout the Indian Himalaya. Areas that have triggered major earthquakes ($M \geq 8$) in the past or may be triggered in the future are considered Category-1 seismic gaps. These include Kashmir seismic gap, the West Himachal-Pradesh seismic gap, Uttarakhand-Dharchula seismic gap, the Central Nepal-Bihar seismic gap, the Arunachal seismic gap and the Shillong seismic gap. The areas where major earthquakes ($M_w < 8$) have triggered in the past or may trigger in the future are considered category-2 seismic gaps. These comprise Jammu seismic gap, the East Himachal-Pradesh seismic gap, the Western Nepal seismic gap and the Sikkim-Bhutan seismic gap. Our region of interest, the Uttarakhand-Dharchula Seismic gap, is located in the central seismic gap (Fig. 11.1) and is a deponent of the Kumaun earthquake of 1720 and the M_w 7.8 Garhwal earthquake of 1803. No major earthquake

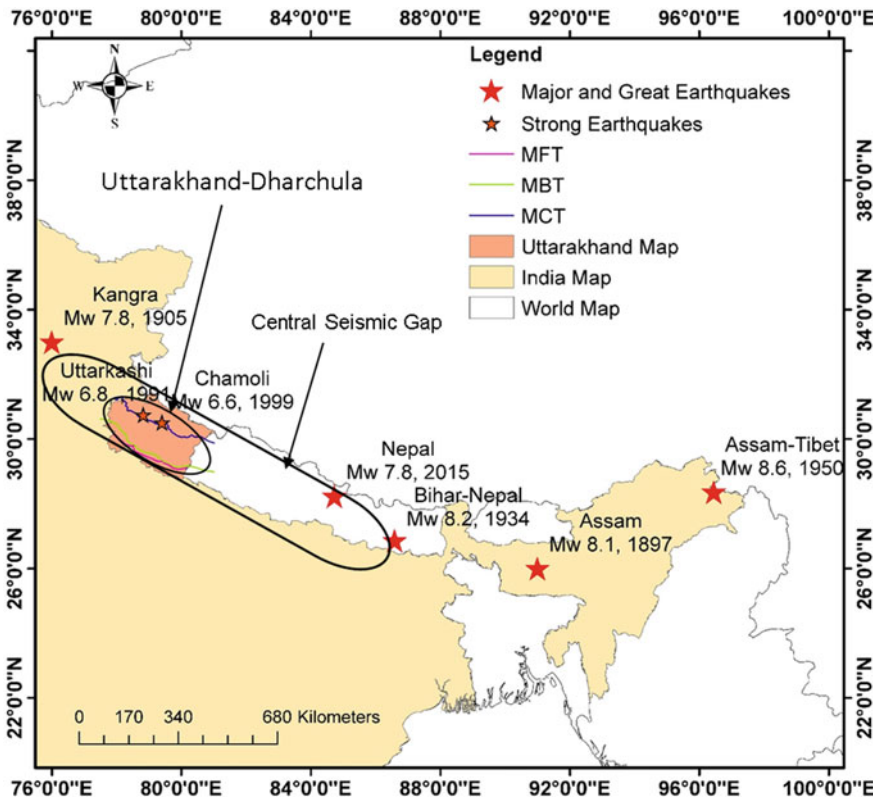

Fig. 11.1 Major earthquakes in the Himalayas and Uttarakhand region and the seismic gaps present in the study area (Khatri 1987; Srivastava et al. 2015)

event has occurred in this region since 1803. This seismic gap of around 800 km long un-ruptured part of the Himalayan arc is also known as Garhwal-Kumaun Himalaya (Khattri 1987). Global positioning system measurements shows strain accumulation and it is still outstanding which is capable of generating one or more destructive earthquakes in the region (Bilham et al. 2001; Bilham 2004). Enormous construction activities, rapid development, fast urban sprawling and high infrastructure growth in this Uttarakhand-Dharchula seismic gap region increase the risk of seismic hazards. There will be thousands of casualties and economic losses worth billions of dollars if a great earthquake hits this seismic gap region (Wyss et al. 2006). The population and infrastructure have already increased manifolds compared to the past in this region, so thus the loss would be enormous (Bansal and Verma 2013; Gupta 2000).

11.3 Geological and Tectonic Settings of the Selected Region

The Himalayan orogenic belt is the outcome of the convergence and collision of the Indian and Asian plates since the early Riphean period. The evolution of the Himalayas is completed in four distinct phases: late Cretaceous to Paleocene (Karakoram phase), late Eocene to Oligocene (Malla Johar phase), middle Miocene to Pontian (Sirmurian phase), and late Pliocene to middle Pleistocene (Siwalik phase). The process of continental convergence was active during the Karakoram phase, while collision and subduction were active during the Malla Johar phase. The Sirmurian phase contributed to the development of distinctive structural characteristics of the Himalayas' main tectonic features (Valdiya 1984b). The tectonostratigraphic studies have subdivided the Himalaya into zones based on distinctive stratigraphy and are bounded by major faults that persist throughout the Himalayas. Notable distinct tectonics from south to north are MFT, Subhimalaya, MBT, Lesser Himalayan Sedimentary Zone (LHSZ), Lesser Himalayan Chrystline Neppes, MCT, Higher (or greater) Himalayan Crystallines (HHC), South Tibetan Detachment system (STD), Tythes Himalaya and the northmost tectonic plate boundary, ITSZ. This plate boundary marks the Hindukush-Pamir-Karakoram-Tibet-Shan Plateau-Malaysia orogenic belt of the Asian plate to the Indian plate. The ITSZ region forms an island arc complex with ophiolites and ophiolites mélanges and calc-alkaline volcanics (Valdiya 1980).

The Sub or Outer Himalayas form the low-altitude hills lying between MBT in the north and MFT in the south. Evidence of erosion and weathering of rocks/debris and fragments of post-collision are often found in this area. These clues were percolated and deposited by the rivers and formed the for-deep basin called Murree-Siwalik Basin. The Lower or Lesser Himalayas is limited by the MCT in the north and MBT in the south. This region comprises marine sediments of the Proterozoic to Cambrian age and some sedimentary records of transgressing shallow sea during the Permian, Upper Cretaceous and Middle Eocene. In general, the deposits found in the Lesser Himalayan Basin provide information about the tectonic changes and associated magmatism that occurred in the basin and its surrounding areas during the Proterozoic and Phanerozoic periods eras. The southern limit of the Great or High Himalayas is marked by the MCT, while its northern boundary is defined by the Tethyan Detachment Fault (TDF). This region comprises the Tertiary leucogranites, Cambro-Ordovician granites/orthogneisses and high-grade Precambrian crystallines. The Tethys Himalaya is limited between the north of Indus-Tsangpo Suture and TDF in the south. This region comprises the deposits of marine sediments of the Tethyan Sea of the period from late Precambrian to Phanerozoic (Palaeozoic-Mesozoic). The Trans-Himalaya or ITSZ includes the oceanic crust of the Neo-Tethys, sediments of deep-sea trenches, subduction and island arc magmatic rocks, sediments related to arc-derived accretion prisms and subduction slices of post-collision Kargil molassic sediments.

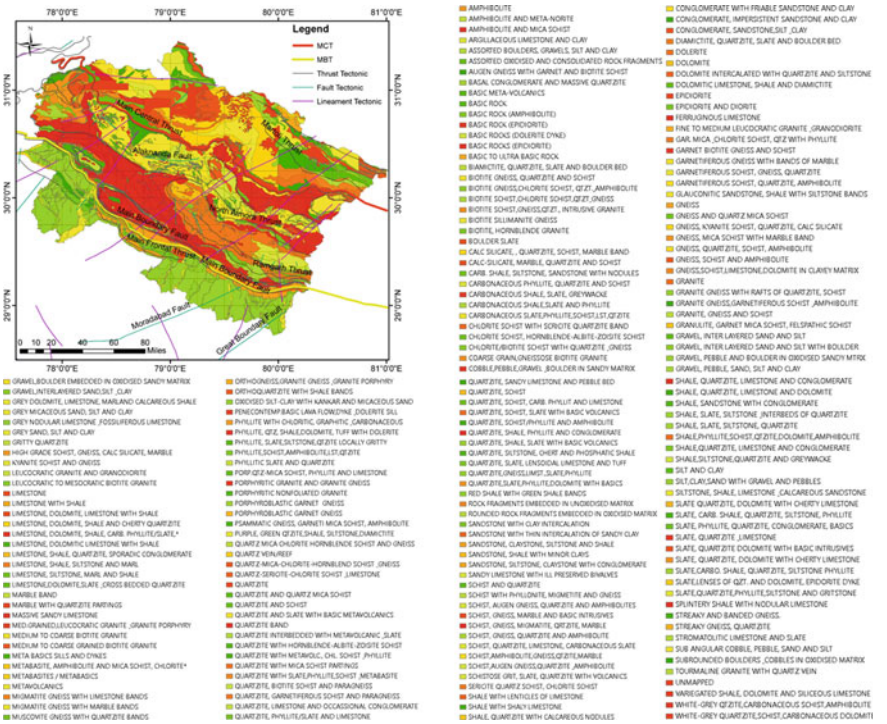

Fig. 11.2 Tectonic and geological features present in Uttarakhand (Bhukosh 2023)

The MCT has pushed high-grade gneisses (from the Higher Himalayas) over lower-grade schists (from the Lesser Himalayas). At the same time, MBT has brought these schists next to unaltered Miocene-Pleistocene molasses in the sub-Himalaya region. The continuous push of the Indian plate against the Asian plate creates friction, crustal shortening, complex geodynamics and faults/thrusts in the Himalayan region. The collision and resulting underthrusting and upheaval of the mountain range make the Himalayan region one of the most seismically active regions in the world (Gansser 1964; Rastogi 1974). Figure 11.2 shows the tectonics and geological features present in the Uttarakhand region.

11.4 Instrumentation of Seismic Array

Due to high seismic risk in Uttarakhand, disaster risk reduction strategies and mitigation measures need to be implemented. After studying the high seismic risk and the sporadic distribution of high-risk zones in the Uttarakhand-Dharchula seismic gap, an earthquake early warning system has been developed for this region (Chamoli et al. 2019; Kumar 2020; Kumar et al. 2023; Kumar et al. 2022a, b).

The Garhwal region in the central Himalayas between Joshimath in the East (30.5616°N, 79.5594°E) and Mori in the west (31.0183°N, 78.0409°E) was selected for the initial phase of instrumentation. This region covers an area of ~150 × 50 km in five districts of Uttarakhand province, namely Uttarkashi, Tehri, Rudraprayag, Pauri and Chamoli. A dense network is preferred for a regional earthquake early warning system. Therefore, low-cost sensors based on Mecro-Electromechanical Systems (MEMS) technology were selected which have lower dynamic range compared to the conventional high-cost and large dynamic-range forced balance accelerometers. The MEMS-based accelerometers fulfill an EEW system's requirement. The required EEW parameter (low pass filtered vertical displacement, P_d) is calculated efficiently from the data retrieved from these sensors. These sensors are tested and effectively deployed in the EEW system for Taiwan and many other countries also (Mittal et al. 2016, 2018, 2019, 2022; Wu and Lin 2014; Wu et al. 2013, 2016, 2019; Wu and Mittal 2021). The name of these accelerometers is pAlert. These sensors are coupled with 16 bits tri-axial MEMS accelerometers and 16-bit 80-MHz CPU.

The pAlert can send the data on two servers through TCP/IP protocol and auto-update its time through Network Time Protocol (NTP) server. A PC-Utility software is used to access it remotely and provide a platform for their configuration. From 2014 to mid-2017, the first phase of the EEW system for Uttarakhand was completed as a pilot project. Figure 11.3 shows the location of the 84 sensors installed in this phase. These sensors are installed on the ground floor of government-owned offices of Bharat Sanchar Nigam Limited (BSNL) and the State Wide Area Network (SWAN) available in Garhwal.

Further extension of the instrumentation for the Kumaun region of Uttarakhand was decided in mid of 2017. The seismogenic part of this region covers four districts, namely Bageshwar, Pithoragarh, Champawat and Nainital. This time, an upgraded version of the sensor (pAlert+) was chosen. These sensors are coupled with 24-bit tri-axial MEMS accelerometers with an internal memory of 8 GB. These sensors are also installed on the ground floor of BSNL and SWAN buildings in the Kumaun region. As a result, the installation of the Kumaun region has 85 sensors as shown in Fig. 11.3. Thus, a total of 169 sensors of both pAlert and pAlert + types have been installed as shown in Fig. 11.3. Inter spacing of sensors is around 10–20 km. Hence, the network is dense and fulfills the requirement of a regional EEW system for Uttarakhand for strong and higher magnitude earthquakes.

11.5 Server Setup

Sensors installed in BSNL and SWAN buildings send the sensed ground motion data to servers at EEW Systems Laboratory, CoEDMM, IIT Roorkee over a dedicated private network on 24×7 basis. Figure 11.4 shows flowchart of networking of EEW system for Uttarakhand. The sensors send data through the TCP/IP protocol bundled in 1200 bytes packets every second. NTP server is used to sync clocks across the network.

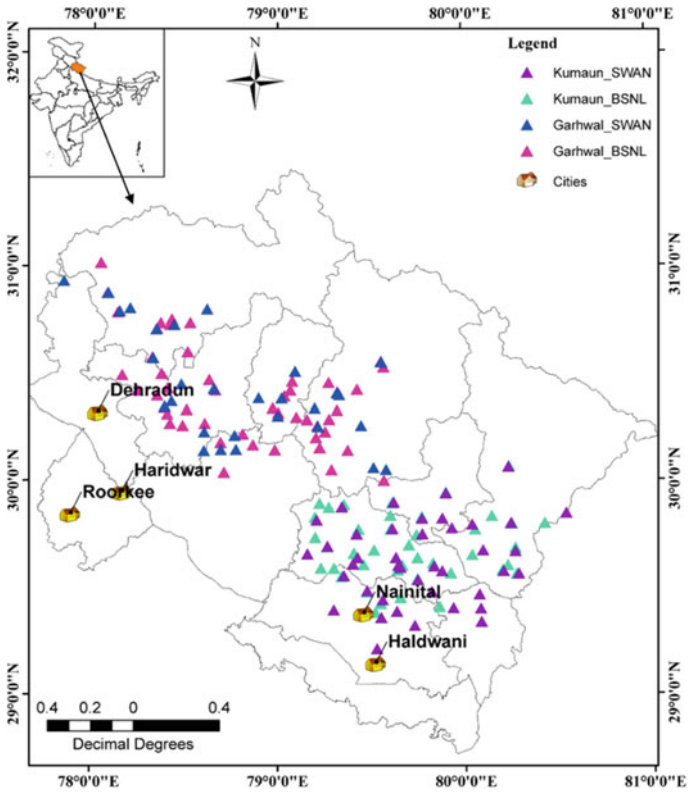

Fig. 11.3 Location of sensors installed in Garhwal and Kumaon region connected through SWAN and BSNL network

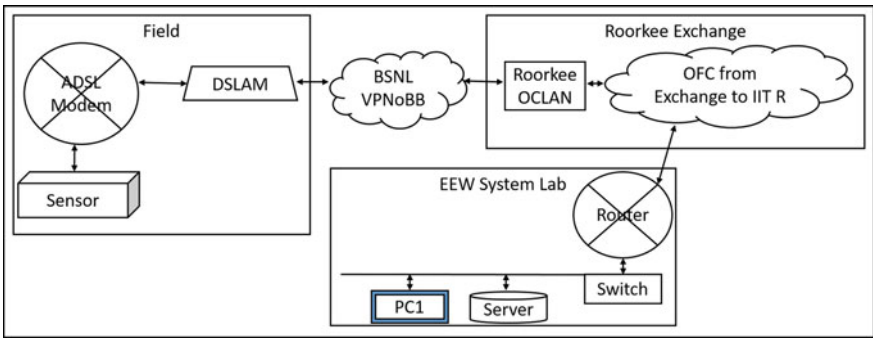

Fig. 11.4 Flowchart of the network

11.6 Warning Dissemination

The dissemination of warnings and their successful reception by users is a top priority of any early warning system. There are several ways of disseminating warning messages to the public. The EEW system of Uttarakhand alerts people through its indigenously developed siren units and mobile application. Sirens have been installed in government-owned buildings, schools, colleges, hospitals, police stations of Dehradun and Haldwani cities and all the district emergency operation centers of Uttarakhand. The warning sirens are connected to the warning server via the internet. In severe earthquake events, the installed sirens are triggered by a command from the server, and installed hooters loudly sound a warning message. Mock drills are also conducted in coordination with the Government of Uttarakhand. A past earthquake event is fed into the system at the scheduled date and time, and a warning trigger is sent to sound the sirens. Mock drill practices simulate scenarios similar to real-time earthquake events. Participating stakeholders like disaster management authorities, fire departments, emergency operation centers, police and NGOs, etc., who deal with disaster response operations, can rehearse their preparedness and improve their standard operating procedures. By doing so, responsible agencies and general public get firsthand information on how to respond during an earthquake. Mock drills are practiced for them as if it were a real earthquake. This can help them change their inappropriate practices to respond during earthquakes and improve their preparedness to respond earthquake events in real time. Mock drill allows all stakeholders to manage post-disaster operations. It also helps in revising and improving their existing standard operating procedures. This lead to a change in the behavior of the residents and forces them to react quickly to earthquake events.

Warnings may be issued to the public in a variety of ways, such as application-specific sirens, television, AM/FM radio broadcasts, mobile messaging, cell broadcast centers and mobile applications. Under this EEW system for Uttarakhand, till now people are warned in two ways through sirens and mobile app. EEW system laboratory indigenously manufactures siren units. Figure 11.5 shows location of sirens installed at the state emergency operation center in Dehradun, the capital city of Uttarakhand, all-district emergency operation centers of the state and significant government buildings in two major cities of the state, Dehradun and Haldwani.

As the Government of Uttarakhand in collaboration with IIT Roorkee has installed public sirens in the two major cities of Dehradun and Haldwani as well as in the district emergency operation centers, too many sirens would be required for covering the whole Uttarakhand and this can cost a massive amount of money and time. This reason prompted us to investigate other options to increase the utility of the developed system. Mobile phones operating on the Android and iOS platforms are ubiquitous in today's world and are owned by a significant portion of the population. Therefore, it is imperative that warning messages are disseminated through mobile App as well. Mobile App should be designed to generate a distinct sound on the mobile phone to notify users when an alert is received. Mobile App should include guidance on the necessary actions to be taken in the event of an earthquake, such as how to locate

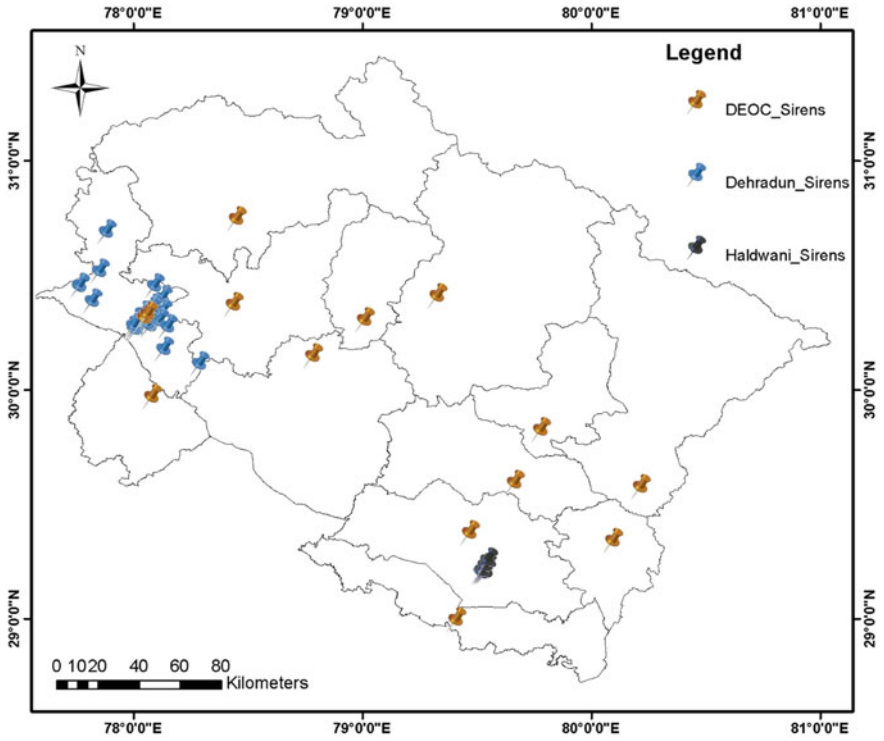

Fig. 11.5 Location of siren units installed in Uttarakhand

a safe place at home to take cover. Additionally, the App should provide a visual representation of the current estimated locations of the P and S waves and the time remaining for the S wave to reach at user's location.

Therefore, IIT Roorkee has developed a smartphone App for earthquake early warning dissemination. This App is designed to broadcast earthquake early warnings to users so that they can protect themselves before harmful earthquake waves reach at their locations. To receive an earthquake's early warning, user has to install the App and fill in the required information during installation process. This App contains informational videos that guide the users to follow the steps to save themselves during an earthquake. At present, this App gives advance warnings of the damaging earthquake in Uttarakhand.

The warnings are issued to the public when the server estimates that the impending earthquake is damaging, while only notifications are issued for non-damaging earthquakes. This App requires user's location-sharing permission to send SMS to registered relatives or friends and disaster management authority on press of SOS button just after of earthquake events. It is always recommended to allow location sharing with Uttarakhand State Disaster Management Authority during App installation. After an earthquake, or in an emergency, this location sharing helps search and

rescue teams to start their operations as quickly as possible. The App receives alerts through the internet, so users are requested to be connected to the internet at all times. The App uses data only during earthquake notifications. This App also shows the demo video and instructions. Please read it at least once to know about the steps to be followed during an earthquake for your safety. Video links are also provided within the App for earthquake preparedness and better understanding.

On August 4, 2021, this App was publicly launched by the Honorable Chief Minister of Uttarakhand. Figure 11.6 represents the first page of the mobile App after installation.

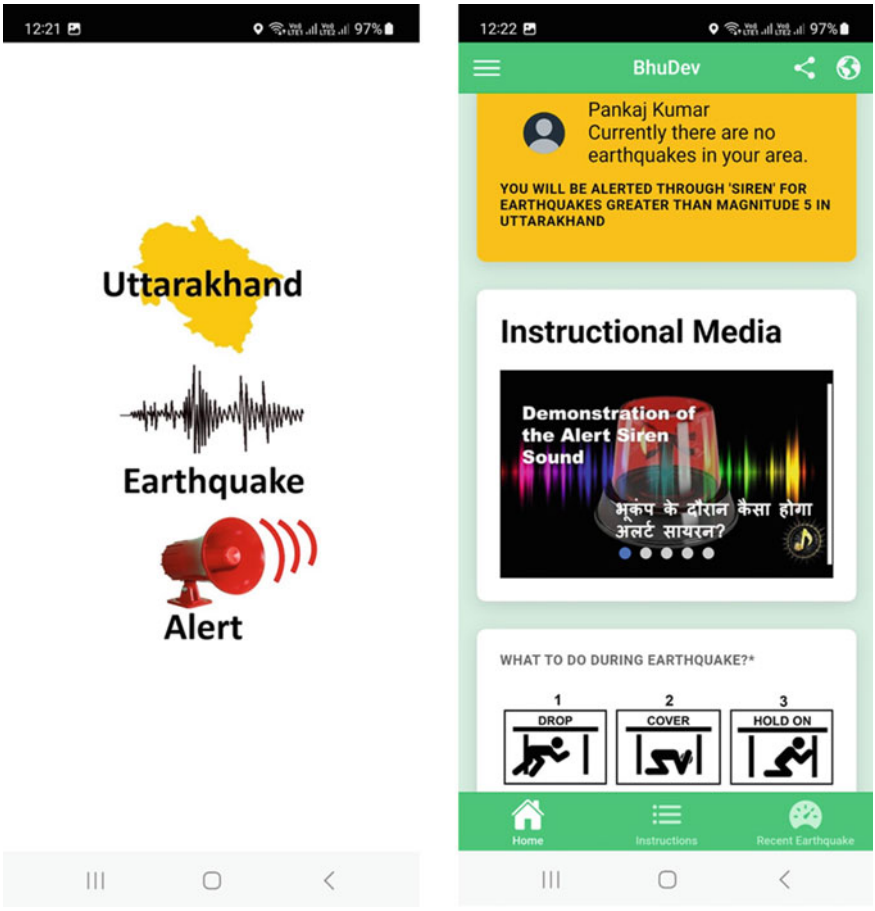

Fig. 11.6 The homepage of the developed mobile app after installation and registration

11.7 Achievements

The earthquake early warning system in the state of Uttarakhand has demonstrated its effectiveness in detecting and issuing warnings of light to moderate earthquake events. Since the launch of the mobile App on August 4, 2021, eight mild earthquakes have been recorded in the Uttarakhand region. Table 11.2 lists earthquake events for which alerts and notifications were issued to the public. A minor earthquake mentioned at serial number 2 in this table, for which the server generated reports and notifications were issued to the public (Table 11.1).

Issuing alerts for all mild earthquakes has increased our confidence in the system's ability and we are sure that the system will successfully generate alerts for moderate and high-magnitude earthquakes in the future. The early warning system is expected to protect lives, jobs and infrastructure while promoting long-term sustainability. In addition, the system provides government officials and administrators with the means to make long-term plans, reduce costs and protect the economy. The government of Uttarakhand in collaboration with EEWS Laboratory conducts mock drills designed to raise public awareness about earthquakes and encourage adherence to guidelines given in the Dos and Don'ts list. The concerned departments take these drills like a

Table 11.1 List of occurred earthquakes in Uttarakhand region for which alerts and notification were issued to the public

Event number	Date	Origin time (UTC)	Location		Mag	Depth (Km)	Region
			Lat	Long			
1	23/05/2021	19:01:45	30.94	79.44	4.3	22	Chamoli, Uttarakhand
2	28/06/2021	06:48:05	30.08	80.26	3.7	10	Pithoragarh, Uttarakhand
3	11/09/2021	00:28:33	30.36	79.13	4.7	5	Chamoli
4	29/12/2021	19:08:21	29.75	80.33	4.1	10	Pithoragarh
5	24/01/2022	19:39:00	29.79	80.35	4.3	10	Pithoragarh
6	11/02/2022	23:33:34	30.72	78.85	4.1	28	Tehri Garhwal
7	09/04/2022	11:22:36	30.92	78.21	4.1	10	Uttarkashi
8	11/05/2022	04:33:09	29.73	80.34	4.6	5	Pithoragarh
9	06/11/2022	03:03:03	30.67	78.60	4.5	5	Tehri Garhwal
10	08/11/2022	20:27:24	29.24	81.06	5.8	10	Dipayal, Nepal

Table 11.2 Site class scheme for stations of EEW system for Uttarakhand after modifying Borchardt (1994)

Site class	General description	Shear wave velocity
A	Firm or hard rocks and compact metamorphic rocks (e.g., gneiss, schist, migmatites, phyllites, quartzites, dolomites, conglomerates), and igneous rocks (e.g., granites, granodiorites, granitoid and basic volcanics)	700 m/sec–1620 m/sec
B	Rocks with a soft to firm consistency (including sedimentary rocks such as sandstone and shale, as well as gravel, siltstone, and limestone)	375 m/sec–700 m/sec
C	Soils (alluvium, slope wash material, Aeolian, silt loams and sandy clay, medium stiff to hard clays, and silty clays)	200 m/sec–375 m/sec

real-time scenario events to assess their preparedness and practice their standard operating procedures. Additionally, mock drills can be helpful during post-earthquake operations.

11.8 Strong Ground Motion Data

EEW System's seismic array for Uttarakhand has recorded almost all earthquakes that have occurred in the Uttarakhand region since 2015. These data are beneficial for earthquake and civil engineering applications. Figure 11.7a shows three channels' motions recorded at the Kanalichina site (lat 29.67, long 80.27) of November 8, 2022, 20:27:24 UTC, M_w 5.8 Dipayal Nepal earthquake (lat 29.24, long 81.06). The epicentral distance of Kanalichina site was 90 km. During this earthquake, the EEW system for Uttarakhand issued an alert to the public on the successfully installed Uttarakhand Bhucamp Alert mobile App. This was a success of the earthquake early warning system developed for the Uttarakhand region. The lead time for the Capital City was ~46 s. Similarly, Fig. 11.7b shows three channels' motions recorded at the Ganai-Gangoli site (lat 29.67, long 80.09) of January 22, 2023, M_w 3.8 Pithoragarh earthquake (lat 29.78, long 80.13). The epicentral distance of the Ganai-Gangoli site was 15 km.

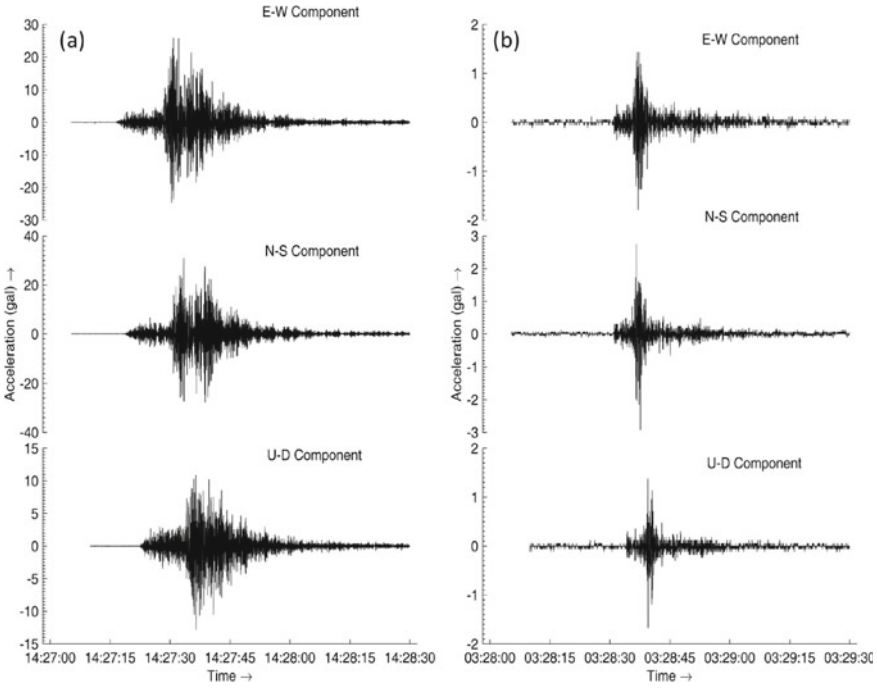

Fig. 11.7 **a** The movement of the components in the east–west (EW), north–south (NS) and up-down (UD) directions at Kanalichina site during the Dipayal Nepal earthquake on November 08, 2022. **b** The detected movement of the east–west (EW), north–south (NS) and up-down (UD) components at the Ganai-Gangoli site during the Pithoragarh earthquake on January 22, 2023

11.9 Site Characterization

It is common for certain structures to remain unaffected after an earthquake, while other similar structures in the same vicinity may exhibit damage (Lachet and Bard 1994). One of the major factors contributing to this phenomenon is the variation in site response characteristics within the region, as the surface layers underneath these structures behave in distinct ways during seismic activity (Kanamori 2005). To minimize the effects of earthquakes, it is crucial to investigate how surface layers react to seismic activities. Undoubtedly, drilling exploration is the most reliable technique for studying the dynamic characteristics of surface layers as it enables precise estimation of geotechnical properties. However, this approach requires significant investment in terms of effort, finances, human resources and time, particularly for investigating broad areas (Borchardt 1970).

Ground motion data recorded from earthquakes are influenced by local site conditions, which can either amplify or deamplify specific period ranges in response spectra. Hence, it is crucial to account for the local site conditions when conducting ground motion analysis and designing structures that can resist earthquakes (Mohraj

1976; Seid et al. 1976). The horizontal-to-vertical (H/V) spectral ratio of an earthquake's ground motion recorded in the S-wave window can reflect the overall influence of subsurface layers on specific frequency ranges, whereas site response has little or no effect on ground motion frequencies in the P-wave window. Field and Jacobs (1995) noted this difference. Satoh et al. (2001) provide a detailed explanation of the H/V ratio for various parts of the ground motion record (P-wave, S-wave, coda). Fourier spectra smoothing of each component's motion is often required during the H/V spectral ratio analysis when a clear peak is not visible. This smoothing helps to extract the spikes corresponding to the site response characteristics from the unsmoothed spectra with multiple spikes. Consistency in smoothing method and smoothing threshold for the entire dataset is crucial during H/V spectral ratio analysis. To obtain more accurate results it is desirable to have multiple records at a station. Averaging the spectral ratios of the entire available record can suppress any spike that is not related to the site response. However, this smoothing process can be time-consuming and requires significant effort, especially when analyzing H/V spectral ratio for many records and stations. The natural frequency range of each site class is a crucial factor in site classification. Soft surface layers tend to exhibit more prominent horizontal motion compared to vertical motion, while rigid surface layers show similar maximum values and waveforms for both horizontal and vertical motions (Nakamura 2008). H/V spectral ratio curves can reveal the dominant periods of a site, regardless of time, location and season (Nakamura 1989), but the amplification of the site obtained from these curves may not always be consistent. Therefore, other methods are necessary to simultaneously obtain the shear wave velocity profile (Dal Moro 2019). Some researchers have combined surface geology and shear-wave velocity for site classification (Borchardt 1994).

In this article, the site characterization of the instrumented sensors is done by modifying the Borchardt (1994) classification approach, which is shown in Table 11.2 (Mittal et al. 2012). In classification, a physical description of the near-surface material is used. Therefore, the classification is mainly based on the type of rock/soil. The information about the site geology is collected from the geological map of Uttarakhand (Bhukosh 2023) and the Seismotectonic Atlas of India and its environs (GSI 2023) (Fig. 11.2).

11.10 Result and Discussion

Since 2014, the starting year of this project, no strong earthquakes have occurred in the instrumented region. But for all light earthquakes that occurred in the instrumented region after August 4, 2021, notifications were issued to the public through the mobile App. These few events have inspired the researchers involved in this project and they are expecting best performance during strong earthquakes. To raise awareness about earthquakes, the EEWS research team conducts a mock drill on the first day of every month at 12 noon. This drill allows the state and district disaster management authorities to assess their preparedness and educate the public on how

to respond during a real event. The team has also distributed pamphlets and other awareness materials across the state.

The site classification of the instrumented site is purely theoretical, and a detailed investigation is required to know more precise results of the effects of local geology on ground motions. This carried-out classification, as given in Appendix 1, gives a general glimpse of the sub/surficial characteristics of the instrumented sites.

Acknowledgements The authors express their gratitude to the Government of Uttarakhand and USDMA for providing the necessary funds for this project. The authors are also thankful to NCS for funding the pilot project. The authors also acknowledge the valuable discussions held with officials from the Uttarakhand Administration, National Disaster Management Authority and National Center for Seismology. The authors thank the project staff for their hard work and contributions and Centre of Excellence in Disaster Mitigation & Management IIT Roorkee for their support.

Appendix

List of stations, their location, site geology and site characterization.

Station number	Station name	Lat	Long	Site class	Site geology according to the seismotectonic atlas
1	Adibadri	30.16	79.23	A	Quartzite and slate with basic meta-volcanics
2	Augustmuni	30.40	79.04	A	Schistose grit, slate, and quartzite with volcanics
3	Auli	30.53	79.57	A	Schist, gneiss, marble, and basic intrusives
4	Bhiri	30.47	79.08	A	Schistose grit, slate, and quartzite with volcanics
5	Chandrapuri	30.43	79.07	C	Grey sand, silt, and clay
6	Chhaam	30.50	78.38	A	Phyllite, quartz, shale, dolomite, tuff with dolerite
7	Chamba	30.35	78.39	A	Quartzite, shale, phyllite, and conglomerate
8	Chamiyala	30.47	78.63	A	Quartzite and slate with basic meta-volcanics
9	Chinyalisour	30.58	78.33	B	Gravel, pebbles, sand, silt, and clay
10	Dhanaulti	30.42	78.25	B	Diamictite, quartzite, slate, and bouldered bed
11	Dhauntri	30.60	78.52	A	Quartzite and slate with basic meta-volcanics
12	Dunda	30.71	78.35	A	Basic meta-volcanics

(continued)

(continued)

Station number	Station name	Lat	Long	Site class	Site geology according to the seismotectonic atlas
13	Gaza	30.27	78.42	A	Phyllite, quartz, shale, dolomite, tuff with dolerite
14	Gaucher	30.29	79.16	B	Gravel, pebbles, sand, silt, and clay
15	Ghurdauri	30.18	78.69	A	Phyllite, quartz, shale, dolomite, tuff with dolerite
16	Gwaldom	30.00	79.57	A	Granite, gneiss and schist
17	Gholteer	30.30	79.10	B	Gravel, pebbles, sand, silt, and clay
18	Ghansali	30.43	78.66	A	Quartzite and slate with basic meta-volcanics
19	Gopeshwar	30.42	79.32	A	Basic meta-volcanics
20	Gairsain	30.05	79.29	A	Garnet mica and chlorite schist, quartzite with phyllite
21	Gyanshu	30.73	78.42	B	Gravel, pebbles, sand, silt, and clay
22	Jhaknidhar	30.34	78.51	A	Phyllite, quartz, shale, dolomite, tuff with dolerite
23	Jamnikhal	30.27	78.61	A	Phyllite, quartz, shale, dolomite, tuff with dolerite
24	Joshimath	30.56	79.56	A	Gnesis, kyanite schist, quartzite, calc silicate
25	Kandikhal	30.44	78.41	A	Phyllite, quartz, shale, dolomite, tuff with dolerite
26	Karanprayag	30.26	79.22	A	Quartzite and slate with basic meta-volcanics
27	Kanatal	30.40	78.35	A	Phyllite, quartz, shale, dolomite, tuff with dolerite
28	Khirsu	30.17	78.87	A	Quartzite, shale, phyllite, and conglomerate
29	Kanskhet	30.04	78.71	A	Phyllite, quartz, shale, dolomite, tuff with dolerite
30	Koteshwar	30.26	78.49	A	Phyllite, quartz, shale, dolomite, tuff with dolerite
31	Mahidanda	30.76	78.43	A	Basic meta-volcanics
32	Maneri	30.74	78.53	A	Quartzite and slate with basic meta-volcanics
33	Mori	31.02	78.05	A	Quartz-mica-chlorite-hornblend schist and gneiss
34	Matli	30.74	78.37	B	Gravel, pebbles, sand, silt, and clay

(continued)

(continued)

Station number	Station name	Lat	Long	Site class	Site geology according to the seismotectonic atlas
35	Naugaon	30.79	78.14	A	Quartzite, slate, phyllite, dolomite with Basics
36	Narainbagar	30.15	79.38	C	Gray sand, silt, and clay
37	Nauti	30.21	79.21	A	Quartzite and slate with basic meta-volcanics
38	Pipalkoti	30.43	79.43	A	Limestone, dolomite, shale, carb. phyllite/Slate
39	Purola	30.88	78.08	A	Quartz-mica-chlorite-hornblend schist and gneiss
40	Paithani	30.15	78.99	A	Quartzite, shale, phyllite, and conglomerate
41	Ranichauri	30.31	78.41	A	Quartzite, shale, phyllite, and conglomerate
42	Srikot	30.22	78.81	B	Gravel, pebbles, sand, silt, and clay
43	Saterakhal	30.32	79.00	A	Basic meta-volcanics
44	Thatyur	30.50	78.16	A	Phyllite, quartz, shale, dolomite, tuff with dolerite
45	Tilwara	30.34	78.97	A	Quartzite and slate with basic meta-volcanics
46	Ukhimath	30.51	79.09	A	Schist, gneiss, marble, and basic intrusives
47	Augustmuni	30.39	79.02	A	Schistose grit, slate, and quartzite with Volcanics
48	Bhilangna	30.43	78.66	A	Quartzite and slate with basic meta-volcanics
49	Barkot	30.81	78.20	B	Gravel, pebbles, sand, silt, and clay
50	Bhatwari	30.80	78.62	A	Quartzite, schist/phyllite and amphibolite
51	Chamoli	30.40	79.33	C	Gray sand, silt, and clay
52	Chinyalisaur	30.57	78.33	B	Gravel, pebbles, sand, silt, and clay
53	Chamba	30.35	78.39	A	Quartzite, shale, phyllite, and conglomerate
54	Duggada	29.80	78.63	B	Splintery shale with nodular limestone
55	Dhumakot	29.75	79.02	A	Phyllite, quartz, shale, dolomite, tuff with dolerite
56	Dunda	30.71	78.35	B	Gravel, pebbles, sand, silt, and clay

(continued)

(continued)

Station number	Station name	Lat	Long	Site class	Site geology according to the seismotectonic atlas
57	Deval	30.06	79.58	A	Schist, augen gneisis, quartzite, and amphibolite
58	Devprayag	30.14	78.60	B	Shale, quartzite, limestone and dolomite
59	Ghat	30.26	79.45	B	Quartz-sericite-chlorite schist and limestone
60	Gopeshwar	30.41	79.32	A	Quartzite and slate with basic meta-volcanics
61	Hindolakhal	30.23	78.61	A	Phyllite, quartz, shale, dolomite, tuff with dolerite
62	Jakholi	30.39	78.90	A	Porphyritic nonfoliated granite
63	Joshimath	30.56	79.56	A	Gnesis, kyanite schist, quartzite, calc silicate
64	Kot	30.15	78.70	A	Phyllite, quartz, shale, dolomite, tuff with dolerite
65	Karanprayag	30.26	79.22	A	Quartzite and slate with basic meta-volcanics
66	Naugaon	30.79	78.15	A	Quartzite, slate, phyllite, dolomite with basics
67	Pokhri	30.34	79.20	A	Schistose grit, slate, and quartzite with volcanics
68	Pauri	30.15	78.78	A	Phyllite, quartz, shale, dolomite, tuff with dolerite
69	Pokhra	29.92	78.92	A	Phyllite, quartz, shale, dolomite, tuff with dolerite
70	Purola	30.88	78.09	A	Quartz-mica-chlorite-hornblend schist and gneiss
71	Pratapnagar	30.45	78.48	A	Quartzite, slate, lensoidal limestone, and tuff
72	Rudhraprayag	30.31	79.00	A	Quartzite, slate, lensoidal limestone, and tuff
73	Rikhnikhal	29.77	78.87	B	Massive sandy limestone
74	Srinagar	30.22	78.77	B	Gravel, pebbles, sand, silt, and clay
75	Satpuli	29.92	78.71	A	Shale, quartzite, limestone, and conglomerate
76	Tehri	30.38	78.43	A	Phyllite, quartz, shale, dolomite, tuff with dolerite
77	Thauldhar	30.51	78.38	A	Phyllite, quartz, shale, dolomite, tuff with dolerite

(continued)

(continued)

Station number	Station name	Lat	Long	Site class	Site geology according to the seismotectonic atlas
78	Thalisain	30.02	79.05	A	Garnet mica and chlorite schist, quartzite with phyllite
79	Tharali	30.06	79.51	A	Schist, augen gneisis, quartzite, and amphibolite
80	Tiuni	30.93	77.85	A	Shale, quartz, limestone, and conglomerate
81	Ukhimath	30.51	79.09	A	Schist, gneiss, marble, and basic intrusives
82	Uttarkashi	30.73	78.44	B	Gravel, pebbles, sand, silt, and clay
83	Vikas Nagar	30.45	77.75	B	Gravel, pebbles, and boulder in oxidized Sandy MTRX
84	Yamkeshwar	29.98	78.42	A	Phyllite, quartz, shale, dolomite, tuff with dolerite
85	Artola	29.62	79.83	A	Garnet mica and chlorite schist, quartzite with phyllite
86	Bageshwar	29.83	79.77	A	Quartzite and slate with basic meta-volcanics
87	Bhowali	29.39	79.52	B	Penecontemporary basic lava flow, dyke, and dolerite sill
88	Baijnath	29.90	79.61	A	Schist, augen gneisis, quartzite, and amphibolite
89	Bhikiasen	29.69	79.27	C	Grey micaceous sand, silt, and clay
90	Baluakot	29.80	80.43	A	Limestone, dolomite, shale, carb. phyllite/slate
91	Barecheena	29.64	79.75	A	Garnet mica and chlorite schist, quartzite with phyllite
92	Berinag	29.77	80.06	A	Quartzite and slate with basic meta-volcanics
93	Basoli	29.70	79.70	A	Quartzite and slate with basic meta-volcanics
94	Bhatrojkhan	29.59	79.30	A	Quartzite, shale, phyllite, and conglomerate
95	Betalghat	29.56	79.34	A	Shale, quartzite, limestone, and conglomerate
96	Chaubatia	29.61	79.46	A	Garnet mica and chlorite schist, quartzite with phyllite
97	Chillianaula	29.66	79.41	A	Garnet mica and chlorite schist, quartzite with phyllite
98	Deghat	29.90	79.22	A	Garnet mica and chlorite schist, quartzite with phyllite

(continued)

(continued)

Station number	Station name	Lat	Long	Site class	Site geology according to the seismotectonic atlas
99	Didihat	29.80	80.25	A	Schist, augen gneisis, quartzite, and amphibolite
100	Danya	29.57	79.93	A	Garnet mica and chlorite schist, quartzite with phyllite
101	Dol	29.54	79.75	A	Garnet mica and chlorite schist, quartzite with phyllite
102	Devidhura	29.41	79.86	A	Leocaratic granite and granodiorite
103	Dwarahat	29.78	79.43	A	Garnet mica and chlorite schist, quartzite with phyllite
104	Ganai Gangoli	29.65	80.04	A	Limestone, dolomite, shale, carb. phyllite/slate
105	Ganai	29.89	79.36	A	Garnet mica and chlorite schist, quartzite with phyllite
106	Garampani	29.48	79.48	B	Penecontemporary basic lava flow, dyke, and dolerite sill
107	Hawal Bagh	29.64	79.63	A	Garnet mica and chlorite schist, quartzite with phyllite
108	Jhajjardeval	29.61	80.23	C	Gray sand, silt, and clay
109	Jaurasi	29.88	79.27	A	Garnet mica and chlorite schist, quartzite with phyllite
110	Kafligair	29.75	79.74	A	Metabasite, amphibolite and micaschist, chlorite[a]
111	Kanalicheena	29.69	80.27	A	Quartzite and slate with basic meta-volcanics
112	Kapkot	29.95	79.90	B	Gravel, boulder embedded in oxidized sandy matrix
113	Karbala	29.58	79.64	A	Garnet mica and chlorite schist, quartzite with phyllite
114	Kausani	29.84	79.60	A	Carbonaceous phyllite, quartzite, and schist
115	Laxmeshwar	29.61	79.67	A	Garnet mica and chlorite schist, quartzite with phyllite
116	Machor	29.59	79.23	A	Phyllite, quartz, shale, dolomite, tuff with dolerite
117	Majkhali	29.68	79.52	A	Garnet mica and chlorite schist, quartzite with phyllite
118	Mukteshwar	29.68	79.52	A	Garnet mica and chlorite schist, quartzite with phyllite
119	Manila	29.74	79.20	A	Garnet mica and chlorite schist, quartzite with phyllite

(continued)

(continued)

Station number	Station name	Lat	Long	Site class	Site geology according to the seismotectonic atlas
120	Munsiari	30.07	80.24	A	Schist, gneiss, marble, and basic intrusives
121	Pandey Gaon	29.58	80.20	A	Limestone, dolomite, shale, carb. phyllite/slate
122	Ramgarh	29.43	79.55	A	Biotite schist, chlorite schist, quartzitet, and gneiss
123	Someshwar	29.78	79.60	A	Quartzite and slate with basic meta-volcanics
124	Syaldey	29.83	79.20	A	Garnet mica and chlorite schist, quartzite with phyllite
125	Thal	29.84	80.15	A	Schist, augen gneisis, quartzite, and amphibolite
126	Tarikhet	29.61	79.40	A	Garnet mica and chlorite schist, quartzite with phyllite
127	Wadda	29.57	80.28	A	Limestone, dolomite, shale, carb. phyllite/slate
128	Almora	29.61	79.64	A	Garnet mica and chlorite schist, quartzite with phyllite
129	Bageshwer	29.83	79.77	A	Limestone, dolomite, shale, carb. phyllite/slate
130	Bhikiasen	29.70	79.27	C	Grey micaceous sand, silt, and clay
131	Bhimtal	29.36	79.55	B	Penecontemporary basic lava flow, dyke and dolerite sill
132	Bhanoli	29.60	79.84	A	Garnet mica and chlorite schist, quartzite with phyllite
133	Barakot	29.47	80.08	A	Carbonaceous phyllite, quartzite, and schist
134	Berinag	29.80	80.04	A	Quartzite and slate with basic meta-volcanics
135	Betalghat	29.56	79.35	A	Quartzite, shale, phyllite, and conglomerate
136	Chaukhutia	29.88	79.34	A	Garnet mica and chlorite schist, quartzite with phyllite
137	Champawat	29.34	80.09	A	Leocaratic granite and granodiorite
138	Dharchula	29.85	80.55	A	Limestone, dolomite, shale, carb. phyllite/slate
139	Dhauladevi	29.58	79.88	A	Garnet mica and chlorite schist, quartzite with phyllite
140	Dwarahat	29.75	79.42	A	Garnet mica and chlorite schist, quartzite with phyllite

(continued)

(continued)

Station number	Station name	Lat	Long	Site class	Site geology according to the seismotectonic atlas
141	Didihat	29.80	80.25	A	Schist, augen gneisis, quartzite, and amphibolite
142	Dhaulachina	29.67	79.78	A	Garnet mica and chlorite schist, quartzite with phyllite
143	Dhari	29.39	79.64	A	Shale, quartzite, limestone, and conglomerate
144	Gangolihat	29.68	80.04	A	Metabasite, amphibolite and micaschist, chlorite[b]
145	Garur	29.90	79.62	A	Schist, augen gneisis, quartzite, and amphibolite
146	Haldwani	29.22	79.53	C	Silt, sand with gravel and pebbles
147	Hawal Bagh	29.64	79.63	A	Garnet mica and chlorite schist, quartzite with phyllite
148	Jainti	29.48	79.82	A	Carbonaceous phyllite, quartzite, and schist
149	Kafligair	29.75	79.77	A	Quartzite, slate, lensoidal limestone, and tuff
150	Kosia Katoli	29.49	79.48	B	Penecontemporary basic lava flow, dyke and dolerite sill
151	Kanda	29.83	79.88	A	Quartzite and slate with basic meta-volcanics
152	Kanalichina	29.67	80.27	A	Limestone, dolomite, shale, carb. phyllite/slate
153	Kapkot	29.94	79.90	B	Gravel, boulder embedded in oxidized sandy matrix
154	Kotabagh	29.40	79.30	C	Oxidized silt–clay with kankar and micaceous sand
155	Lohaghat	29.40	80.08	A	Carbonaceous phyllite, quartzite, and schist
156	Lamgara	29.54	79.75	A	Garnet mica and chlorite schist, quartzite with phyllite
157	Munakot	29.57	80.29	A	Limestone, dolomite, shale, carb. phyllite/slate
158	Munsiari	30.07	80.24	A	Schist, gneiss, marble, and basic intrusives
159	Nainital	29.38	79.46	A	Carbonaceous phyllite, quartzite, and schist
160	Okhal Kanda	29.32	79.73	A	Biotite schist, chlorite schist, quartzitet, and gneiss
161	Pati	29.41	79.94	A	Leocaratic granite and granodiorite

(continued)

(continued)

Station number	Station name	Lat	Long	Site class	Site geology according to the seismotectonic atlas
162	Pithoragarh	29.58	80.21	A	Limestone, dolomite, shale, carb. phyllite/slate
163	Ramgarh	29.45	79.56	A	Shale, quartzite, limestone, and conglomerate
164	Ranikhet	29.64	79.43	A	Garnet mica and chlorite schist, quartzite with phyllite
165	Sult	29.66	79.16	A	Phyllite, quartz, shale, dolomite, tuff with dolerite
166	Someshwer	29.78	79.61	A	Quartzite, slate, lensoidal limestone, and tuff
167	Syaldey	29.82	79.21	C	Grey micaceous sand, silt, and clay
168	Tarikhet	29.61	79.40	A	Garnet mica and chlorite schist, quartzite with phyllite
169	Vikas Bhawan	29.61	79.65	B	Gravel, pebble, and boulder in oxidized sandy MTRX

References

Ambraseys NN, Douglas J (2004) Magnitude calibration of north Indian earthquakes. Geophys J Int 159(1):165–206. https://doi.org/10.1111/j.1365-246X.2004.02323.x

Arjun K, Ashwani K, Gupta SC, Himanshu M, Arup S (2014) Earthquake source parameters and their scaling for the uttarakhand region of north-west himalaya. Disaster Adv. 7:28–41

Bansal BK, Verma M (2013) Science and technology based earthquake risk reduction strategies: the Indian scenario. Acta Geophys 61(4):808–821. https://doi.org/10.2478/s11600-013-0105-5

Bhatia SC, Kumar MR, Gupta HK (1999) A probabilistic seismic hazard map of India and adjoining regions. Ann. Di Geofis. 42:1153–1164

Bhukosh (2023) OCBIS Portal, Geological Survey of India [WWW Document]. https://bhukosh.gsi.gov.in/Bhukosh/Public. https://bhukosh.gsi.gov.in/Bhukosh/Public

Bilham R (2004) Earthquakes in India and the Himalaya: tectonics geodesy and history. Ann Geophys 47(2–3). https://doi.org/10.4401/ag-3338

Bilham R, Gaur VK, Molnar P (2001) Himalayan seismic hazard. Science 293(5534):1442–1444. https://doi.org/10.1126/science.1062584

Borcherdt RD (1970) Effect of local geology on ground motion near San Francisco bay*. Bull Seismol Soc Am 60:29–61

Borcherdt RD (1994) Estimates of site-dependent response spectra for design (Methodology and Justification). Earthq Spectra

BSSC (2004) NEHRP recommended provisions for seismic regulations for new buildings and other structures (FEMA 450). 2003 Edition. Part 1: provisions, building seismic safety council, national institute of building sciences, Washington, D.C.

Chamoli BP, Kumar A, Chen D-Y, Gairola A, Jakka RS, Pandey B, Kumar P, Rathore G (2019) A prototype earthquake early warning system for northern India. J Earthq Eng 0: 1–19

Chaudhary C, Sharma ML (2017) Probabilistic models for earthquakes with large return periods in Himalaya region. Pure Appl Geophys 174:4313–4327
Dal Moro G (2019) Effective active and passive seismics for the characterization of urban and remote areas: four channels for seven objective functions. Pure Appl Geophys 176:1445–1465
DiPietro JA, Pogue KR (2004) Tectonostratigraphic subdivisions of the Himalaya: a view from the west. Tectonics 23:1–20
ENVIS Centre on Himalayan Ecology (2020) The Himalaya (abode of snow). The Highest Mountain Region in the World [WWW Document]. ENVIS. http://gbpihedenvis.nic.in/indian_him_reg.htm
Field EH, Jacob KH (1995) A comparison and test of various site response estimation techniques, including three that are not reference site dependent. Bull Seismol Soc Am 85:1127–1143
Fukushima Y, Bonilla LF, Scotti O, Douglas J (2007) Site classification using horizontal-to-vertical response spectral ratios and its impact when deriving empirical ground-motion prediction equations. J Earthq Eng 11:712–724
Gade M, Raghukanth STG (2017) Simulation of strong ground motion for a Mw 8.5 hypothetical earthquake in central seismic gap region. Himalaya Bull Earthq Eng 15:4039–4065
Gansser A (1964) Geology of the Himalaya, Library of. ed, Printed in Switzerland by Orell FUlsli, Arts graphiques S. A., Zurich. interscience publishers, a division of John Wiley & Sons Ltd, London, New York, Sydney
GSI (2023) Geological Survey of India [WWW Document]. https://www.gsi.gov.in/webcenter/portal/OCBIS. https://www.gsi.gov.in/webcenter/portal/OCBIS
Gupta H, Gahalaut VK (2014) Seismotectonics and large earthquake generation in the Himalayan region. Gondwana Res 25:204–213
Gupta HK (2000) Major and great earthquakes in the Himalayan region: an overview. In: Balassanian S, Cisternas A, Melkumyan M (eds) Earthquake hazard and seismic risk reduction. Advances in natural and technological hazards research, vol 12. Springer, Dordrecht. https://doi.org/10.1007/978-94-015-9544-5_9
Gupta HK (2015) The Mw 7.8 April 25, 2015 Nepal earthquake (End of a long-term seismic quiescence?). J Geol Soc India 85(6):641–646. https://doi.org/10.1007/s12594-015-0261-0
Gupta HK, Bhatia SC (1981) A review of the long period surface waves studies in the himalaya and nearby regions, geodynamic. ed, zagros, hindu kush, himalaya: geodynamic evolution. American Geophysical Union, 2000 Florida Avenue, N.W. Washington, DC 20009, Geological Society of America, 3300 Penrose Place; P.o. Box 9140 Boulder, Colorado 80301, Washindton, D.C, Boulder, Colorado
Gupta HK, Rao NP, Rastogi BK, Sarkar D (2001) The deadliest intraplate earthquake. Science (80). 291: 2101–2102
Gupta HK, Rao VD, Singh J (1982) Continental collision tectonics: evidence from the Himalaya and the neighbouring regions. Tectonophysics 81:213–238
Gupta HK, Singh HN (1989) Earthquake swarms precursory to moderate to great earthquakes in the northeast India region. Tectonophysics 167(2–4):285–298. https://doi.org/10.1016/0040-1951(89)90079-6
Höbusch H (2016) Mountain of destiny: nanga parbat and its path into the German imagination (Studies in German literature, linguistics, and culture). Camden House
Humar JM, Lau D, Pierre JR (2001) Performance of buildings during the 2001 Bhuj earthquake. Can J Civ Eng 28:979–991
Inaba T, Dohi H, Okuta K, Sato T, Akagi H (2000) Nonlinear response of surface soil and NTT building due to soil-structure interaction during the 1995 Hyogo-ken Nanbu (Kobe) earthquake. Soil Dyn Earthq Eng 20:289–300
Jade S, Shrungeshwara TS, Kumar K, Choudhury P, Dumka RK, Bhu H (2017) India plate angular velocity and contemporary deformation rates from continuous GPS measurements from 1996 to 2015. Sci Rep 7:1–16
Kanamori H (2005) Real-time seismology and earthquake damage mitigation. Annu Rev Earth Planet Sci 33:195–214

Khattri KM, Tyagi AK (1983) Seismicity patterns in the himalayan plate boundary and identification of the areas of high seismic potential. Tectonophysics 96:281–297
Khattri KN (1987) Great earthquakes, seismicity gaps and potential for earthquake disaster along the Himalaya plate boundary. Tectonophysics 138:79–92
Kumar P (2020) Earthquake early warning system : site classification, intensity map and attributes. Thesis, centre of excellence in disaster Mitigation & Management, Indian Institute of Technology Roorkee, India
Kumar P, Pandey B, Kamal K, Kumar A (2022a) Site classification of seismic recording stations of Garhwal region of earthquakes early warning system for Uttarakhand, India. Vietnam J Earth Sci 44:369–394
Kumar P, Sharma ML, Jakka RS, Kumar A, Joshi GC, Rautela P (2023) Successful alert issuance with sufficient lead time by uttarakhand state earthquake early warning system: case study of nepal earthquakes. J Geol Socienty India 99:303–310
Kumar R, Mittal H, Babita S (2022b) Earthquake genesis and earthquake early warning systems: challenges and a way forward. Surv Geophys 43:1143–1168
Lachet C, Bard PY (1994) Numerical and theoretical investigations on the possibilities and limitations of nakamura's technique. J Phys Earth 42:377–397
Langston CA (1979) Structure under mount rainier, washington, inferred from teleseismic body waves. J Geophys Res 84:4749–4762
Macau A, Benjumea B, Gabas A, Figueras S, Vila M (2014) The effect of shallow quaternary deposits on the shape of the h/v spectral ratio. Surv Geophys 36:1–24
Malik JN, Nakata T, Philip G, Suresh N, Virdi NS (2008) Active fault and paleoseismic investigation: evidence of a historic earthquake along Chandigarh fault in the frontal himalayan zone, NW India. Himal Geol 29:109–117
Martin SS, Hough SE, Hung C (2015) Ground motions from the 2015 Mw 7.8 Gorkha, Nepal, earthquake constrained by a detailed assessment of macroseismic data. Seismol Res Lett 86(6):1524–1532. https://doi.org/10.1785/0220150138
Mittal H, Kumar A, Ramhmachhuani R (2012) Indian national strong motion instrumentation network and site characterization of its stations. Int J Geosci 03:1151–1167
Mittal H, Wu YM, Kumar A, Kumar A, Sharma B (2016) Evaluating the effects of ground motion parameters on response spectra in Uttarakhand Himalayas, India. Arab J Geosci 9
Mittal H, Wu YM, Lal M, Benjamin S, Yang M, Gupta S (2018) Testing the performance of earthquake early warning system in northern India. Acta Geophys
Mittal H, Wu YM, Sharma ML, Yang BM, Gupta S (2019) Testing the performance of earthquake early warning system in northern India. Acta Geophys 67:59–75
Mittal H, Yang BM, Wu YM (2022) Progress on the earthquake early warning and shakemaps system using low-cost sensors in Taiwan. Geosci Lett 9
Mohraz B (1976) A study of earthquake response spectra for different geological conditions. Bull Seismol Soc Am 66:915–935
Nakamura Y (1989) A method for dynamic characteristics estimation of subsurface using microtremor on the ground surface, railway technical research institute/Tetsudo Gijutsu Kenkyujo. Railway Technical Research Institute/Tetsudo Gijutsu Kenkyujo, TOKYO, Japan
Nakamura Y (2008) On the H/V spectrum. In: The 14 world conference on earthquake engineering October 12–17, 2008, Beijing, China. Beijing, pp 1–10
Neate J (1989) High Asia: an illustrated history of the 7,000 Metre Peaks. Mt. Seattle 213
New Zealand Standard (2004) Structural design actions Part 5: earthquake actions – New Zealand. NZS 1170(5):1–87
Patriat P, Achache J (1984) India-Eurasia collision chronology has implications for crustal shortening and driving mechanism of plates. Nature 311:615–621
Paudyal H, Panthi A (2010) Seismic vulnerability in the Himalayan Region. Himal Phys 1:14–17
Perron V, Gélis C, Froment B, Hollender F, Bard PY, Cultrera G, Cushing EM (2018) Can broad-band earthquake site responses be predicted by the ambient noise spectral ratio? Insight from observations at two sedimentary basins. Geophys J Int 215:1442–1454

Phillips WS, Aki K (1986) Site amplification of coda waves from local earthquakes in central California. Bull Seismol Soc Am 76:627–648
Rastogi BK (1974) Earthquake mechanisms and plate tectonics in the himalayan region. Tectonophysics 21:47–56
Satoh T, Kawase H, Matsushima S (2001) Differences between site characteristics obtained from microtremors, S-waves, P-waves, and codas. Bull Seismol Soc Am 91:313–334
Seed HB, Ugas C, Lysmer J (1976) Site-dependent spectra for earthquake-resistant design. Bull Seismol Soc Am 66:221–243
Sharma ML (2003) Seismic hazard in the northern India region. Seismol Res Lett 74:141–147
Sharma ML, Arora MK (2005) Prediction of seismicity cycles in the himalayas using artificial neural network. Acta Geophys Pol 53:299–309
Singh DD, Gupta HK (1980) Source dynamics of two great earthquakes of the Indian subcontinent: the Bihar-Nepal earthquake of January 15, 1934 and the Quetta earthquake of May 30, 1935. Bull Seismol Soc Am 70(3):757–773. https://doi.org/10.1785/BSSA0700030757
Srivastava HN (1992) Earthquake prediction studies in Himalaya critical evaluation. Mem Geol Soc India 23:151–172
Srivastava HN (2004) Earthquakes: forecasting and mitigation, reprint. ed. National Book Trust, India
Srivastava HN, Verma M, Bansal BK, Sutar AK (2015) Discriminatory characteristics of seismic gaps in Himalaya. Geomatics. Nat Hazards Risk 6:224–242
Steckler MS, Akhter SH, Seeber L (2008) Collision of the Ganges–Brahmaputra delta with the burma arc: implications for earthquake hazard. Earth Planet Sci Lett 273:367–378
UBC (1994) Uniform building code, structural engineering design provisions, volume 2, international conference of building officials, 5360 workman mill road whittier. California 90601–2298(310):699–0541
Valdiya KS (1980) Geology of the kumaun lesser Himalaya: Dehradun 289
Valdiya KS (1984) Aspects of TECTONICS: focus on south central Asia. Tata McGraw-Hill Pub. Co., New Delhi, India
Valdiya KS (1984b) Evolution of the Himalaya. In: Naqvi SM, Gupta HK, Balakrishna S (eds) Lithosphere: structure, dynamics and evolution. tectonophysics, pp 229–248
Wu Y-M, Lin T-L (2014) A test of earthquake early warning system using low cost accelerometer in Hualien, Taiwan. In: Wenzel FJ Zschau (eds) Early Warn. Geol. Disasters - Sci. Methods Curr. Pract. Adv. Technol. Earth Sci. Springer Berlin Heidelberg, New York, pp 307–331
Wu YM, Chen DY, Lin TL, Hsieh CY, Chin TL, Chang WY, Li WS, Ker SH (2013) A high-density seismic network for earthquake early warning in Taiwan based on low cost sensors. Seismol Res Lett 84:1048–1054
Wu YM, Liang WT, Mittal H, Chao WA, Lin CH, Huang BS, Lin CM (2016) Performance of a low-cost earthquake early warning system (P-Alert) during the 2016 ML 6.4 Meinong (Taiwan) earthquake. Seismol Res Lett 87:1050–1059
Wu YM, Mittal H (2021) A review on the development of earthquake warning system using low-cost sensors in taiwan. Sensors 21
Wu YM, Mittal H, Huang TC, Yang BM, Jan JC, Chen SK (2019) Performance of a low-cost earthquake early warning system (P-ALErt) and shake map production during the 2018 M w 6.4 Hualien, Taiwan, earthquake. Seismol Res Lett 90:19–29
Wyss M, Gupta S, Rosset P (2018) Casualty estimates in repeat himalayan earthquakes in India. Bull Seismol Soc Am 108:2877–2893
Wyss M, Wang RJ, Zschau J, Xia Y (2006) Earthquake loss estimates in near real-time. Eos Trans Ame Geophys Union 87(44):477–478. https://doi.org/10.1029/2006EO440001
Xie J, Zimmaro P, Li X, Wen Z, Song Y (2016) VS30 empirical prediction relationships based on a new soil-profile database for the beijing plain area, China. Bull Seismol Soc Am 106:1–12

Zhang P, Yang Z, Gupta HK, Bhatia SC, Shedlock KM (1999) Global seismic hazard assessment program (GSHAP) in continental Asia. Ann Di Geofis 42:1167–1190

Zhao JX, Irikura K, Zhang J, Fukushima Y, Somerville PG, Asano A, Ohno Y, Oouchi T, Takahashi T, Ogawa H (2006) An empirical site-classification method for strong-motion stations in Japan using H/V response spectral ratio. Bull Seismol Soc Am 96:914–925

Chapter 12
Overview of Artificial Intelligence (AI) and Machine Learning (ML) in Seismology

Harendra Kumar Dadhich

Abstract Undoubtedly one of the most destructive natural catastrophes is an earthquake. Around the world, they frequently result in significant losses in terms of people, structures, economies, and societies. It is still impossible to accurately anticipate the location and timing of catastrophic occurrences, despite the fact that analytical and measuring techniques have advanced steadily over the previous few decades. The chapter provides an overview of applications of machine learning (ML) and Artificial Intelligence (AI) in seismology so that above mentioned problems in this field can be resolved. The ML Model helps to identify unseen signals and patterns to extract features that might improve our physical understanding of earthquakes. The modeling capabilities of the ML-based methods have resulted in their extensive applications in science and engineering. Herein, the role of ML as an effective approach for solving some problems in geosciences will be highlighted. ML algorithms in seismology address various problems like earthquake detection, phase picking, EEW, ground-motion prediction, seismic tomography, and earthquake geodesy. AI-based algorithms are used for earthquake analysis and prediction, deciphering complex stress development patterns, and developing fully automatic seismic event detection using SVM. ML techniques, such as ANN and GA, estimate earthquake source parameters, while classification algorithms like Artificial Neural Network (ANN) and Support Vector Machine (SVM) have been used to study to identify shallow focus (depth < 70 km) tsunami genic earthquakes at a regional distance. Also, a lot of ML and AI models can be used in seismology to resolve various key problems of seismology from detection to prediction tasks.

Keywords Machine learning · Artificial intelligence · Seismology · Early warning · Classification

H. K. Dadhich (✉)
Birla Soft Pvt. Limited, Noida, India
e-mail: dadhich.harendra@gmail.com

Sandeep et al. (eds.), *Geohazards*, Advances in Natural and Technological Hazards Research 53, https://doi.org/10.1007/978-981-99-3955-8_12

12.1 Introduction

Seismology is the scientific study of earthquakes and the propagation of seismic waves through the Earth. Machine learning techniques have been applied to various problems in seismology, such as earthquake prediction, analysis of seismic data, and identification of patterns in seismic activity. One example of the use of machine learning in seismology is the development of predictive models for earthquakes. These models can be trained on data about past earthquakes, such as their locations, magnitudes, and timing, to predict the likelihood of future earthquakes in a given area. Machine learning algorithms can also be used to analyze large amounts of seismic data to identify patterns and trends that may not be immediately apparent to humans. Another application of machine learning in seismology is in the development of algorithms to detect and classify different types of seismic waves. Seismologists use a variety of sensors to measure ground motion during an earthquake, and machine learning algorithms can be used to analyze these data to identify different types of seismic waves, such as P-waves, S-waves, and surface waves. Overall, the use of machine learning in seismology has the potential to improve our understanding of earthquakes and improve our ability to predict and prepare for them.

The rapid advancement of sensing technology and resolving techniques has led to significant progress in seismology. This progress is primarily driven by the increased computational capacity, allowing for the analysis of massive tectonic datasets. Whereas former research principally used established dossier mining forms, again, artificial intelligence (AI) supports adept tools to address that dossier and extract valuable information to form trustworthy predictions and conclusions in seismology. Therefore, AI-enhanced seismology considerably depends on how to use AI approaches (such as machine intelligence (ML) or deep learning (DL)) to get productive detecting data with buzz and detect temblor occurrences that are at or below the roar level.

In recent years, seismology has focused most of its efforts on improving the sensitivity of phase detection while processing large amounts of real-time acquired data. Due to the inefficiency of earthquake experts visually examining recorded data at various stages, it is desirable to be able to predict earthquakes in a rational and reliable manner using data collected in real time (Lary et al. 2015). A short-term (long-term) average (STA/LTA) prediction algorithm was developed and later replaced by the phase assignment method because the former cannot distinguish between impulsive transient seismic signals. The latter was developed to summarize seismic phases to determine whether earthquakes will occur (Shahin et al. 2016; Ross et al. 2018, 2019). However, these conventional approaches fall short of detecting smaller, more frequent seismic events. As a result, AI tools are deployed to handle the complex scenarios of earthquake prediction. AI plays a key role in modern earthquake detection systems as it increases detection efficiency and mitigates the effects of noisy data. Figure 12.1a shows the interrelationship between AI and data science techniques in seismology. Comparing various AI algorithms in seismology, supervised and unsupervised ML approaches have received significant research attention (Sick et al. 2015;

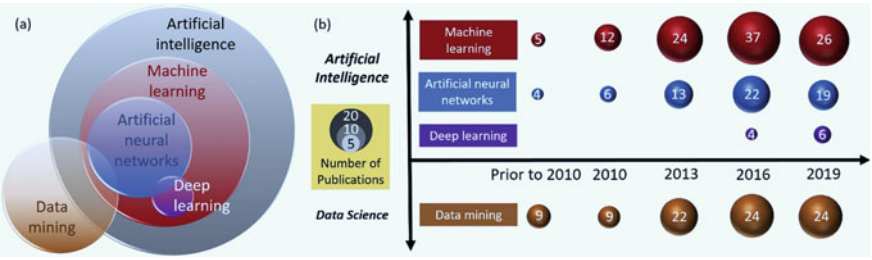

Fig. 12.1 Existing AI and data science studies in seismology. **a** Illustration of the interrelation between AI and data science techniques in seismology. **b** Summary of the published AI-based studies in seismology during 1999–2019. *Source* https://doi.org/10.1016/j.gsf.2019.10.004

Wang et al. 2019; Woo 2019). In the field of ML, various algorithms, including Artificial Neural Networks (ANN), Genetic Programming (GP), Self-Organizing Maps (SOM), Support Vector Machines (SVM), and Decision Trees (DT), are employed to implicitly determine earthquake events. Among these, Deep learning, utilizing the concept of ANNs, stands out as one of the most advanced techniques (Kundu et al. 2017). Deep learning allows for learning generalized representations of datasets across different domains and capturing complex nonlinear relationships between variables. Define ML's powerful capabilities on sequential datasets make it an excellent choice for phase assignment problems in seismology. This is suitable for phase assignment in real-time seismic networks as it processes one element of the sequence at a time. Figure 12.1b summarizes his AI-based research in seismology published from 1999 to 2019. As you can see, ANN is the most widely used ML method in this area. Moreover, there has recently been a growing interest in the use of deep learning techniques in seismology.

12.2 Machine Learning and Artificial Intelligence Approaches in Seismology

There are several ways in which artificial intelligence (AI) approaches, including machine learning, can be used in seismic analysis:

- Classification of seismic events: Machine learning algorithms can be used to classify different types of seismic events, such as earthquakes, explosions, and volcanic eruptions, based on the characteristics of the seismic waves they produce.
- Earthquake prediction: Machine learning algorithms can be trained on data about past earthquakes to predict the likelihood of future earthquakes in a given area.
- Seismic data analysis: Machine learning algorithms can be used to analyze large amounts of seismic data to identify patterns and trends that may not be immediately apparent to humans.

- Seismic hazard assessment: Machine learning algorithms can be used to assess the likelihood of earthquakes occurring in a given area based on various factors, such as the geology of the region, the history of seismic activity, and the presence of faults or other geologic features.
- Seismic event monitoring: Machine learning algorithms can be used to monitor seismic activity in real time, providing early warning of earthquakes (Kumar et al. 2022) and other seismic events.

Overall, the use of AI approaches in seismic analysis can help seismologists better understand earthquakes and other seismic events and improve our ability to predict and prepare for them.

12.3 Traditional Methods Used in Seismology

Seismology is the study of earthquakes and the Earth's structure and behavior through the analysis of seismic waves. There are several traditional methods used in seismology to study earthquakes and the Earth's structure, including:

Seismic refraction: This method involves the use of seismic waves to determine the composition and structure of the Earth's crust. Seismic waves are sent through the Earth and their path is monitored to determine the properties of the layers of the Earth.

Seismic reflection: This method involves the use of seismic waves to create an image of the Earth's crust. Seismic waves are sent through the Earth and reflected off different layers, creating an image of the Earth's structure.

Gravity surveys: This method involves the measurement of the Earth's gravity field to determine the density of the Earth's crust. The density of the Earth's crust can be used to infer the composition and structure of the Earth's crust.

Magnetic surveys: This method involves the measurement of the Earth's magnetic field to determine the composition and structure of the Earth's crust. The Earth's magnetic field is influenced by the presence of iron-bearing minerals in the crust.

Tomography: This method involves the use of seismic waves to create a three-dimensional image of the Earth's interior. Seismic waves are sent through the Earth and their path is monitored to create a detailed image of the Earth's structure.

InSAR: This method involves the use of satellite imagery to measure ground deformation caused by earthquakes. The satellite images can be used to create a detailed map of the ground deformation and infer the location and size of the earthquake.

Besides this many more traditional methods are there like GPS for crustal deformation, Receiver function, and Inversion that involves solving an inverse problem to determine the structure of the Earth's interior. In this technique, seismologists use mathematical models and algorithms to analyze the data collected from seismic

waves and determine the properties of different layers of the Earth's interior; physical modeling involves constructing a physical model of the Earth's interior and subjecting it to seismic waves to study the behavior of these waves and understand how they interact with different layers of the Earth. This technique allows seismologists to test different hypotheses about the structure of the Earth and verify their accuracy.

12.4 Machine Learning Architecture: Features and Techniques

ML, a branch of AI, involves systems that automatically learn from data, recognize patterns, and make decisions. What's special about ML is that computers can learn without being explicitly programmed. Most ML-based methods are intrinsically inspired by biological learning. In seismology, ML uses a series of techniques to find inherent rules and dependencies among data and classify or regress them. ML is also commonly used to classify and analyze unseen patterns and features in detected data. This is because, unlike seismologists who use intuition and logic to analyze data, they detect unknown features that are beyond human capabilities (Kong et al. 2019). Figure 12.2 shows the main components of ML. This can be divided into supervised and unsupervised (Salehi and Burgueno 2018). The former typically consists of regression and classification techniques, while the latter includes reduction and clustering techniques. There is also another category called semi-supervised learning algorithms that can clean data and make predictions.

However, ML in seismology can be divided into supervised and unsupervised learning to (1) collect and (2) split seismic data for training and testing; the basic exploratory data analysis (EDA) has been done on seismic datasets for better understanding. (3) the training model uses a numerical optimization algorithm to tune the seismic variables, (4) the test data is used to evaluate the model in terms of prediction accuracy, and (5) the ML algorithm is used to add new data for prediction and generate. In general, ML can be categorized into three applications in seismology. This includes code accelerator tools for reducing the computational cost of deterministic models, developing empirical models when deterministic models are not possible, and handling classification problems (Lary et al. 2015). In the field of ML, ANNs have found many applications in seismology (Azamathulla Md et al. 2005; Alavi and Gandomi et al. 2011a; Alavi et al. 2011b). ANN, like many other ML methods, is considered a black-box model generator because it cannot produce practical prediction equations.

This limitation has been addressed by other ML methods such as GP and Decision Trees (DT). Neural Networks generally consist of multiple processing components, usually grouped into layers; an input layer, some hidden layers, and an output layer (Salehi and Burgueno et al., 2018). In seismology, ANN models start with information propagation in the input layer. The network evaluates and adjusts the weights on the

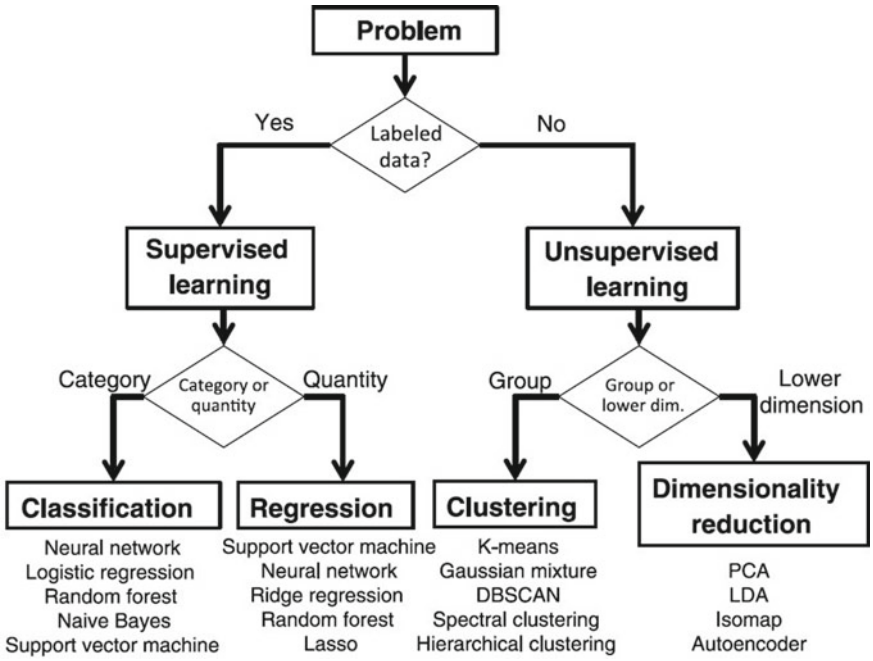

Fig. 12.2 Machines learning (ML) algorithm types. Supervised machine learning (ML) builds models that predict categorical or quantitative target variables from labeled datasets. Unsupervised machine learning (ML) groups data by similarity or decreases the dimensionality of the input datasets by operating on unlabeled datasets. The bottom of each category has a list of popular ML algorithms

presentation of the training data set, uses learning techniques to find the set of weights, and establishes the relationship between the input and output data with minimal error (Giacinto et al. 1997). Through the training process, the performance of ANN models can be validated against independent datasets.

12.5 Future Trends

Machine learning, a subset of artificial intelligence, has the potential to revolutionize the field of seismology by enabling faster and more accurate analysis of seismic data. Some potential applications of machine learning in seismology include earthquake prediction; in this, Machine learning algorithms can be used to analyze large datasets of seismic activity and identify patterns that may indicate the likelihood of an earthquake. By predicting earthquakes in advance, seismologists can better prepare for and mitigate the impacts of these natural disasters. Also, Seismic wave analysis (LeCun 2015, Li et al. 2018), in this Machine learning algorithm, can be

used to classify and identify different types of seismic waves, such as P-waves and S-waves, and to accurately measure the magnitude and location of earthquakes. This can help seismologists to better understand the properties of earthquakes and the structure of the Earth's interior. In Seismic imaging, Machine learning algorithms can be used to improve the accuracy and resolution of seismic imaging techniques, such as seismic tomography, by analyzing large datasets of seismic data and identifying patterns and structures within the Earth's interior. In Hazard assessment, Machine learning algorithms can be used to analyze the impact of earthquakes on different types of infrastructure, such as bridges and buildings, and to predict the likelihood of damage in different scenarios. This can help seismologists to develop strategies for mitigating the impacts of earthquakes and reducing the risk of damage to infrastructure. In Data visualization, Machine learning algorithms can be used to visualize and analyze large datasets, such as those collected from seismic networks, in ways that are not possible using traditional methods. By using machine learning to visualize and analyze seismic data, seismologists can gain insights and discover patterns that may not be apparent using other methods.

Overall, the use of machine learning in seismology has the potential to greatly enhance our understanding of earthquakes and the Earth's interior structure, and to improve our ability to predict and prepare for these natural disasters.

12.6 Prediction Systems

AI technology can be used to eliminate the effects of seismic noise by setting the's self-adaptive limit states. To avoid the effects of low-amplitude seismic noise, a limit state can be defined. The intelligent data-driven earthquake prediction system can adjust the limit state in terms of periods, the frequency of events occurring, detection accuracy, cost analysis, etc. On the other hand, it is important to improve the performance of seismic monitoring sensors, such as using self-powered seismic sensors that harvest energy from the environment. AI-assisted earthquake prediction models are expected to reduce energy dissipation from seismic sensors and improve data transformation for detection (Larose et al. 2015). Additionally, it is important to consider the impact of location and modify the forecast model accordingly. Clearly, the AI model trained on the North American earthquake data is different from the model developed on the Middle East data.

12.7 Conclusion

Earthquake prediction is important for risk assessment, prevention, and safety design of large structures. However, it is usually difficult to characterize the seismic response and reveal features from large amounts of continuously acquired noisy data. To address these serious challenges in seismology, AI technology was used as a powerful

statistical tool to address data-related problems. In the path, AI demonstrates the benefits of large-scale acceptance emerging in seismology to open up promising directions for AI-assisted seismic analysis. This contrasts with the traditional approach that has been prevalent in seismic regions so far. The exciting debut of ML over the last decade and its robust branches like DL-like, coupled with the emergence of cluster computing environments and more powerful personal computers has made it possible to process mass seismological data and provides immediate potential solutions to areas of need. A seismic prediction model that identifies seismic responses from noisy data (i.e., valid seismic data) while revealing unseen patterns and features from detected seismic data (i.e., undetected seismic data) Preliminary efforts were made to use DL analysis with the goal of developing earthquake. Here we take a step forward to envision future development trends for DL Enhanced Seismology in IoT platforms. Aside from the fact that DL seismic analysis is still in its early stages, the IoT is just at the peak of Gartner's hype cycle. Integrating the state-of-the-art of DL and IoT technology and applying them to seismic data will greatly advance the development of seismology.

References

Alavi AH, Gandomi AH (2011a) Prediction of principal ground-motion parameters using a hybrid method coupling artificial neural networks and simulated annealing. Comput Struct 89:2176–2194

Alavi AH, Gandomi AH, Modaresnezhad M, Mousavi M (2011b) New ground-motion prediction equations using multi expression programing. J Earthq Eng 15:511–536

Azamathulla Md H, Deo MC, Deolalikar PB (2005) Neural networks for estimation of scour downstream of a ski-jump bucket. ASCE J H draul Eng 131(10):898–908

Giacinto G, Paolucci R, Roli F (1997) Application of neural networks and statistical pattern recognition algorithms to earthquake risk evaluation Pattern. Recognit Lett 18:1353–1362

Kumar R, Mittal H, Sandeep et al (2022) Earthquake genesis and earthquake early warning systems: challenges and a way forward. Surv Geophys 43: 1143–1168. https://doi.org/10.1007/s10712-022-09710-7

Kundu A, Bhadauria YS, Basu S, Mukhopadhyay S (2017) Application of ann and svm for identification oftsunamigenic earthquakes from 3- component seismic data. In: 2017 2nd IEEE international conference on recent trends in electronics, information & communication technology (RTEICT). IEEE, pp 10–13

Kong DT, Trugman ZE, Ross MJ, Bianco BJ, Meade P (2019) Gerstoft machine learning in seismology: turning data into insights. Seismol Res Lett 90(1): 3–14

Kortström J, Uski M, Tiira T (2016) Automatic classification of seismic events within a regional seismograph network. Comput Geosci 87: 22–30

Larose E, Carriere S, Voisin C, Bottelin P, Baillet L, Gueguen P, Walter F, Jongmans D, Guillier B, Garambois S, Gimbert F, Massey C (2015) Environmental seismology: what can we learn on earth surface processes with ambient noise? J Appl Geophysics 166(2015):62–74

Lary D, Alavi A, Gandomi A, Walker A (2015) Machine learning in geosciences and remote sensing. Geosci Front 7.https://doi.org/10.1016/j.gsf.2015.07.003

LeCun Y, Bengio Y, Hinton G (2015) Deep learning. Nature 521:436–444

Li Z, Meier M, Hauksson E, Zhan Z, Andrews J (2018) Machine learning seismic wave discrimination: application to earthquake early warning. Geophys Res Lett 45:4773–4779

Perol T, Gharbi M, Denolle M (2018) Convolutional neural network for earthquake detection and location. Sci Adv 4: e1700578

Ross ZE, Meier M, Hauksson E, Heaton TH (2018) Generalized seismic phase detection with deeplearning. Bull Seismol Soc Am 180(5A): 2894–2901

Ross ZE, Yue Y, Meier M, Hauksson E, Heaton TH (2019) PhaseLink: a deep learning approach to seismic phase association. J Geophys Res: Solid Earth 124:856–869

Shahin MA (2016) State-of-the-art review of some artificial intelligence applications in pile foundations. Geosci Front 7(1): 33–44. ISSN 1674-9871.https://doi.org/10.1016/j.gsf.2014.10.002

Sick B, Guggenmos M, Joswig M (2015) Chances and limits of single-station seismic event clustering by unsupervised pattern recognition. Geophys J Int 201:1801–1813

Salehi H, Burgueno R (2018) Emerging artificial intelligence methods in structural engineering 171: 170–189

Schmid Huber J (2015) Deep learning in neural networks: an overview. Neural Netw 61: 85–117

Wang R, Pan C, Wang X, Xu F, Jiang S, Li M (2019) The impact of tracheotomy timing in critically ill patients undergoing mechanical ventilation: A meta-analysis of randomized controlled clinical trials with trial sequential analysis, Heart & Lung 48(1):46–54, ISSN 0147-9563. https://doi.org/10.1016/j.hrtlng.2018.09.005

Woo TH (2019) Analysis of earthquake management design for nuclear power plants (NPPs) incorporated with artificial intelligence (AI) method. Energy Sources, Part A: Recovery, Utilization, Environ Effects 41(17):2104–2113